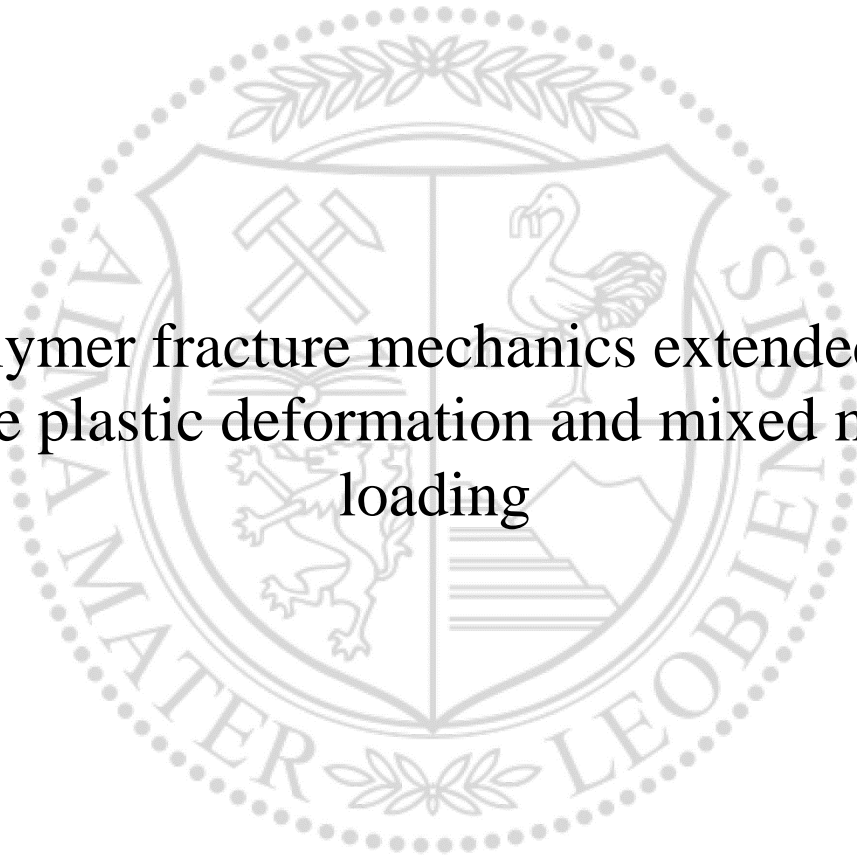




Materials Science and Testing of Polymers

Doctoral Thesis

The background features a large, faint watermark of the University of Leoben seal. The seal is circular and contains a shield with various symbols: crossed hammers, a swan, a lion, and a mountain range. The text 'UNIVERSITAS MONTANA LEOBENSIS' is written around the perimeter of the seal.

Polymer fracture mechanics extended to
large plastic deformation and mixed mode
loading

Dipl.-Ing. Anja Gosch, BSc

March 2021



EIDESSTÄTTLICHE ERKLÄRUNG

Ich erkläre an Eides statt, dass ich diese Arbeit selbständig verfasst, andere als die angegebenen Quellen und Hilfsmittel nicht benutzt, und mich auch sonst keiner unerlaubten Hilfsmittel bedient habe.

Ich erkläre, dass ich die Richtlinien des Senats der Montanuniversität Leoben zu "Gute wissenschaftliche Praxis" gelesen, verstanden und befolgt habe.

Weiters erkläre ich, dass die elektronische und gedruckte Version der eingereichten wissenschaftlichen Abschlussarbeit formal und inhaltlich identisch sind.

Datum 22.03.2021

A handwritten signature in blue ink, appearing to read 'Anja Gosch', written over a horizontal line.

Unterschrift Verfasser/in
Anja Gosch

Anja Gosch

Dissertation

Polymer fracture mechanics extended to large plastic deformation and mixed mode loading

March 2021

This cumulative Dissertation was authored by

DI Anja Gosch

born 27th January 1993

in Bruck an der Mur (Styria, Austria)

Materials Science and Testing of Polymers

Department Polymer Engineering and Science, Montanuniversitaet Leoben

*Everything great that ever happened in this world
happened first in somebody's imagination.*

Astrid Lindgren

Preamble

Acknowledgement

The research work of this thesis was performed at the Materials Science and Testing of Polymers/ Montanuniversitaet Leoben within the framework of the COMET-program of the Federal Ministry for Climate Action, Environment, Energy, Mobility, In-novation and Technology and the Federal Ministry for Digital and Economic Affairs with contributions by the Polymer Competence Center Leoben GmbH, the Institute of Physics of Materials (AS CR/Czech Republic), the Università degli Studi di Brescia (Dipartimento di Ingegneria Meccanica e Industriale/Italy) and the Doctoral Center for Engineering Sciences of the Research Campus of Central Hessen under the supervision of the Justus-Liebig-University Gießen in cooperation with the University of Applied Sciences of Central Hessen (Technische Hochschule Mittelhessen/Germany). The PCCL is funded by the Austrian Government and the State Governments of Styria, Lower Austria and Upper Austria.

I would like to take the opportunity to express my gratitude and thankfulness to all people supporting and inspiring me while working on my thesis.

First of all, I would like to thank both of my supervisors Dr. FLORIAN ARBEITER (Materials science and testing of polymers, Montanuniversitaet Leoben) and Dr. MICHAEL BERER (PCCL GmbH, Leoben) for their support and guidance through my PhD work. It was a pleasure for me to work with both of you and to get the possibility of developing my own way as PhD student. With the help of your scientific background it was possible to develop new experimental procedures and explore new fields of polymer fracture mechanics. Even though, the fact of having two supervisors was sometimes quite challenging, I always had the benefit of a broad scientific discussion and the input of several aspects in the end. I am very thankful for your support during my PhD thesis.

Second, I would like to thank Univ.-Prof. Dr. GERALD PINTER (Materials science and testing of polymers, Montanuniversitaet Leoben) for the opportunity to perform my PhD thesis within his working group and for the

welcoming and cooperative atmosphere at our institute. It was a pleasure to experience the positive impact of social commitment on the way of working.

Furthermore, I wanted to thank my mentor Assoc.-Prof. Dr. FRANCESCO BALDI (Dipartimento di Ingegneria Meccanica e Industriale, Universita Degli Studi di Brescia, Italy) and his team for their support during my thesis and the opportunity to visit him in Brescia and fulfil my work around the J-Integral. In addition, I wanted to thank the whole team from the Institute of Physics of Materials in Brno for the cooperation in the field of mixed mode loading.

I am also very grateful to the whole team of our Institute (Materials science and testing of polymers), who made all the coffee breaks in the morning and the lunchtime so entertaining and amusing. Without this nice atmosphere all around the office, my PhD time would not have been as great as it was. Special thanks goes to my office colleagues ANDREA and JÜRGEN. It was a pleasure for me to share the office with you both. Furthermore, I wanted to thank all my colleagues from the RELIABLE-group. I especially wanted to thank SANDRA for her charming personality. I also wanted to take the chance to thank FRANZ, from whom I learned a lot about manufacturing techniques.

Outside of work, I wanted to take the opportunity to thank my friends MIRIAM, JULIA, MARIE, LISA, ANJA and SUSANNE who stand by my side since ground school. Furthermore, I wanted to thank all my friendships with the starting point in Leoben (SILVIA, JOHANNES, MARTIN, MANUELA, KATHARINA, HANS, ELISA, CHRISTOPH, LAURA and MARTIN). You made my time as a student in Leoben to a very important and special part of my whole life.

Furthermore, I wanted to thank my boyfriend THOMAS, who always supported my ideas and gave me the trust I needed to complete this thesis. You always find the right words to cheer me up when I am lost in my thoughts and you encouraged me to work for my dreams. Furthermore, you are my favourite travelling partner to fulfil my craving for learning about new cultures and countries.

Finally, yet importantly, I wanted to say thank you to my family who enabled myself to do whatever I wanted to do. My parents HERMANN and PETRONELLA, who showed me what is important for a happy life and my brother DANIEL, for his humorously thoughts in hard times. With all their never-ending love I had experienced in my life, I was able to complete this thesis.

Kurzfassung

Die Analyse und Weiterentwicklung bruchmechanischer Ansätze für Kunststoffe wurde zum Fokus zahlreicher Forschungsarbeiten, sowohl im Bereich von theoretischen Ansätzen als auch bei der Entwicklung verbesserter Testmethoden. Vom heutigen Standpunkt aus, gibt es jedoch noch immer Bereiche in der Bruchmechanik von unverstärkten Kunststoffen, wie die elastisch plastische Bruchmechanik und sogenannte „Mixed Mode“ Belastungen, die wenig bis gar nicht untersucht wurden. Genau diese genannten Bereiche wurden in dieser Arbeit untersucht und weiterentwickelt, um sie bei Kunststoffen in Zukunft noch breiter anwenden zu können.

Im Bereich der elastisch plastischen Bruchmechanik gibt es bereits verschiedene Prüfmethoden, welche auch bei Kunststoffen angewendet werden. Dennoch stellt sich die Ermittlung von adäquaten bruchmechanischen Kennwerten von Polymeren noch immer als schwierig heraus. In dieser Arbeit wurde deshalb die Anwendbarkeit verschiedener Testmethoden der elastisch plastischen Bruchmechanik in Kombination mit unterschiedlichen Methoden zur Minimierung der Messdatenstreuung für Kunststoffe überprüft. Basierend auf diesen Ergebnissen wurde die Geometrieabhängigkeit von elastisch plastischen Bruchparametern anhand einer Testmethode der „European Structural Integrity Society (ESIS TC 4)“ untersucht. Die ermittelten Initiierungsparameter zeigten eine Abhängigkeit von der Probekörpergröße, während keine Geometrieabhängigkeit der Risswachstumskurve festgestellt wurde. Zusätzlich wurden verschiedene Initiierungsparameter der untersuchten Geometrien mit physikalischen Vorgängen während des Rissinitiierung korreliert. Die gewonnenen Erkenntnisse sollen in Zukunft als Grundlage für die Simulation komplexer Bauteile herangezogen werden.

Um ein größeres Verständnis für das Mixed Mode Materialverhalten von unverstärkten Kunststoffen zu schaffen, wurden in dieser Arbeit verschiedene Probekörpergeometrien und auch Testmethoden untersucht. So wurden Mixed Mode I/III Ermüdungsmessungen mit reiner Mode I Belastung verglichen. Es wurde eine verringerte Lebensdauer durch Mixed Mode I/III

Belastung im Vergleich zu reiner Mode I Last festgestellt. Um die Vorhersagefähigkeit von Lebensdauermodellen zu erhöhen wurde ein äquivalenter Bruchparameter errechnet (equivalent stress intensity parameter ΔK_{eq}), welcher beide Riss Modi (Mode I und Mode III) miteinbezieht. Messeinflüsse wie Reibung und Verschleiß steigerten im Versuch die Prüfkörpertemperatur und konnten auch in einer anschließenden optischen Untersuchung detektiert werden. Zusätzlich wurden quasi-statische Messungen in Mode I und Mode III an dünnwandigen Proben durchgeführt. Durch die Erkenntnisse im Bereich „Mixed Mode“ Risswachstum von unverstärkten Kunststoffen ist es möglich, diese Belastungsart während der Bauteilauslegung zu berücksichtigen und somit die Berechnung von Lebensdauern zu verbessern. Die gefundenen Einflussfaktoren können in Zukunft bei diesen Belastungsfällen von Anfang an berücksichtigt werden. Zusätzlich dienen die gefundenen experimentellen Ansätze als Startpunkt für weitere Untersuchungen im Mode II Bereich.

Abstract

The proper characterization of occurring fracture mechanisms in polymers, the design of sufficient testing methods, and its theoretical aspects are gaining more and more in importance. However, there are still less investigated areas of research within polymer fracture mechanics, such as elastic plastic fracture mechanics (EPFM) and mixed mode fracture of bulk polymers. In order to increase the knowledge in these areas, a detailed scientific study was conducted in the present work.

In the past, a lot of effort was put into the assessment of testing procedures in the area of EPFM, in order to characterize ductile polymers with large plastic deformations. However, with the procedures available for polymers it can still be challenging to evaluate reproducible fracture parameters. Therefore, several testing methods of EPFM were applied in combination with scatter reduction procedures in this thesis to evaluate the fracture behaviour of polymers. Additionally, the evaluation of size-independent fracture parameters was evaluated by the application of a testing scheme developed by the European Structural Integrity Society (ESIS TC 4). The determined fracture initiation parameters showed size dependent values, whereby, the calculated crack growth resistance curve (J-R curve) displayed one overlapping curve without any sign of size dependency. Furthermore, the crack initiation parameters were correlated with occurring fracture processes for the different specimen sizes. In the future, the conducted measurements on different specimen sizes can be used in combination with numerical simulations for component design with more complex geometries.

In the case of mixed mode loading, several specimen configurations and testing procedures were developed within this study to characterize bulk polymeric materials. Mixed mode I/III fatigue fracture tests were conducted and compared to pure mode I fatigue results. A significant life-time reduction was observed for mixed mode I/III loaded samples in comparison to pure mode I loading. The results led to the development of an equivalent stress intensity

factor range ΔK_{eq} , which takes both loading cases into account. The introduction of ΔK_{eq} is especially beneficial, to assess different mixed mode problems using one fracture mechanical parameter. During mixed mode loading the crack flanks can stay close, which may result in wear abrasion and friction. This was also detected in the current work, by an increasing surface temperature during the mode I/III fatigue tests. For the investigation of quasi-static mixed mode conditions, measurements of pure mode I and pure mode III were conducted on thin-walled specimens. The obtained results of this study can be used to improve life-time estimation of mixed mode loaded applications. Additionally, the observed experimental test approaches can act as starting point for further measurements of mode II loaded cracks.

Symbols

| Designation | Unit | Description |
|-------------------|----------------------|--|
| a | [mm] | Crack length |
| a_0 | [mm] | Initial crack length |
| A_{el} | [J] | Elastic part of the area under the load displacement curve |
| A_{pl} | [J] | Plastic part of the area under the load displacement curve |
| B | [mm] | Specimen thickness |
| b | [mm] | Remaining ligament length |
| C_0 | [mm/N] | Initial elastic compliance |
| dJ_R/da | [kJ/m ³] | Slope of the J-R curve |
| da/dN | [mm/-] | Crack growth rate |
| E | [MPa] | Young's Modulus |
| G | [J/m ²] | Energy release rate |
| $G(b/W)$ | [-] | Geometry function |
| $H(u_{pl}/W)$ | [N] | Material deformation function |
| <i>J-Integral</i> | [kJ/m ²] | J-Integral |
| J_{tip} | [kJ/m ²] | J-Integral close to the crack tip |
| J_{far} | [kJ/m ²] | J-Integral far from the crack tip |
| J_{IC} | [kJ/m ²] | Initiation toughness value |
| $J_{I,lim}$ | [kJ/m ²] | Initiation toughness value |

Symbols

| | | |
|------------------|------------------------|--|
| $J_{0.2}$ | [kJ/m ²] | J-Integral at 0.2 mm crack advancement |
| J_{bl} | [kJ/m ²] | Intersection of J-R curve with the blunting line |
| K | [MPam ^{0.5}] | Stress intensity factor |
| ΔK | [MPam ^{0.5}] | Stress intensity factor range |
| ΔK_I | [MPam ^{0.5}] | Stress intensity factor range in mode I |
| ΔK_{II} | [MPam ^{0.5}] | Stress intensity factor range in mode II |
| ΔK_{III} | [MPam ^{0.5}] | Stress intensity factor range in mode III |
| ΔK_{eq} | [MPam ^{0.5}] | Equivalent stress intensity factor range |
| K_{IC} | [MPam ^{0.5}] | Critical stress intensity factor in mode I |
| $K_{I,th}$ | [MPam ^{0.5}] | Threshold stress intensity factor in mode I |
| P | [N] | Applied load |
| S_{ij} | [-] | Load separation parameter |
| S_{sb} | [-] | Load separation parameter (blunt notched bN and sharp notched sN specimen) |
| T | [MPa] | Traction vector |
| T_{app} | [-] | Applied tearing modulus |
| T_R | [-] | Tearing modulus |
| u | [mm] | Displacement |
| u_{pl} | [mm] | Plastic displacement |
| W | [mm] | Specimen width |

Symbols

| | | |
|--------------------|---------------------|--|
| w | [J/m ³] | Strain energy density |
| ε_{ij} | [-] | Strain tensor |
| Δa | [mm] | Crack advancement |
| η_{el} | [-] | Geometry dependent factor (elastic part) |
| η_{pl} | [-] | Geometry dependent factor (plastic part) |
| μ | [N/m ²] | Shear modulus |
| σ_{ij} | [MPa] | Stress tensor |
| σ_y | [MPa] | Yield stress |

Contents

| | |
|--|-----------|
| Outline and summary | 1 |
| 1. Motivation and background | 2 |
| 2. Structure of the thesis | 5 |
| 3. Elastic plastic fracture mechanics | 9 |
| 3.1. The J-Integral – Theory and preconditions..... | 9 |
| 3.2. Evaluation of the J-R curve | 13 |
| 3.3. Evaluation of the J-R curve for polymers | 16 |
| 3.4. Effect of specimen size on the J-R curve evaluation for polymers | 24 |
| 4. Mixed mode fracture of polymers | 27 |
| 4.1. Mixed mode crack growth | 27 |
| 4.2. Mixed mode specimen configurations | 30 |
| 4.3. Fatigue fracture of polymers extended to mixed mode loading | 33 |
| 4.4. Crack path development in mixed mode fatigue crack growth | 38 |
| 5. Summary and Conclusions | 43 |
| 6. Outlook | 47 |
| Appendix | 49 |
| List of additional publications within the framework of this thesis | 50 |
| Conference contributions | 51 |
| Supervised thesis | 52 |
| References | 53 |

Outline and summary

1. Motivation and background

In recent years, society has put an increased focus on the environmental challenges rooted in using polymer (plastic) goods in all kinds of applications. However, plastics have become indispensable in our everyday life. Starting from easy food packaging to keep our daily meal fresh, to a substantial portion of modern construction materials of our homes, plastics are at the base of many technological advantages. Modern transportation with lightweight bikes and electric cars as well as communication via smartphones would be straight up impossible without polymeric products. Since plastic products are such an integral element in our modern life, significant efforts have to be made to reduce their ecological impact across the entire life cycle. One has to start with improving the production of polymers from fossil fuels, and reducing its contribution to overall CO₂ emission further, even though the manufacturing footprint of polymers is small compared to other materials such as glass or steel [1]. On the other hand, end-of life options and recycling opportunities have to be explored [2,3]. Thus, impact of plastics through their lifecycle has to be understood, new sustainable plastics have to be developed, a closed loop recycling is recommended, and it is necessary to understand and control plastic degradation [3].

However, one additional approach to reduce the environmental impact of plastic products is to design in a way that ensures longevity and easy recovery at the end-of-life. Therefore, the design and production of more complex long-life structural components is mandatory. Simultaneously, safety without catastrophic failure during application has to be guaranteed before product release, which can be especially challenging for complex, optimized structures. In order to meet the requirements for long-life polymer products, it is necessary to consider restrictions arising from the chosen material class accurately and understand the material behaviour and possible failure mechanisms. During the construction and design process of a component, several aspects have to be considered e.g. the mechanical behaviour, the thermal resistances or the influence of aging and media. Based on the

described relationships, the focus of this thesis was put on the fracture mechanical properties of the material.

Fracture mechanical aspects in component design are especially important, even though they are often still not considered precisely. Small defects, plastic deformation or cracks due to the manufacturing process of the chosen material cannot be avoided. Hence, it is necessary to be aware of the likelihood of failures. When dealing with polymers, there are further restrictions for component design arising from the material itself, such as the viscoelastic material behaviour and the change of mechanical properties with temperature, which have to be addressed. Based on the described situation, it is necessary to increase the knowledge of material failure mechanisms, take uncertainties into account, and, as a result, ensure a safe component operation [4,5].

To determine the material resistance against crack growth, several methods and standards are available nowadays. However, the choice of the method is based on considerations on the expected fracture characteristics of a given material [5]. The basic theory of all fracture mechanical approaches is linear elastic fracture mechanics (LEFM). Hence, it is especially important to understand its fundamental assumptions. The stress intensity factor K and the energy release rate G are toughness parameters from LEFM. For both toughness parameters K and G , quantitative relationships were developed for all three loading cases of the crack tip: mode I, mode II and mode III.

The application of fracture mechanics to polymers has gained lots of interest in recent years and increased the knowledge significantly to understand crack propagation in polymeric materials. To name some examples, the Technical Committee 4, "Polymers, Polymer Composites and Adhesives", of the European Structural Integrity Society (ESIS TC4) summarized the fundamental relationships of polymer fracture mechanics in [6]. This elementary work was extended and applied to various types of polymers, e.g. thermoplastic materials, elastomers or fibre reinforced composites [7–14]. The described procedures are an important step towards the design and construction of engineering components made of polymers. However, in order to directly transfer the fracture-parameters from the laboratory to the application further steps are required.

Application of fracture mechanics

For the design of engineering structures, three essential criterions have to be considered:

- i. the applied stress,
- ii. defects in the material and defect sizes and
- iii. fracture toughness of the chosen material.

Fracture parameters can provide information about the resistance against crack initiation or growth and are determined experimentally, as discussed in the following section. The crack driving force is given by the external stress and the size of flaws and defects. Generally, a crack starts to grow when the driving force exceeds the crack growth resistance. Once crack growth has initiated, it is often the origin of complete component failure and break down of the system. Extensive knowledge is already available on applied fracture mechanics in polymers, e.g. for determining the life-time of polymer pipes [13,15–20], or for the evaluation of cylindrical elements made of polymers [21].

However, the aforementioned fracture mechanical tools are accompanied by many restrictions and are not valid for every loading case and every type of polymer. For example, methods based on LEFM are not applicable to polymers showing strong non-linear material behaviour and large plastic deformations. In the described situation, methods from elastic plastic fracture mechanics (EPFM) are required. Furthermore, most of the fracture mechanical experiments are only designed for mode I testing, even though shear crack opening (mode II and mode III) is required for a complete understanding of engineering applications. In three-dimensional components, which contain internal flaws, inhomogeneities, pores or holes, significant amounts of shear forces can be present directly at the crack tip. Based on the described situation, the aim of this thesis is to investigate two specific topics in more detail:

- i. the elastic plastic fracture mechanics, EPFM, of polymers and
- ii. mixed mode loading of polymeric bulk materials.

The following chapters provide an overview of the most important issues regarding these two topics.

2. Structure of the thesis

To increase the knowledge in polymer fracture mechanics, it is essential to extend the available fracture-mechanical methods towards elastic plastic fracture mechanics and mixed mode fracture analysis, as indicated in the introduction. In the next section, a brief description of the research conducted in this work shall be given.

EPFM was already investigated intensively for various types of polymers in the last decades. Thus, a collection of procedures and testing methods is already available. However, appropriate protocols for the evaluation of the crack initiation and crack growth behaviour, reaching acceptable reproducibility and repeatability, are still missing [22]. Therefore, it is important to understand the available procedures, methods, and arising challenges of determining the crack resistance curve (J - R curve). Furthermore, the influence of different specimen sizes and subsequent constraint issues on the fracture response of the material should be investigated.

In the topic of mixed mode fracture mechanics of polymers, many analyses dealing with laminates and fibre composites are documented in literature [23–25]. For bulk polymeric materials comparably little data is available [26,27]. Therefore, it is of great interest to develop adequate specimen geometries and testing methods for bulk polymers within this work.

To enhance the methods and models available in elastic plastic fracture mechanics for polymers, as well as mixed mode fracture, the following key objectives were defined as the goal of this thesis:

EPFM of polymers

- a. Extensive review of EPFM and the used methods and procedures to characterize polymeric materials
- b. Applicability of EPFM to various types of polymers

- i. Characterization of a crack growth resistance curve via different experimental procedures
 - ii. Determination of the fracture behaviour close to the glass transition temperature of three different polypropylene types
 - iii. Screening of data reduction methods to diminish scattering
- c. Examining the influence of specimen size on fracture mechanical parameters
 - i. Influence of specimen size on initiation and crack growth parameters
 - ii. Determination of constraint differences within specimen geometries

Mixed mode fracture of polymers

- a. Extensive review of mixed mode fracture analysis and the used specimen configurations and methods to characterize bulk polymeric materials
- b. Development of adequate specimen geometries for mixed mode I/III **fatigue** testing
 - i. Development of specimen geometries and testing procedures to characterize mode I/III fatigue fracture
 - ii. Fracture mechanical analysis of mixed mode I/III loading
 - iii. Evaluation of an equivalent stress intensity factor for life-time estimation
- c. Understanding the influence of mixed mode fatigue loading on the fracture surface appearance
 - i. Analysis of the influence of friction and abrasion on the resulting fracture surface of mode I/III specimens
 - ii. Determination of mixed mode mechanisms (e.g. factory roof formations)
- d. Validation of mixed mode behaviour of different polymers
- e. Development of adequate specimen geometries for **monotonic** mode III testing

-
- f. Investigation of specimen geometries for monotonic mode I and mode III testing
 - i. Examination of pure monotonic mode I loading of thin walled polymer bulk specimens extended to different fracture parameter
 - ii. Examination of pure monotonic mode III loading of thin walled polymer bulk specimens

Based on the outlined objectives of this work, the following structure was chosen to display the scientific progress and research in the area of polymer fracture mechanics. The thesis is divided into three parts:

- i. Preamble
- ii. Outline and summary
- iii. List of publications

The preamble contains the mandatory sections of the thesis (e.g. abstract) as well as contents such as affidavit, acknowledgement and the table of content.

In the second part, the motivation and some background related topics of this thesis are presented. This leads to the objectives and the definition of the two investigated topics of polymer fracture mechanics within this thesis. The first topic deals with elastic plastic fracture mechanics (EPFM) of polymers and the second topic is focused mixed mode fracture analysis extended to unreinforced polymers. Both parts provide an overview about the most important theoretical aspects and results of the publications, which are marked at the respective place. Furthermore, a summary of the main results is outlined in this section and leads to the conclusions and outlook.

In the last part, a collection of publications, with information on the scientific journals where they are published or intended to be published, is added to illustrate the progress in the area of polymer fracture mechanics:

Publication 1: Comparison of *J-integral* methods for the characterization of tough polypropylene grades close to the glass transition temperature

Publication 2: J-testing of polymers via the load separation criterion based ESIS TC4 procedure: Effect of the specimen size

Publication 3: Size induced constraint effects on crack initiation and propagation parameters in ductile polymers

Publication 4: Mixed Mode I/III fatigue fracture characterization of Polyoxymethylene

Publication 5: Fatigue characterization of polyethylene under mixed mode I/III conditions

Publication 6: Fracture of thin-walled Polyoxymethylene bulk specimens in modes I and III

3. Elastic plastic fracture mechanics

For polymers, LEFM is only applicable under certain restrictions, since polymers tend to non-linearity, highly ductile material behaviour and large amounts of plastic deformation in front of the crack tip. For some types of polymers, it is nearly impossible to characterize the crack growth behaviour with methods based on LEFM. Thus, methods of EPFM have to be utilized to characterise the crack growth behaviour of polymers. An overview of the theoretical background and the state of the art in EPFM of polymers is given in this chapter. Furthermore, a short summary of both, developed methods and findings, are presented.

3.1. The J-Integral – Theory and preconditions

A common parameter in EPFM is the *J-Integral* and the characterization of a crack-resistance curve (*J-R* curve, *J-Integral* depending on the crack advancement Δa) to evaluate non-linear crack growth behaviour of a material [5,10,28–30]. The *J-Integral* was first proposed by Rice [31], and is defined as the difference between the external and the internal work, within an arbitrary area around the notch tip surrounded by a curve (contour Γ) for two dimensional problems (Figure 1), and is given by

$$J = \int_{\Gamma} \left(w \, dy - T \frac{du}{dx} \, ds \right) \quad (1)$$

where w is the strain energy density, T the traction vector, u the displacement vector and ds the length increment along the contour.

The strain energy density w is defined by following relationship

$$w = \int_0^{\varepsilon_{ij}} \sigma_{ij} \, d\varepsilon_{ij} \quad (2)$$

where σ_{ij} is the stress tensor and ε_{ij} the strain tensor.

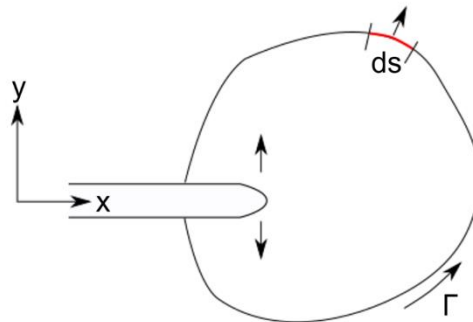


Figure 1. Loaded two-dimensional notch tip surrounded by a contour Γ to calculate the J -Integral, according to [31].

The traction vector is defined as the stress vector at a given point n_{ij} along the contour:

$$T = \sigma_{ij} n_{ij} . \quad (3)$$

The J -Integral summarizes the thermodynamic crack driving force (e.g. the energy released per unit crack extension) and the nonlinear elastic crack tip deformation of the material [31,32].

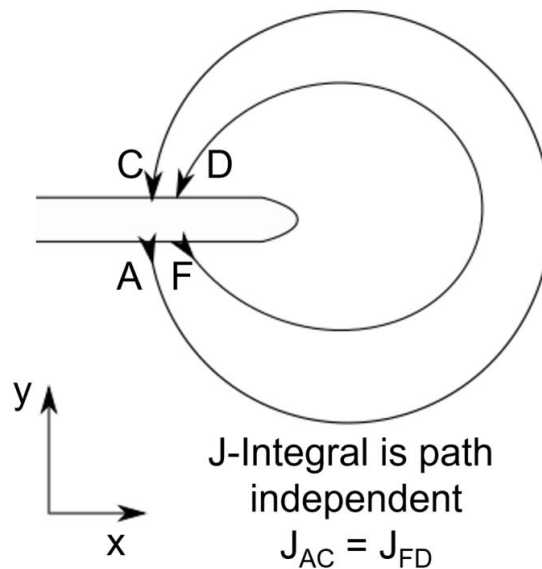


Figure 2. Different contours surrounding a two-dimensional crack tip to prove the path independency of the J -Integral (contour A-C and F-D).

A typical characteristic of the *J-Integral* is its path-independency [31,33]. Hence the integration path (contour Γ in Figure 1) is not important as long as the whole crack tip is included, as shown in Figure 2. In a homogeneous body, the path independency can also be written in terms of

$$J_{tip} = J_{far} \quad (4)$$

where J_{tip} is the *J-Integral* close to the crack tip and J_{far} is the *J-Integral* on a far-field contour. The evaluation of J_{tip} is often hardly feasible in experiments. However, J_{far} can be determined in a straight forward fashion as the total energy release during crack extension in a body [34].

The general assumptions for the application of the *J-Integral* are based on Rice [31], and are only valid by treating elastic plastic deformations as if they were nonlinear elastic (the difference between nonlinear elastic and a nonlinear elastic plastic material is depicted in Figure 3).

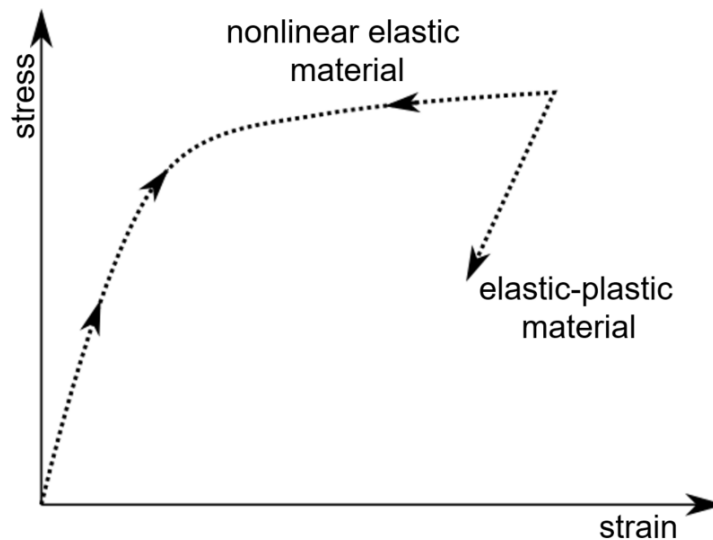


Figure 3. Representative stress-strain curve of a nonlinear elastic material and an elastic-plastic material, according to [5].

The major difference between a nonlinear elastic and an elastic-plastic deformation response is noticeable in the unloading process: a nonlinear elastic material follows the same stress strain curve during loading and unloading, whereas, the elastic-plastic material displays irreversible deformation. Thus, plastic deformation and unloading processes are limiting the applicability of the *J-Integral*. Rice proved the applicability of the *J-Integral* to non-linear material behaviour [31]. Hutchison [35], Rice, and Rosengren [33] showed independently of each other the possibility of using the *J-Integral* to also describe crack tip conditions in a non-linear material. However, as long

as no unloading occurs, elastic plastic material behaviour can also be represented via the *J-Integral* [5].

There are some further restrictions regarding the application of the *J-Integral* [28]:

- i. the deformation in the third direction has to be neglected (minimum specimen thickness in relation to the yield zone),
- ii. the material temperature has to be constant during testing (otherwise the path independency is no longer valid) and
- iii. no kinetic effects may occur.

In order to apply the *J-Integral* as an experimental fracture parameter, several forms were developed and are summarized chronologically in [36]. The *J-Integral* enjoyed great success in the characterization of nonlinear materials, which is discussed extensively in literature [5,28,31,36–38]. Some of the most important steps towards the development of the *J-Integral* as a fracture parameter should be named separately: The first experiments for the characterization of an initiation value (J_{IC}) were published by Begley and Landes [38]. Their early work deals with the application of the *J-Integral* to geometrically similar specimens with different crack lengths. This procedure is strongly restricted, limiting its widespread application. However, it was the starting point for further investigations and testing series in EPFM.

A more general form of the *J-Integral* was proposed by Sumpter and Turner in [39]. This form denotes the *J-Integral* as the sum of an elastic and a plastic part as follows

$$J = J_{el} + J_{pl} = \frac{\eta_{el} A_{el}}{b B} + \frac{\eta_{pl} A_{pl}}{b B} \quad (5)$$

where η_{el} and η_{pl} are the elastic and plastic geometry factors (depending on the notch length over width ratio a/W), A_{el} is the elastic area under the load displacement curve, A_{pl} is the plastic area under the load displacement curve, b is the remaining ligament length ($W-a$) and B the specimen thickness. In general, the evaluation of the elastic part of the *J-Integral*, J_{el} , is straightforward and is defined as (according to LEFM) [36]

$$J_{el} = \frac{K_I^2}{E'} \quad (6)$$

where K_I is the stress intensity factor and $E' = E$, the Young's Modulus of plane stress and of plane strain $E' = E/(1-\nu^2)$. Hence, the evaluation of η_{pl} is central to this *J-Integral* estimation, which is extensively discussed in literature [36]. The most accurate way to characterize the η_{pl} factor is via numerical

simulations. However, the following definitions led to sufficiently accurate results in the full range of crack sizes for SE(B) specimens [36]:

$$\eta_{pl} = \begin{cases} 2, & \frac{a}{W} > 0.282 \\ 0.32 + 12 \left(\frac{a}{W}\right) - 49.5 \left(\frac{a}{W}\right)^2 + 99.8 \left(\frac{a}{W}\right)^3, & \frac{a}{W} \leq 0.282 \end{cases} \quad (7)$$

Splitting the *J-Integral* into an elastic and a plastic part led to the first application of the often used multispecimen method, where several identical specimens are loaded to different amounts of displacement and the resulting crack advancement is measured afterwards by a complete break of the specimen [36,40].

3.2. Evaluation of the J-R curve

The typical failure mechanisms of components made of a tough material (elastic plastic material behaviour) are triggered by exceeding a specific *J-Integral* value. The fracture process can result in a stepwise failure due to crack growth, which is accompanied by large plastic deformations in front of the crack tip [5]. The typical *R-curve* (crack growth resistance curve), where the *J-Integral* increases with increasing crack advancement Δa , is characteristic for the aforementioned material behaviour [41]. The fracture behaviour can no longer be described by a single parameter, since the crack growth parameter varies with the value of Δa . A typical J-R curve (*J-Integral* depending on the crack length Δa) is shown in Figure 4.

At the origin of the *J-R* curve, the material behaviour is governed by the blunting process. Crack tip blunting is a typical deformation mechanism at the beginning of an experiment, where the sharp notch deforms to a round notch due to high stress concentrations close to the crack tip [42,43]. Figure 5 presents an example of the ongoing deformation process during the blunting phase on the fracture surface of a random polypropylene copolymer (PP-R). Directly after the initial notch (marked as the crack tip) the characteristic blunting phase is detected, where polymer fibrils are stretched and deformed in crack growth direction before the crack growth initiates (**publication 1** [44]).

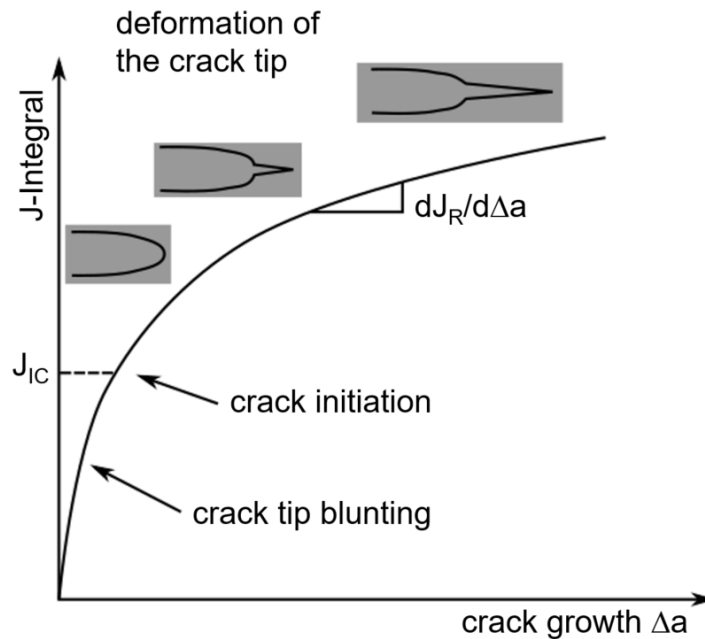


Figure 4. The J-Integral increases with growing crack advancement Δa representing the crack growth resistance curve (J-R-curve) and its typical initial states, the crack tip blunting and the crack initiation according to [5].

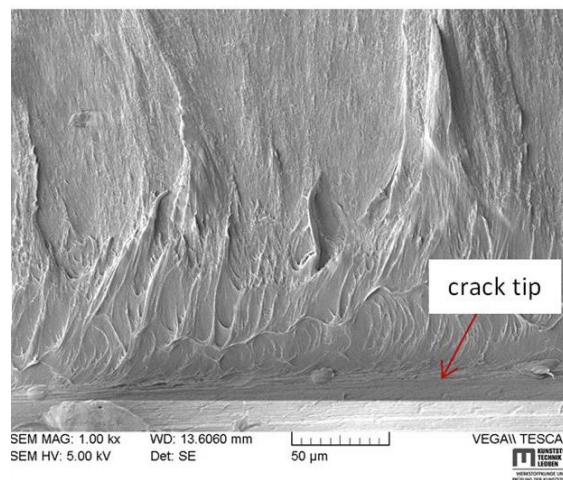


Figure 5. Crack tip blunting on a fracture surface close to the initial notch of a random polypropylene copolymer, adapted from [44].

Depending on the investigated material, the blunting process is often highly challenging to distinguish from actual crack initiation [12]. Theoretically, the end of the blunting phase is marked by a local failure, caused by the first real crack advancement (crack initiation in Figure 4). In practical investigations, the accuracy of crack advancement measurements is limited by the experimental methods available, and as a result, a focus was put on developing

mathematical relationships to evaluate the blunting-to crack growth transition [12]. If all preconditions for the application of the *J-Integral* are met, stable crack growth is visible in strictly monotonously increasing *J-R* plots. Generally, there are several parameters that can be calculated from the *J-R* curve. However, the most common one is the initiation value (J_{IC}).

Initiation toughness parameter

For the determination of a crack growth initiation parameter J_{IC} , based on the *J-R* curve, two methods are available:

- i. the evaluation of the value $J_{0.2}$, which is the *J-Integral* at 0.2 mm crack advancement

This level of crack advancement ensures visible cracks for evaluation, while still providing a viable toughness value.

- ii. the use of the blunting line to determine J_{bl} .

J_{bl} is the intersection of the *J-R* curve with the blunting line, which is defined as

$$J_{bl} = 2 m \sigma_y \Delta a \quad (8)$$

where the plastic constraint factor m is usually assumed to be equal to 1 and σ_y is the uniaxial yield stress determined at a similar speed as the *J-R*-curve [45].

The crack growth initiation value J_{IC} is defined as the lower value of $J_{0.2}$ or J_{bl} [5,12,28,46,47]. An example for the evaluation of J_{IC} from the *J-R* curve is presented in Figure 6, where the crack growth behaviour (*J-R* curve) of polypropylene-block-copolymer (PP-B) is depicted (**publication 1** [44]).

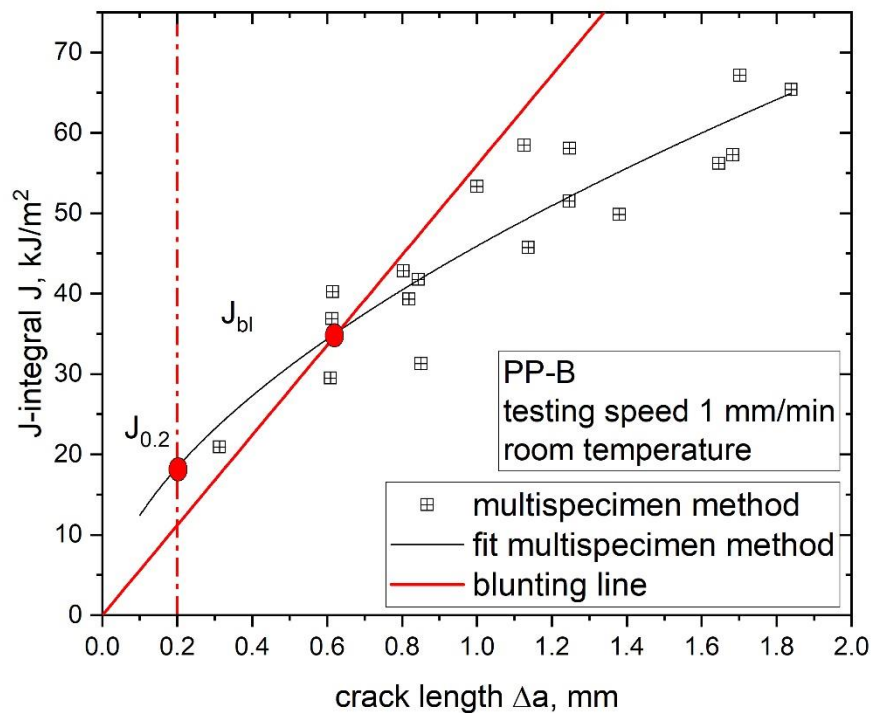


Figure 6. Determination of the crack growth initiation parameter J_{IC} from the J - R curve of a polymer – evaluation of the parameter $J_{0.2}$ at 0.2 mm crack advancement and J_{bl} from the blunting line, adapted from [44].

3.3. Evaluation of the J - R curve for polymers

In the area of EPFM of polymers several forms of J - R curve evaluations are available, causing different forms of experimental procedures to be viable, depending on the investigated conditions (temperature and testing speed) [36,40,48–57]. However, constructing the J - R curve requires the evaluation of the J -Integral as a function of the crack advancement Δa . Here, one of the most common methods is the multispecimen method [5,28,36]. For polymers in particular, there are still some open questions regarding the validity of this method, which require detailed analyses.

Multispecimen method

A testing procedure for the application of the multispecimen method on polymers was developed by the ESIS TC4 [28] and the ASTM [58]. The procedure requests the testing of several identical specimens, up to different amounts of crack advancement Δa . The Δa generated in the experiment is evaluated after the test via an optical analysis after breaking the specimen

apart in an individual procedure. To evaluate the *J-Integral*, the load-displacement plot is required and in combination with Δa , one tested specimen leads to one data point in the crack resistance curve (Figure 7).

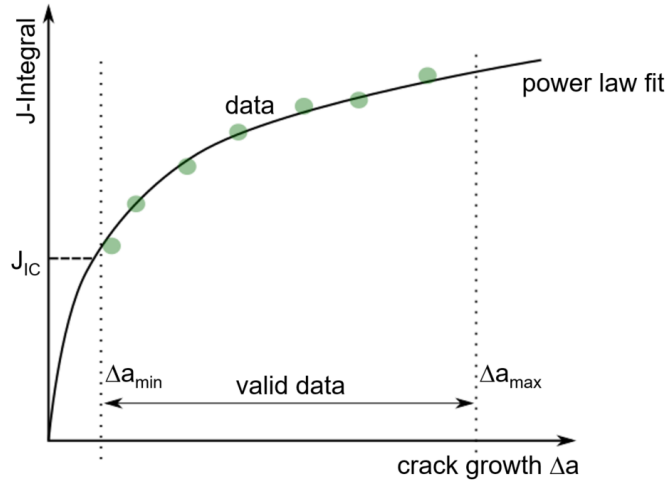


Figure 7. Calculated data points from the multispecimen approach to evaluate the crack resistance curve (*J-R* curve), with the initiation value J_{IC} and the limit points Δa_{min} and Δa_{max} according to [5].

To break a specimen for Δa measurement after testing, several techniques exist, such as cryo-fracturing, impact tests or fatigue cycling of specimens. For polymers, the cryo-fracturing is used most of the time, since it primarily causes brittle fracture. Brittle fracture patterns are especially important because they can be distinguished from the ductile fracture surface more clearly.

Additionally, for a valid *J-R* curve, some restrictions are defined in [28], which lead to a minimum necessary value of Δa_{min} (0.05 mm) and a maximum value of Δa_{max} :

$$\Delta a_{max} = 0.1 (W - a_0) \quad (9)$$

where W is the specimen width and a_0 the initial crack length of the specimen. Furthermore, there are at least 7 data points required within the valid area of Δa for a representative *J-R* curve. Finally, valid data of the crack resistance curve is fitted via a power law fit [28]

$$J = A \Delta a^N \quad (10)$$

where A and N are fitting parameters. When the fitting parameter N is smaller than or equal to 1, the calculated *J-R* curve can be seen as valid. The described multispecimen method has been widely used for the fracture mechanical characterization of polymers [50,59–64].

Challenges concerning the crack length determination of polymers

In the case of polymers, several established methods for the determination of Δa are not applicable. For example, the potential drop method, the partial unloading or heat tinting procedure cannot be used, which makes the characterization of an exact value challenging. Furthermore, the accurate definition of the crack front and crack advancement is influenced by large plastic deformations in front of the crack tip, the used method for breaking the specimen and subjective interpretation by the operator [28]. A representative fracture surface, which can be used to illustrate the difficulties during determination of Δa is shown in Figure 8 (**publication 1** [44]).

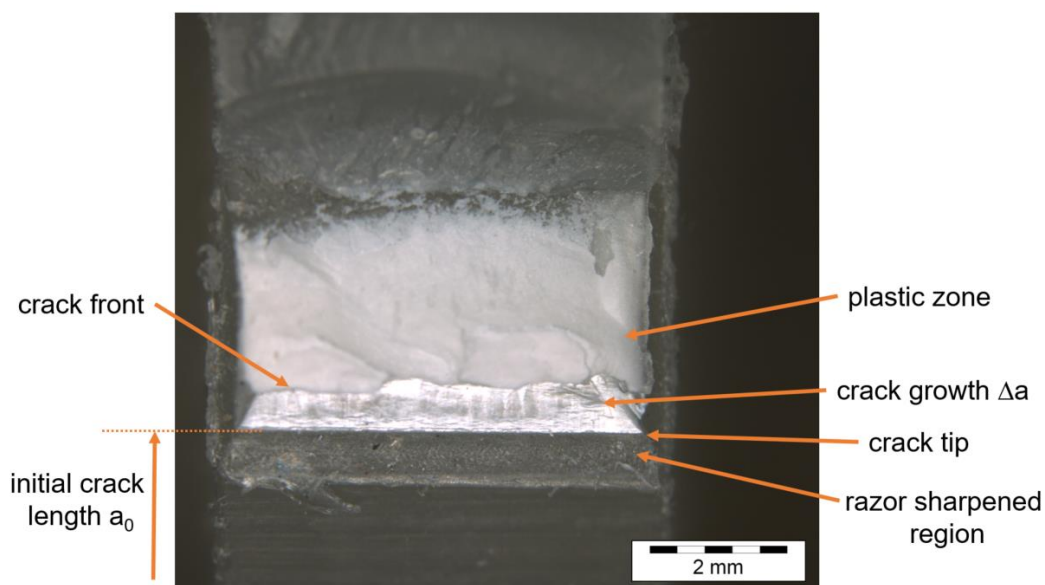


Figure 8. Fracture surface of a tested random polypropylene copolymer specimen showing the notch tip, stable crack propagation and the plastic zone, adapted from [44].

These difficulties make the precise determination of the crack tip and the crack advancement Δa challenging. This is reflected in a high data scattering of the corresponding J - R curve (**publication 1** [44]).

Therefore, two correction procedures for calculating the J - R curves from the multispecimen method were applied to reduce the present data scattering. First, the correction with the Δa – time plot was used, to ensure steady state crack propagation in the tests, which is a precondition for the use of the J -Integral. The second correction procedure was based on the load separation method. This correction procedure excluded data points from the J - R curve obtained by means of the multispecimen method, which either did not fulfil the power law fitting precondition, or showed a strongly deviating curve shape.

Doing so, it was possible to reduce the data scattering and exclude measurements with vastly different fracture behaviour (**publication 1** [44]).

To conclude, the measurement of Δa in polymeric materials is quite complicated and prone to errors. Hence, the development of alternative methods to evaluate the J - R curve of a polymer became an important research area in recent years. An example for alternative methods are the so-called single specimen methods. These methods are convincing because they only require a few specimens and the evaluation of Δa on the fracture surface is no longer necessary. One of these approaches, the load separation method, will be described in detail in the next section.

Single specimen methods

Beside the multispecimen procedure, there are some single specimen methods, which gained more and more interest in recent years for the characterization of ductile polymers [10,12,29,46,60,65–71]. Single specimen methods require only two specimens for the evaluation of an entire J - R curve. Many of these methods are connected by the basic assumption of load-separability, which acts as a precondition for a specific form of the J - $Integral$ [72]. The load-separability assumes that the load for the same material, geometry and constraint can be written as a product of two independent functions in the plastic region [73,74]

$$P = G\left(\frac{b}{W}\right) H\left(\frac{u_{pl}}{W}\right) \quad (11)$$

where $G(b/W)$ is the geometry function, $H(u_{pl}/W)$ is the material deformation function, b the ligament length, W the specimen width and u_{pl} the plastic displacement. The plastic displacement is calculated from the applied displacement u

$$u_{pl} = u - P C_0 \quad (12)$$

where P is the applied load and C_0 the initial elastic compliance of the load displacement curve. Based on the load separation property, two testing methods were developed for polymers: The load separation and the normalization method. However, both single specimen methods are currently still under development and need further detailed investigation for a successful application to characterize the fracture behaviour of polymers.

Originally the load separation method was intended for the evaluation of the geometry factor η_{pl} [72]. Afterwards the method was extended to growing crack experiments and to evaluate an initiation toughness value without the need of

constructing the whole J - R curve [10,22,46,60,69,75–77]. Generally, the load separation parameter S_{ij} is defined as

$$S_{ij} = \frac{P(b_i)}{P(b_j)} \Big|_{u_{pl}} \quad (13)$$

where P represents the applied load on a specimen with the ligament length b . By substituting the load, the parameter S_{ij} can be written as:

$$S_{ij} = \frac{G\left(\frac{b_i}{W}\right) H\left(\frac{u_{pl}}{W}\right)}{G\left(\frac{b_j}{W}\right) H\left(\frac{u_{pl}}{W}\right)} \Big|_{u_{pl}} = \frac{G\left(\frac{b_i}{W}\right)}{G\left(\frac{b_j}{W}\right)} \Big|_{u_{pl}} \quad (14)$$

For stationary crack experiments (testing of a blunt notched (bN) specimen with a round notch tip) the geometry function $G(b/W)$ is constant. Hence, also the parameter S_{ij} takes a constant value, which can be used to evaluate η_{pl} and verify the load separation principle. The load separation parameter is also defined in a way that enables the characterization of growing cracks. Therefore, the parameter S_{sb} can be estimated from the applied load of a sharp notched (sN) specimen P_s and a bN specimen P_b :

$$S_{sb} = \frac{P_s}{P_b} \Big|_{u_{pl}} \quad (15)$$

The parameter S_{sb} represents the crack growth behaviour in the sN specimen in comparison to a stationary crack experiment of the bN specimen. Therefore, the S_{sb} parameter is no longer constant over the whole testing range. When the crack starts to propagate in the sN specimen, the parameter S_{sb} will decrease with increasing u_{pl} , as shown in Figure 9).

The development of crack growth parameters directly from the S_{sb} -curve is of great interest. An example was proposed by the ESIS TC4, which developed a testing approach for the characterization of two additional fracture parameters from the S_{sb} -curve [22]. The usability of the proposed procedure was shown in a recent round robin study [66]. The two additional parameters, the initiation toughness value $J_{I,lim}$ and the parameter m_s , should be used to strengthen the results from the multispecimen method. The $J_{I,lim}$ value can be determined from the load displacement curve of a sN specimen with the help of the S_{sb} -curve. The point of fracture initiation is evaluated after the maximum of the S_{sb} -curve, at $0.995 \cdot S_{sb,max}$ (marked in Figure 10). The parameter m_s is marked in the last region of the normalized load separation curve. A representative normalized load separation plot is shown in Figure 10 (**publication 2** [78]).

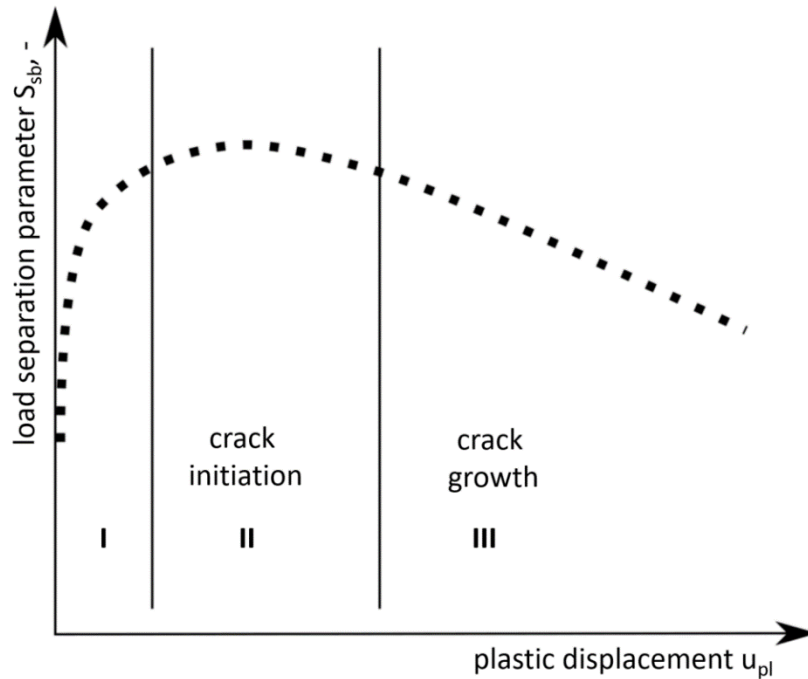


Figure 9. Load separation curve representing the crack initiation process and crack growth, adapted from [44].

Influence of specimen constraint

Another advantage of the load-separation principle is the possibility to use it in the form of the material key curve to evaluate the constraint in a specimen. Thickness variations within a specimen or a component can influence the constraint levels (triaxiality in front of the crack tip), and subsequently the fracture behaviour [5,79,80]. Thus, the characterization of constraint states and variations is of great importance.

The constraint information in a component can be represented by a calibration function. A common way to obtain a calibration function is by evaluating the material key curve derived from the load separation principle (as shown in Ref. [80]). The evaluation of the material key curve is based on the geometry function, $H(u_{pl}/W)$, evaluated as:

$$H\left(\frac{u_{pl}}{W}\right) = \frac{P}{G\left(\frac{a}{W}\right)} = \frac{P}{\left(1 - \frac{a}{W}\right)^2} \quad (16)$$

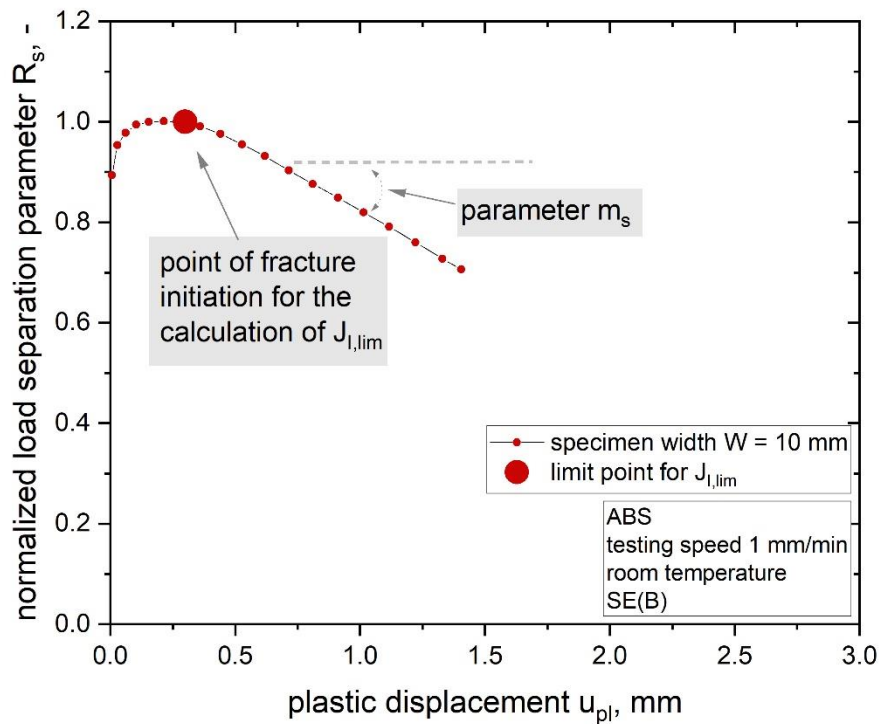


Figure 10. Normalized load separation curve for the calculation of the initiation toughness value $J_{I,lim}$ and the parameter m_s according to [22] (adapted from [78]).

The normalized load, P_N , can be evaluated as follows:

$$P_N = \frac{P}{B W \left(1 - \frac{a}{W}\right)^2} \quad (17)$$

The material key curve (normalized load, P_N depending on the ratio of plastic displacement over width, u_{pl}/W) provides information about changes in the constraint in front of the crack tip. An example for a material key curve evaluated from stationary crack experiments on bN specimens with varying specimen width W ($W = 5$ to 50 mm see Figure 11) is presented in Figure 12 (**publication 3**).

Changing constraint levels in the crack initiation phase were found for the smallest (W is 5 mm) and the largest (W is 50 mm) specimen size of ABS. However, all investigated specimen sizes in between (W ranges from 10 to 40 mm) displayed a similar constraint for the crack initiation and the crack growth phase (**publication 3**).

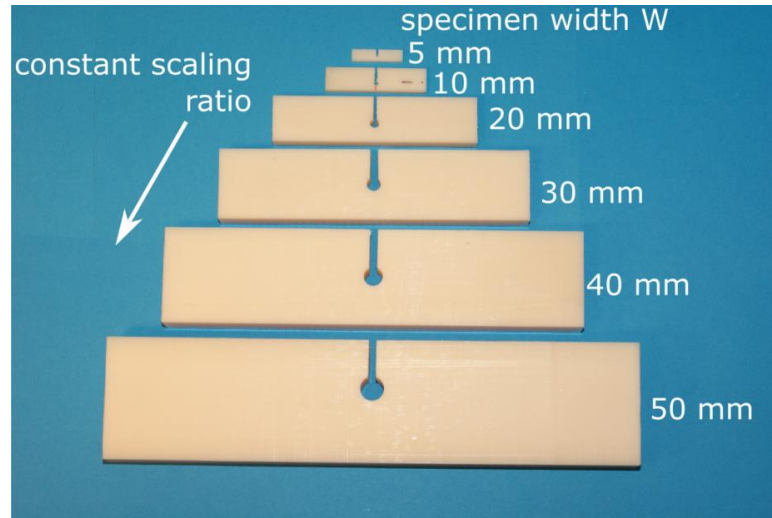


Figure 11. Up-scaled blunt notched single edge notched in bending specimens showing the constant up-scaling ratio, adapted from [78].

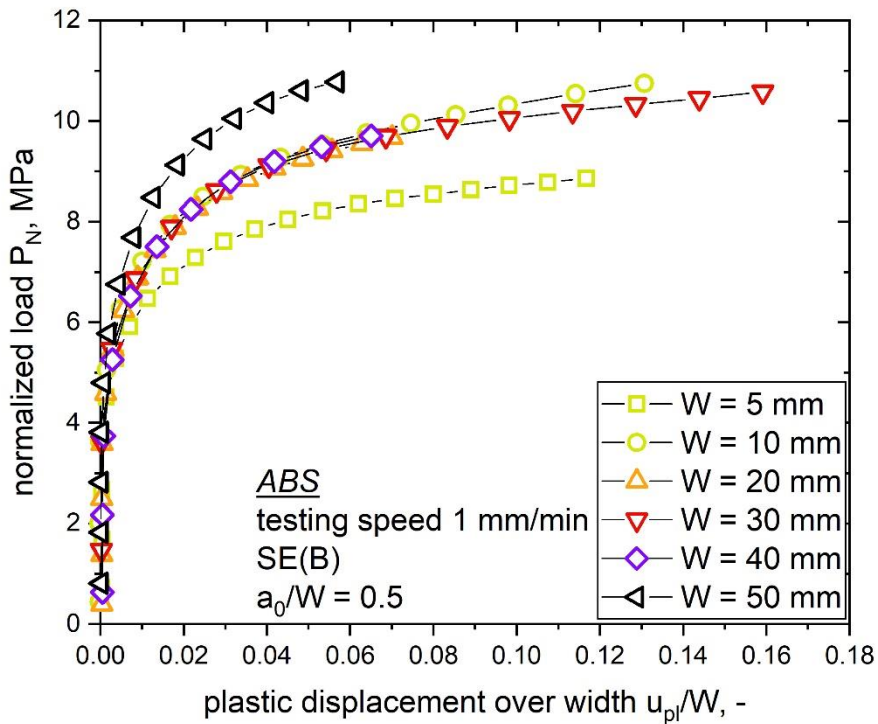


Figure 12. Material key curves obtained for acrylonitrile-butadiene-styrene copolymer with up-scaled specimen sizes in order to evaluate constraint differences, adapted from publication 3.

3.4. Effect of specimen size on the J-R curve evaluation for polymers

To characterize the effect of specimen size on the fracture behaviour, single edge notched in bending SE(B) specimens with a maximum up-scaling ratio of 10 (Figure 11) were analysed in **publication 3**. For this scale-up, specimens with a width W ranging from 5 to 50 mm were investigated in detail. The crack growth behaviour of varying specimen sizes was determined via the multispecimen procedure and a combined J-R curve is shown in Figure 13.

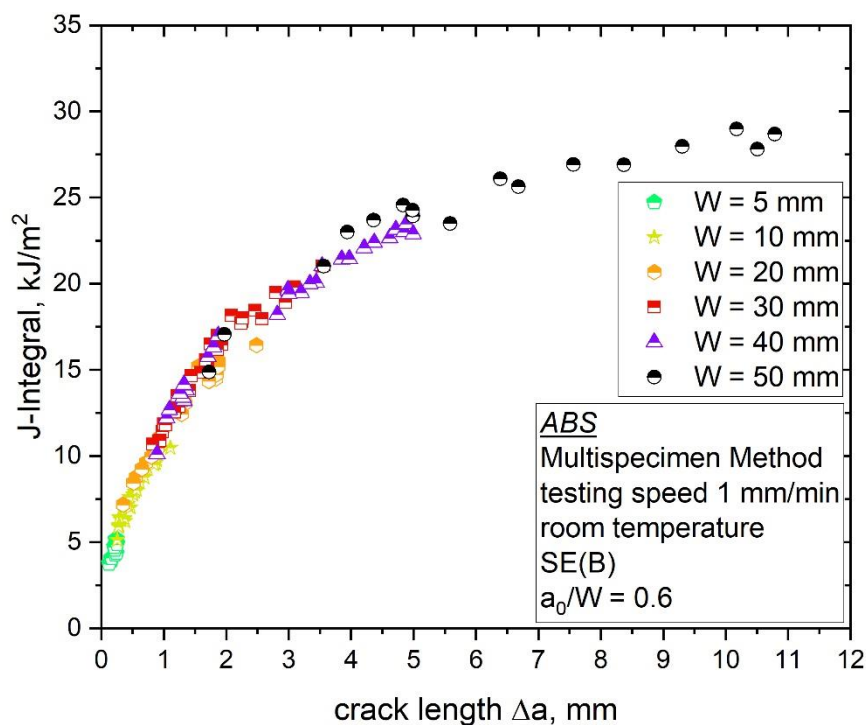


Figure 13. Combined J-R curve obtained for acrylonitrile-butadiene-styrene copolymer with examined specimen sizes (specimen width W from 5 to 50 mm), adapted from publication 3.

The resulting J-R curve obtained for ABS shows one overlapping curve for all tested specimen sizes. However, for the smallest and the largest specimen size some changes in the fitted J-R curves were detected, which support the results of changing constraint levels for these two specimen sizes. Nevertheless, a size independent crack resistance curve could be confirmed for specimen sizes ranging from W is 10 to 40 mm (**publication 2** [78] and **publication 3**).

Furthermore, four representative crack initiation parameters were characterized:

- $J_{0.2}$ (apparent), which is based on the technological evaluation of the J-R curve [28], displayed slowly increasing initiation values for specimens with W is 10 to 40 mm
- J_{bl} (apparent), which is also based on the evaluation of the J-R curve [28], displayed the lowest initiation values and a similar behaviour as $J_{0.2}$
- J_{ini} , which is based on the initiation time t_{ini} as discussed in [48], displayed increasing crack initiation values with increasing specimen size, where small deviations were detected for changing constraint states
- $J_{l,lim}$, which is based on the ESIS TC4 LS method [22], displayed similar results as J_{ini} and supports the size-dependent fracture initiation behaviour (initiation parameters increase with increasing specimen size)

A comparison of all crack initiation parameters investigated is shown in Figure 14 (**publication 3**).

$J_{0.2}$ and J_{bl} have to be seen as apparent values, since the experimental data points at low amounts of Δa were limited. Especially for larger specimen sizes J_{bl} and $J_{0.2}$ displayed a similar trend with slightly increasing initiation toughness values, which can be partly related to missing Δa -values at very low levels. However, J_{bl} showed the lowest fracture initiation values and is therefore the representative initiation toughness value according to the multispecimen procedure [28]. The calculated J_{ini} and $J_{l,lim}$ values grow continuously with increasing specimen size. The contrary behaviour of these two parameters, compared to the former two, give rise to the assumption that these parameters mark two different stages during the fracture process. $J_{0.2}$ and J_{bl} are marking crack initiation, whereby the other two parameters, J_{ini} and $J_{l,lim}$, are representing the onset of stable crack growth. In the case of increasing specimen sizes these two events during a fracture process (crack initiation and onset of stable crack growth) are not necessarily at the same time, which is also shown in Figure 14. This is supported by the principle nature of crack initiation, which is typically a continuous process starting with crack tip blunting until a complete crack front is developed over the whole specimen thickness [12].

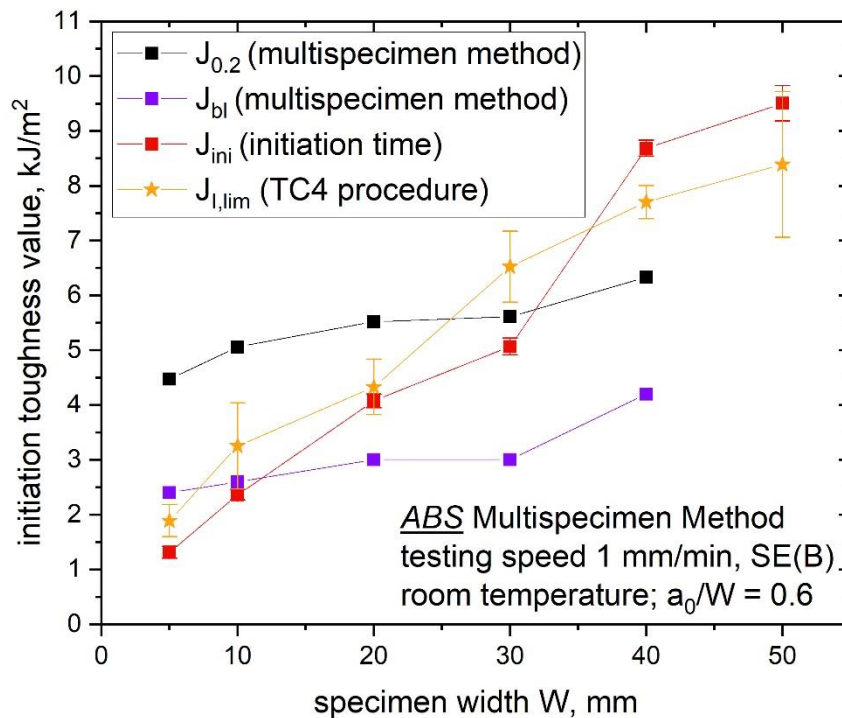


Figure 14. Comparison of initiation toughness parameters $J_{0.2}$ (multispecimen procedure), J_{bl} (multispecimen procedure), J_{ini} (based on the initiation time t_{ini}) and $J_{l,lim}$ (ESIS TC 4 draft protocol) for increasing specimen sizes, adapted from publication 3.

The results of the investigations suggest the use of the initiation parameters based on the multispecimen procedure ($J_{0.2}$ and J_{bl}) for material ranking and comparison, whereby, the parameters representing stable crack growth (J_{ini} and $J_{l,lim}$) are necessary for evaluation of geometry aspects and to mark the event of a fully developed crack front. Further details about the influence of the specimen size on the fracture parameters of polymers are given in **publication 2** [78] and in **publication 3**.

4. Mixed mode fracture of polymers

Polymer fracture mechanics is a powerful tool to investigate failure mechanisms and damage of structural components and technical applications. Besides the basic information for engineering components such as material strength and stiffness, mode I fatigue fracture experiments have become more and more central in avoiding component failure. However, during actual application, mixed mode loading can occur and should be included in calculations of various engineering components, such as rolling bearing elements [21], gears [81], torsionally stressed shafts for transport vehicles [82] and rolls with grooves [83].

4.1. Mixed mode crack growth

Mixed mode loading is a combined loading of crack opening forces in tensile (mode I) and shear loading (in plane - mode II and out of plane - mode III), as shown in Figure 15.

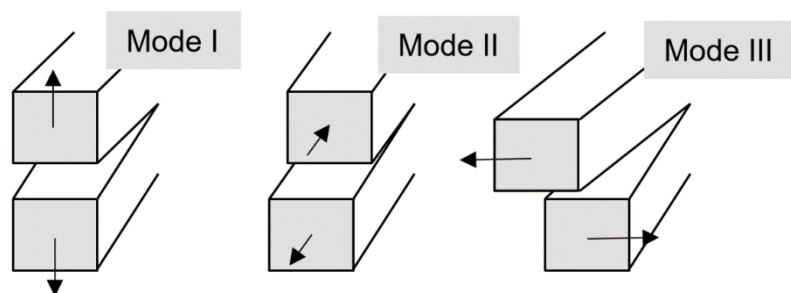


Figure 15. Loading modes of the crack tip according to [5].

While a useful amount of research is available for laminates [24,25,84], it is not possible to apply all found relationships to unreinforced bulk polymers. Additionally, it is necessary to understand the fundamentals of all three loading modes separately, in order to deepen the understanding for the combined mixed mode loading situation.

As a starting point, the basic mixed mode loading relationships according to LEFM are stated. When all three loading modes (mode I, mode II and mode III) are present at the crack tip, the energy release rate G is given by [5]

$$G = \frac{K_I^2}{E'} + \frac{K_{II}^2}{E'} + \frac{K_{III}^2}{2\mu} \quad (18)$$

where K_I , K_{II} and K_{III} are the stress intensity factors in each loading mode, E' the Young's modulus (in plane stress or plane strain state) and μ is the shear modulus. Based on this relationship, it is possible to combine each loading mode present at the crack tip via one representative parameter. However, during mixed mode loading an additional parameter is influencing the fracture behaviour. A crack in a loaded body is always propagating in the path of least resistance and maximum driving force. Hence, the growing crack does not always stay in its initial plane during mixed mode loading, as in the case shown in Figure 16. This change of direction is quantified by the crack growth angle. For example, it is quite common that mixed mode cracks propagate orthogonal to the maximum principal stress (i.e. in mode I loading) [5], as shown in Figure 16. A crack growth deviating from the initial pre-crack plane is also known as a mode I branch [85–87], where a crack tries to change its plane of crack growth to reach pure mode I.

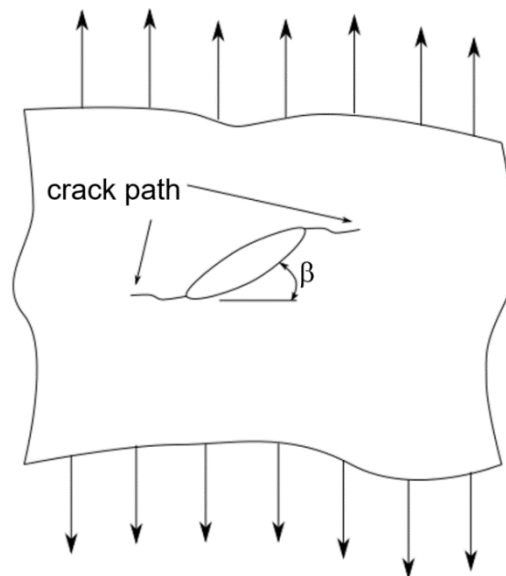


Figure 16. Mixed mode loaded crack propagates orthogonal to the maximum principal stress in mode I, according to [5].

Figure 17 shows the switch from mode II or mode III loading to mode I via the formation of a mode I branch. The mode I branches differ in direction, depending on the actual loading mode (shown in Figure 17 for mode II and

mode III). In mode II, the entire crack tip is changing its direction, whereas in mode III the twist starts only at one point along the crack front. One of the simplest twisting angles in pure mode III is 45° . In this particular loading case the mode III amount decreases to zero and only mode I is acting as the crack driving force [87]. Additionally, the crack path is strongly influenced by the material itself.

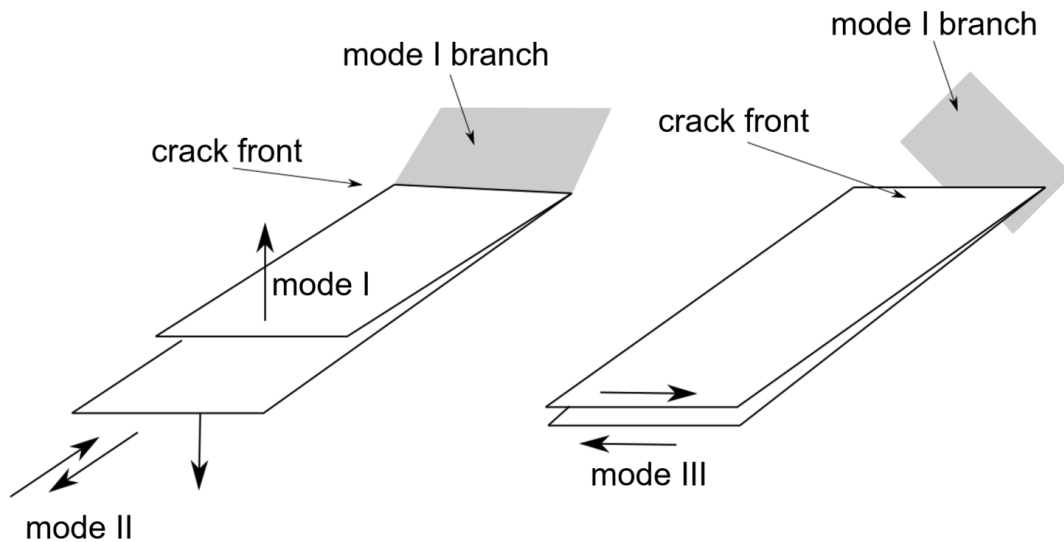


Figure 17. Mode I branches in front of a mixed mode I/II and a mixed mode I/III loaded crack tip, according to [87].

An example for a mode I branch in high density polyethylene is given in Figure 18, where the crack path twisted directly after the initial notch. The observed crack path deflection is typically for mixed mode I/III tested specimens and further details regarding the measurements of such phenomena are given in **publication 5** [88].

As mentioned in this short introduction, there are many aspects, which have to be considered during mixed mode loading. In **publication 4** [89] and **publication 5** [88], mixed mode loading was mainly investigated in fatigue experiments, where in the past a lot of effort has been put into the application of fatigue fracture mechanics to model crack growth in various types of polymers and composites under pure mode I [7,9,16,18,19,25].

Subsequently, the next chapter provides a rough overview of the background, as well as newly found results regarding the fatigue crack growth behaviour in polymers extended to shear mode-loading.

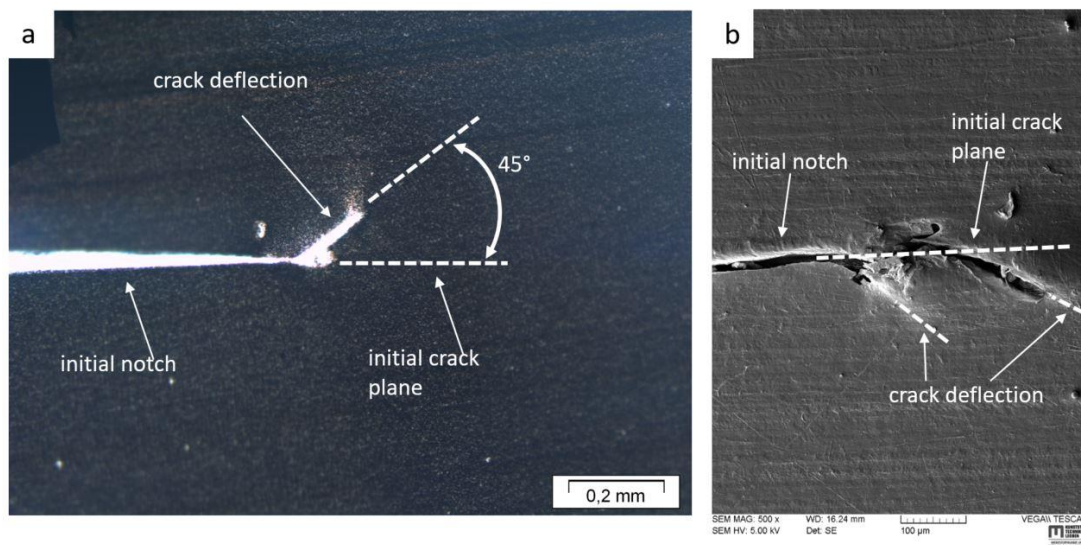


Figure 18. Twisted crack path during a mixed mode I/III experiment – both specimens are analysed via crack freezing experiments and a light microscope is used in (a) and a scanning electron microscope in (b), adapted from [88].

4.2. Mixed mode specimen configurations

Various types of mixed mode specimen configurations were used to test the behaviour of bulk materials in the past, as illustrated in Figure 19 [85,90]. The least complex experiment type is the plate specimen in tension with an initially inclined crack or an inclined edge crack (Figure 19-a and -b). Another specimen configuration is shown in Figure 19-c. Here, a disc specimen with an inclined crack in the centre is loaded in compression. Shear specimens loaded in 3- or 4-point bending configuration were used in early mixed mode experiments and are still used in recent studies to show the influence of friction and abrasion between crack flanks in mode II and mode III [91,92]. Figure 19-e shows a circumferentially notched bar loaded with a torsional load [93–95]. Nowadays more advanced specimen configurations are used like the all fracture mode (AFM) specimen and the newly developed compact tension shear rotation (CTSR) specimen [96,97].

In **publication 4** [89] and **publication 5** [88] mixed mode I/III fatigue behaviour was investigated for two polymers, namely a polyoxymethylene (POM) and polyethylene (PE) via a cracked round bar (CRB) as shown in Figure 20. Previous research, mainly on metals, displayed good results for a comparison of mode I and mode III in one test set-up [98–103]. To determine the pure mode I crack growth characteristics, a tensile fatigue load was applied (Figure 20-a). Mixed mode I/III conditions were achieved by applying both, tensile

(mode I) and torsional fatigue loads (mode III) as shown in Figure 20-b. CRB specimens have the advantage of a uniform mode III loading, without the influence of mode II, due to corner singularities. In contrast, rectangular-shaped specimens always contain corners, which induce a coupling of mode II and mode III [104] (**publication 4** and **publication 5** [88,89]).

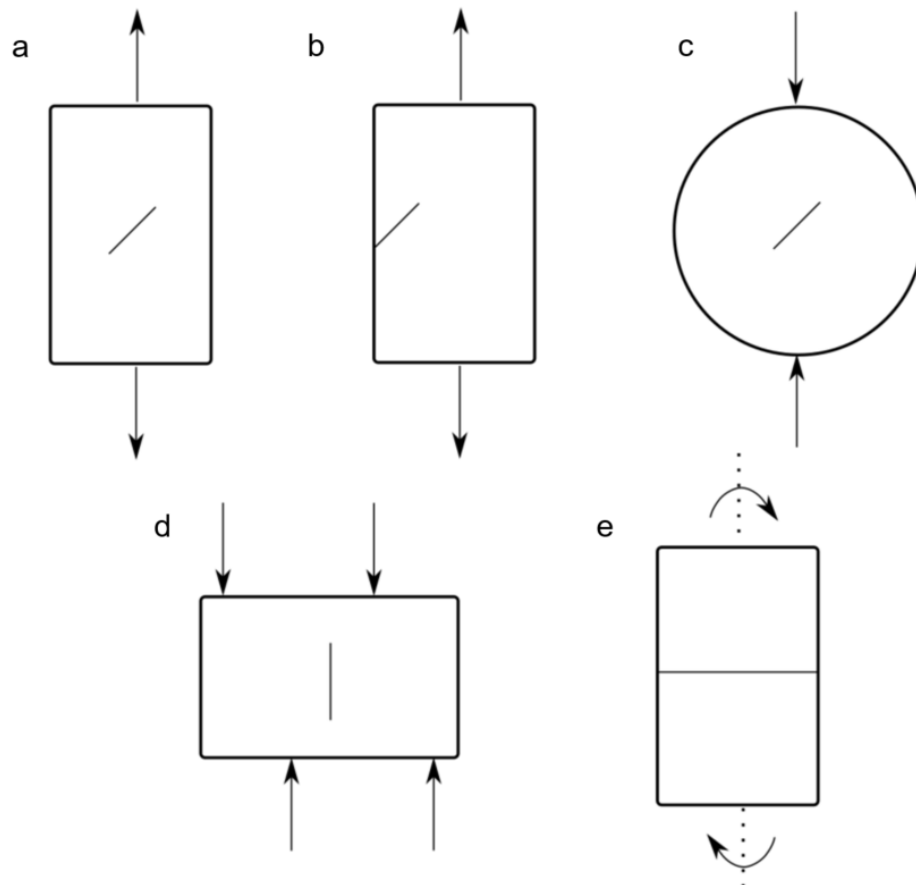


Figure 19. Commonly used specimen geometries in early scientific studies of mixed mode fracture and mixed mode fatigue fracture (a-e), according to [85,90].

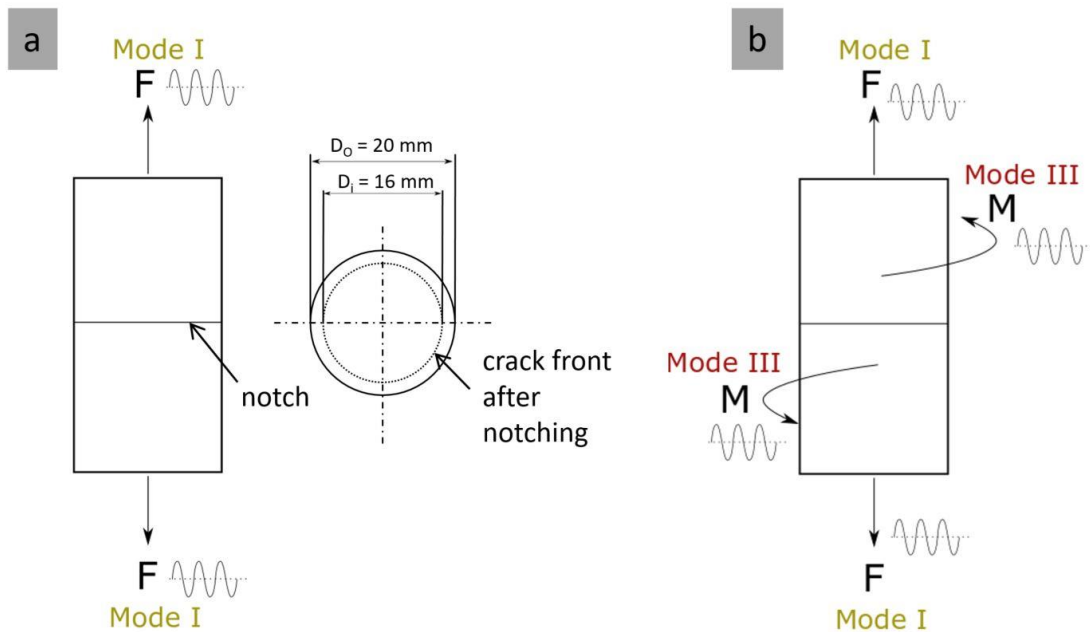


Figure 20. Cracked round bar specimen used to characterize pure mode I (a) and mixed mode I/III (b) fatigue loading in polymers, adapted from [89].

To determine the fracture mechanical properties in pure mode I and III under monotonic loading, two experimental setups based on the double cantilever beam (DCB) and the out-of-plane double cantilever beam (ODCB) have been proposed in **publication 6** [105]. An overview of the used experimental setup is given in Figure 21. To achieve monotonic mode I loading, the DCB specimen is loaded with a tensile force (axial loading). For monotonic mode III loading the ODCB specimen is loaded with a constant angle-rate (torsional loading). The setup (shown in Figure 21) consists of two orthogonal linear sliders below the bottom clamping device to avoid lateral forces. Both presented testing setups provided good results for the characterization of pure mode I and mode III loading (**publication 6** [105]).

In the present study no results dealing with mode II fracture of polymers are presented, due to the more complex specimen configurations and required experimental set-ups. However, mode II loading of polymers was also investigated within the framework of this thesis, but it is still under investigation and the aim of future works (further details in the outlook).

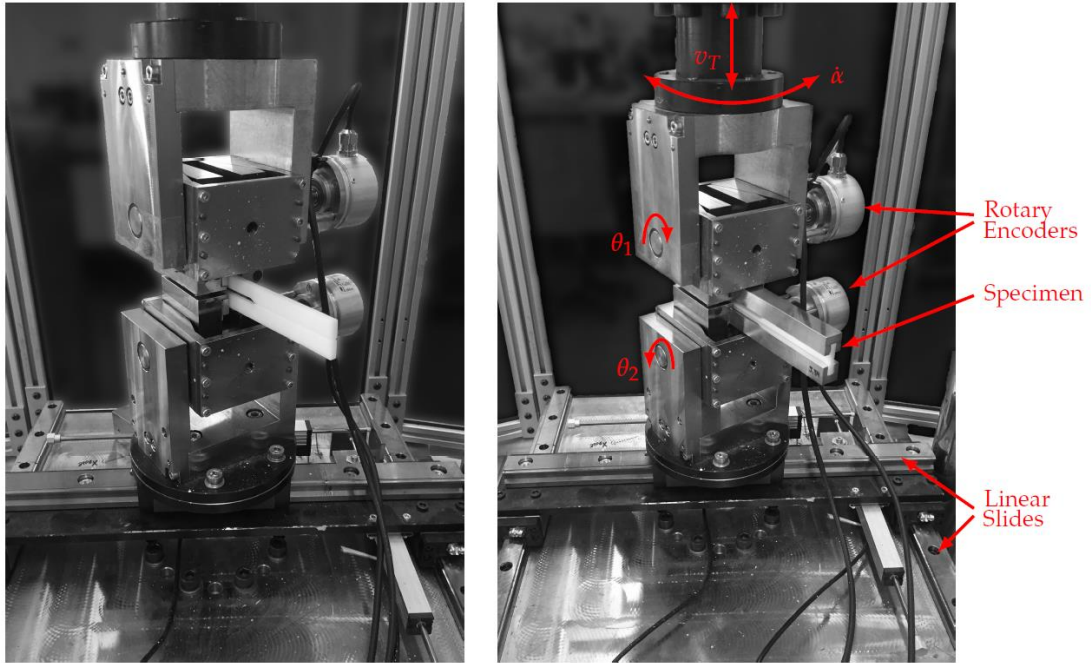


Figure 21. Experimental set-up for pure mode I (double cantilever beam) and mode III (out-of-plane double cantilever beam) fracture mechanical characterization, adapted from [105].

4.3. Fatigue fracture of polymers extended to mixed mode loading

Fatigue testing is, due to the applied cyclic loading, the most critical load case for life-time estimation of a component. Based on the assumption of small scale yielding, as shown in Figure 22, the application of LEFM concepts (e.g. the stress intensity factor concept) is possible to model crack advancement in order to perform lifetime analysis. The stress intensity factor range ΔK for fatigue loading is defined as [104]

$$\Delta K = K_{max} - K_{min} \quad (19)$$

where K_{max} and K_{min} are the stress intensity factors at the maximum and the minimum of the cyclic loading (see Figure 22).

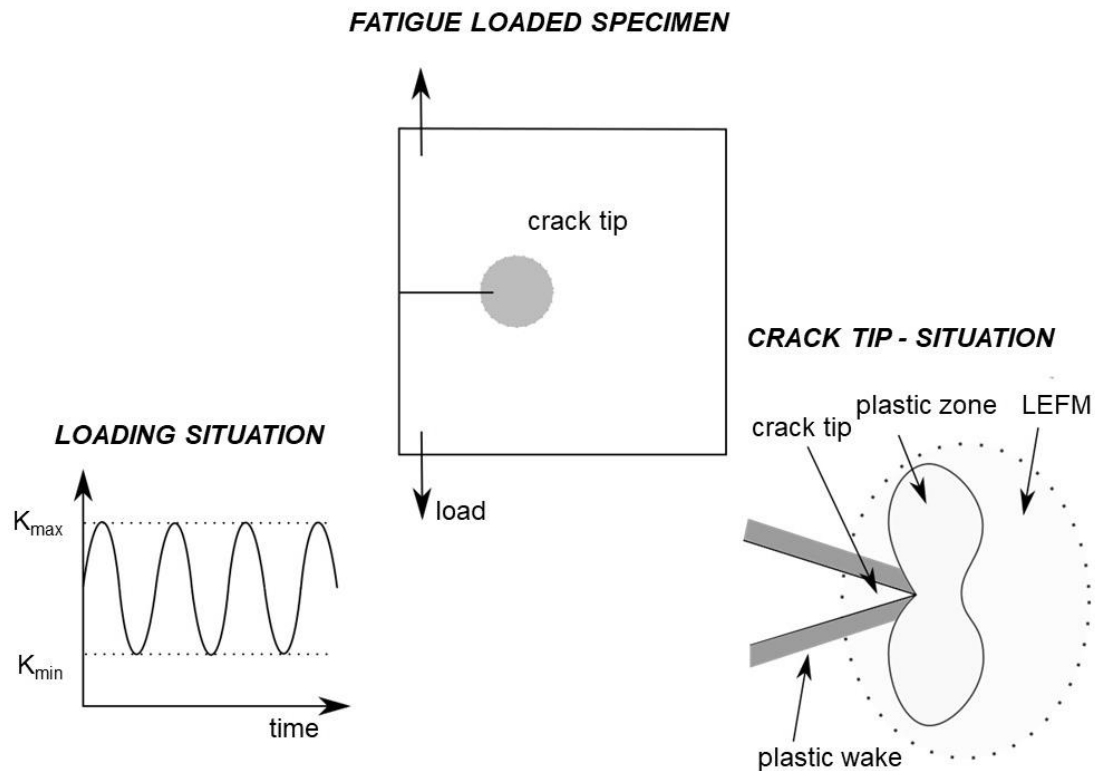


Figure 22. Fatigue loaded specimen (loading situation is defined by K_{max} and K_{min}) where the crack tip situation is defined by small scale yielding (the plastic zone, the plastic wake and the area of LEFM), according to [5].

For polymeric materials, several external and internal effects are influencing the fatigue fracture behaviour such as [106]:

- Testing frequency
- Testing temperature
- Testing environment
- Applied mean stress and load history
- Morphology and molecular properties

An increasing testing frequency can cause localized heating at the crack tip, which can lead to thermally induced changes in the failure behaviour [106]. An example for the influence of an increased surface temperature is shown in Figure 23, where two mixed mode I/III loaded specimens led to different surface temperatures (measured via an IR camera during testing).

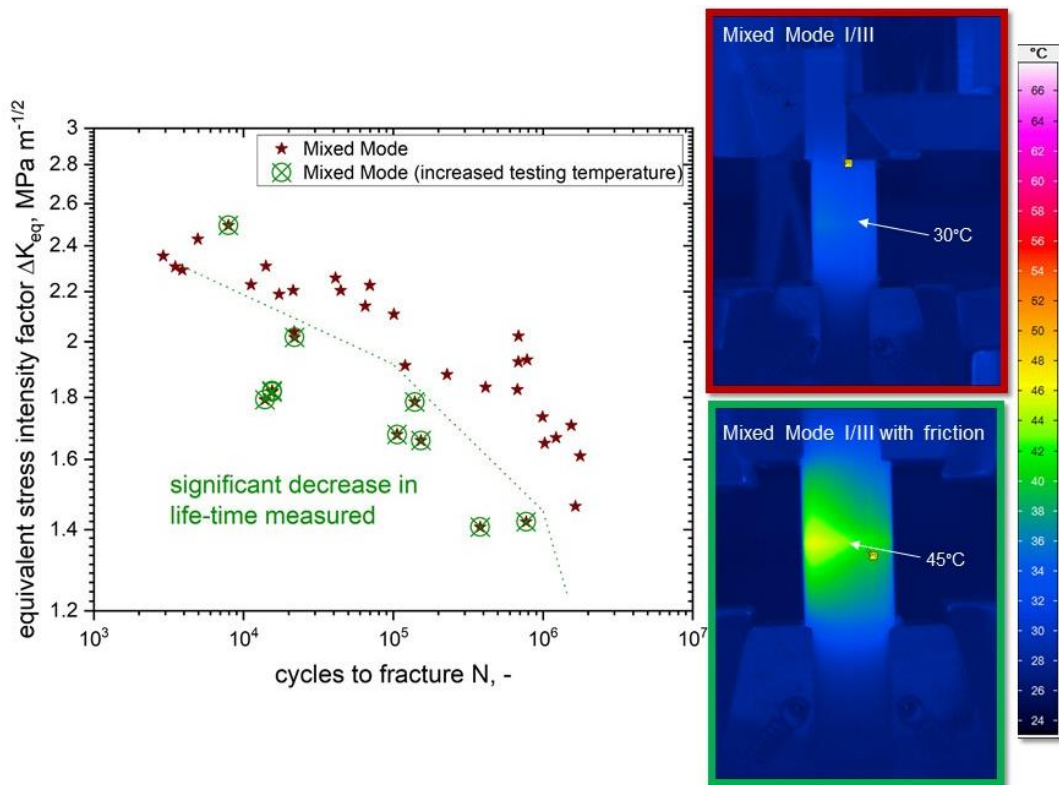


Figure 23. Influence of increased surface temperature during mixed mode I/III loading – increased surface temperature (green image frame) leads to lifetime reduction compared to moderate level of surface temperature (red image frame), adapted from [89].

A significant increase in the measured surface temperature during testing (shown in Figure 23) led to a significant lifetime reduction. At the surface directly next to the crack tip, a temperature of 45°C was measured for the green marked specimen (**publication 4** [89]). An increased specimen surface temperature during testing is especially critical for polymers, since they are highly sensitive to temperature changes, as stated above.

One method to further quantify the crack propagation behaviour of a material is to use a fully logarithmic plot, where the crack growth rate da/dN is shown as a function of the applied ΔK . However, in certain cases it is not possible to measure the crack growth rate during fatigue testing due to the experimental testing set-up or the restrictions arising with the specimen configuration. In this case, it is common to look at the fatigue fracture curve (stress intensity factor range ΔK versus the cycles to failure N_f). This was done to determine the difference between pure mode I and mixed mode I/III fatigue loading conditions on Polyethylene (shown in Figure 24).

By a comparison of applied ΔK_I and corresponding failure cycles N_f , the additional loading in mode III led to a significant decrease in the measured cycles to failure compared to pure mode I fatigue experiments. Via mode III loading a similar slope as for the pure mode I quasi-brittle curve was observed only shifted to a lower life-time with increasing ΔK_{III} (**publication 5** [88]).

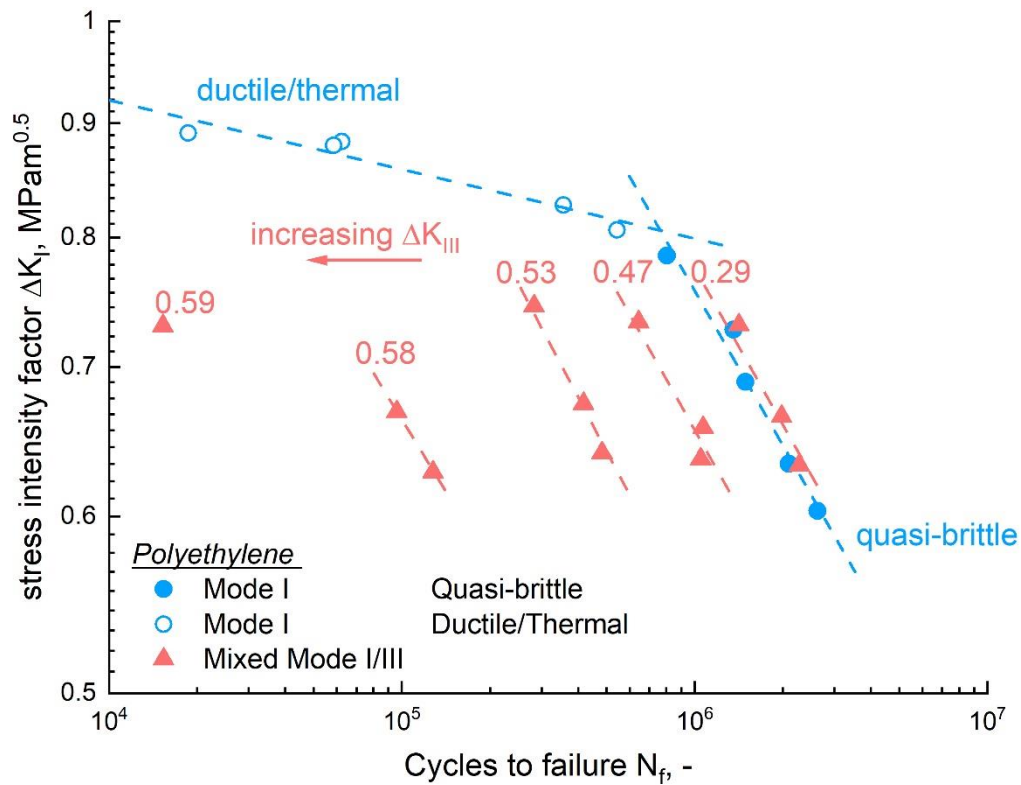


Figure 24. Fatigue fracture behaviour of PE evaluated in pure mode I and mixed mode I/III fatigue testing: an increasing mode III amount (caption of mixed mode I/III data points is the mean value of ΔK_{III}) leads to a decrease in the cycles to fracture, adapted from [88].

For lifetime estimation based on LEFM, it is of high interest to represent both loading cases with a single parameter, which simultaneously takes mode I and mode III loading into account, like the equivalent stress intensity factor range ΔK_{eq} .

The equivalent stress intensity factor (ΔK_{eq}) represents all three loading cases and according to the principle assumptions of LEFM is defined as [5]:

$$\Delta K_{eq} = \sqrt{\Delta K_I^2 + \Delta K_{II}^2 + \frac{1}{1-\nu} \Delta K_{III}^2} \quad (20)$$

Commonly, individual loading cases are not represented in equal parts in application. Thus, various types of equations for ΔK_{eq} have been proposed in literature [90,107,108]. An example of ΔK_{eq} is presented in Figure 25, where following equation was used to describe the mixed mode behaviour of PE:

$$\Delta K_{eq} = \sqrt{\Delta K_I^2 + 0.9 \left(\frac{\Delta K_{III}}{\Delta K_I} \right) \Delta K_{III}^2} \quad (21)$$

In this case the applied ratio of mode III/mode I ($\Delta K_{III}/\Delta K_I$) is considered. Using this formula, data points of both loading cases coincided well as shown in Figure 25.

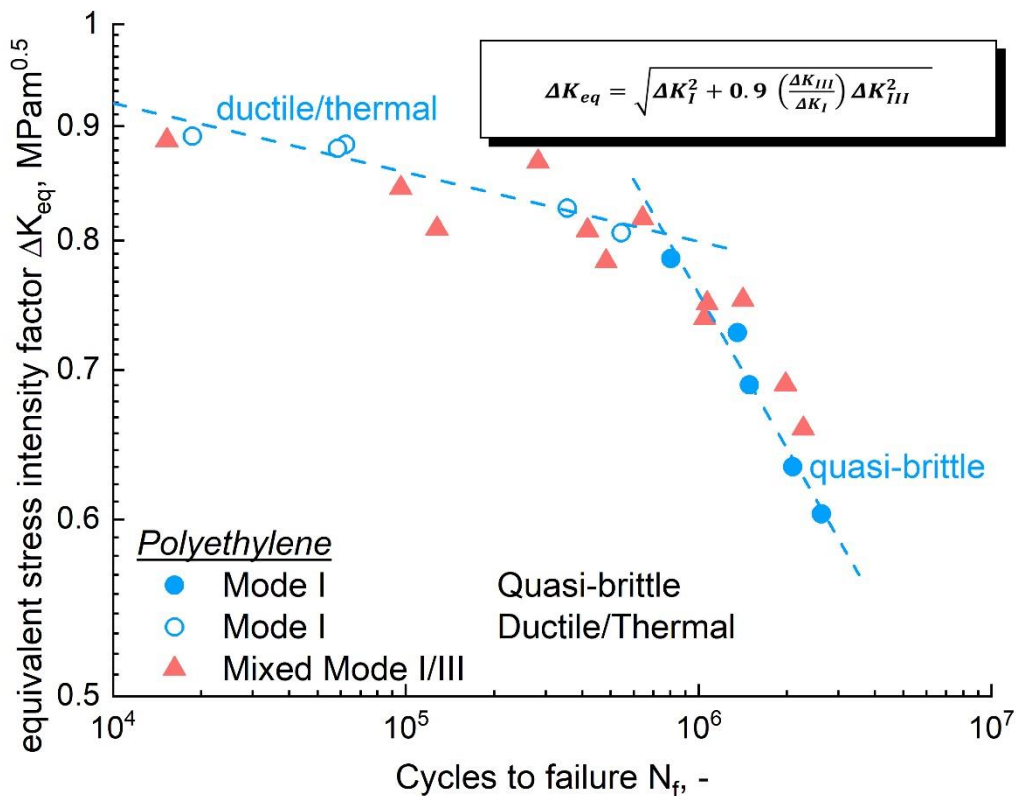


Figure 25. Calculated equivalent stress intensity factor ΔK_{eq} in pure mode I and mixed mode I/III representing the fatigue fracture behaviour of Polyethylene, adapted from [88].

The application of the adapted ΔK_{eq} equation enables the explicit description of the relationship between applied loading and subsequent cycles to failure over the whole testing range. Based on the good correlation of the two loading cases, the proposed equation is expected to be usable for life-time prediction of mixed mode I/III loaded polyethylene components (**publication 5** [88]).

The discussed fundamentals of mixed mode crack growth and fatigue fracture characterization should provide a rough overview for the more complex mixed mode fatigue fracture analysis discussed in the next section.

4.4. Crack path development in mixed mode fatigue crack growth

Mixed mode crack propagation is influenced by two mechanisms: intrinsic and extrinsic mechanisms [85,109]. Crack driving forces and the generation of new fracture surfaces are summarized as intrinsic mechanisms, including fatigue crack propagation. Intrinsic mechanisms are controlled by the applied stress and strain field and the cyclic deformation is controlling the crack growth [110]. Extrinsic mechanisms influence the deformation in front of the crack tip and can act as shielding or anti-shielding effects [110]. Depending on the resulting effect the crack driving force can be reduced or increased during testing by extrinsic mechanisms. This has a significant impact on the resulting crack growth. Hence, it is important to be aware of extrinsic effects during mixed mode testing and to take a close look at ongoing processes close to the crack tip.

Generally, extrinsic mechanisms such as crack deflection, wedging, bridging, sliding or zone shielding are categorized in following groups: geometric, zone and contact shielding or a combination of them, see Figure 26 [109,110]. This area of research is well investigated for metals and some examples are given for extrinsic crack growth effects in [109,110].

As an example, for geometric extrinsic effects, a simple crack deflection can be named. Here, the crack deflects from the initial crack plane due to the specific stress fields in mixed mode loading. An example for crack deflection is shown in Figure 27, where the fracture surface of a mixed mode I/III loaded specimen displayed so called “factory roof” formations. Factory roof formations are mixed mode facet formations occurring directly after the crack initiation phase with a 45° sloping “roof” [93,95,100]. This is the result of cracks, trying to propagate in local mode I by twisting the crack plane, and was found in two different polymers (POM and PE, for more details see **publication 4** and **publication 5** [88,89]). The observed “factory roof formations” were highly sensitive to the applied mode III amount. The influence of increasing mode III loading (increased from 1 to 4) can be observed from Figure 27. With increasing mode III loading the clear factory roof formations disappear and a tangentially deformed texture appears on the fracture surface (**publication 5** [88]).

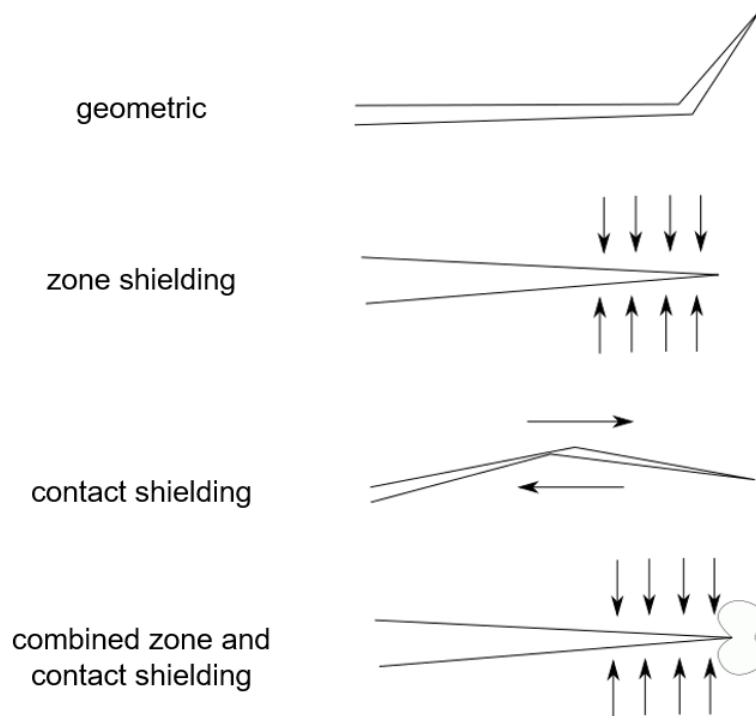


Figure 26. Classes of extrinsic mechanisms during mixed mode loading, according to [109,110].

Zone shielding effects are commonly observed when plastic deformation occurs, or residual stresses are present in front of the crack tip. Contact shielding is always combined with a reduction in the monotonic and cyclic forces acting at the crack tip. One example is, roughness induced crack closure effects, where the friction between the crack flanks influences the crack path direction and the crack propagation [111]. In addition, crack bridging and sliding crack flanks are categorized as contact shielding. Finally, the combination of zone and contact shielding effects can occur, which is also listed in Figure 26. Depending on the present extrinsic effect, the crack driving force, which is a combination of intrinsic and extrinsic effects, can be increased or reduced [109,110].

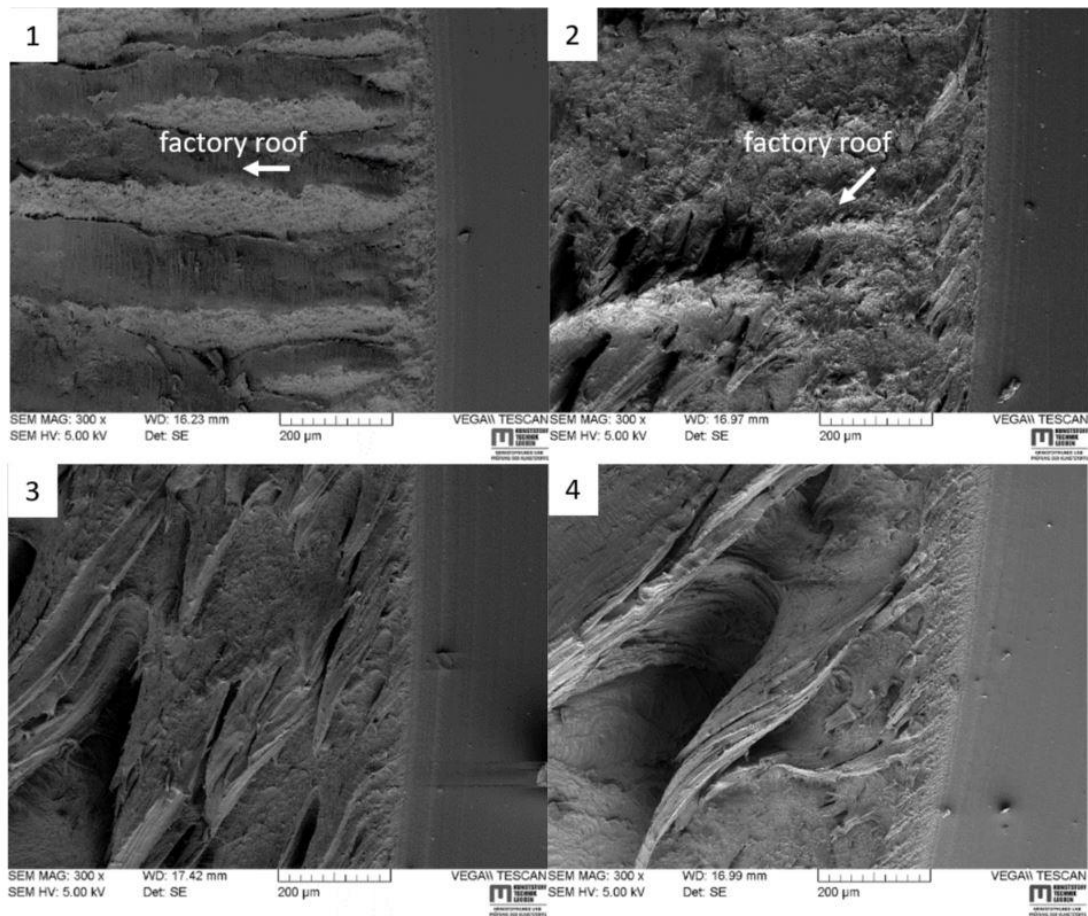


Figure 27. Scanning electron microscopy images of “factory roof” formations on the fracture surface after mixed mode I/III testing – with increasing mode III amount (1 to 4) the formations decrease and change to a more tangential direction, adapted from [88].

Some of the described extrinsic effects were also found in **publication 5** [88]. The simultaneous occurrence of the described effects led to a reduction of the crack driving forces, also in the case of polymers. One example are “factory roof” formations detected on the fracture surface of mode I/III fatigue tests, which led to crack closure effects (see Figure 28 and **publication 5** [88]). Crack closure effects are commonly found in metals [85,99–101,110,111]. The contact between the fracture surfaces hinders the crack propagation and the acting driving force directly on the crack tip is reduced, which can influence the measured cycles to failure.

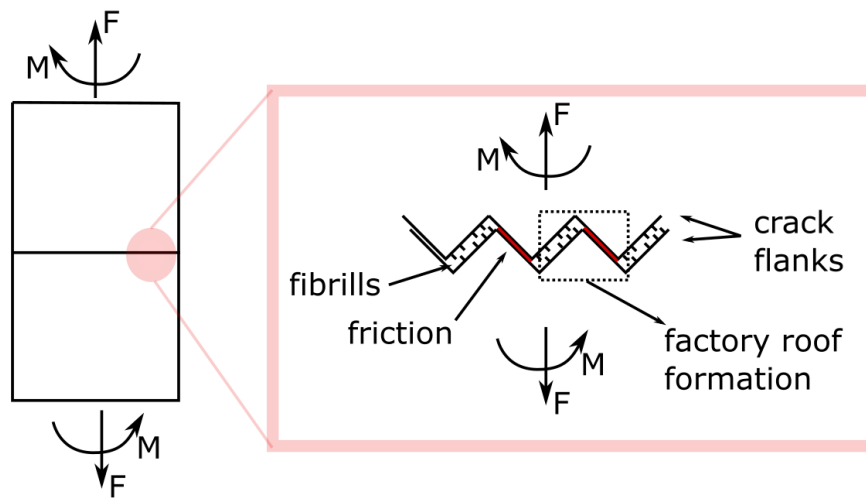


Figure 28. Schematic illustration of crack closure effects arising from “factory roof” formations in mixed mode I/III fatigue testing of polymers, adapted from [88].

In Figure 29, microscope images of different effects influencing mixed mode I/III fatigue fracture of PE are associated with the stress intensity factor level, at which they most commonly occurred. Three zones were identified and marked as: (1) crack closure effect, (2) mixed mode I/III crack growth and (3) thermally induced failure in Figure 29. For mixed mode I/III data points with low amounts of mode III (marked as 1) a slight increase in the measured number of cycles to failure was detected. This increase in life-time can be explained by the crack closure effect, where the driving force for crack growth is reduced due to a closed crack tip. Mixed mode I/III specimens from area (2), appear to be no longer influenced by crack closure effects and display a satisfying correlation with the resulting ΔK_{eq} of pure mode I data points. Finally, the thermally induced failure (marked as 3), which is governed by frictional heating through abrasion between the crack flanks and hysteretic heating, is shown on the left side of the plot (**publication 4** and **publication 5** [88,89]).

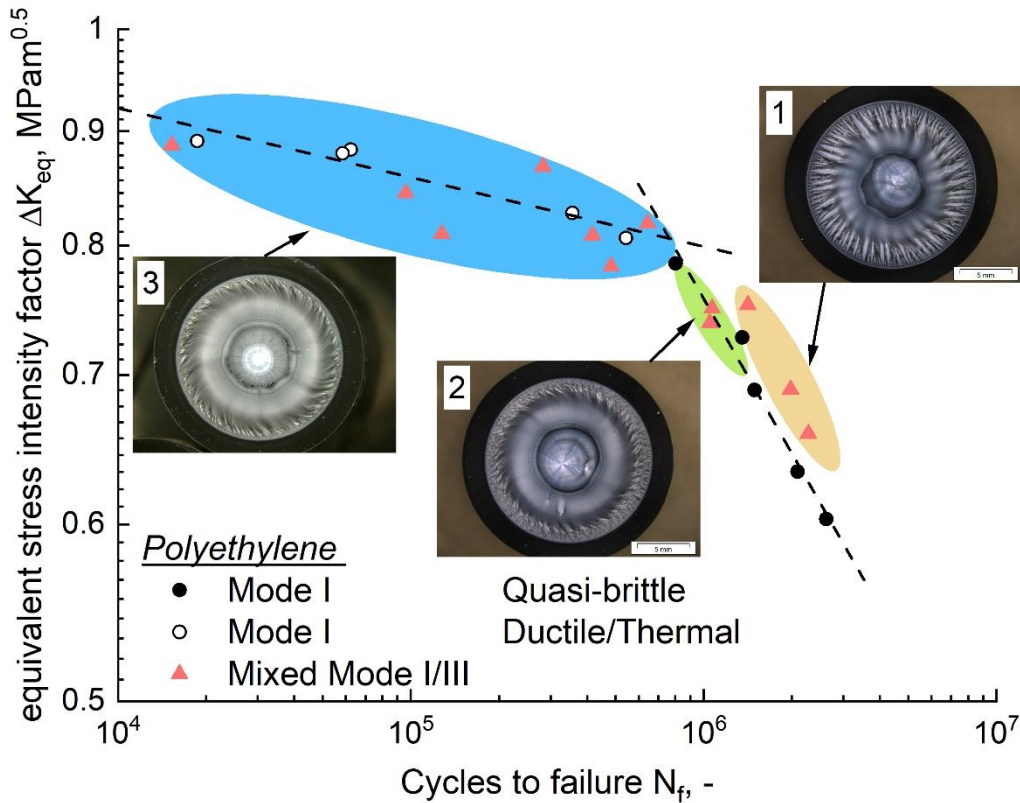


Figure 29. Effects influencing the fatigue fracture behaviour of polyethylene: (1) crack closure effect leads to increased number of cycles to failure, (2) mixed mode I/III fracture and (3) thermally induced failure, adapted from [88].

The acquired knowledge in mixed mode I/III fatigue fracture mechanics could act as foundation for future lifetime prediction. A relationship of the mixed mode fatigue crack growth rate and the applied loading has already been proposed [108]. There, the mixed mode loading is summarized as the equivalent stress intensity factor range ΔK_{eq} . Hence, the Paris relationship [112] is extended by the equivalent stress intensity factor range ΔK_{eq} as following [90]

$$\frac{da}{dN} = A \Delta K_{eq}^m \quad (22)$$

where da/dN is the crack growth rate and A and m are constants depending on the investigated material. The evaluation of the crack growth rate and its relationship with the applied load is a major goal in fatigue fracture characterization and the basic information for life-time prediction.

5. Summary and Conclusions

Fracture mechanical approaches are a powerful tool in the design process of reliable and high-performing products. Theories and methods based on fracture mechanics are nowadays in use to rank new material classes or to model their long-term behaviour. However, when it comes to polymer fracture mechanics, essential aspects are still under investigation. The aim of this thesis was to expand the knowledge in the area of polymer fracture mechanics towards high plastic deformations in front of the crack tip and mixed mode loading applications.

Basic principles of elastic plastic fracture mechanics (EPFM) have already been applied to various types of polymers in literature. However, the available protocols do not provide satisfying results so far. There is also a lack of knowledge and scientific background, when it comes to component design and upscaling of EPFM fracture parameters. To address this issue, EPFM of polymers was adapted towards the reduction of data scattering in the J - R curve and the scaling possibility of fracture parameters (e.g. crack initiation $J_{0.2}$ or blunting value J_{bl}) in the present thesis. For this reason, the available testing procedures for the evaluation of the crack resistance curve (J - R curve, J -*Integral* depending on the crack advancement Δa) - the multispecimen and the load separation method - were compared for three types of polypropylene (PP) in the vicinity of the glass transition in **publication 1**. The used multispecimen method displayed significant data scattering. Especially, the collected Δa -data scattered significantly. The load separation method, a single specimen method requiring only one sharp notched and one blunt notched specimen, also displayed significant data scattering within the resulting J - R curves of the examined PP types. Therefore, several data reduction procedures were examined and showed promising results for the calculation of reliable fracture parameters in **publication 1**: (i) correction with the Δa -time plot, (ii) evaluation of the power-law fit for the load separation curves, (iii) statistical Weibull approach, and (iv) application of the normalized load separation method.

Before the results of laboratory tests can be used for real-life applications, it is necessary to investigate the scaling possibility of the fracture parameters. In **publication 2**, fracture parameters according to an ESIS TC 4 procedure were studied on different specimen sizes (geometrically similar specimens with a scaling ratio of 10) of acrylonitrile-butadiene-styrene copolymer (ABS). Single edge notched bending (SEN(B)) specimens with a specimen width W ranging from 5 to 50 mm were used. An initiation crack growth parameter ($J_{I,lim}$) and a parameter describing the crack advancement (m_s) were evaluated within this study. For both parameters, a specimen size dependency was observed. The initiation value $J_{I,lim}$ increased with increasing specimen size, which was in agreement with the observed plastic zone size in front of the crack tip. For the parameter m_s , which represents the crack advancement per unit of plastic displacement, a decrease with increasing specimen size was perceived. The evaluated specimen size dependency of m_s was expected, since this parameter is a specimen characteristic. In contrast to the found size dependencies for $J_{I,lim}$ and m_s , the separately determined J - R curves of all specimen sizes overlapped without showing any size dependency.

To increase the knowledge of up-scaling fracture parameters, a comprehensive literature study on the influence of constraint (triaxiality in front of the crack tip) was conducted. Based on this review, experimental methods for the evaluation of constraint differences and a detailed study of various approaches for the calculation of initiation toughness and crack growth parameters were compared in **publication 3**. Specimens made from ABS with the same scaling and loading as in the previous study were analysed. For the investigations of constraint differences, two experimental approaches (material key curve and comparison of specimens with and without side-grooves) were carried out. Via the material key curve, differences in the constraint were determined for the smallest and the largest specimen size. The specimen sizes in between (specimen width W from 10 to 40 mm) displayed no influence, which was confirmed by the testing of side-grooved specimens. In the second part of **publication 3**, a geometry independent J - R curve was observed for specimen sizes ranging from W is 10 to 40 mm. Furthermore, the influence of the specimen size on the fracture initiation was investigated. Therefore, four different crack initiation parameters were compared: apparent $J_{0.2}$ (from the J - R curve), apparent J_{bl} (from the J - R curve), J_{ini} (evaluated from the crack propagation kinetics) and $J_{I,lim}$ (based on the ESIS TC 4 procedure). The observed parameter displayed contrary behaviour. While J_{bl} and $J_{0.2}$ are nearly constant, J_{bl} and $J_{I,lim}$ increase with increasing specimen size. This can be explained by the used experimental approach, where parameters based on the J - R curve ($J_{0.2}$ and J_{bl}) are describing the crack initiation, J_{ini} and $J_{I,lim}$ are

correlating with the physical crack initiation and mark the point of stable crack growth.

The second part of this thesis was focused on mixed mode fracture of bulk polymeric materials. Due to the complexity of mixed mode crack growth, the development of adequate specimen configurations and testing procedures was realized prior to testing. In the presented thesis, mixed mode I/III fatigue testing was analysed for various types of unreinforced polymers with the aim of developing possibilities to implement mixed mode behaviour into calculations for crack growth kinetics-based life-time evaluations. As a starting point, in **publication 4**, the mode I/III fatigue loading of polyoxymethylene (POM) was compared to the well investigated pure mode I loading. In comparison to pure mode I loading, the applied mixed mode I/III fatigue load led to a significant life-time reduction due to wear and induced heating between the closed crack flanks. To address the influence of friction and wear abrasion in mixed mode loading, an IR camera was installed to measure the temperature increase close to the crack tip. The concept of an equivalent stress intensity factor ΔK_{eq} was introduced to combine both loading cases into one parameter which can be used for life-time prediction of mixed mode loaded cracks.

The observations of mixed mode loaded POM acted as the starting point for further investigations to gain a deeper understanding of crack growth mechanisms in mixed mode. A well-investigated polymer (polyethylene, PE) with well-known fracture mechanisms was chosen for further analysis under mixed mode I/III fatigue loading in **publication 5**. Similar to the previous study on POM, fatigue fracture curves were calculated in two ways. In the first fatigue fracture plot, the applied mode I depending on the cycles was shown, where a life-time reduction with increasing mode III was observed. In the second fatigue fracture curve, the combined parameter ΔK_{eq} was used to include the influence of mixed mode I/III loading. With this approach, areas with different dominating effects in mixed mode I/III fatigue fracture, such as crack closure, mixed mode crack growth, and thermally induced failure could be distinguished.

Thin-walled polymeric specimens were examined in monotonic mode I and mode III loading in **publication 6**. Two experimental set-ups based on the double cantilever beam (DCB) and out-of-plane double cantilever beam (ODCB) were used to investigate POM specimens. The used methods provide the possibility to evaluate the energy release rate based on the J-Integral for pure mode I and mode III loading. In addition, it was possible to convert the results into stress intensity factors in both loading cases due to quasi-brittle failure of the investigated material. The optical analysis of the fracture surface

confirmed the quasi-brittle failure mechanisms, since no signs of plastic deformation were found close to the initial crack tip. In the case of mode III loading, some twisting and deflection of the crack plane was observed, which is typical for this loading case. During these experiments, pop-in fracture was observed, which can act limiting in various applications.

6. Outlook

The new methods and procedures for fracture mechanical investigations of polymers presented in this thesis increase the knowledge regarding plastic deformation and mixed mode crack growth. However, in both areas of polymer fracture mechanics open questions still have to be addressed.

To make EPFM applicable for component design of polymers, the relationship between crack growth parameters and geometry changes have to be known. In the conducted thesis, a size dependency was found for several different crack initiation parameters of polymers ($J_{0.2}$, $J_{I,lim}$, J_{ini} and $J_{II,lim}$). Even though, the global fracture behaviour (J-R curve) was size independent and displayed one overlapping curve. Further investigations of the changing constraint state for very small and large specimens are planned. With the help of numerical methods, it should also be possible to consider varying specimen geometries and to evaluate geometry independent crack growth parameters for elastic-plastic material behaviour in the future.

Furthermore, the observed results in the area of EPFM are only representative for quasi-static loading conditions and one specific material class. To further increase the knowledge towards real life applications, it is necessary to gain more information about changing testing conditions and the influence of viscoelasticity on fracture parameters from EPFM. Moreover, all investigations were made at room temperature and leads to the necessity of further experiments at different testing temperatures.

Beside the mixed mode specimen configurations discussed in this thesis, a high number of testing set-ups and specimens are available in the area of metals. In the future, these methods and specimen configurations have to be verified for additional polymers and compared to the gained mixed mode I/III data of the present study.

The missing loading case of mode II crack tip opening is necessary to fully understand mixed mode loading in unreinforced bulk polymers. Therefore, reliable specimen configurations and testing procedures have to be developed.

Outlook

This missing loading case can help to complete the calculations based on the equivalent stress intensity factor and to improve life-time estimations. Furthermore, the investigation of fracture mechanisms in mode II loading can lead to a deeper understanding of the influence of friction and wear abrasion during mixed mode loading.

Appendix

List of additional publications within the framework of this thesis

Journal Publication, F.J. Arbeiter, M. Spoerk, J. Wiener, A. Gosch, G. Pinter; *Fracture mechanical characterization and lifetime estimation of near-homogeneous components produced by fused filament fabrication*, Polymer Testing; 66, 2018, 105-113; <https://doi.org/10.1016/j.polymertesting.2018.01.002>

Journal Publication, O. Slavik, P. Hutar, M. Berer, A. Gosch, F.J. Arbeiter, L. Nahlik; *Numerical Modelling of Cylindrical Specimen under Mixed-Mode Loading Conditions*, Key Engineering Materials, Trans Tech Publications; 774, 6, 325-330; doi:10.4028/www.scientific.net/KEM.774.325

Journal Publication, P. Dlhy, J. Poduska, L. Nahlik, M. Berer, A. Gosch, G. Pinter, P. Hutar; *Compression-Loaded Cracked Cylinder - Stress Intensity Factor Evaluation*, Key Engineering Materials, Trans Tech Publications; Key Engineering Materials, Trans Tech Publications; 774, 6, 331-336; doi:10.4028/www.scientific.net/KEM.774.331

Journal Publication, O. Slavik, P. Hutar, A. Gosch, M. Berer, T. Vojtek, F.J. Arbeiter, G. Pinter, L. Nahlik; *Fatigue Crack Propagation under Mixed Mode I and III in Polyoxymethelene Homopolymer*, Trans Tech Publications; Key Engineering Materials, 827, 6, 404-409; doi.org/10.4028/www.scientific.net/KEM.827.404

Journal Publication, A. Gosch, J. Geier, F.J. Arbeiter, M. Berer, G. Pinter; *Methods for automated crack length detection in fracture mechanical fatigue tests of unreinforced polymers*, Structural Integrity Procedia,

Conference contributions

Gosch A., Arbeiter F., Pinter G. (2017), *Experimental methods to characterize the nonlinear elastic plastic fracture behaviour of polymers, as a starting point for multi-layered structures*, Oral presentation, 8th International Conference on fracture of polymers, composites and adhesives (ESIS TC4), Les Diablerets (Switzerland)

A. Gosch, M. Berer, P. Dlhy, P. Hutar, F. Arbeiter, G. Pinter (2018), *Mode III fatigue in technical thermoplastics*, Poster, 17th International conference on Deformation Yield and Fracture of Polymers (TU Eindhoven), Kerkrade (Netherlands)

A. Gosch, F. Arbeiter, M. Berer, J. Wiener, A. Frank, G. Pinter (2018), *Application of J-integral methods to tough pipe materials*, Oral presentation, ANTEC 2018: The Plastics Technology Conference (SPE Society of Plastic Engineers), Orlando (USA)

A. Gosch, F. Arbeiter, M. Berer, G. Pinter (2020), *Methods for automated crack length detection in fatigue tests of unreinforced polymers*, Oral presentation, 1st Virtual European Conference of Fracture (European Structural Integrity Society)

Supervised thesis

Geier J. (2019) *Automated crack growth detection of unreinforced polymers*.
Master thesis, Montanuniversitaet Leoben.

References

- [1] Center for International Environmental Law. Plastic & Climate: The Hidden Costs of a Plastic Planet; Available from: <https://www.ciel.org/wp-content/uploads/2019/05/Plastic-and-Climate-FINAL-2019.pdf>.
- [2] Ellen MacArthur Foundation. The New Plastics Economy: Rethinking the future of plastics; Available from: <https://www.ellenmacarthurfoundation.org/publications/the-new-plastics-economy-rethinking-the-future-of-plastics>.
- [3] Royal Society of Chemistry. Science to enable sustainable plastics; Available from: <https://www.rsc.org/new-perspectives/sustainability/progressive-plastics/>.
- [4] Hertzberg RW, Vinci RP, Hertzberg JL. Deformation and fracture mechanics of engineering materials. 5th ed. Hoboken, NJ: Wiley; 2013.
- [5] Anderson TL. Fracture Mechanics: Fundamentals and Application. CRC Press - Taylor & Francis Group; 2005.
- [6] Blackman B, Davies P, Moore DR, Pavan A, Reed P, Williams JG (eds.). Fracture Mechanics Testing Methods for Polymers, Adhesives and Composites. Kidlington, Oxford; 2001.
- [7] Arbeiter F, Schrittester B, Frank A, Berer M, Pinter G. Cyclic tests on cracked round bars as a quick tool to assess the long term behaviour of thermoplastics and elastomers. *Polym Test* 2015;45:83–92. <https://doi.org/10.1016/j.polymertesting.2015.05.008>.
- [8] Berer M, Pinter G. Determination of crack growth kinetics in non-reinforced semi-crystalline thermoplastics using the linear elastic fracture mechanics (LEFM) approach. *Polym Test* 2013;32:870–9. <https://doi.org/10.1016/j.polymertesting.2013.03.022>.
- [9] Berer M, Pinter G, Feuchter M. Fracture Mechanical Analysis of Two Commercial Polyoxymethylene Homopolymer Resins. *J Appl Polym Sci* 2014;131:1–15. <https://doi.org/10.1002/APP.40831>.
- [10] Frontini PM, Fasce LA, Rueda F. Non linear fracture mechanics of polymers: Load Separation and Normalization methods. *Eng Fract Mech* 2012;79:389–414. <https://doi.org/10.1016/j.engfracmech.2011.11.020>.
- [11] Agnelli S, Balasooriya W, Bignotti F, Schrittester B. On the experimental measurement of fracture toughness in SENT rubber specimens. *Polym*

-
- Test 2020;87:106508.
<https://doi.org/10.1016/j.polymertesting.2020.106508>.
- [12] Baldi F, Agnelli S, Rico T. On the determination of the point of fracture initiation by the load separation criterion in J-testing of ductile polymers. *Polym Test* 2013;32:1326–33.
<https://doi.org/10.1016/j.polymertesting.2013.08.007>.
- [13] Pinter G, Arbeiter F, Berger IJ, Frank A. Correlation of fracture mechanics based lifetime prediction and internal pipe pressure tests. Unpublished; 2014.
- [14] Stelzer S, Brunner AJ, Argüelles A, Murphy N, Pinter G. Mode I delamination fatigue crack growth in unidirectional fiber reinforced composites: Development of a standardized test procedure. *Composites Science and Technology* 2012;72(10):1102–7.
<https://doi.org/10.1016/j.compscitech.2011.11.033>.
- [15] Arbeiter F, Pinter G, Lang RW, Frank A. Fracture Mechanics Methods to Assess the Lifetime of Thermoplastic Pipes. In: Grellmann W, Langer B, editors. *Deformation and Fracture Behaviour of Polymer Materials*. Cham: Springer International Publishing; 2017, p. 33–54.
- [16] Frank A, Pinter G, Lang RW. Fracture Mechanics Lifetime Prediction of PE 80 and PE 100 Pipes under Complex Loading Conditions. Unpublished; 2010.
- [17] Pinter G, Haager M, Balika W, Lang RW. Cyclic crack growth tests with CRB specimens for the evaluation of the long-term performance of PE pipe grades. *Polym Test* 2007;26(2):180–8.
<https://doi.org/10.1016/j.polymertesting.2006.09.010>.
- [18] Andena L, Rink M, Frassine R, Corrieri R. A fracture mechanics approach for the prediction of the failure time of polybutene pipes. *Engineering Fracture Mechanics* 2009;76(18):2666–77.
<https://doi.org/10.1016/j.engfracmech.2009.10.002>.
- [19] Lang RW, Stern A, Doerner G. Applicability and limitations of current lifetime prediction models for thermoplastics pipes under internal pressure. *Angew. Makromol. Chemie* 1997;247(1):131–45.
<https://doi.org/10.1002/apmc.1997.052470109>.
- [20] Parsons M, Stepanov EV, Hiltner A, Baer E. Correlation of stepwise fatigue and creep slow crack growth in high density polyethylene. *Journal of Materials Science* 1999;34(14):3315–26.
<https://doi.org/10.1023/A:1004616728535>.
- [21] Berer M, Mitev I, Pinter G. Finite element study of mode I crack opening effects in compression-loaded cracked cylinders. *Eng Fract Mech* 2017;175:1–14. <https://doi.org/10.1016/j.engfracmech.2017.03.008>.

-
- [22] Agnelli S, Baldi F. A testing protocol for the construction of the load separation parameter curve for plastics. ESIS TC4 communication 2015.
- [23] Jones R, Stelzer S, Brunner AJ. Mode I, II and Mixed Mode I/II delamination growth in composites. *Composite Structures* 2014;110:317–24. <https://doi.org/10.1016/j.compstruct.2013.12.009>.
- [24] Brunner AJ, Stelzer S, Pinter G, Terrasi GP. Mode II fatigue delamination resistance of advanced fiber-reinforced polymer–matrix laminates: Towards the development of a standardized test procedure. *International Journal of Fatigue*, 50, 57-62 2013. <https://doi.org/10.1016/J.IJFATIGUE.2012.02.021>.
- [25] Stelzer S, Pinter G. Fatigue Delamination Growth in CFRP Composites: From Pure Mode I and Mode II to Mixed Mode I/II. *MSF* 2015;825-826:914–21. <https://doi.org/10.4028/www.scientific.net/MSF.825-826.914>.
- [26] R. Lach. *Mixed Mode Fracture Mechanics Behaviour of PMMA*. Weinheim:1–6; 2017.
- [27] Smith DJ, Ayatollahi MR, Pavier MJ. The role of T-stress in brittle fracture for linear elastic materials under mixed-mode loading. *Fatigue Fract Eng Mater Struct* 2001;24:137–50.
- [28] Hale GE, Ramsteiner F (eds.). *J-Fracture toughness of polymers at slow speed*. Oxford, UK: Elsevier; 2001.
- [29] Agnelli S, Baldi F, Castellani L, Pisoni K, Vighi M, Laiarinandrasana L. Study of the plastic deformation behaviour of ductile polymers: Use of the material key curves. *Mechanics of Materials* 2018;117:105–15. <https://doi.org/10.1016/j.mechmat.2017.11.002>.
- [30] Huang DD, Li S, Williams GJ. Materials selection using fracture mechanics. In: Moore DR, editor. *Application of Fracture Mechanics to Polymers, Adhesives and Composites*. Elsevier; 2003, p. 121–127.
- [31] Rice JR. A path independent integral and the approximate analysis of strain concentration by notches and cracks. *J Appl Mech* 1968;35:379–86.
- [32] Rice JR. Mathematical analysis in the mechanics of fracture. *Mathematical Fundamentals* 1968;2:191–311.
- [33] Rice JR, Rosengren GF. Plane strain deformation near a crack tip in a power-law hardening material. *J Mech Phys Solids* 1968;16:1–12.
- [34] Kolednik O. A simple model to explain the geometry dependence of J-Da curves. *Int J Fracture* 1993;63:263–74.
- [35] Hutchinson JW. Singular behaviour at the end of a tensile crack in a hardening material. *J Mech Phys Solids* 1968;16:13–31.

-
- [36] Zhu X-K, Joyce JA. Review of fracture toughness (G, K, J, CTOD, CTOA) testing and standardization. *Eng Fract Mech* 2012;85:1–46. <https://doi.org/10.1016/j.engfracmech.2012.02.001>.
- [37] Ernst H, Paris PC, Rossow M, Hutchinson JW. Analysis of Load-Displacement Relationship to Determine J-R Curve and Tearing Instability Material Properties. *American Society of Testing and Materials*;1979:581–99.
- [38] Begley JA, Landes DL. The J-Integral as a fracture criterion. *National Symposium on Fracture mechanics 1972(Part II, ASTM STP 514)*:1–20.
- [39] Sumpter JDG, Turner CE. Method for Laboratory Determination of. In: Pukui MK, editor. *Cracks and fracture: 9th conference stp 601*. [Place of publication not identified]: Astm; 1976, 3-3-16.
- [40] Grellmann W, Seidler S, Jung K, Kotter I. Crack-Resistance Behavior of Polypropylene Copolymers. *J Appl Polym Sci* 2001;79:2317–25.
- [41] Erdogan F. Fracture mechanics. *International Journal of Solids and Structures* 2000;37(1-2):171–83. [https://doi.org/10.1016/S0020-7683\(99\)00086-4](https://doi.org/10.1016/S0020-7683(99)00086-4).
- [42] Samuel BA, Haque MA. Visualization of crack blunting using secondary fluorescence in soft polymers. *Polym Test* 2008;27:404–11. <https://doi.org/10.1016/j.polymertesting.2007.12.007>.
- [43] Kinloch AJ, Williams JG. Crack blunting mechanisms in polymers. *Journal of Materials Science*, 15(4), 987-996 1980. <https://doi.org/10.1007/BF00552112>.
- [44] Gosch A, Arbeiter FJ, Berer M, Pinter G. Comparison of J-integral methods for the characterization of tough polypropylene grades close to the glass transition temperature. *Eng Fract Mech* 2018. <https://doi.org/10.1016/j.engfracmech.2018.06.002>.
- [45] Lach R, Frontini PM, Grellmann W. On the Plastic Constraint Factor of Polymers. *Macromol. Symp.* 2017;373(1):1600117. <https://doi.org/10.1002/masy.201600117>.
- [46] Baldi F, Agnelli S, Ricco T. On the applicability of the load separation criterion in determining the fracture resistance (J_{Ic}) of ductile polymers at low and high loading rates. *Int J Fracture* 2010;165:105–19. <https://doi.org/10.1007/s10704-010-9510-9>.
- [47] Malito LG, Sov JV, Gludovatz B, Ritchie RO, Pruitt LA. Fracture toughness of ultra-high molecular weight polyethylene: A basis for defining the crack-initiation toughness in polymers. *J Mech Phys Solids* 2019;122:435–49. <https://doi.org/10.1016/j.jmps.2018.09.022>.
- [48] Lach R, Krolopp T, Hutar P, Grellmann W. Influence of the interface and the additional layer on the stable crack propagation through polyolefin

-
- bilayered structures. *Procedia Mater Sci* 2014;3:867–72.
<https://doi.org/10.1016/j.mspro.2014.06.141>.
- [49] Seidler S, Koch T, Kotter I, Grellmann W. CRACK INITIATION BEHAVIOUR OF PP-MATERIALS. San Sebastian: ECF13; 2000.
- [50] Seidler S, Koch T, Kotter I, Grellmann W. Crack Tip Deformation and Toughness in Polypropylenes. Honolulu, Hawaii: ICF10; 2001.
- [51] Lach R, Seidler S, Grellmann W. Resistance Against the Intrinsic Rate of Fracture Mechanics Parameters for Polymeric Materials Under Moderate Impact Loading. *Mech Time-Depend Mater* 2005;9:103–19.
- [52] Cocco RG, Frontini PM, Perez Ipin JE. Threshold toughness of polymers in the ductile to brittle transition region by different approaches. *Eng Fract Mech* 2007;74:1561–78.
<https://doi.org/10.1016/j.engfracmech.2006.09.011>.
- [53] Cocco RG, Frontini PM, Perez Ipin JE. Fracture Toughness of Polymers in the Ductile-to-Brittle Transition Region: Statistical Approach and Lower Bound Determination. *J. Polym Sci Part B Polym Phys* 2005;43:3674–84.
<https://doi.org/10.1002/polb.20600>.
- [54] Džugan J, Viehrig H-W. Application of the normalization method for the determination of J–R curves. *Mater Sci Eng A* 2004;387-389:307–11.
<https://doi.org/10.1016/j.msea.2004.01.067>.
- [55] Fasce L, Pettarin V, Bernal C, Frontini P. Mechanical Evaluation of Propylene Polymers under Static and Dynamic Loading Conditions. *J Appl Polym Sci* 1999;74:2681–93.
- [56] Frontini P, Santarelli E. The Effects of Specimen Size and Testing Conditions on Fracture Toughness Evaluation of Polypropylene Homo polymer. *Polym Eng Sci* 2001;41:1803–14.
- [57] Kolednik O, Schöngrundner R, Fischer FD. A new view on J-integrals in elastic–plastic materials. *Int J Fracture* 2014;187:77–107.
<https://doi.org/10.1007/s10704-013-9920-6>.
- [58] ASTM D6068. Test Method for Determining J-R Curves of Plastic Materials. West Conshohocken, PA: ASTM International.
<https://doi.org/10.1520/D6068-10R18>.
- [59] Bernal CR, Cassanelli AN, Frontini PM. A Simple Method for J-R Curve Determination in ABS Polymers. *Polym Test* 1995;14:85–96.
- [60] Wainstein J, Frontini PM, Cassanelli AN. J-R curve determination using the load separation parameter Spb method for ductile polymers. *Polym Test* 2004;23:591–8.
<https://doi.org/10.1016/j.polymertesting.2003.10.010>.
- [61] Salazar A, Frontini PM, Rodriguez J. Determination of fracture toughness of propylene polymers at different operating temperatures. *Eng Fract*

-
- Mech 2014;126:87–107.
<https://doi.org/10.1016/j.engfracmech.2014.04.023>.
- [62] Fasce LA, Frontini PM, Wong S-C, Mai Y-W. Polypropylene Modified with Elastomeric Metallocene- Catalyzed Polyolefin Blends: Fracture Behavior and Development of Damage Mechanisms. *J. Polym Sci Part B Polym Phys* 2004;42:1075–89.
- [63] Narisawa I. Fracture and toughness of crystalline polymer solids. *Polym Eng Sci* 1987;27(1):41–5. <https://doi.org/10.1002/pen.760270107>.
- [64] Salazar A, Rodriguez J, Martinez AB. The role of notch sharpening on the J-fracture toughness of thermoplastic polymers. *Eng Fract Mech* 2013;101:10–22. <https://doi.org/10.1016/j.engfracmech.2012.07.006>.
- [65] Baldi F, Ricco T. High-rate J-testing of toughened polyamide 6/6: Applicability of the load separation criterion and the normalization method. *Eng Fract Mech* 2005;72:2218–31. <https://doi.org/10.1016/j.engfracmech.2005.02.002>.
- [66] Agnelli S, Baldi F, Blackman BRK, Castellani L, Frontini PM, Laiariandrasana L et al. Application of the load separation criterion in J-testing of ductile polymers: A round-robin testing exercise. *Polym Test* 2015;44:72–81. <https://doi.org/10.1016/j.polymertesting.2015.03.019>.
- [67] Bernal C, Cassanelli A, Frontini P. On the applicability of the load separation criterion to acrylonitrile/butadiene/styrene terpolymer resins. *Polymer* 1996;37:4033–9.
- [68] Bernal CR, Montemartini PE, Frontini PM. The Use of Load Separation Criterion and Normalization Method in Ductile Fracture Characterization of Thermoplastic Polymers. *J. Polym Sci Part B Polym Phys* 1996;34:1869–80.
- [69] Rodriguez C, Maspoch ML, Belzunce FJ. Fracture characterization of ductile polymers through methods based on load separation. *Polym Test* 2009;28:204–8. <https://doi.org/10.1016/j.polymertesting.2008.12.004>.
- [70] Salazar A, Rodriguez J. The use of the load separation parameter Spb method to determine the J–R curves of polypropylenes. *Polym Test* 2008;27:977–84. <https://doi.org/10.1016/j.polymertesting.2008.08.013>.
- [71] Morhain C, Velasco JI. Determination of J-R curve of polypropylene copolymers using the normalization method. *J Mater Sci* 2001, 2001:1487–99.
- [72] Sharobeam MH, Landes JD. The load separation and npl development in precracked specimen test records. *Int J Fracture* 1993;59:213–26.
- [73] Ernst H, Paris PC, Landes JD. Estimations on J-Integral and tearing modulus T from a single specimen test record. *American Society of Testing and Materials* 1981:476–502.

-
- [74] Joyce JA. Fracture toughness evaluation of polytetrafluoroethylene. *Polym Eng Sci* 2003;43(10):1702–14. <https://doi.org/10.1002/pen.10144>.
- [75] Sharobeam MH, Landes JD. The load separation criterion and methodology in ductile fracture mechanics. *Int J Fracture* 1991;47:81–104.
- [76] Cassanelli AN, Cocco R, Vedia LA de. Separability property and η_{pl} factor in ASTM A387-Gr22 steel plate. *Eng Fract Mech* 2003;70(9):1131–42. [https://doi.org/10.1016/S0013-7944\(02\)00095-4](https://doi.org/10.1016/S0013-7944(02)00095-4).
- [77] Salazar A, Rodriguez J, Segovia A, Martinez AB. Influence of the notch sharpening technique on the fracture toughness of bulk ethylene–propylene block copolymers. *Polym Test* 2010;29:49–59. <https://doi.org/10.1016/j.polymertesting.2009.09.004>.
- [78] Gosch A, Arbeiter FJ, Agnelli S, Berer M, Pinter G, Baldi F. J-testing of polymers via the load separation criterion based ESIS TC4 procedure: Effect of the specimen size. *Polym Test* 2020;89:106637. <https://doi.org/10.1016/j.polymertesting.2020.106637>.
- [79] Donoso JR. Common format for developing calibration curves in elastic plastic fracture mechanics. *Eng Fract Mech* 1994;47:619–28.
- [80] Donoso JR, Landes JD. The role of constraint on the calibration functions for the prediction of ductile fracture behavior in structural components. *Int J Fracture* 1993;63:275–85.
- [81] Fajdiga G, Sraml M, Flasker J. Surface Fatigue of Gear Teeth Flanks. In: Gdoutos EE, editor. *Fracture of nano and engineering materials and structures: Proceedings of the 16th European Conference of Fracture*, Alexandroupolis, Greece, July 3-7, 2006. Dordrecht: Springer; 2006, p. 197–198.
- [82] Beretta S, Desimone H, Madia M, Poli A. Multiaxial fatigue and defect assessment of truck stabilisers. *IJVD* 2006;40(1/2/3):212. <https://doi.org/10.1504/IJVD.2006.008462>.
- [83] Domazet Ž, Lukša F, Šušnjar M. Failure analysis of rolls with grooves. *Engineering Failure Analysis* 2007;14(6):1166–74. <https://doi.org/10.1016/j.engfailanal.2006.11.067>.
- [84] Rizov V. Mixed-mode I/II fracture study of polymer composites using Single Edge Notched Bend specimens. *Computational Materials Science* 2013;77:1–6. <https://doi.org/10.1016/j.commatsci.2013.04.021>.
- [85] Pokluda J, Pippan R, Vojtek T, Hohenwarter A. Near-threshold behaviour of shear-mode fatigue cracks in metallic materials. *Fatigue and fracture of engineering materials and structures* 2013;37:232–54. <https://doi.org/10.1111/ffe.12131>.
- [86] Pook LP. *Crack paths*. Southampton: WIT Press; 2002.

-
- [87] Pook LP. Mixed-mode fatigue crack growth thresholds: A personal historical review of work at the National Engineering Laboratory, 1975–1989. *Eng Fract Mech* 2018;187:115–41. <https://doi.org/10.1016/j.engfracmech.2017.10.028>.
- [88] Gosch A, Arbeiter FJ, Berer M, Vojtek T, Hutař P, Pinter G. Fatigue characterization of polyethylene under mixed mode I/III conditions. *International Journal of Fatigue* 2021;145:106084. <https://doi.org/10.1016/j.ijfatigue.2020.106084>.
- [89] Gosch A, Berer M, Hutař P, Slávik O, Vojtek T, Arbeiter FJ et al. Mixed Mode I/III fatigue fracture characterization of Polyoxymethylene. *International Journal of Fatigue* 2020;130:105269. <https://doi.org/10.1016/j.ijfatigue.2019.105269>.
- [90] Qian J, Fatemi A. Mixed mode fatigue crack growth: A literature survey. *Eng Fract Mech* 1996;55:969–90.
- [91] Doquet V, Bui QH, Bertolino G, Merhy E, Alves L. 3D shear-mode fatigue crack growth in maraging steel and Ti-6Al-4V. *Int J Fract* 2010;165(1):61–76. <https://doi.org/10.1007/s10704-010-9504-7>.
- [92] Saboori B, Ayatollahi MR. A novel test configuration designed for investigating mixed mode II/III fracture. *Eng Fract Mech* 2018;197:248–58. <https://doi.org/10.1016/j.engfracmech.2018.04.048>.
- [93] Tschegg EK. Mode III and Mode I fatigue crack propagation behaviour under torsional loading. *J Mater Sci* 1983;18:1604–14.
- [94] Tschegg EK, Ritchie RO, McClintock FA. On the influence of rubbing fracture surfaces on fatigue crack propagation in Mode III. *Int J Fatigue* 1983:29–35.
- [95] Tschegg FK. SLIDING MODE CRACK CLOSURE AND MODE III FATIGUE CRACK GROWTH IN MILD STEEL. *Acta metall* 1983;9:1323–30.
- [96] Richard HA, Eberlein A. Material characteristics at 3D-mixed-mode-loadings. *Procedia Structural Integrity* 2016;2:1821–8. <https://doi.org/10.1016/j.prostr.2016.06.229>.
- [97] Richard HA, Kuna M. Theoretical and experimental study of superimposed fracture modes I, II and III. *Eng Fract Mech* 1990;35(6):949–60. [https://doi.org/10.1016/0013-7944\(90\)90124-Y](https://doi.org/10.1016/0013-7944(90)90124-Y).
- [98] Pokluda J, TRATTNIG G, MARTINSCHITZ C, Pippan R. Straightforward comparison of fatigue crack growth under modes II and III. *Int J Fatigue* 2008;30(8):1498–506. <https://doi.org/10.1016/j.ijfatigue.2007.09.009>.
- [99] Vojtek T, Pippan R, Hohenwarter A, Holan L, Pokluda J. Near-threshold propagation of mode II and mode III fatigue cracks in ferrite and austenite.

-
- Acta Mater 2013;61:4325–635.
<https://doi.org/10.1016/j.actamat.2013.04.033>.
- [100] Vojtek T, Pokluda J, Hohenwarter A, Pippan R. Three-dimensional morphology of fracture surfaces generated by modes II and III fatigue loading in ferrite and austenite. *Eng Fract Mech* 2013;108:285–93. <https://doi.org/10.1016/j.engfracmech.2013.02.022>.
- [101] Vojtek T, Pokluda J, Šandera P, Horníková J, Hohenwarter A, Pippan R. Analysis of fatigue crack propagation under mixed mode II+III in ARMCO iron. *Int J Fatigue* 2015;76:47–52. <https://doi.org/10.1016/j.ijfatigue.2014.09.018>.
- [102] Vojtek T, Pokluda J, Hohenwarter A, Pippan R. Progress in understanding of intrinsic resistance to shear-mode fatigue crack growth in metallic materials. *Int J Fatigue* 2016;89:36–42. <https://doi.org/10.1016/j.ijfatigue.2016.01.009>.
- [103] Vojtek T, Pippan R, Hohenwarter A, Pokluda J. Prediction of effective mode II fatigue crack growth threshold for metallic materials. *Eng Fract Mech* 2017;174:117–26. <https://doi.org/10.1016/j.engfracmech.2016.11.024>.
- [104] Pook LP. Crack profiles and corner point singularities 2000;23:141–50.
- [105] Schrader P, Gosch A, Berer M, Marzi S. Fracture of Thin-Walled Polyoxymethylene Bulk Specimens in Modes I and III. *Materials (Basel)* 2020;13(22). <https://doi.org/10.3390/ma13225096>.
- [106] Hertzberg RW, Manson JA. *Fatigue of engineering plastics*. New York, NY: Acad. Press; 1980.
- [107] Richard HA, Schramm B, Schirmeisen N-H. Cracks on Mixed Mode loading – Theories, experiments, simulations. *Int J Fatigue* 2014;62:93–103. <https://doi.org/10.1016/j.ijfatigue.2013.06.019>.
- [108] Tanaka K. Fatigue crack propagation from a crack inclined to the cyclic tensile axis. *Eng Fract Mech* 1974;6:493–507.
- [109] Ritchie RO. Mechanisms of fatigue crack propagation in metals, ceramics and composites: Role of crack tip shielding. *Materials Science and Engineering: A* 1988;103(1):15–28. [https://doi.org/10.1016/0025-5416\(88\)90547-2](https://doi.org/10.1016/0025-5416(88)90547-2).
- [110] Pippan R, Hohenwarter A. Fatigue crack closure: a review of the physical phenomena. *Fatigue & Fracture of Engineering Materials & Structures* 2017;40(4):471–95. <https://doi.org/10.1111/ffe.12578>.
- [111] Suresh S, Ritchie RO. A Geometric Model for Fatigue Crack Closure Induced by Fracture Surface Roughness. *MTA* 1982;13A.

[112] Paris P, Erdogan F. A Critical Analysis of Crack Propagation Laws.
Journal of Basic Engineering 1963;85(4):528–33.
<https://doi.org/10.1115/1.3656900>.

List of publications

Publication 1

Bibliographic information

Title: Comparison of J-Integral methods for the characterization of tough Polypropylene grades close to the glass transition temperature

Authors: Anja Gosch¹, Florian J. Arbeiter¹, Michael Berer², Gerald Pinter^{1,2}

Affiliation:

1. Materials Science and Testing of Polymers, Montanuniversitaet Leoben, Otto Glöckel-Strasse 2, 8700 Leoben, Austria
2. Polymer Competence Center Leoben GmbH, Roseggerstr. 12, 8700 Leoben, Austria

Periodical: Engineering Fracture Mechanics

DOI: doi.org/10.1016/j.engfracmech.2018.06.002

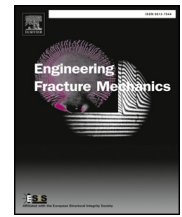
Relevant contributions to this publication

| | |
|-----------------------------|--|
| Conceptualization: | Anja Gosch, Florian Arbeiter |
| Methodology: | Anja Gosch, Florian Arbeiter |
| Validation: | Anja Gosch |
| Investigation: | Anja Gosch |
| Writing - Original Draft: | Anja Gosch |
| Writing - Review & Editing: | Florian Arbeiter, Michael Berer, Gerald Pinter |



Contents lists available at ScienceDirect

Engineering Fracture Mechanics

journal homepage: www.elsevier.com/locate/engfracmech

Comparison of J-integral methods for the characterization of tough polypropylene grades close to the glass transition temperature

Anja Gosch^a, Florian J. Arbeiter^{a,*}, Michael Berer^b, Gerald Pinter^{a,b}^a Materials Science and Testing of Polymers, Montanuniversitaet Leoben, Otto-Gloeckel-Str. 2, 8700 Leoben, Austria^b Polymer Competence Center Leoben GmbH, Roseggerstr. 12, 8700 Leoben, Austria

A B S T R A C T

The fracture mechanical characterization of very tough Polypropylene at room temperature is of great interest for many technical applications. Precision and validity of obtained values can significantly be influenced by notching and crack length determination, which has thoroughly been shown in literature. Additionally, the proximity to the glass transition temperature can induce further uncertainties.

The aim of this study is to compare different J-integral methods of elastic plastic fracture mechanics to determine J-R curves for tested materials. Methods consist of the classical multi-specimen, a single specimen method (load separation) and a statistical approach (Weibull). Specific data reduction procedures based on physical principles were applied to reduce scattering and achieve reliable values. In this way, a reliable fracture mechanics characterization of Polypropylene at room temperature was achieved with a critical verification of the used methods. Finally, the determined fracture toughness value showed a good agreement with the surface texture of inspected fracture surfaces.

1. Introduction

The applicability of Polypropylene (PP) in various technical applications is widely accepted. Especially in the case of piping it is often used due to low manufacturing costs, the possibility of recycling and the extremely tough fracture behaviour. Above all, the characterization of the crack resistance requires a detailed investigation to guarantee safety during the application. Therefore, the influence of chemical and morphological parameters (molecular weight, degree of crystallinity or the size and distribution of crystalline regions and spherulites [1–6]) on the fracture behaviour of PP has been subject to rigorous study. In particular Polypropylene is very well investigated at high loading rates and low temperatures [5,7,8], where the crack resistance is not particularly influenced by any transition region. However, several applications of PP are at or close to room temperature and under moderate to static loading conditions. As proposed in literature [7,9–15] there is a strong sensitivity of fracture toughness to notching procedures, geometry dimensions and strain rate for PP at room temperature. Therefore, it is necessary to understand and reliably determine the fracture behaviour of Polypropylene at moderate loading rates and at room temperature, which is especially vital in critical applications, such as pressurized vessels or components in long-term use.

For many polymeric materials like Polyoxymethylene, Polyethylene, Polyamides, etc. linear elastic fracture mechanics gives good and plausible results at room temperature [16–19]. However, the determination of the crack resistance of PP at room temperature (which inherently is also close to the glass transition region for the investigated types of Polypropylene) cannot be conducted using

* Corresponding author.

E-mail address: florian.arbeiter@unileoben.ac.at (F.J. Arbeiter).<https://doi.org/10.1016/j.engfracmech.2018.06.002>

Received 18 January 2018; Received in revised form 16 May 2018; Accepted 2 June 2018

Available online 22 June 2018

0013-7944/ © 2018 Elsevier Ltd. All rights reserved.

| Nomenclature | | | |
|----------------|---|------------------|--|
| a_0 | initial crack length | S_{pb} | load separation parameter |
| a_p | crack length during testing in the sharp notched specimen | $S_{pb,plateau}$ | point of crack growth initiation according to load separation method |
| a_b | initial crack length of the blunt notched specimen | T_g | glass transition temperature |
| B | specimen thickness | U | area under the load displacement curve |
| C | initial compliance of the specimen | W | specimen width |
| $dJ/d\Delta a$ | slope of the crack resistance curve at 0.2 mm crack propagation | $\tan(\delta)$ | loss factor |
| J_{bl} | J-integral at the intersection of blunting line with the crack resistance curve | Δa | crack propagation |
| J_C | initiation toughness value | η | geometry dependent factor |
| J_0 | J-integral before crack initiation | ν | displacement |
| $J_{0,th}$ | threshold fracture parameter, determined via Weibull analysis | ν_{pl} | plastic displacement |
| $J_{0,2}$ | J-integral at 0.2 mm crack propagation | ν_{el} | elastic displacement |
| m_s | parameter which describes the slope of region III in the normalized load separation curve | bN | blunt notched |
| P_p | load in the sharp notched specimen | EPFM | elastic plastic fracture mechanics |
| P_b | load in the blunt notched specimen | ESIS | European Structural Integrity Society |
| R_s | normalized load separation curve | J-R curve | J-R curve crack resistance curve |
| | | LS method | load separation method |
| | | MS method | multi-specimen method |
| | | PP | polypropylene |
| | | PP-B | polypropylene-Block-copolymer |
| | | PP-R | polypropylene-Random-copolymer |
| | | sN | sharp notched |

this concept [20]. Instead, methods based on elastic plastic fracture mechanics (EPFM) are applied and so-called “crack resistance curves” (“J-R curves” - (J-integral depending on the crack length Δa) are generated.

1.1. Multi-specimen method (MS method)

The most common approach to determine a crack resistance curve is the multi-specimen method. In this procedure, several identical specimens are loaded to different amounts of displacement. For each specimen, the required energy is determined and interpreted as a J-integral value. These values are plotted against the crack growth Δa thus creating the J-R curve. The procedure for the multi-specimen method (MS method) is described in the literature [21,22] and can be performed using the following steps:

- i. Several pre-cracked specimens are loaded to different amounts of displacement.
- ii. Determination of the crack propagation Δa on the fracture surface after cryo-fracturing.
- iii. Evaluation of J_0 , which does not include the crack propagation during testing, using the following equation:

$$J_0 = \frac{\eta U}{B(W-a_0)} \quad (1)$$

in which η is a geometry dependant factor (2 for single edge notched bending (SENB) specimens), U is the area under the load displacement curve, B the specimen thickness, W the width and a_0 the initial crack length.

- iv. Correction of the calculated J_0 by the amount of energy needed for crack growth Δa during testing in order to determine the J-integral value for a specific amount of Δa

$$J = J_0 \left[1 - \frac{(0.75\eta-1)\Delta a}{W-a_0} \right] \quad (2)$$

- v. The crack resistance curve (J-R curve) is constructed by plotting the result of Eq. (2) against the corresponding crack length Δa .

The experimental procedure for the multi-specimen method is very time consuming in terms of specimen preparation and additionally it has a high material consumption. The reliability of this method is strongly influenced by the correct measurement of the exact crack growth on the fracture surface. Especially for Polypropylene, which is referenced as difficult to characterize by the European Structural Integrity Society (ESIS), this characterization proves challenging. Therefore, the development of single specimen methods, where only a single pre-cracked and a single blunt notched specimen is required, are of high interest.

1.2. Load separation method (LS method)

One of the developed single specimen procedures is the so called load separation method. The procedure for the load separation

method is based on the principle developed by Ernst et al. [23]. The construction of a load separation parameter curve is required to determine the crack propagation in a sharp notched specimen during testing. If this load separation parameter curve can be established it is possible to construct the whole J-R curve (J-integral depending on the crack length Δa) with just two specimens. The main steps of the procedure are described below and can be found in detail in [24]:

- i. Loading of a sharp notched specimen sN (sharp crack tip) and a blunt notched specimen bN (round (blunt) crack tip) to a certain amount of displacement ν , where crack growth in the sharp notched specimen is ensured but no crack growth in the blunt notched specimen (only plastic deformation or blunting) occurs.
- ii. Determination of the plastic displacement ν_{pl} during testing for both specimens, by subtracting the elastic displacement as shown in Eq. (3).

$$\nu_{pl} = \nu - \nu_{el} = \nu - PC \quad (3)$$

in which ν is the measured displacement and ν_{el} the elastic displacement calculated from the load P and the initial compliance C .

- iii. Characterization of the load separation parameter S_{pb} by dividing the measured forces of both specimens at identical plastic displacements

$$S_{pb} = \frac{P_p}{P_b}, \nu_{pl,p} = \nu_{pl,b} \quad (4)$$

in which P_p is the resulting load to the sharp notched specimen and P_b is the applied load to the blunt notched specimen. Using S_{pb} and ν_{pl} the load separation curve as shown in Fig. 1 can be constructed. The load separation curve shows three typical regions. First, the early region of plastic displacement (region I), also named the “unseparable region” where no load separation is valid. The region where the load separation parameter reaches a maximum (region II), represents the blunting process in the sharp notched specimen. Within region II the crack usually starts to propagate. Therefore, the initiation point of crack growth has to be defined in this region. Finally in region III, where the load separation parameter S_{pb} decreases, the propagation in the sharp notched specimen occurs.

- iv. With the load separation curve it is possible to calculate the crack propagation a_p during testing using Eq. (5),

$$a_p = a_b (S_{pb})^{1/m}, S_{pb} (\nu_{pl} \geq \nu_{pl,plateau}) \quad (5)$$

in which a_b is the initial crack length of the blunt notched specimen and S_{pb} is taken from the load separation curve in the area of stable crack growth (Fig. 1, III). To clearly define the start of region III, the initiation point of crack growth $S_{pb,plateau}$ was defined as the maximum value $S_{pb,max}$ minus 0.1 as it is proposed in literature [26,27]. This initiation point of crack growth $S_{pb,plateau}$ can be used in substitution of the parameter $J_{0.2}$ (see Section 3.2.1) to characterize crack growth onset and is much closer related to the actual physics of the fracture onset process [28]. However, since this method is not yet fully understood it was not used to determine crack initiation in this study.

- v. Finally, the crack length in the sharp notched specimen associated with each point of the load-displacement record is known. Hence the calculation of the J-integral and construction of J-R curve can be continued as described for the MS method starting at point iii.

Unfortunately, single specimen methods are influenced by several aspects (sensitivity to the initiation criterion, load separation

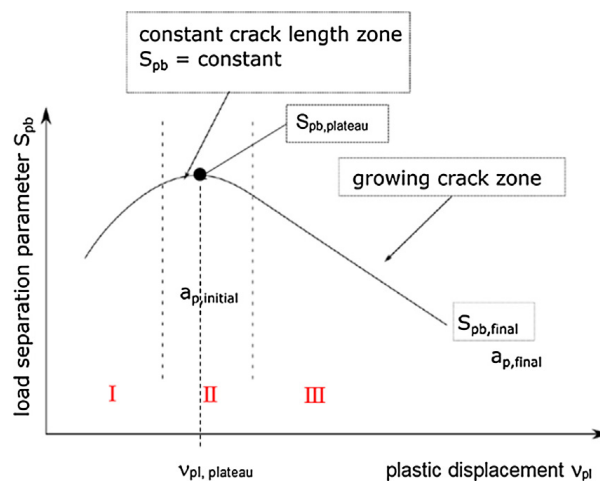


Fig. 1. Load separation parameter curve to determine the crack growth initiation point ($S_{pb} = \text{constant}$) and the area of stable crack growth according to [25].

property, kind of blunt notched specimen used in specific) [14,26,28,29]. Hence, the fracture behaviour characterized with single specimen methods is usually used in combination with the multi-specimen method to strengthen the results of the J-R curve.

For Polypropylene the fracture test results at room temperature, which were the main intention for this study, are strongly influenced by the notch, geometrical dimensions and the strain rate. Small changes can already be sufficient to significantly influence the results, or even change the local type of failure from brittle to ductile or vice versa. Consequently, results show significant scattering and it is difficult to clearly characterize the crack resistance of chosen PP-types at room temperature.

The aim of this study is to determine reliable crack resistance curves of Polypropylene near their application temperature (room temperature). Hence, two additional experimental procedures to reduce scattering by excluding data sets based on physical principles were applied. Furthermore, a statistical approach in the form of a three-parameter Weibull fit was used to calculate a threshold fracture parameter $J_{0,th}$ [14].

2. Materials and methods

2.1. Materials

Two different types of pipe grade PP were used for the experiments: polypropylene block-copolymer (PP-B) and polypropylene random-copolymer (PP-R). The general material data was taken from the data sheets or from previous experiments [30–33]. For the sake of convenience, several important properties which strongly influence the fracture toughness, such as the molecular weight M_w , are shown in Table 1.

To investigate the glass transition temperature the dynamic-mechanical properties of the tested materials were measured in previous studies [30] and are shown in Fig. 2. The glass transition peak temperature of PP-B is around 5–10 °C and –5 to 0 °C for PP-R. Hence, the experimental conditions at room temperature did not lie within the peak of the glass transition, but in the glass transition region. This can be seen by the curve shape of the loss factor $\tan\delta$ and the loss modulus E'' (Fig. 2), where both still display a negative slope around room temperature.

2.2. Experimental procedure

To characterize the fracture behaviour under aforementioned conditions the multi-specimen method (MS method) [21] and a single specimen method (LS method [26]) were used as described in the introduction. Both methods can be used to generate whole J-R curves of the materials, which show the necessary energy in terms of J-integral, depending on the amount of produced crack propagation Δa . Both MS and LS method were evaluated for the same specimens and in accordance with the proceeding discussed in chapter 1.

Single edge notched bending specimens (shown in Fig. 3) were used to test the materials in a three point bending configuration. The specimen geometry was $6.5 \times 16 \times 70.4$ mm for PP-R and $10.2 \times 20.5 \times 95$ mm for the PP-B specimens. The difference in the dimensions is owed to availability issues. Generally, all specimens were sidegrooved with a root radius around 0.25 mm and a total reduction in thickness of maximum 0.2B according to [34]. For each material 30 sharp notched specimens (sN) were tested for the MS method. Additionally to the sharp notched specimens, one blunt notched specimen per material (bN) was produced for the application of the LS method (Fig. 3). The bN specimens were machined with a round crack tip with a radius of 2 mm. With the bN specimen, all sN specimens used for the MS method were additionally analysed following the LS method. In general, all specimens were side-grooved to generate a straight crack front and to suppress the plane stress state at the specimen's side surfaces.

The notching process has a major influence on the quality of the results, and affects not only the crack growth initiation but also the whole fracture process. Hence, the experimental notching procedure to generate the sharp crack tip is extremely important to get representative results for the fracture behaviour of the materials tested [24,35]. Therefore, the notches of the sN specimens were sharpened using a new razor blade. By sliding the blade along the crack front using a microtome a sharp and uniform crack tip was achieved. The crack lengths obtained after notching satisfied the requirement $0.55 \leq a_0/W \leq 0.65$.

The tests were performed under displacement control at a constant crosshead displacement of 1 mm/min. As shown in Fig. 3, a support length of 4 times the specimen width W was used, which is in accordance with the recommendations in [21]. The mechanical tests were carried out on a Zwick Z010 (Zwick GmbH & Co.KG, Germany) and a contact extensometer for the displacement measurement. For the measurement of the crack growth Δa on the fracture surface, specimens were cryo-fractured and examined using an optical microscope. The length of Δa was taken as the average value of several measurements, equidistantly distributed along the notch. Fracture surfaces were examined using an optical microscope SZX12 from Olympus (Olympus Life Science Europe GmbH,

Table 1
Material properties of Polypropylene resins used in this study [30].

| Property | PP-B | PP-R |
|-------------------------------------|----------------|----------------|
| Young's Modulus (MPa), 23 °C | 1300 | 900 |
| Yield Stress (MPa), 23 °C | 28 | 25 |
| Density (kg/m ³), 23 °C | 900 | 905 |
| Glass transition temperature (°C) | 5–10 | –5 to 0 |
| Molecular weight M_w (kg/mol) | 605,000 | 538,000 |

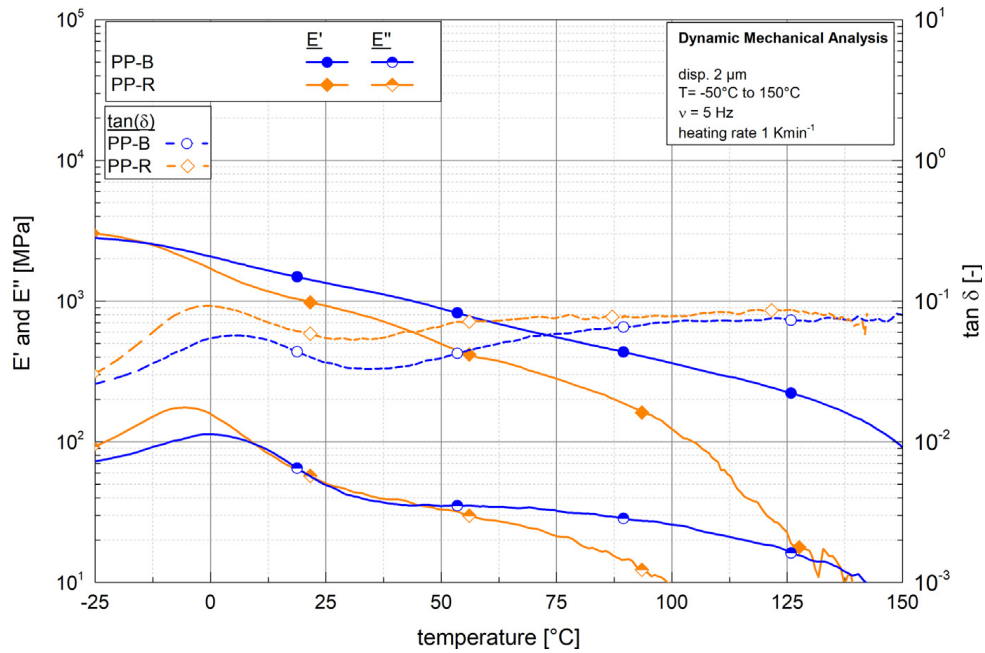


Fig. 2. Examination of dynamic mechanical properties of the tested materials (PP-B and PP-R) according to [30].

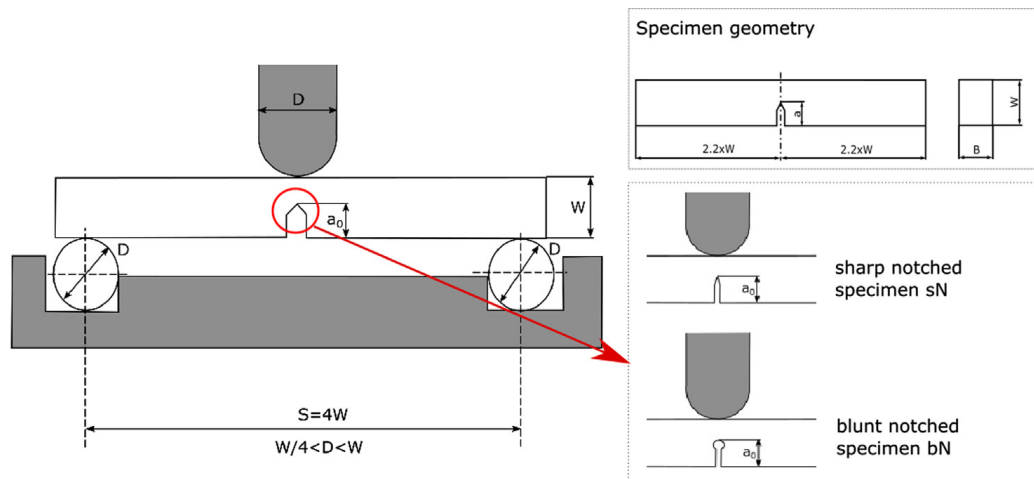


Fig. 3. Set-up and specimen configurations used in this study – three point bending of single edged notched specimens with sharp notch (sN) and blunt notch (bN) according to [21,36].

Germany) and a scanning electron microscope Vega II from TeScan (Brno, Czech Republic), for closer examination of deformation and fracture mechanisms.

3. Results and discussion

The results for the two materials investigated in this study (PP-B and PP-R) are presented and discussed in the following. In accordance with Section 3.2 the discussion of the results will start with the uncorrected J-R curves obtained for the MS method and the LS method. Afterwards the results obtained for the m_c -parameter will be discussed. Subsequently, the influence of the two correction techniques on the J-R curves will be analysed. Finally, the Weibull analysis will be compared to different parameters obtained from the (untreated and treated) J-R curves.

3.1. Crack resistance (J-R) curves

For both materials under investigation it was possible to determine a crack resistance curve at room temperature using the classical MS method and the LS method. Untreated results are shown in Figs. 4 and 5. Specimens which could not be evaluated due to experimental reasons (e.g. clear determination of crack propagation Δa not possible, notch quality) were excluded prior to data treatment.

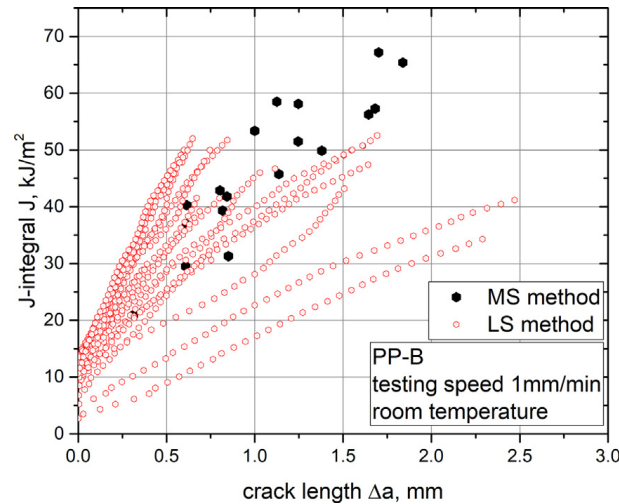


Fig. 4. J-integral versus crack length Δa determined with the multi-specimen method (MS) and the load separation method (LS) for PP-B.

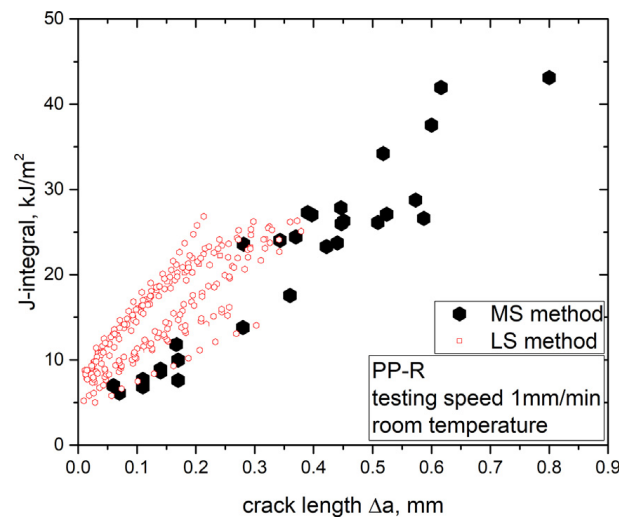


Fig. 5. J-integral versus crack length Δa determined with the multi-specimen method (MS) and the load separation method (LS) for PP-R.

As mentioned before the glass transition region of PP is close to room temperature. Here highly dissipative shear processes dominate the crack growth of PP [13]. For the materials tested glass transition temperature (T_g) values are around $T_g = 5$ to 10 °C for PP-B and $T_g = -5$ to 0 °C for PP-R [30]. Even though the T_g values are below the testing temperature of 23 °C the influence is still present due to phasing out of the damping peak of the material (observed e.g. in dynamic mechanical analysis (Fig. 2)) which accompanies T_g . This could be an additional reason why the J-R curve of the MS method shows significant data scattering for both materials. For a reliable material characterization it is necessary to reduce this scattering.

Another strong source for the data scattering in the J-R curves is the determination of the crack growth Δa for the MS method. For the PP materials examined in this study, the determination of the final crack front position was very difficult due to various deformation and damage mechanisms, which occurred during testing. In order to illustrate this situation Fig. 6 shows representative fracture surfaces of PP-B and PP-R.

The tested PP-B specimens Fig. 6 show a rather well visible region of stable crack growth and the crack propagation length could easily be determined via optical microscope for most specimens. Contrary, for PP-R the crack tip and thus the crack propagation length could not always be determined precisely. Additionally, crack fronts of PP-R were not always straight even though specimens were side-grooved as suggested in [37]. This is reflected in a higher data scattering of the corresponding J-R curve.

The results of the LS method, with the big advantage of constructing a whole J-R curve with only one sharp notched specimen, show not always the same tendency as the J-R curve of the MS method. Plotting all J-R curves leads to high scatter, as shown in Figs. 4 and 5. Compared to experimental aspects as discussed for the MS method above, the LS method is also dependent on additional theoretical parameters [14,26,28,29], which influence the procedure and results (like the chosen blunt notched specimen, the used calibration points and the point chosen as crack growth onset ($S_{pb,plateau}$)). Hence, the use of the LS method to characterize the fracture behaviour of a complex material such as PP at room temperature without a combined J-R curve from the MS method bears certain risks when looking at $J - \Delta a$ values. To improve results further data analysis is recommended.

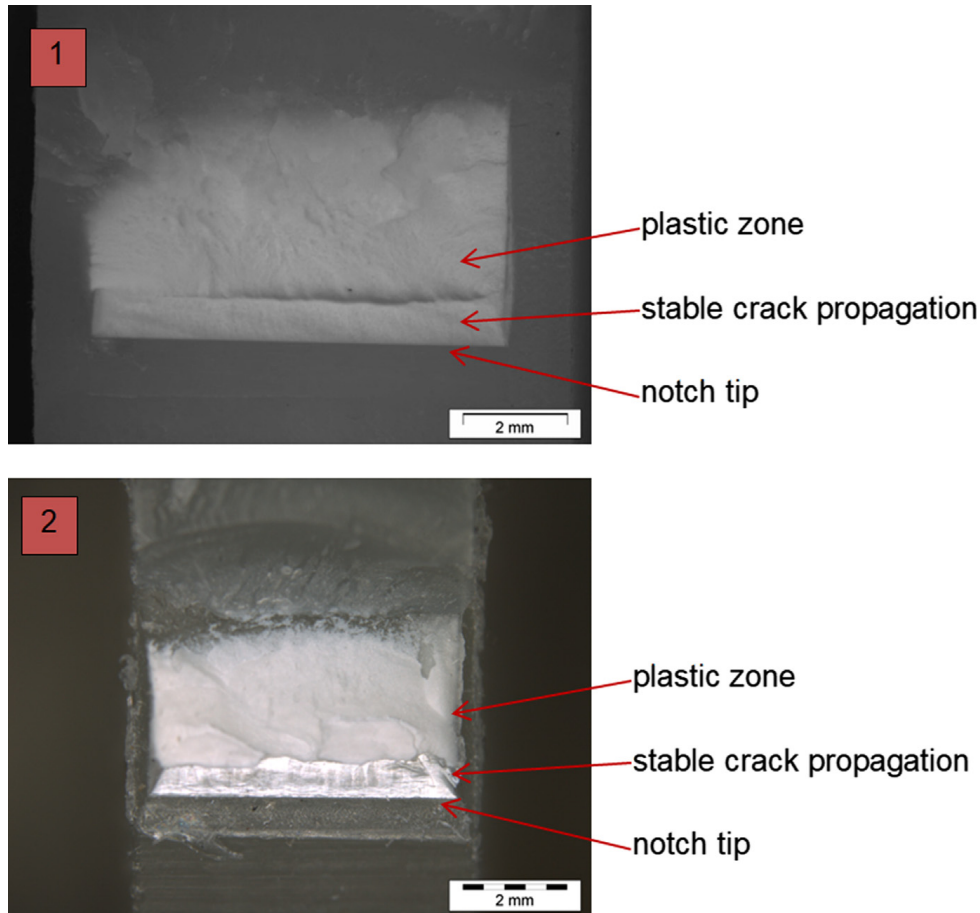


Fig. 6. Fracture surface of PP-B (1) and PP-R (2) to characterize the crack growth Δa – both specimens were sidegrooved.

3.2. Data analysis

Polypropylene has both, its glass transition temperature and its ductile to brittle transition in the vicinity of the test temperature (room temperature). Hence, tested Polypropylene showed strong scattering under the mentioned testing conditions. To achieve desired information regarding fracture toughness nonetheless, the following procedures, which are explained in detail below, were applied

- Standard procedure for the generation and analysis of the J-R curve using no specific correction
- The m_s -parameter as an additional parameter to rank the tested materials
- Correction of the J-R curve using the Δa -time plot
- Correction of the J-R curve using the load separation method
- Weibull analysis of the J-R curves

3.2.1. Standard procedure for the J-R curve

Both, the MS method as well as the LS method were analysed in accordance with the procedure discussed in Section 1. The J-R curves constructed of both methods were fitted by a power law in the form of $J = C\Delta a^n$, where a requirement of the validity of the J-R curve is that $n \leq 1$ [14]. The crack resistance curve provides a further value, the initiation toughness J_C , which is used to describe the early region of crack propagation. This initiation toughness value J_C is defined as the lower value of $J_{0.2}$ (J-integral at 0.2 mm crack propagation) or a J_{bl} value (intersection of the blunting line with the J-R curve) [21]. The blunting line is traced according to the following analytical expression [28]:

$$J = 2\sigma_y \Delta a \quad (6)$$

in which σ_y is the yield stress in uniaxial tension and Δa the crack propagation. This procedure was applied on both methods (MS method and LS method) to calculate an initiation toughness value J_C . Another value that was calculated from the crack resistance curve was the slope of the curve tangent at $\Delta a = 0.2$ mm ($dJ/d\Delta a$). According to e.g. Lach et al. [38] this parameter characterizes the crack propagation. It is often used for materials where crack initiation and propagation can be clearly identified and scatter is low enough to justify the application of a fitted curve. In the case of high scattering of the data points, which has to be expected for PPat room temperature, fitting might lead to unreliable data [14].

3.2.2. The m_s parameter - an extension of the LS method

In a previous study of Baldi et al. [36] a more sophisticated analysis of the LS method is discussed. They suggest to interpret the “region III – slope” of the normalized load separation curve (region of steady state stable crack growth) as inherent property of ductile polymers. This parameter will be termed as “ m_s – parameter” in the following. In [36] the m_s – parameter was used to characterize the fracture behavior of ductile polymers. It revealed a high reproducibility, which made it interesting for the materials examined in this work. The normalized load separation curve $R_s(\nu_{pl})$ can be calculated according to:

$$R_s(\nu_{pl}) = \frac{S_{pb}(\nu_{pl})}{S_{pb,max}} \quad (7)$$

in which the load separation curve $S_{pb}(\nu_{pl})$ is divided and normalized by its maximum value $S_{pb,max}$. The m_s -parameter is defined as the negative slope in region III of this normalized load separation curve (region III in analogy to the “conventional” load separation curve shown in Fig. 1):

$$m_s = -\frac{dR_s}{d\nu_{pl}} R_s(\nu_{pl} \geq \nu_{pl,max}) \quad (8)$$

It indicates the crack advancement produced per unit of plastic displacement. Generally, it can attain values between 0 (only crack blunting) and values near 1. For the later, linear elastic fracture mechanics can be used to describe the fracture behaviour. In our study, the m_s -parameter was calculated for both materials. It was determined for all specimens analysed with the LS method and summarized using average and standard deviation.

3.2.3. Correction of the J-R curve using the Δa -time plot

This rather empirical procedure is a correction procedure typically used for the MS method. Hence, it was also used to correct the J-R curves obtained by the MS method in this study. The procedure is based on the definition of the J-integral. According to the thermodynamics the J-integral describes the energy field around a moving crack but only in the case of steady state crack propagation. Generally, the fracture process can be understood as a three-phase process (phase I: crack tip blunting/crack initiation; phase II: non stationary stable crack growth; phase III: steady state stable crack growth). For steady state stable crack growth the crack propagation rate \dot{a} has to be constant after the crack initiation. To ensure this, the crack propagation Δa evaluated for each specimen tested was plotted as a function of the corresponding total testing time. Subsequently, the data was fitted with a linear fit and strongly deviating data points, which in fact had a different crack speed \dot{a} , were removed (Fig. 7). Similar data treatment was done by Lach et al. [39,40]. The idea of this procedure is to exclude measurements, for which either the fracture behaviour (due to changing fracture mechanism, geometrical factors such as notching or impurities etc.) is different or the pre-conditions for the application of the J-integral (steady state stable crack growth) are no longer fulfilled [38,39]. After removal of the excluded data points the MS method was re-evaluated to generate the corrected J-R curve.

3.2.4. Correction of the J-R curve using the load separation method

The second procedure used to reduce the scattering in the MS method was to combine it with LS method. While the LS method can be used to establish whole J-R curves, previous study have shown that the absolute values of these curves can vary significantly, depending on the specimens used. Nevertheless, the slope of these J-R curves was found to be rather constant for the different specimens, as long as the fracture behaviour remains unchanged [26,36].

Based on these previous findings, J-R curves of every individually tested sample of the MS method were calculated using the LS method and compared to the J-R curve obtained when using the MS method for the analysis. In case of extreme differences between the slopes of the J-R curves obtained from LS method and MS method (specimen 2 in Fig. 8) the data point (specimen) was removed. Alternatively, if the J-R curve of the LS method did not fulfil the requirements of the power law $J = C\Delta a^n$ ($n \leq 1$, specimen 1 in Fig. 8) the data point was also removed since it was expected that this specimen failed in a different manner. After removal of the excluded data points the MS method was re-evaluated to generate the corrected J-R curve.

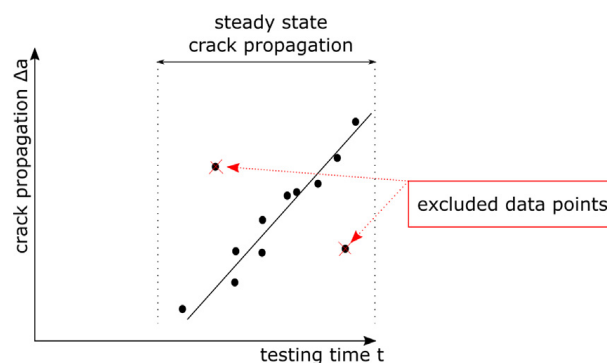


Fig. 7. Data correction procedure using the Δa – time plot – data points with significantly different crack propagation rates were removed.

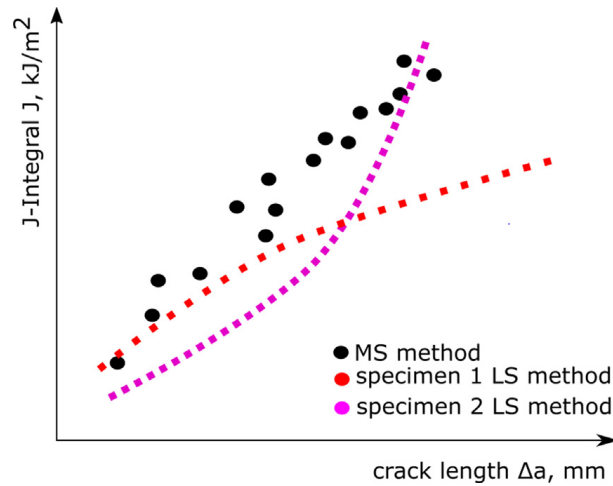


Fig. 8. Data correction procedure for the MS method based on its combination with the LS method – specimens, which did not fulfill the power law requirements (specimen 1) or which had a slope completely different to the one obtained from the MS method (specimen 2) were removed.

3.2.5. Weibull analysis of the J-R curves

Additionally to the reduction of scattering using the two correction procedures described above, a statistical model was included in the data analysis. For this, a statistical approach based on the weakest link model was selected. As discussed in literature [14], this statistical approach assumes the smallest J-value along the crack front as the critical fracture toughness for crack initiation in the specimen. In analogy to the literature [9,14,41,42] the J-R curves in this study were analysed with a three-parameter Weibull model given in the following equation:

$$F(J) = 1 - \exp\left\{-\left[\frac{J - J_{0,th}}{C - J_{0,th}}\right]^m\right\} \tag{9}$$

Therein $F(J)$ is the cumulative distribution function, J the evaluated J-integral of individual data sets, $J_{0,th}$ is a threshold toughness parameter independent of size, C is a scale parameter and m is the shape parameter. Using this approach it is possible to calculate the minimum threshold toughness value $J_{0,th}$. J-integrals below this value cause a zero probability of failure inside the corresponding specimen. To apply this statistical approach on the J-R curves the following procedure was used:

- i. The J-integral values determined were arranged from the lowest to the highest value, and assigned with an index number i .
- ii. Calculation of the cumulative probabilities using the following equation,

$$F(J_i) \approx P_i = \frac{i - 0.5}{N} \tag{10}$$

where N is the total number of data points.

- iii. The cumulative distribution function was rearranged to obtain the expression of a straight line:

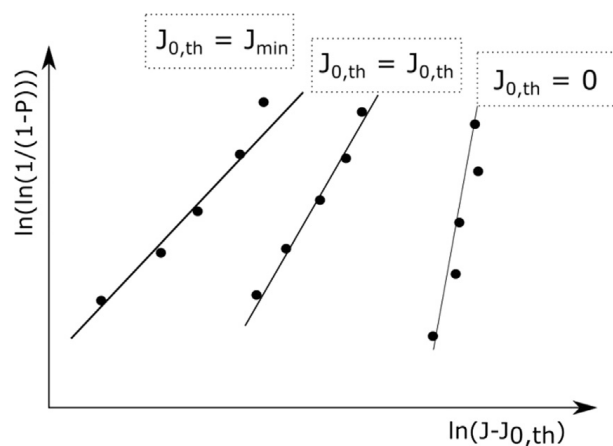


Fig. 9. Weibull-Fit to determine the threshold toughness value $J_{0,th}$ according to [42]. This method is stated for stationary cracks.

$$\ln \left[\ln \left[\frac{1}{1-P_i} \right] \right] = m \ln(J - J_{0,th}) - m \ln(C - J_{0,th}) \quad (11)$$

where m is the slope of the straight line and C is obtained from the ordinate ($m \ln(C - J_{0,th})$). Using an iterative approach, $J_{0,th}$ can then be calculated as the value that best fitted all the experimental data points of the J-R curve (maximum coefficient of correlation (R^2)). In general, $J_{0,th}$ can assume values between 0 and the lowest fracture toughness value $J_{c,min}$ of the experimental data. The illustration in Fig. 9, shows the Weibull-Fit with different threshold toughness values $J_{0,th}$ used.

To apply these statistical approach on growing cracks a censoring strategy is usually used as described in literature [41,42]. Hence, specimens with a crack growth larger than 10% of the original remaining ligament were excluded in the regression analysis.

3.3. Evaluation of the parameter m_s

This parameter is calculated using the normalized load separation curve R_s , which is based on the LS method. The normalized load separation curves $R_s(v_{pl})$ obtained in this study are plotted in Fig. 10. The m_s - parameter is evaluated from region III (after the maximum, refer to Section 3.2.2 for more details) of this curve, which is the region of crack growth in the sN specimen. The m_s - parameter depends on the specimen geometry and the material. It is used to classify the crack propagation process as a function of the amount of plastic displacement. For materials, which reveal a m_s - parameter of nearly 0 mm^{-1} (indicating only crack tip blunting), the common procedures of elastic plastic fracture mechanics to characterize fracture processes, like the MS method, are likely to fail. On the other side, materials with an m_s -parameter around 1 mm^{-1} are usually suitable to be investigated using linear elastic fracture mechanics. The general idea of the m_s -parameter is to use it as a criterion for the application of the multi-specimen approach [36]. As shown in Fig. 10, the slope in region III of the normalized load separation curve (which represents the m_s -parameter) is rather uniform for PP-B. For PP-R on the other hand, there is more variation, especially at higher levels of plastic displacement v_{pl} . This difference is also represented in the m_s - parameter values and their corresponding standard deviation in Table 2.

Compared to other materials the determined m_s values for PP-B and PP-R are relatively low, which indicates the fracture process is mainly dominated by blunting [36]. This extremely tough material behaviour should also be reflected in initiation toughness values. To correlate the m_s - parameter with the fracture process, the fracture surfaces of PP-B and PP-R are presented in Fig. 11 for three different specimens. Looking at the fractured specimens, the PP-R surfaces show much more crack-asymmetry than the PP-B specimens, even though specimens were side-grooved. The latter look more uniform in terms of crack shape and crack front. Based on these results, the consistency of the region III-slopes of the normalized load separation curve (quantified as the m_s - parameter) appears to be a good indication for the uniformity of the fracture behaviour during testing.

3.4. Effect of J-R curve correction

Two types of corrections were tested for the J-R curves of the MS method (refer to Sections 3.2.3 and 3.2.4 for details): the correction with the Δa -time plot and the correction using the LS method. The more established Δa - time plot correction was used to ensure steady state stable crack growth in tests, which is a precondition for the application of the J-integral. The corresponding plots crack propagation Δa as a function of the testing time t are shown in Fig. 12 for both materials. The data points plotted show a quite linear trend, which indicates steady state stable crack propagation in almost all specimens. Only one data point for PP-B and three data points for PP-R were excluded. The resulting J-R curves are the ones showed in Fig. 13. It is obvious that the J-R curves corrected with this technique still show significant scattering. A general problem with the Δa - time plot correction is that the criterion for the exclusion of the data points is quite subjective.

For the second J-R curve correction method, every single specimen of the MS method was used to calculate a J-R curve with the LS

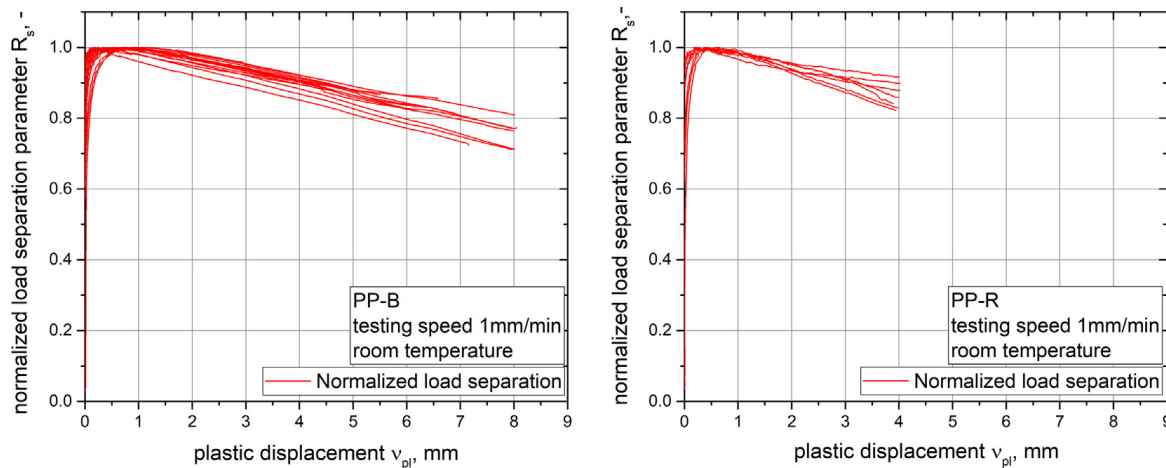


Fig. 10. Normalized load separation parameter R_s as a function of the plastic displacement v_{pl} for several tested specimens of PP-B (left) and PP-R (right).

Table 2
 m_s – parameter with standard deviation for PP-B and PP-R at room temperature.

| Material | m_s – parameter (mm^{-1}) | Standard deviation (mm^{-1}) |
|----------|--|---|
| PP-B | 0.032 | 0.004 |
| PP-R | 0.037 | 0.013 |

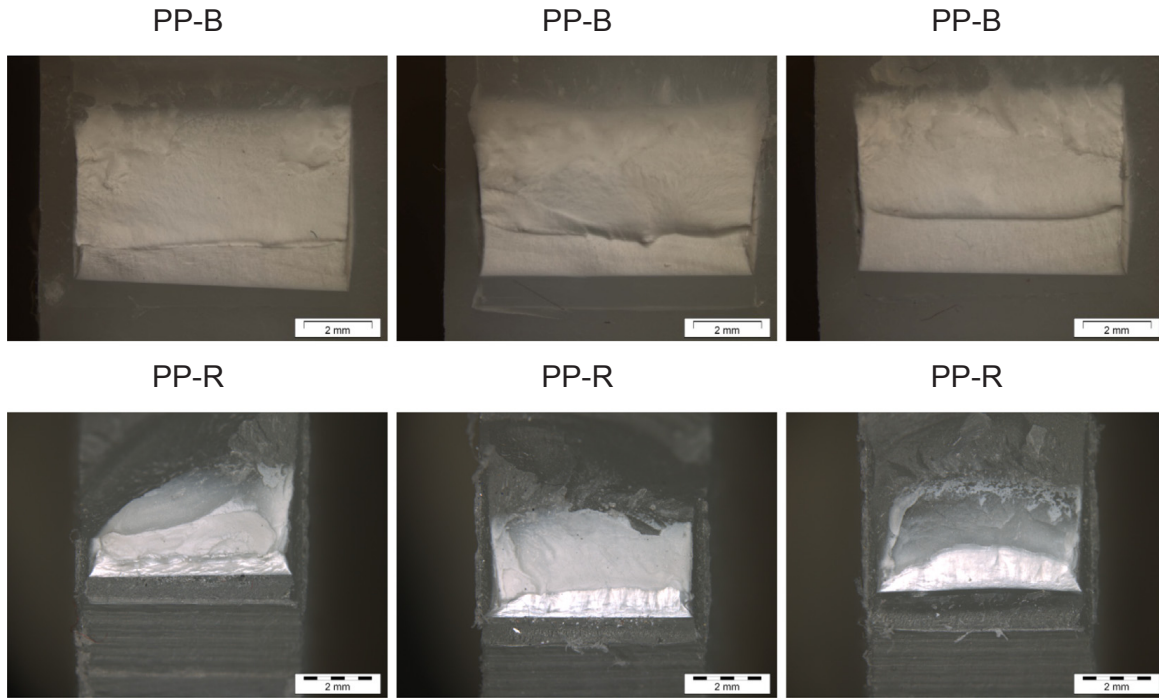


Fig. 11. Fracture surface of PP-B and PP-R to present differences in the crack shape and the crack front.

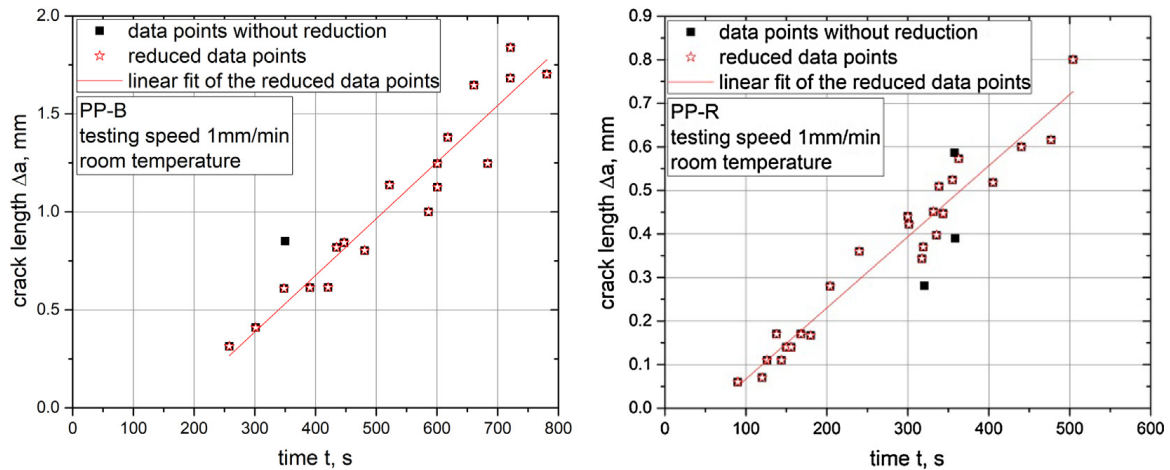


Fig. 12. Crack length Δa as a function of the testing time t - original and reduced data points of PP-B (left) and PP-R (right).

method. Specimens with J-R curves either extremely different to the one obtained from the MS method or which did not meet the shape requirements of the power law fit (refer to Section 3.2.4 for details) were removed. Subsequently, the J-R curves were recalculated with the corrected data set. The corresponding curves are shown in Fig. 14. Generally, the data treatment using the LS method worked well for the materials tested and it gave similar results to the MS method. Compared to the uncorrected J-R curve, the slope of the LS method corrected one is slightly higher for both materials. Especially for PP-R, this correction procedure removed mainly data points far away from the fitted MS curve.

To quantify the results, parameters commonly used, such as J_c and $dJ/d\Delta a$ at a crack growth of 0.2 mm were determined [21,38]. They are presented in Table 3 for PP-B and Table 4 for PP-R. For both materials the $J_{0.2}$ (J-integral at 0.2 mm crack growth) was the lower value (as presented in Fig. 15) and is used as fracture initiation value.

The tables show that the initiation toughness $J_{0.2}$ is higher for PP-B than for PP-R ($J_{0.2} = 18.1\text{--}19.6 \text{ kJ/m}^2$ for PP-B and $J_{0.2}$

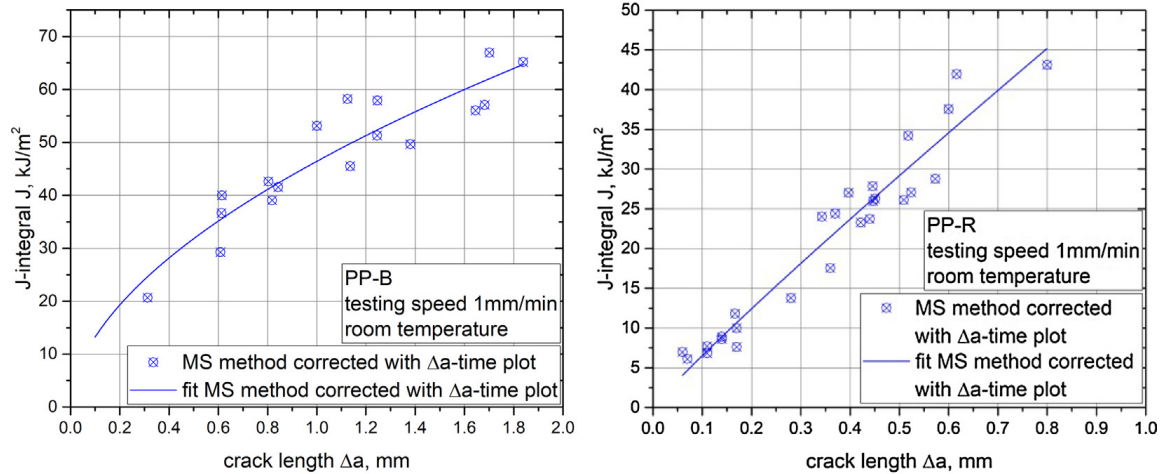


Fig. 13. J-integral versus crack length Δa corrected with the LS method for PP-B (left) and PP-R (right).

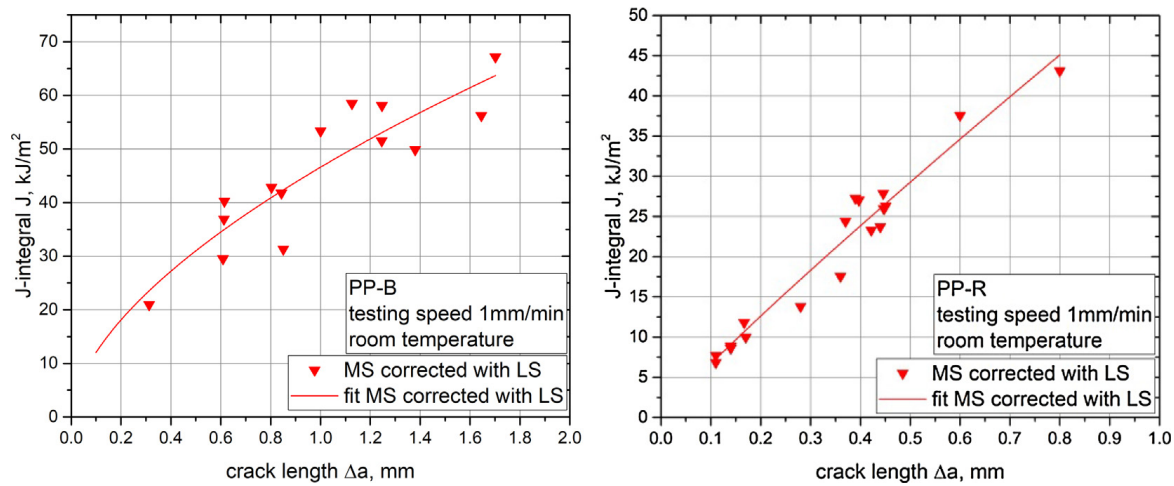


Fig. 14. J-integral versus crack length corrected with the LS method for PP-B (left) and PP-R (right).

Table 3

Weibull parameters, initiation toughness $J_{0.2}$ and slope of the J-R curve at 0.2 mm crack propagation $dJ/d\Delta a$ for PP-B at room temperature.

| Method | R^2 (Weibull) | $J_{0,th}$ (kJ/m ²) | $J_{0.2}$ (kJ/m ²) | $dJ/d\Delta a$ (kJ/(m ² mm)) |
|---|-----------------|---------------------------------|--------------------------------|---|
| MS method | 0.99 | 0.0 | 18.4 | 52.2 |
| Corrected with Δa -time | 0.98 | 0.0 | 19.4 | 52.6 |
| Corrected with LS method | 0.98 | 4.6 | 18.1 | 53.1 |
| Arbitrary LS curve ^a | 0.98 | 8.7 | 19.6 | 56.0 |
| Load separation method – average of all specimens | 0.94 | 2.3 | – | – |

^a For one specific specimen with a J-R curve similar to that from the MS method, not representative for all specimens.

Table 4

Weibull parameters, initiation toughness $J_{0.2}$ and slope of the J-R curve at 0.2 mm crack propagation $dJ/d\Delta a$ for PP-R at room temperature.

| Method | R^2 (Weibull) | $J_{0,th}$ (kJ/m ²) | $J_{0.2}$ (kJ/m ²) | $dJ/d\Delta a$ (kJ/(m ² mm)) |
|---|-----------------|---------------------------------|--------------------------------|---|
| MS method | 0.93 | 5.9 | 13.1 | 57.0 |
| Corrected with Δa -time | 0.94 | 6.5 | 12.4 | 58.0 |
| Corrected with LS method | 0.95 | 6.4 | 12.6 | 57.9 |
| Arbitrary LS curve ^a | 0.98 | 3.7 | 15.5 | 40.9 |
| Load separation method – average of all specimens | 0.99 | 2.3 | – | – |

^a For one specific specimen with a J-R curve similar to that from the MS method, not representative for all specimens.

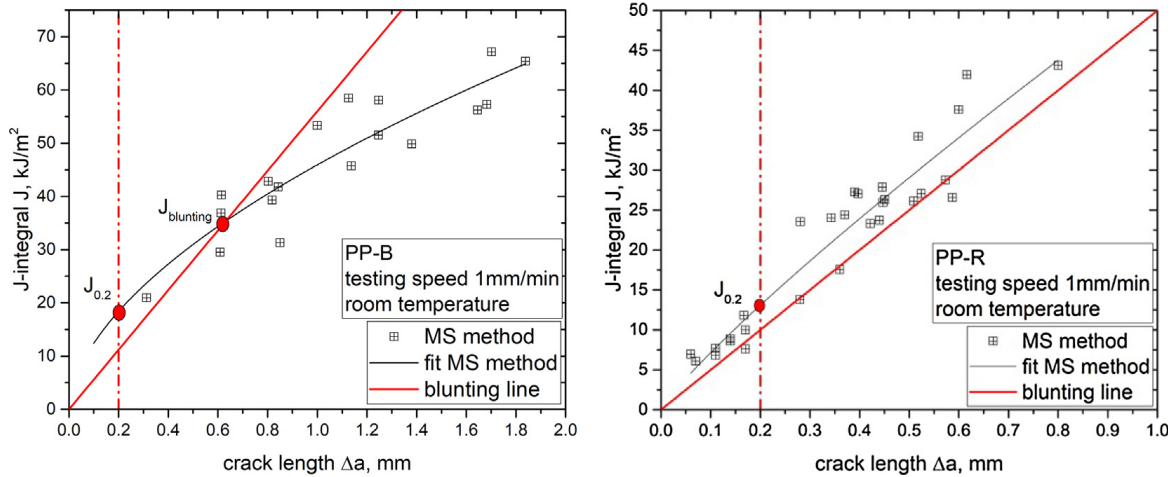


Fig. 15. J-integral versus crack length Δa for the determination of the initiation toughness value J_c for PP-B (left) and PP-R (right).

= 12.4–15.5 kJ/m² for PP-R, depending on the method to generate the J-R curve). At this point it has to be mentioned that the blunting line for both materials is rather shallow and in the case of PP-R does not even cross the J-R curve. This is a clear indication of a fracture process which is highly dominated by blunting. Typically for materials with high toughness values and a low yield stress [43,44]. The slope of the J-R curve was found to be steeper for PP-R. This is reflected in the slope values calculated at 0.2 mm crack propagation ($dJ/d\Delta a$), where PP-R reveals values from 57.0 to 58.0 kJ/(m² mm) compared to PP-B with values between 52.2 and 53.1 kJ/(m² mm), again depending on the method used to calculate the J-R curve. The highly deviating values of 40.9 kJ/(m² mm) for PP-R and 56.0 kJ/(m² mm) for PP-B are based on the J-R curve of just one single specimen of the LS method. Due to the discussed scattering of single tests, they cannot be seen as representative. These values were added to illustrate the uncertainty in the results when using just one single specimen to characterize the fracture behaviour of Polypropylene at room temperature. The results ($J_{0.2}$ and $dJ/d\Delta a$) indicate that PP-B shows a higher crack initiation resistance at $\Delta a = 0.2$ mm but PP-R has a higher resistance against further crack propagation due to the steeper slope.

3.5. Weibull analysis of the J-R curves

In order to statistically analyse determined J-R curves, a Weibull model was used in this study. With this model the threshold toughness parameter $J_{0,th}$ was calculated as it was done in previous studies [9,14,41,41,42]. Generally, the fracture toughness (J-value) varies along the crack front in a specimen. For this, the threshold toughness parameter $J_{0,th}$ represents the lowest fracture resistance along the crack front (weakest-link model) [41,42]. The results for $J_{0,th}$ are summarized in Table 3 (PP-B) and Table 4 (PP-R). For PP-B this threshold parameter varies between 0 kJ/m² and 8.7 kJ/m² (result of arbitrary curve, added for illustration purpose) As discussed in the theory, $J_{0,th}$ can assume values between 0 and J_c . The determined results differ highly depending on the correction procedure (see value of LS correction). The exclusion of data points has a major influence on the initiation toughness value. Therefore, a higher number of tests is necessary to provide a reliable threshold parameter for PP-B at room temperature. This explains a threshold value of 0 kJ/m², which is not reasonable from a physical point of view. The $J_{0,th}$ results of PP-R are between 2.3 and

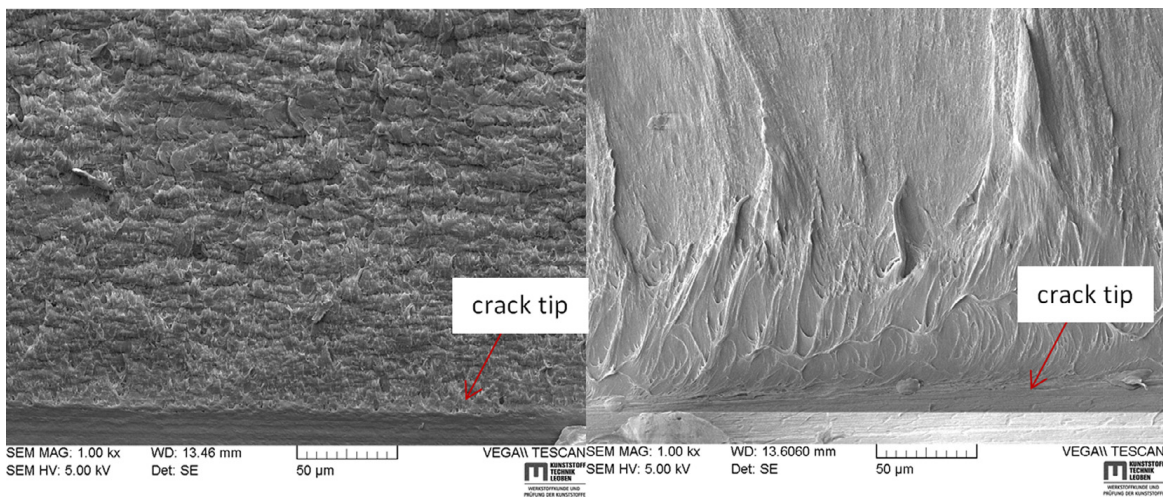


Fig. 16. Fracture surfaces of PP-B (left picture) and PP-R (right picture) close to the initial notch.

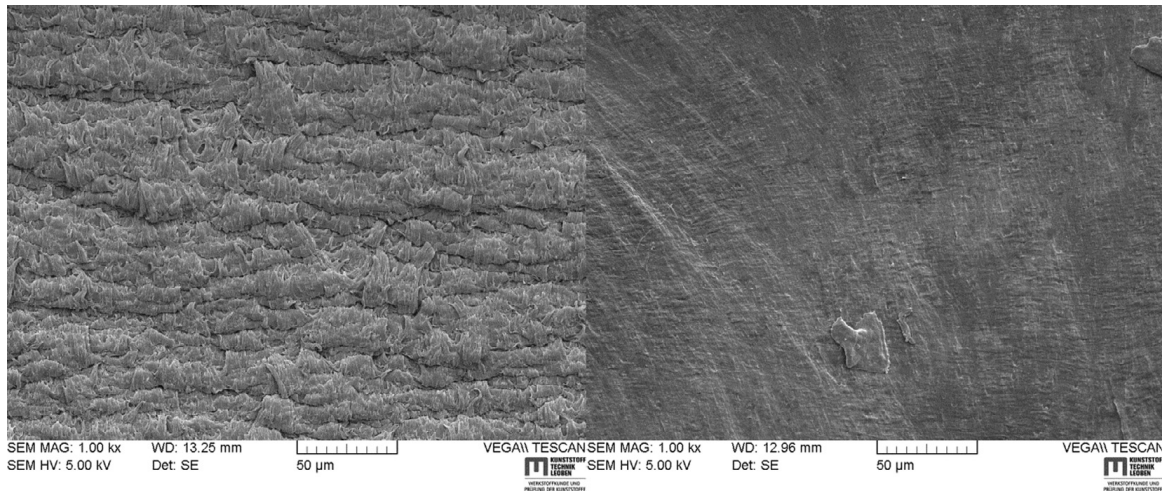


Fig. 17. Fracture surfaces of PP-B (left picture) and PP-R (right picture) after significant crack propagation.

6.5 kJ/m². The value of 2.3 kJ/m² is the average of all LS method J-R curves (for the single specimen it is 3.7 kJ/m²). The values of the uncorrected and corrected MS method J-R curves are between 5.9 and 6.5 kJ/m², respectively. Thus the initiation toughness values based on the MS method (both uncorrected and corrected) are lower for PP-B than for PP-R, whereas the averaged values obtained for the LS method are similar.

In order to find a physical explanation for the $J_{0,th}$ values determined SEM pictures with a magnification of 1000 were taken. The images are shown in Figs. 16 and 17. PP-B has a quite coarse structure near the initial notch. Near the crack tip some blunting mechanism is observable by small fibrils which are oriented in the crack growth direction. Hence, morphology of crack tip blunting instead of real crack growth can be assumed near the crack tip. After the first few µm of crack propagation, the amount of plastic deformation seems to increase. Moreover, an additional effect is visible on the fracture surfaces of PP-B: apparent surface cracks, which are roughly parallel to the crack front. These cracks are links to further crazes, which were formed during the crack propagation process. The formation of multiple crazes ahead of the crack tip is reported in the literature e.g. for PP-B [30] and iPP [13]. For illustration purposes the effect is shown in Fig. 18. With increasing distance to the razor blade notch, the spacing between the surface cracks increases. This is interpreted as decrease of the “multiple crazing” effect. The texture of the fracture surface of PP-R on the other hand indicates more pronounced plastic deformation near the notch which is related to a blunting process. After the first few µm of crack growth, the fracture surfaces of PP-R change to a rather smooth appearance, which remains until the end of the test (Fig. 17).

The surface textures of the fracture surfaces fit quite well to the J-R curves of PP-B and PP-R (Figs. 4 and 5) and the corresponding results in Table 3 and Table 4. The $J_{0,th}$ values, which are related to crack initiation or very small levels of crack propagation, are higher for PP-R (ductile behaviour near the notch) than for PP-B (brittle behaviour near the notch). Obviously, “multiple crazing” of PP-B has no effect yet. Subsequently, the next parameter determined on the crack propagation path is $J_{0,2}$ (J-integral for 0.2 mm of crack extension). This value was found to be higher for PP-B than for PP-R. This is attributed to a strong contribution of the “multiple crazing” effect at the beginning of crack propagation in PP-B. Obviously, this effect dissipates more energy than the plastic deformation in PP-R (Fig. 18). However, the $dJ/d\Delta a$ value at $\Delta a = 0.2$ mm (slightly higher for PP-R than for PP-B) and the J-R curve (constant slope for PP-R, varying slope for PP-B) are a strong indication that the effect of “multiple crazing” in PP-B decreases slightly with continuing crack propagation. On the other hand, for PP-R the fracture surface texture remains rather unchanged after 50–100 µm (Figs. 16 and 17) which seems to be reflected in the resulting J-R curve (slope in J-R curve does not change).

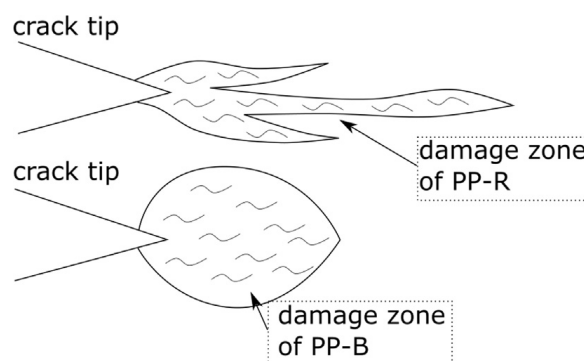


Fig. 18. Damage zones observed in front of cyclically loaded crack tips of PP-B and PP-R according to [13,30,45,46].

4. Conclusion

The crack resistance (J-R) curve of Polypropylene measured at room temperature reveals a significant amount of scattering, due to the vicinity to the glass transition temperature of this material. This behaviour was also found in the current study. The characterization using only the multi-specimen method only, where the measurement of the crack growth Δa has a major influence on the results, proved rather difficult. With the load separation method it was possible to calculate a whole J-R curve with one sharp notched and one blunt notched specimen. However, the J-R curves from the load separation method obtained for the individual specimens also showed significant scattering for the materials tested.

To reduce the data scattering two correction procedures for the J-R curves from the multi-specimen method were used. First, the correction with the Δa – time plot was applied, to ensure steady state crack propagation in the tests, which is a precondition for the use of the J-integral. This experimental procedure excludes data points with different fracture behaviour and crack speeds. The application of this procedure is rather easy and it should be used every time the multi-specimen method is conducted. A disadvantage here is the subjectivity of the criterion for the data point exclusion. A discussion of a more objective criterion (confidence intervals) within the scientific community is suggested. The second correction procedure used was based on the load separation method. Here all specimens with J-R curves, which either did not fulfil the power law fit precondition or which showed a strongly deviating curve shape were removed from the data set of the J-R curve obtained via MS method. This correction procedure excluded more data points than the Δa -time plot procedure for tested materials.

The application of the statistical approach (Weibull analysis) to evaluate a threshold toughness parameter $J_{0,th}$ worked well for both materials investigated. The resulting $J_{0,th}$ values were compared with SEM images and they could be successfully correlated to the corresponding fracture surface textures. However, a higher number of specimens is suggested to avoid invalid results (e.g. 0 kJ/m²) due to statistical results.

Additionally, a still rather unconventional approach, the normalized load separation curve, was analysed for its slope in the crack propagation region. The so-called m_s -parameter was determined to characterize the crack propagation as a function of the amount of plastic displacement. This parameter was rather constant for all tested samples of PP-B. For PP-R the values of the m_s -parameter showed comparatively high scatter which was related to the high crack asymmetry found for this material.

The crack resistance (J-R) curves determined for PP-R and PP-B at room temperature allow the following conclusions for the different approaches examined:

- I. Both, the multi-specimen method as well as the load separation method lead to high data scattering in the data points.
- II. By using the correction procedures discussed in this study, it is possible to reduce the data scattering and exclude measurements with vastly different fracture behaviour.
- III. The statistical Weibull analysis provided an initiation toughness parameter $J_{0,th}$ to describe fracture initiation.
- IV. The normalized load separation curves and the corresponding m_s -parameter gave information about the uniformity of the crack growth process.
- V. The use of the load separation method to characterize a J-R curve of PP close to the glass transition temperature, without a combined multi specimen method, is not recommended.

For the two types of Polypropylene investigated some differences were found. The region of stable crack growth was clearly visible for PP-B, while for PP-R the crack front could not always be precisely determined. PP-R showed significant crack-asymmetry in both, the fracture surfaces and the corresponding m_s -parameter. Generally, it was possible to describe the fracture behaviour of PP-B and PP-R with three parameters (the threshold toughness parameter $J_{0,th}$, the initiation toughness $J_{0,2}$ and the slope of the J-R curve at 0.2 mm crack propagation $dJ/d\Delta a$), which describe different regions of the fracture behaviour. It was found that for PP-R the threshold toughness parameter $J_{0,th}$ is higher, the $J_{0,2}$ value is smaller and the slope $dJ/d\Delta a$ is steeper compared to the corresponding values of PP-B. These quantitative fracture parameters were also compared with SEM images of the fracture surfaces of both materials. A good correlation between these parameters, the J-R curves and the textures on the fracture surfaces was found for both materials.

Acknowledgement

The research work of this paper was performed at Materials Science and Testing of Polymers/Montanuniversitaet Leoben within the framework of the COMET-program of the Federal Ministry for Transport, Innovation and Technology and the Federal Ministry of Science, Research and Economy with contributions by the Polymer Competence Center Leoben GmbH.

Appendix A. Supplementary material

Supplementary data associated with this article can be found, in the online version, at <http://dx.doi.org/10.1016/j.engfracmech.2018.06.002>.

References

- [1] Kim GM, Michler GH, Gahleitner M, Fiebig J. Relationship between morphology and micromechanical toughening mechanisms in modified polypropylenes. *J Appl Polym Sci* 1996;60:1391–403.
- [2] Gaymans RJ. Fracture of polypropylene I. The effect of molecular weight and temperature at low and high test speed. *Polymer* 1998;39:5467–75.
- [3] Radusch HJ. Fracture characteristics and deformation behavior of heterophasic ethylene-propylene copolymers as a function of the dispersed phase composition. *Polymer* 2005;46:9411–22.
- [4] Starke JU, Michler GH, Grellmann W, Seidler S, Gahleitner M, Fiebig J, et al. Fracture toughness of polypropylene copolymers: influence of interparticle distance and temperature. *Polymer* 1997;39:75–82.
- [5] Karger-Kocsis J, Varga J, Ehrenstein GW. Comparison of the fracture and failure behavior of injection-molded A- and B-Polypropylene in high-speed three-point bending tests. *J Appl Polym Sci* 1997;64:2057–66.
- [6] Fayolle B, Tcharkhtchi A, Verdu J. Temperature and molecular weight dependence of fracture behaviour of polypropylene films. *Polym Test* 2004;23:939–47.
- [7] Fasce LA, Frontini PM, Wong SC, Mai YW. Polypropylene modified with elastomeric metallocene-catalyzed polyolefin blends: fracture behavior and development of damage mechanisms. *J Polym Sci Part B Polym Phys* 2004;42:1075–89.
- [8] Tjong SC, Shen JS, Li RK. Impact fracture toughness of beta-form polypropylene. *Scr Metall* 1995;33:503–8.
- [9] Frontini P, Santarelli E. The effects of specimen size and testing conditions on fracture toughness evaluation of polypropylene homo polymer. *Polym Eng Sci* 2001;41:1803–14.
- [10] Fasce L, Pettarin V, Bernal C, Frontini P. Mechanical evaluation of propylene polymers under static and dynamic loading conditions. *J Appl Polym Sci* 1999;74:2681–93.
- [11] Lapique F, Meakin P, Feder J, Jossang T. Relationships between microstructure, fracture-surface morphology, and mechanical properties in ethylene and propylene polymers and copolymers. *J Appl Polym Sci* 2000;2370–82.
- [12] Grellmann W, Seidler S, Jung K, Kotter I. Crack-resistance behavior of polypropylene copolymers. *J Appl Polym Sci* 2001;79:2317–25.
- [13] Gensler R, Plummer C, Grein C, Kausch H-H. Influence of the loading rate on the fracture resistance of isotactic polypropylene and impact modified isotactic polypropylene. *Polymer* 2000;41:3809–19.
- [14] Salazar A, Frontini PM, Rodriguez J. Determination of fracture toughness of propylene polymers at different operating temperatures. *Eng Fract Mech* 2014;126:87–107.
- [15] Fernando PL, Williams JG. Plane stress and plane strain fractures in polypropylene. *Polym Eng Sci* 1980;20:215–20.
- [16] Berer M, Pinter G, Feuchter M. Fracture mechanical analysis of two commercial polyoxymethylene homopolymer resins. *J Appl Polym Sci* 2014;131:1–15.
- [17] Berer M, Pinter G. Determination of crack growth kinetics in non-reinforced semi-crystalline thermoplastics using the linear elastic fracture mechanics (LEFM) approach. *Polym Test* 2013;32:870–9.
- [18] Arbeiter F, Schrittmesser B, Frank A, Berer M, Pinter G. Cyclic tests on cracked round bars as a quick tool to assess the long term behaviour of thermoplastics and elastomers. *Polym Test* 2015;45:83–92.
- [19] Frank A, Freimann W, Pinter G, Lang RW. A fracture mechanics concept for the accelerated characterization of creep crack growth in Pe-Hd pipe grades. *Eng Fract Mech* 2009;76:2780–7.
- [20] Agarwal BD, Patro BS, Kumar P. J-Integral as fracture criterion for short fibre composites: an experimental approach. *Eng Fract Mech* 1984;19:678–84.
- [21] Hale GE, Ramsteiner F. J-Fracture toughness of polymers at slow speed. In: Blackman B, Davies P, Moore DR, Pavan A, Reed P, Williams JG, editors. *Fracture mechanics testing methods for polymers, adhesives and composites*, Kidlington, Oxford; 2001, p. 123–57 En.
- [22] Ernst H, Paris PC, Landes JD. Estimations on J-integral and tearing modulus T from A single specimen test record. *American Society of Testing And Materials* 1981. p. 476–502.
- [23] Ernst H, Paris PC, Rossow M, Hutchinson JW. Analysis of load-displacement relationship to determine J-R curve and tearing instability material properties. *American Society of Testing And Materials*; 1979. p. 581–99.
- [24] Salazar A, Rodriguez J, Segovia A, Martinez AB. Influence of the notch sharpening technique on the fracture toughness of bulk ethylene-propylene block copolymers. *Polym Test* 2010;29:49–59.
- [25] Wainstein J, Frontini PM, Cassanelli AN. J-R curve determination using the load separation parameter Spb method for ductile polymers. *Polym Test* 2004;23:591–8.
- [26] Salazar A, Rodriguez J. The use of the load separation parameter Spb method to determine the J-R curves of polypropylenes. *Polym Test* 2008;27:977–84.
- [27] Wainstein JE, Cocco RG, De Vedia LA, Cassanelli AN. Influence of the calibration points on the spb parameter behavior. *J Test Eval* 2007;35.
- [28] Baldi F, Agnelli S, Rico T. On the determination of the point of fracture initiation by the load separation criterion in J-testing of ductile polymers. *Polym Test* 2013;32:1326–33.
- [29] Bernal CR, Cassanelli AN, Frontini PM. A simple method for J-R curve determination in abs polymers. *Polym Test* 1995;14:85–96.
- [30] Arbeiter FJ, Frank A, Pinter G. Influence of molecular structure and reinforcement on fatigue behavior of tough polypropylene materials. *J Appl Polym Sci* 2016;133.
- [31] Borealis Polyolefine GmbH. BA202E: polypropylene block copolymer for non-pressure pipes. Material Data Sheet HA.
- [32] Borealis Polyolefine GmbH. Polypropylene BE 50: polypropylene homopolymer for non pressure pipes and extruded sheets. Material Data Sheet EN.
- [33] Borouge. Polypropylene RA130E: polypropylene random copolymer for pressure pipes systems. Material Data Sheet VI.
- [34] Esis Publication 28. Fracture mechanics testing methods for polymers adhesives and composites. Oxford, UK; 2001.
- [35] Salazar A, Rodriguez J, Martinez Ab. The role of notch sharpening on the J-fracture toughness of thermoplastic polymers. *Eng Fract Mech* 2013;101:10–22.
- [36] Baldi F, Agnelli S, Blackann BR, Castellani L, Frontini PM, Laiariandrasana L, et al. Application of the load separation criterion in j-testing of ductile polymers: a round-robin testing exercise. *Polym Test* 2015;44:72–81.
- [37] ESIS procedure for determining the fracture behaviour of materials. Geesthacht: ESIS European Structural Integrity Society; 1992.
- [38] Lach R, Krolopp T, Hutar P, Grellmann W. Influence of the interface and the additional layer on the stable crack propagation through polyolefin bilayered structures. *Proc Mater Sci* 2014;3:867–72.
- [39] Lach R, Grellmann W. Time-and temperature-dependent fracture mechanics of polymers: general aspects at monotonic quasi-static and impact loading conditions. *Macromol Mater Eng* 2008;293:555–67.
- [40] Lach R, Seidler S, Grellmann W. Resistance against the intrinsic rate of fracture mechanics parameters for polymeric materials under moderate impact loading. *Mech Time-Depend Mater* 2005;9:103–19.
- [41] Cocco RG, Frontini PM, Perez Ipina JE. Fracture toughness of polymers in the ductile-to-brittle transition region: statistical approach and lower bound determination. *J Polym Sci Part B Polym Phys* 2005;43:3674–84.
- [42] Cocco RG, Frontini PM, Perez Ipin JE. Threshold toughness of polymers in the ductile to brittle transition region by different approaches. *Eng Fract Mech* 2007;74:1561–78.
- [43] Baldi F, Agnelli S, Ricco T. On the applicability of the load separation criterion in determining the fracture resistance (JIC) of ductile polymers at low and high loading rates. *Int J Fract* 2010;165:105–19.
- [44] Frontini PM, Fasce LA, Rueda F. Non linear fracture mechanics of polymers: load separation and normalization methods. *Eng Fract Mech* 2012;79:389–414.
- [45] Seidler S, Koch T, Kotter I, Grellmann W. Crack tip deformation and toughness in polypropylenes, ICF10. Honolulu, Hawaii; 2001.
- [46] Seidler S, Koch T, Kotter I, Grellmann W. Crack initiation behaviour of PP-materials, ECF13. San Sebastian; 2000.

Publication 2

Bibliographic information

Title: J-testing of polymers via the load separation criterion based ESIS TC4 procedure: Effect of the specimen size

Authors: Anja Gosch¹, Florian J. Arbeiter¹, Silvia Agnelli³, Michael Berer², Gerald Pinter^{1,2}, Francesco Baldi³

Affiliation:

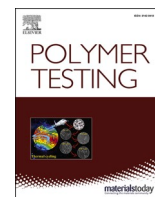
1. Materials Science and Testing of Polymers, Montanuniversitaet Leoben, Otto Glöckel-Strasse 2, 8700 Leoben, Austria
2. Polymer Competence Center Leoben GmbH, Roseggerstr. 12, 8700 Leoben, Austria
3. Dipartimento di Ingegneria Meccanica e Industriale, Università degli Studi di Brescia, Via Branze 38, Brescia 25123, Italy

Periodical: Polymer Testing

DOI: doi.org/10.1016/j.polymertesting.2020.106637

Relevant contributions to this publication

| | |
|-----------------------------|---|
| Conceptualization: | Anja Gosch, Florian Arbeiter, Silvia Agnelli, Francesco Baldi |
| Methodology: | Anja Gosch, Francesco Baldi |
| Validation: | Anja Gosch |
| Investigation: | Anja Gosch |
| Writing - Original Draft: | Anja Gosch |
| Writing - Review & Editing: | Florian Arbeiter, Silvia Agnelli, Michael Berer, Gerald Pinter, Francesco Baldi |



Test Method

J-testing of polymers via the load separation criterion based ESIS TC4 procedure: Effect of the specimen size

Anja Gosch^a, Florian J. Arbeiter^{a,*}, Silvia Agnelli^c, Michael Berer^b, Gerald Pinter^a, Francesco Baldi^c

^a Materials Science and Testing of Polymers, Montanuniversitaet Leoben, Otto-Gloeckel-Str. 2, 8700, Leoben, Austria

^b Polymer Competence Center Leoben GmbH, Roseggerstr. 12, 8700, Leoben, Austria

^c Dipartimento di Ingegneria Meccanica e Industriale, Università Degli Studi di Brescia, Via Branze 38, Brescia, 25123, Italy

ARTICLE INFO

Keywords:

J-integral

Load separation criterion

Scaling effects

ABS (Acrylonitrile-butadiene-styrene)

ABSTRACT

The Technical Committee 4, “Polymers, Polymer Composites and Adhesives”, of the European Structural Integrity Society (ESIS TC4) developed a draft protocol based on the load separation criterion to determine two fracture parameters (an initiation parameter, $J_{I,lim}$, and a crack growth parameter, m_s) without the need to measure the crack growth (Δa). This is especially beneficial, since the measurement of Δa is prone to errors. The developed testing scheme displays promising results, as shown in a round-robin testing exercise. To further push this testing scheme, it is necessary to verify the specimen size scaling possibility. Hence, in this work, single edge notched in bending (SE(B)) specimens with different sizes, but geometrically similar, were manufactured. ESIS TC4 testing scheme was successfully applied to specimens with the different sizes, and data of $J_{I,lim}$ and m_s were obtained. The observed effect of the specimen size on the aforementioned fracture parameters is presented and discussed.

1. Introduction

Detailed knowledge of the material specific fracture behaviour is an important step towards a successful application of an engineering component. However, for polymeric materials exhibiting high amounts of plastic deformation and non-linear behaviour, fracture mechanics testing approaches able to provide reliable results are still under development. Generally, methods from elastic plastic fracture mechanics (EPFM) are needed for these materials. EPFM introduces the parameter “J-Integral” to evaluate the energy required to produce crack growth (Δa). Typically, the crack growth resistance curve (J-R curve), where the J-Integral is plotted against the crack growth Δa , is determined. Based on the J-R curve, several fracture parameters such as $J_{0.2}$ (J-Integral at 0.2 mm crack growth), J_{bl} (blunting value in the J-R curve) and the slope of the J-R curve, $dJ/d\Delta a$, (crack growth resistance) can be determined. The combination of these parameters describes the fracture behaviour of a material and is used as a basic information for component design and simulations based on fracture mechanics.

ESIS TC4 developed a procedure to determine the J-R curve with the so called multi-specimen approach [1], where several nominally

identical specimens are tested in a way to obtain different amounts of crack growth, Δa . This procedure is technically equivalent to that described by ASTM D6068 [2]. The multi-specimen approach displays a high specimen consumption and the results are strongly influenced by the uncertainties from the measurement of Δa , as shown in previous research [3]. Hence, the reliability of the multi-specimen method can be very low and new methods, where the measurement of Δa is no longer required, are of high interest. The single-specimen approaches most commonly examined, the application of which requires only few specimens, are based on the load separation criterion [4], and their application to polymers was verified in previous studies [5–10]. ESIS TC4 decided to investigate the possibility to strengthen the results from the multi-specimen method [1] with two additional fracture parameters determined by means of a load separation criterion-based approach, to characterize the fracture initiation process and the crack growth. Based on this approach (called TC4 LS-method hereafter) the following parameters are proposed: for the fracture initiation, the initiation toughness value $J_{I,lim}$ (fracture resistance parameter) and, to characterize the crack growth, the parameter m_s (it provides a rough measure of Δa per unit of plastic displacement). The reproducibility of the procedure was

* Corresponding author.

E-mail address: florian.arbeiter@unileoben.ac.at (F.J. Arbeiter).

<https://doi.org/10.1016/j.polytest.2020.106637>

Received 2 April 2020; Received in revised form 4 May 2020; Accepted 18 May 2020

Available online 24 May 2020

0142-9418/© 2020 Elsevier Ltd. All rights reserved.

verified in a round-robin test under the direction of ESIS TC4. In this study, the testing scheme was successfully applied to two different materials, and encouraging results were obtained. The detailed test procedure and the results from the round-robin activity were published in literature [11].

The influence of scaling specimen sizes on the results of the described TC4 LS-method has to be assessed and compared to other methods, to further push this new approach dealing with m_s and $J_{I,lim}$. It is known from literature [12], that different specimen geometries and sizes lead to changes in the constraint level (degree of triaxiality) in front of the crack tip, and therefore to different fracture responses at a macroscopic scale (experimentally evidenced also for ductile materials [13–16]). This aspect is especially important for component design, where the results from laboratory tests are used for the development of real-life applications. Hence, the analysis of the ability of a fracture mechanics testing approach to highlight specimen size scaling effects is an important step in the development of a new method. The aim of this work is to examine the applicability of the TC4 LS-method to specimens of different sizes. A suitable polymeric material that exhibits a ductile behaviour was identified (an acrylonitrile-butadiene-styrene, ABS, resin in the form of a thick plate was chosen) and SE(B) specimens with different sizes but geometrically similar, i.e. with the same dimensionless parameters characterizing the geometry, were prepared and tested according to the TC4 LS-method. In the end, the results will provide more information on the influence of the specimen size, on the applicability of the method and on the resulting fracture parameters. Furthermore, some improvements or changes of the ESIS TC4 protocol will be suggested.

2. Theory and method

The TC4 LS-method, for which a specific draft protocol has been prepared recently by ESIS TC4 [13], is based on the load separation concept proposed by Ernst [4], and derived from Sharobeam and Landes' works published in the early 90's [14,15] on metals. The load separation concept is founded on two independent functions, the geometry function G and the material deformation function H . These two functions are able to represent the load P for a defined material, geometry and constraint (during a fracture test on a cracked specimen, in the plastic region), as in equation (1):

$$P = G\left(\frac{b}{W}\right) H\left(\frac{u_{pl}}{W}\right) \quad (1)$$

in which $G(b/W)$ is the geometry function, b is the remaining ligament length, W the specimen width and a_0 the initial notch length; $H(u_{pl}/W)$ is the material deformation function and u_{pl} the plastic displacement defined as:

$$u_{pl} = u - P C\left(\frac{b}{W}\right) \quad (2)$$

where u is the applied displacement during the experiment, P the load and $C(b/W)$ the elastic compliance of the tested specimen. In previous research [5,6,10,16,17] the applicability of the load separation concept on polymeric materials was verified for both, blunting and crack propagation phases.

The TC4 LS-method is based on the evaluation of the "load separation parameter curve" (S_{sb} curve). The procedure describes the construction of this curve from two quasi-static tests carried out on a sharp notched specimen (sN), and a blunt notched specimen (bN). The separation parameter, S_{sb} , is defined as in equation (3):

$$S_{sb} = \frac{P_s}{P_b} \Big|_{u_{pl}} \quad (3)$$

where P_s is the load of a sN specimen, P_b the load of a bN specimen. The ratio is built at the same plastic displacement u_{pl} . Regarding the

determination of u_{pl} (as shown in equation (2)), the protocol suggests to use the initial elastic compliance C_0 value in place of the actual compliance, $C(b/W)$.

Following the TC4 LS-method, the tested specimens have to be of the same dimensions. Finally, the S_{sb} curve is constructed by plotting the load separation parameter S_{sb} as a function of the plastic displacement (shown in Fig. 1a). This curve shows three characteristic regions presented in Fig. 1a: (I) the unseparable region at low values of u_{pl} , (II) the "plateau" region which represents the blunting process before the crack starts to grow and (III) the propagation region, where crack growth occurs in the sN specimen.

According to the TC4 LS-method [13], developed for the SE(B) specimen geometry (see Fig. 2a), it is possible to determine a fracture initiation parameter, that is called $J_{I,lim}$. The $J_{I,lim}$ value is determined from the load displacement curve of the sN specimen with the help of the S_{sb} -curve, as described in the following equation:

$$J_{I,lim} = \frac{2 U_{lim,c}}{B(W - a_0)} \quad (4)$$

$$S_{sb,pl} = 0.9975 S_{sb,max} \quad (5)$$

where B is the specimen thickness and $U_{lim,c}$ is the area under the load-displacement curve up to the limit point u_{lim} (corrected for indentation and machine compliance as described in Ref. [1]), which is corresponding to the limit plastic displacement $u_{pl,lim}$ on the S_{sb} -curve (see Fig. 1). The procedure for the identification of $u_{pl,lim}$ changes according to the type of S_{sb} curve, as described in the TC4 LS-method. First of all, the plateau value of the load separation curve, $S_{sb,pl}$, is required. In this study a broad peak after the unseparable region was found in the S_{sb} -curves, as shown in Fig. 1. This is a typical S_{sb} -curve of "type 2" described in the TC4 LS-method. Hence, the plateau value, $S_{sb,pl}$, is evaluated after the maximum point in the S_{sb} -curve Eq 5, $S_{sb,max}$, as:

The limit plastic displacement, $u_{pl,lim}$, is determined with equations Eq 6 and 7:

$$S_{sb,lim} = 0.9950 S_{sb,max} \quad (6)$$

$$u_{pl,lim} = u_{pl}(S_{sb,lim}) \quad (7)$$

Finally, u_{lim} is calculated from $u_{pl,lim}$ with the help of equation (2) and was taken as the point of fracture initiation. Once the point of fracture initiation is known, the $U_{lim,c}$ value is determined and corrected for indentation and machine compliance as proposed in the ESIS TC4 multi-specimen procedure [1]. The correction curve (evaluated on an identical but unnotched sample) is subtracted from the evaluated load-displacement curve of the investigated sharp notched specimen. In the end, the initiation value $J_{I,lim}$ can be determined as proposed in equation (4).

The second parameter recommended in the TC4 LS-method, is the parameter m_s , which indicates the crack advancement produced per unit of plastic displacement (shown in Fig. 1b). This parameter can be used to estimate the crack growth behaviour before applying a whole multi-specimen procedure to evaluate the crack growth curve. Hence, the parameter m_s is a great tool to rank the crack growth behaviour exhibited by a specimen in a fracture test. Therefore, the normalized load separation parameter, R_s , is defined as shown in equation Eq 8.

$$R_s(u_{pl}) = \frac{S_{sb}(u_{pl})}{S_{sb,pl}} \quad (8)$$

where S_{sb} is the load separation parameter and $S_{sb,pl}$ is the plateau value as described in the previous section. The parameter m_s is evaluated in the region III of the normalized load separation curve (R_s depending on u_{pl}) as the opposite of the slope Eq 9.

$$m_s = \frac{dR_s}{du_{pl}} \Big|_{u_{pl} > u_{pl,lim}} \quad (9)$$

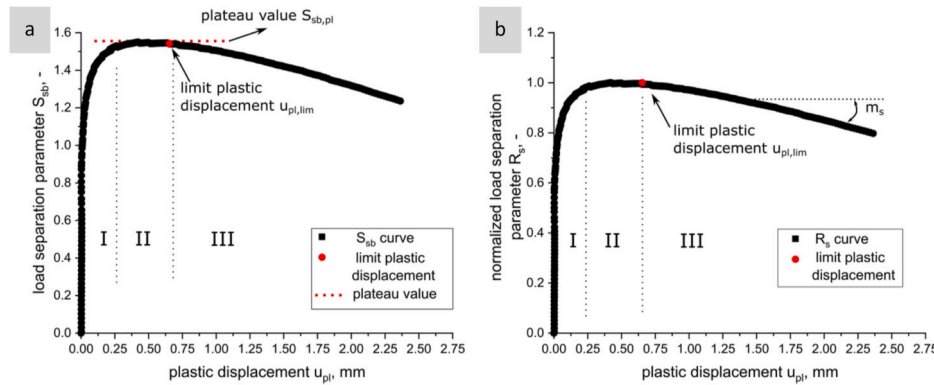


Fig. 1. Example of a load separation S_{sb} curve (a) and of a normalized load separation R_s curve (b). The three regions, the limit point at $u_{pl,lim}$, the plateau value $S_{sb,pl}$ and the parameter m_s are displayed.

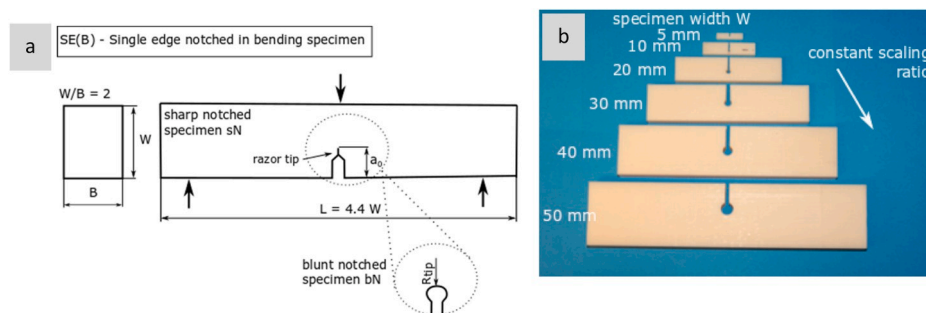


Fig. 2. (a) Scheme of blunt notched and sharp notched SE(B) specimen geometry; (b) example of the blunt notched ABS-specimens manufactured with constant scaling ratio.

This parameter indicates the crack advancement produced per unit of plastic displacement and is dependent on both specimen geometry and material. The parameter m_s can be used as “ductility index”, where with increasing m_s the crack advancement Δa per unit of plastic displacement u_{pl} increases and in the case of pure blunting the parameter m_s is 0.

3. Experimental

3.1. Specimen scaling

In order to prove scaling effects, specimens of different sizes but geometrically similar were manufactured. The examined specimen geometry was SE(B) (see Fig. 2a). Both sN and bN specimens were tested. The specimen scaling was realized from a width, W , of 5 mm–50 mm. A picture of the scaling bN SEN(B) specimens is presented in Fig. 2b. The specimen width to thickness ratio, W/B , as well as the length (L) to width ratio, L/W , were kept constant for all the sizes. These ratios were chosen according to Ref. [1] as 2 and 4.4, respectively. The initial crack length (a_0) over width, a_0/W , ratio was fixed at 0.6 for both sN and bN specimens.

3.2. Material

The material under investigation in this work was an ABS supplied as an extruded plate with a thickness of 50 mm. The length of the plate was 1200 mm with a width of 500 mm. The high thickness of the plate was necessary to realize a high scaling ratio of the manufactured specimens. The ABS-plate is commercially available at Faigle Kunststoffe GmbH (Austria).

3.3. Specimen preparation

SE(B) specimens were manufactured from the plate in a way that the fracture process zone (at the crack tip), once the specimen had been notched, resulted at a fixed x_3 -level of the plate (ref. to Fig. 3, where W_p indicates the thickness of the plate along the x_3 -axis direction), that is at $x_3 = W_p/2$ (mid-thickness of the plate). This is especially important, since some differences were detected in the mechanical behaviour of the material from core and external surfaces of the plate, as reported in the Appendix. The bars for the preparation of the specimens were obtained from the plate via cutting and milling.

As discussed in literature, the notching procedure has a significant influence on the results of fracture mechanical tests [18,19]. Thus the chosen notching procedure for the sN specimen was broaching, which has shown promising results in literature [20]. A commercial microtome was adapted with a razor blade and, by sliding the blade along the notch front, a sharp uniform crack tip was obtained. The length of this sharp notch was roughly 1 mm. The correct value used for the subsequent calculations was verified after testing via optical microscopy. The blunt notch was produced as a key-hole. The round hole was drilled. The notch tip radius, r_{tip} , was changed according to the specimen size, as listed in Table 1.

3.4. Testing procedures

Three-point bending tests were conducted on the notched specimens. All the tests were performed on a Zwick Universal Testing System (Zwick GmbH & Co.KG, Germany), model Z010 and Z250, using load cells with different capacities as shown in Table 1. The measurements were done at 23 °C and with a constant crosshead speed of 1 mm/min. In the SE(B) tests, the span, S , was varied in such a way that the span to specimen width ratio, S/W , kept a constant value of 4 for the various sizes. The

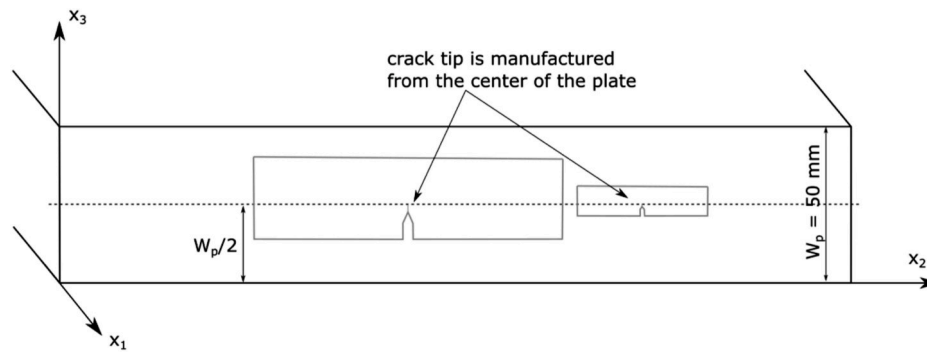


Fig. 3. Scheme of the specimen manufacturing from the centre of the ABS-plate.

Table 1

Test configuration details and bN specimen notch tip radius for the different specimen sizes examined.

| Specimen width W | Span S | Roller radius R | Load cell capacity | Notch tip radius of bN specimen rtip |
|------------------|--------|-----------------|--------------------|--------------------------------------|
| [mm] | [mm] | [mm] | [kN] | [mm] |
| 5 | 20 | 1 | 1 | 0.5 |
| 10 | 40 | 3 | 10 | 1 |
| 20 | 80 | 3 | 10 | 2 |
| 30 | 120 | 5 | 10 | 3 |
| 40 | 160 | 5 | 10 | 4 |
| 50 | 200 | 10 | 10 | 5 |

diameter of the rollers was chosen depending on the specimen size.

In order to check the reproducibility of the results obtained by the application of the TC4 LS-method, fifteen sN specimen and one single bN specimen were tested for each size examined. The ESIS TC4 multi-specimen method was also tentatively applied [1] and, to this aim, the results from the sN specimens were used. To generate different levels of crack growth, for each size, the tests were interrupted at different levels of displacement. After testing the specimens were cryo-fractured and the crack length Δa was identified on the fracture surface as the average value of four measurements distributed equidistantly along the notch. To this aim, an optical microscope SZX12 from Olympus (Olympus Europa SE & CO. KG, Germany) was used. The optical microscope was also used to evaluate the plastic zone radius on the specimen surface.

For each specimen size examined, specific indentation correction tests were carried out on unnotched bars as described in Ref. [1], and the results were used to correct the J -integral values.

4. Results and discussion

4.1. Application of the ESIS TC4 load separation method

For the ABS examined here, the validity of the load separation criterion is assumed, based on previously published works that confirmed the load separation property for several ductile polymers, including ABS [5,7,10,16,21]. The TC4 LS-method requires load, P , vs displacement, u , curves from sN and bN specimens. Fig. 4 provides an overview of the P - u curves obtained from scaling sN specimens. One representative curve is shown for each tested size ($W = 5, 10, 20, 30, 40$ and 50 mm). All specimen sizes tested display non-linear P - u traces, and stable fracture behaviour was observed. Generally, a low amount of data scattering was determined for all the specimen sizes. As expected, with increasing specimen size, the load at a given applied displacement rises. A similar effect was observed also for the curves from the bN specimens. However, crack growth is prevented in the bN specimens by the round crack tip. This was verified for every bN specimen after testing by means of optical microscopy analyses, and it is a precondition for the application of the

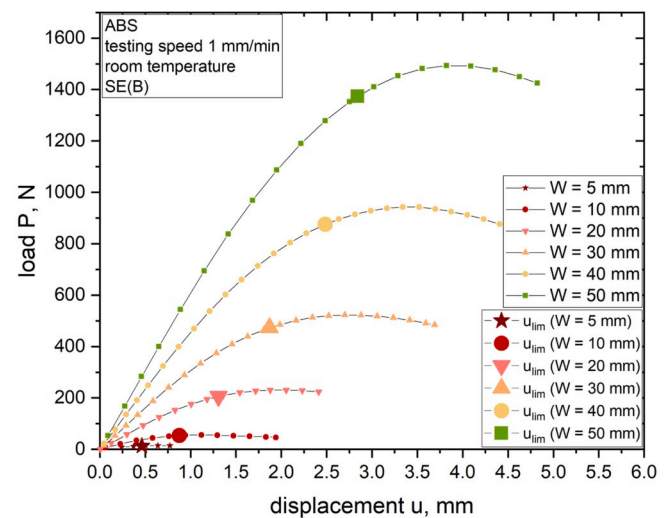


Fig. 4. Load P – displacement u curves obtained from sharp notched specimens of ABS, tested at room temperature at different sizes (width $W = 5, 10, 20, 30, 40$ and 50 mm) with the marked position of the limit point, at u_{lim} .

LS-method.

On each curve in Fig. 4, the corresponding limit point, which should indicate fracture initiation, is also highlighted (at u_{lim}), as determined by the application of the TC4 LS-method (details in section 2). According to the beam theory (elastic material), in three-point bending tests the level of displacement achieved to ensure a given level of strain is proportional to the specimen width, W . This is only valid for unnotched specimens with different sizes and tested keeping the span to width ratio, S/W , fixed. Hence, by supposing that a given minimum level of nominal strain should be reached at the crack tip to promote fracture in the notched specimens here tested (at u_{lim}), higher amounts of displacement are expected for larger specimen sizes to produce crack growth. This is qualitatively confirmed by the position of u_{lim} (the bigger the size, the higher the displacement at the limit point, u_{lim}) as shown in Fig. 4. However, the actual effect of the specimen size on the nominal strain at fracture initiation will be discussed in more detail below, in the section where $J_{I,lim}$ data are discussed.

Based on the P - u curves obtained, the load separation parameter, S_{sb} , and the normalized load separation parameter, R_s , were calculated and plotted as a function of u_{pl} (details for the procedure in section 2). The R_s curves constructed for the fifteen different sN specimens of two of the six sizes examined are shown in Fig. 5. The smallest ($W = 5$ mm, Fig. 5a) and the largest ($W = 50$ mm, Fig. 5b) specimen size are presented.

The curves in Fig. 5 display the characteristic trend expected for a load separation parameter curve (see Fig. 1). For both sizes in Fig. 5, a relatively low amount of scattering in the R_s curves was observed, and

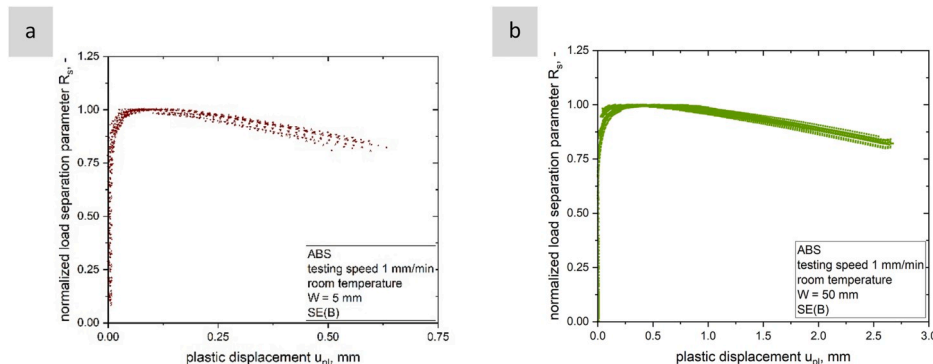


Fig. 5. R_s curves obtained from specimens with width W of 5 mm (a) and 50 mm (b); all fifteen repetitions are reported.

similar degrees of scattering were also obtained for the other specimen sizes in between ($W = 10, 20, 30$ and 40 mm). From Fig. 5, it can be observed that the specimens with $W = 50$ mm were exposed to remarkably higher amounts of plastic displacement u_{pl} compared to the smaller specimens with $W = 5$ mm. A comparison of the determined R_s curves of all tested sizes is given in Fig. 6.

For every size a representative R_s curve was chosen. The specimen size effect on the R_s curve emerges clearly; more specifically, by increasing the specimen size: region I in the R_s -curve expands up to higher values of u_{pl} ; the plateau (region II) becomes longer; the slope of the curve in region III, and hence the value of m_s , decreases (refer to Fig. 1b). In Fig. 7, the R_s data of the curves of Fig. 6 have been plotted as a function of u_{pl}/W . Interestingly, the various curves plotted as in Fig. 7 practically overlap in the region I, indicating that the level of u_{pl} that has to be reached in order to complete the development of the plastic pattern is controlled only by the specimen size. Similar results were determined for the extension of the plateau region (related to crack blunting) as well as for the trend of the curve in the region III (related to crack propagation), where a more complex dependence on the size is observed.

An overview about the decrease of the parameter m_s with increasing specimen size is shown in Fig. 8a. The decrease of m_s indicates a decrease in the crack growth Δa produced per unit of plastic displacement u_{pl} for the larger specimens of ABS. This effect is in agreement with literature [11]. In the analysis of the size effect observed here on m_s , which refers to crack growth in the plastic region, it is not possible to

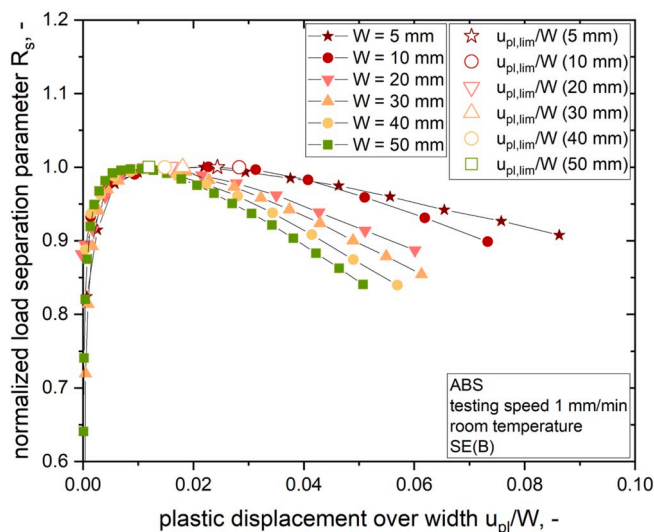


Fig. 7. Representative R_s -curves plotted as a function of the plastic displacement over the width, $u_{pl,lim}/W$, with limit point $u_{pl,lim}/W$ for the different specimen sizes ($W = 5, 10, 20, 30, 40$ and 50 mm).

separate the contribution of the material from that of the geometry. However, a possible explanation for the decreasing m_s with increasing specimen size here observed could be a simple geometrical effect. The results are reported in Fig. 8b as m_s multiplied by W ($m_s \cdot W$) plotted against W . The term $m_s \cdot W$ shows a linear increase with increasing specimen width, and this indicates that, at least in the examined range of W , the dependence of m_s over the size can be described by a very simple expression, which can in principle also be used for the estimation of m_s for sizes not examined experimentally. This result is of particular interest by considering that the m_s parameter is being given a key role in the fracture characterization of ductile polymers within ESIS TC4 [11].

$J_{I,lim}$ values were evaluated at the limit point, i.e. at $u_{pl,lim}$, according to the TC4 LS-method, for the various sizes examined. The corresponding limit points are marked on the R_s -curves in Figs. 6 and 7, and on the loading curves in Fig. 4. $J_{I,lim}$ values are shown in Fig. 8c, as a function of W . The initiation value varies with the specimen size and, more specifically, the higher the specimen size, the higher the initiation fracture resistance is. From Fig. 8c it comes out that the initiation parameter $J_{I,lim}$ displays a higher amount of scattering compared to the parameter m_s . This is based on the determination of $u_{pl,lim}$, where small variations end up in high variations of the initiation value [10]. Nevertheless, the specimen size dependence observed for the parameter $J_{I,lim}$, which should be an initiation fracture resistance parameter, was not expected [12]. $J_{I,lim}$ should have a constant value irrespective of the specimen size to be an initiation fracture resistance parameter, provided

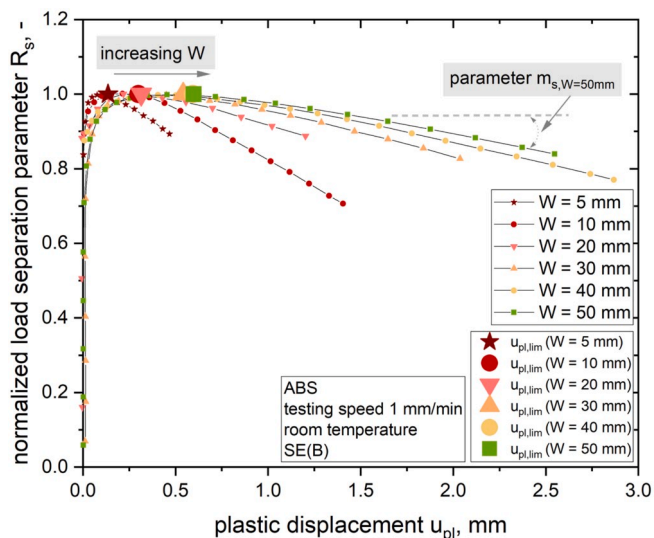


Fig. 6. Representative R_s -curves (normalized load separation parameter R_s) as a function of the plastic displacement u_{pl} with limit point $u_{pl,lim}$ for the different specimen sizes ($W = 5, 10, 20, 30, 40$ and 50 mm).

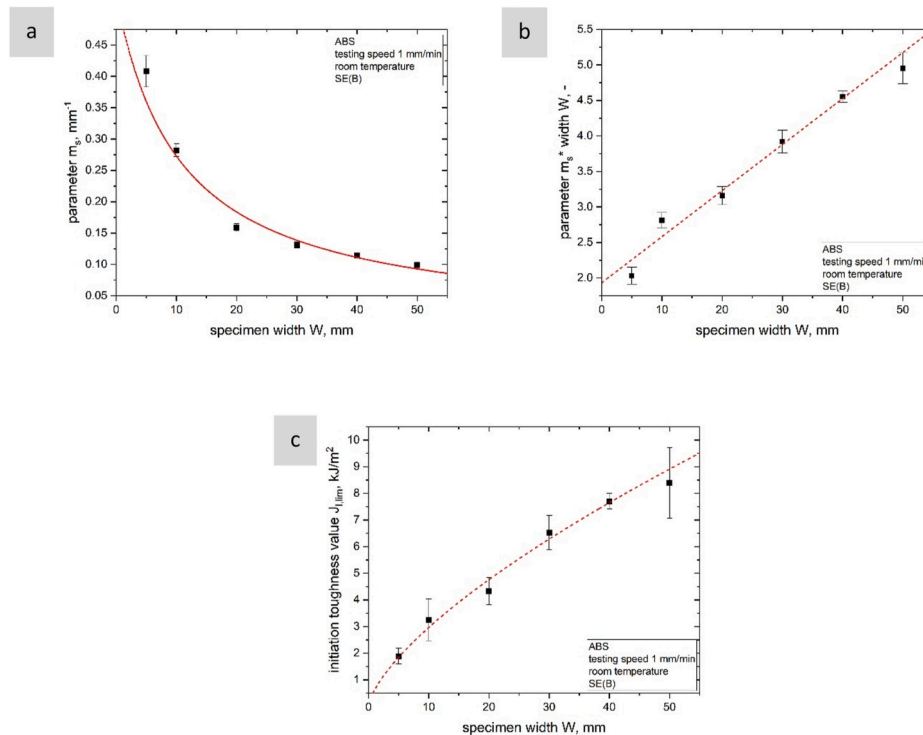


Fig. 8. Parameters m_s (a), $m_s \cdot W$ (b) and $J_{I,lim}$ (c) as a function of the specimen width, W .

the size criteria recommended in Ref. [1] for J_c validity are verified (see Table 2 for the size criteria check on the specimens tested in the present work). Probably, this size effect on $J_{I,lim}$ can be directly related to the peculiar nature of fracture initiation in the ABS examined. As underlined by Baldi et al. in Ref. [8], fracture initiation in ABS is a progressive process characterized by the slow development of the crack front across the thickness of the pre-cracked specimen, which can start even during the development of the plastic pattern. The absence of a sharp blunting-to-fracture initiation process makes the S_{sb} curve intrinsically unable to indicate a variation of crack length in the sN specimen until a small but measurable crack growth has occurred. This degree of uncertainty attributed to the ability of the S_{sb} curve to detect fracture initiation during a fracture test on a ductile polymer is expected to depend on the polymeric material examined, but also on the specimen size used. Therefore, $J_{I,lim}$ has earned the title of “pseudo-initiation” fracture resistance parameter (see also [11]). It is reasonable to suppose that the blunting-to-fracture transition might depend on the length of the crack front, which is the specimen thickness, and, consequently, the degree of effectiveness of the S_{sb} curve to detect that crack has started to grow might result size dependent. This idea seems to suggest that the procedure used here for the identification of the limit point (according to

the ESIS TC4 protocol [13]), described in section 2, and based on the use of a fixed ratio between $S_{sb,lim}$ and $S_{sb,plateau}$, should be modified. Probably a new procedure that takes into account the specific trend of the S_{sb} curve under examination should be considered. These observations will be directly forwarded to ESIS TC4.

The idea that the gradualness of the fracture initiation process might depend on the specimen size seems to be supported by the observation that different contributions of plastic deformation can be achieved to start crack growth in specimens with different sizes. Fig. 9 shows the values of apparent strain at the limit point, $\epsilon_{app,lim}$, evaluated for the different specimen sizes according to this expression:

Table 2
Determined values of plastic zone radius $r_{y,lim}$ and the optically determined plastic zone radius $r_{y,opt}$ for the investigated specimen sizes.

| Width W [mm] | Validity check ^a “B, $W-a_0 > 20 \cdot J_{I,lim}/\sigma_y$ ” ? | Plastic zone radius from $J_{I,lim}$, $r_{y,lim}$ [mm] | r_y , lim/ ($W-a_0$) [%] | Optically determined plastic zone radius, $r_{y,opt}$ [mm] |
|----------------------|--|--|---------------------------------------|---|
| 5 | ok | 0.34 | 15.2 | 0.50 |
| 10 | ok | 0.58 | 13.1 | 1.06 |
| 20 | ok | 0.79 | 8.7 | 1.40 |
| 30 | ok | 1.19 | 8.8 | 2.02 |
| 40 | ok | 1.39 | 7.8 | 2.44 |
| 50 | ok | 1.51 | 6.8 | 2.74 |

^a Size criteria recommended in Ref. [1] for J_c validity.

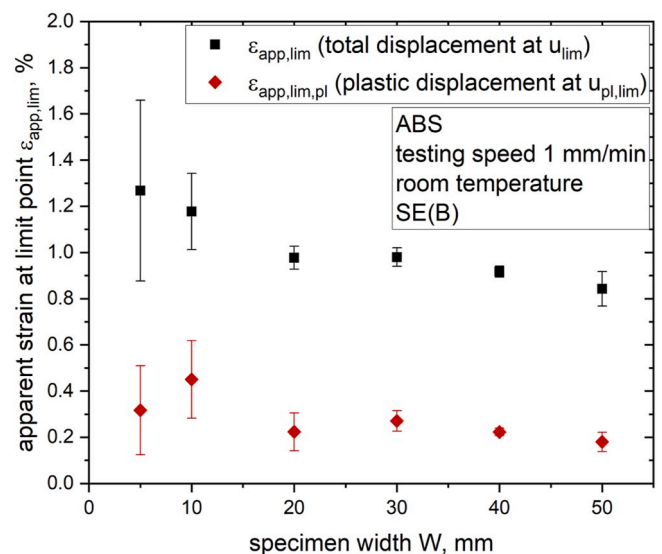


Fig. 9. Apparent strain at limit point $\epsilon_{app,lim}$ (obtained at the total displacement of the limit point, u_{lim}) and the plastic part of the apparent strain at the limit point $\epsilon_{app,lim,pl}$ (obtained at the plastic displacement of the limit point, $u_{pl,lim}$) for every examined specimen size ($W = 5, 10, 20, 30, 40$ and 50 mm).

$$\varepsilon_{app,lim} = 0.15 \frac{u_{lim}}{W} \quad (10)$$

where u_{lim} indicates the displacement at the limit point. In addition to $\varepsilon_{app,lim}$, calculated from the values of total displacement (u_{lim}), also the plastic part of $\varepsilon_{app,lim}$, indicated with $\varepsilon_{app,lim,pl}$, was determined from the plastic displacement at the limit point ($u_{pl,lim}$), and the data are plotted in Fig. 9. Eq. (10) has been obtained by assuming the specimen as a bar (elastic material) with an effective width equal to $(W-a_0)$, and considering the geometrical relationships between a_0 , W and S used in the experiments. An “apparent” character is attributed here to the strain evaluated through Eq. (10), since this equation neglects completely the stress intensification due to the notch, and it applies to elastic materials (the limit points obtained for the various sizes belong to the plastic region). The data obtained for $W = 5$ mm was put aside, because of the quite pronounced standard deviation. However, by considering the data obtained through Eq. (10) only as indexes for a comparative analysis among the various sizes, it can be observed that $\varepsilon_{app,lim}$ decreases by increasing W . $\varepsilon_{app,lim,pl}$ reduces of about 50% from $W = 10$ mm to $W = 20$ mm, whereas for higher W the size effect on $\varepsilon_{app,lim,pl}$ is less pronounced. Interestingly, the contribution of $\varepsilon_{app,lim,pl}$ in $\varepsilon_{app,lim}$ passes from the 38% for $W = 10$ mm, to the 21% for $W = 50$ mm.

In the analysis of the size effect observed for $J_{I,lim}$, also the fact, that the level of constraint undergone by the material at the crack tip might be different in the specimens of the various sizes, should be taken into account. This aspect is at present under analysis, and it is being studied by the construction of the material key curves (directly related to the material deformation function, H (see Eq. (1)), following [22]. The fact that the material is deformed at different nominal strain rates in the specimens of the various sizes (with $W = 5$ mm, the nominal strain rate is ten times that of $W = 50$ mm) can be thought to play only a secondary role.

With respect to the critical points discussed during the evaluation of fracture initiation, it was important to investigate the use of $J_{I,lim}$ as a fracture initiation value. As discussed above, a fracture initiation parameter should be independent of geometry and size (intrinsic to the material). Therefore, two further procedures were applied to gain more information about the influence of the scaling on the fracture behaviour. The first procedure deals with the calculation of the plastic zone radius in front of the crack tip based on the $J_{I,lim}$ values and the experimental determination of the plastic zone radius on the specimens tested. This procedure gives a first impression about the validity of $J_{I,lim}$ as initiation value. The second part deals with the determination of a J-R curve composed of all geometries based on the multi-specimen procedure. This is especially important to check the general comparability of the fracture behaviour for all scaling specimens.

4.2. Initiation check – determination of the plastic zone radius

A validity check for the J-value at fracture initiation, J_c , is recommended in Ref. [1], to verify, a posteriori, whether J_c could be related to plane strain loading conditions and excessive plasticity in the ligament is avoided. For all the specimen sizes investigated here, this validity check to $J_{I,lim}$ data gave a positive outcome (see Table 2), suggesting that plane strain conditions along the notch front are ensured. In consideration of this, Irwin's plane strain plastic zone expression was used for the estimation of the plastic zone radius at the limit point, $r_{y,lim}$, which was calculated from $J_{I,lim}$ as shown in Eq 11 [12,23]:

$$r_{y,lim} = \frac{1}{6\pi} \frac{J_{I,lim} E}{\sigma_y^2 (1 - \nu^2)} \quad (11)$$

where E is the Young's Modulus and σ_y the tensile yield stress of the investigated material (see the Appendix), and ν the Poisson's ratio assumed equal to 0.33. The values of $r_{y,lim}$ are reported in Table 2. In addition, the ratio of $r_{y,lim}$ over the remaining ligament length $(W-a_0)$ is given for each specimen size. It emerges that, by increasing the specimen

size, the extension of the plastic zone at the limit point with respect to the remaining ligament length $(W - a_0)$ decreases; and this makes the possible specimen border-effect, if any are present, less significant.

Further, for each size, the plastic zone radius was measured optically on the lateral external surface of the specimen by means of an optical microscope. The results, indicated with $r_{y,opt}$, are also reported in Table 2. Fig. 10 provides an overview of three optical measurements of $r_{y,opt}$ directly on the specimen surface. For each size, the specimen with the lowest amount of crack growth was selected among the fifteen sN tested specimens, in such a way that $r_{y,opt}$ data could be more closely related to an ideal fracture initiation. The plastic deformation zone, in front of the crack tip, appears as a whitened region whose maximum extension along the x_2 -axis direction (refer to Fig. 3) was taken as $r_{y,opt}$. By comparing $r_{y,lim}$ with $r_{y,opt}$ for each size examined, it emerges that the former is smaller than the latter. This can be explained by considering the different stress conditions which the two different sets of data ($r_{y,lim}$ vs $r_{y,opt}$) refer to: plane strain and plane stress conditions, for $r_{y,lim}$ and $r_{y,opt}$ data, respectively). Interestingly, it can be also observed that $r_{y,opt}$ increases by increasing the specimen size, similar to $r_{y,lim}$. The size dependence observed for $r_{y,lim}$ was expected since $r_{y,lim}$ data are directly calculated from $J_{I,lim}$, by contrast the size dependence of $r_{y,opt}$ was unexpected. It is worth noting that, even if a non-zero degree of uncertainty should be attributed to the $r_{y,opt}$ data, in consideration of the difficulties intrinsically associated to the optical identification of the plastic zone (see Fig. 10), a quite pronounced difference between $r_{y,opt}$ for $W = 50$ and $r_{y,opt}$ for $W = 5$ mm is obtained (the former is more than five times the latter). This effect seems to suggest that fracture initiation actually occurs at different J-values in specimens of different sizes. The possible contribution of different degrees of constraint in specimens with different sizes cannot be ruled out. The understanding of the size effect observed for $r_{y,opt}$ requires further analyses to be carried out. The idea to focus on constraint issues is further supported.

4.3. Application of the multi-specimen method to describe the fracture behaviour

To prove the general comparability of the crack growth behaviour of all investigated specimen sizes, the ESIS TC4 multi-specimen method [1] was applied and, to this aim, the data obtained from the tests carried out on the fifteen different sN specimens were used. The tests for the application of the TC4 LS-method are not perfect for the multi-specimen procedure, since the levels of crack growth, Δa , produced in the former are typically too high. It is worth noting that high Δa levels are necessary for the proper evaluation of the parameter m_s , whereas the multi-specimen method [1] requires small Δa . It is accepted [12] that the expression here adopted for the calculation of J-value at the limit point (Eq. (4)), which is used also for the determination of J-value at the final point of the loading curve in the multi-specimen method, is valid only if the corresponding Δa is lower than $\Delta a_{max} = 0.1(W-a_0)$. Practically, no valid data point (i.e. with short Δa) is available for $W = 30, 40$ and 50 mm. In consideration of this, for the application of the multi-specimen method, the J-values at the final point of the loading curve were determined by resorting to a formula proposed in literature [4] that accounts for Δa higher than Δa_{max} , and J is determined according to Eq 12 and 13:

$$J = J_0 \left[1 - \frac{0.75 \eta - 1}{B} \Delta a \right] \quad (12)$$

$$J_0 = \frac{\eta U_c}{B (W - a_0)} \quad (13)$$

where η the geometry dependent calibration factor (2 for SE(B) specimens), U_c is the area under the load-displacement curve (corrected for indentation and machine compliance as described in Ref. [1]), B the specimen thickness, W the specimen width, a_0 the initial notch length

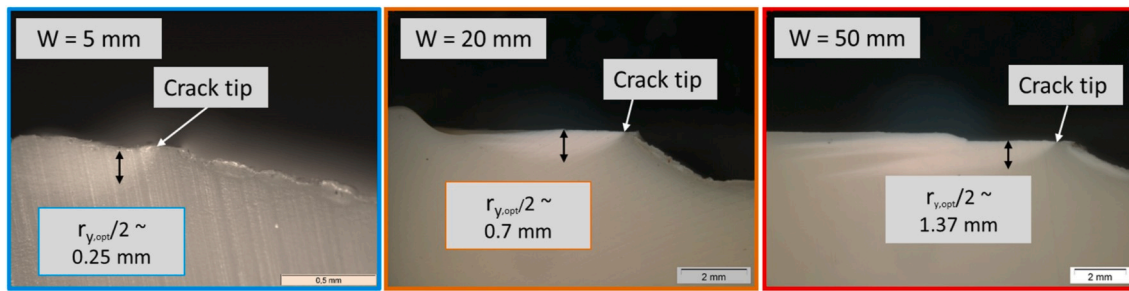


Fig. 10. Light-microscope pictures of selected ABS specimens ($W = 5, 20$ and 50 mm) to measure plastic zone radius $r_{y,opt}$ in front of the crack tip on the specimen surface.

and Δa the amount of crack growth. The J-R curves for the different sizes were tentatively constructed in the knowledge of the restrictions, and they are shown in Fig. 11. Interestingly, the J-R curves for the various sizes are overlapping and practically draw one single curve.

The multi-specimen procedure includes a fitting routine for the measured data according to a simple power-law equation Eq 14:

$$J = c \Delta a^b \tag{14}$$

where c and b are the fitting parameters. For a valid J-R curve, parameter b has to be smaller than 1 according to Ref. [1]. For each size, the evaluated parameter b fulfils this requirement (parameters c and b are presented in Table 3). Nevertheless, the shape of the curve composed of the data points from the various sizes cannot be described via one single power law fitting curve. There seems to be a knee in the curve at a crack length, Δa , of around 2 mm (see Fig. 11). The parameter b increases regularly for specimen sizes from 5 to 30 mm, and afterwards a decrease is observed (for $W = 40$ and 50 mm, the data points belong to the post-knee region, where the curve is less sloped). A steady increase of the parameter c is observed from small to big sizes. At the moment there is no explanation for this change in the curve shape. This may be also connected to constraint issues of the tested specimen geometries, which are under investigation. Furthermore, it is worth pointing out, that further measurements with lower amounts of produced Δa are necessary for the large geometries to make clear suggestions. However, size independent J-R curves were also found for polymeric materials in literature [24].

The J-values at 0.2 mm crack growth (here indicated with $J_{0.2,app}$)

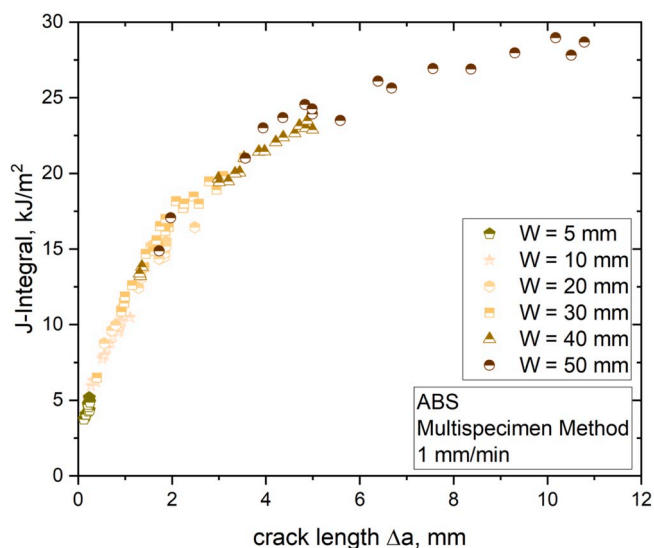


Fig. 11. J-R curve (J-Integral depending on the crack length Δa) for the different specimen sizes ($W = 5, 10, 20, 30, 40$ and 50 mm) determined via the multi-specimen procedure [1].

Table 3

J-R curve power law fitting parameters c and b and values of $J_{0.2,app}$ for all tested sizes.

| Width W [mm] | Parameter c (power-law fit) [kJ/(m ² mm ^b)] | Parameter b (power-law fit) [-] | Initiation value $J_{0.2,app}$ [kJ/m ²] |
|-------------------|---|--------------------------------------|--|
| 5 | 8.66 | 0.41 | 4.42 |
| 10 | 10.39 | 0.45 | 5.01 |
| 20 | 11.44 | 0.44 | 5.31 |
| 30 | 11.93 | 0.47 | 5.94 |
| 40 | 12.18 | 0.41 | 6.31 |
| 50 | 14.59 | 0.29 | 9.20 |

were determined, and they are listed in Table 3. The subscript app in $J_{0.2,app}$, for “apparent”, is added to remark that these values refer to a region of the J-R curve quite far from the experimental data points used for its construction (characterized by Δa values well beyond the limit indicated in the reference protocol). It can be observed that, by increasing the specimen size, the value of $J_{0.2,app}$ increases. This result is in agreement with the size effect observed for $J_{I,lim}$ even if, for this latter set of parameters a more marked size effect is observed.

5. Conclusion

In this work, the draft protocol based on the load separation criterion developed by ESIS TC4 for J-testing of ductile polymers was applied to SE(B) specimens of ABS with different sizes (the maximum scaling ratio examined was 10). Separation parameter, S_{sb} , curves were successfully obtained for all the specimen sizes. Subsequently evaluated data of $J_{I,lim}$ and m_s were consistent with expectations based on the indications provided by the protocol.

By increasing the specimen size the value of m_s , which gives a rough indication of the crack growth, Δa , produced in the plastic region per unit of plastic displacement, progressively decreases (m_s of the smallest size is around 4 times m_s of the biggest one). Considering, that m_s is a specimen characteristic, a specimen size dependence was expected and the results show that such a dependence can be described by a simple analytical expression.

By increasing the specimen size, the value of $J_{I,lim}$, which is presented in the protocol as a material pseudo-initiation fracture resistance parameter, increases ($J_{I,lim}$ of the biggest size is around 4 times $J_{I,lim}$ of the smallest one). Interestingly, the optical measurement of the plastic zone at the crack tip seems to confirm the specimen size dependence noticed for $J_{I,lim}$, at least qualitatively. The increase in $J_{I,lim}$ observed here, has been tentatively explained by considering the peculiar nature of fracture initiation in a ductile polymer, which is a progressive process characterized by the slow development of the crack front across the thickness of the pre-cracked specimen.

The data obtained on the pre-cracked specimens for the application of the load separation criterion-based approach were used also for the construction of the J-R curves for the various specimen sizes. J-R curves

were constructed following the ESIS TC4 multi-specimen approach, slightly modified to take into account the relatively high levels of Δa produced in the fracture tests. The J-R curves obtained for the various sizes overlap and concur to draw one single curve that exhibits a clear discontinuity (a knee) at $\Delta a \approx 2$ mm.

A deeper explanation of the relationships between the specimen size and the fracture properties here examined would require the analysis of the level of constraint undergone by the material at the crack tip in the specimens of the various sizes. This is the matter of further studies, which are currently underway.

Declaration of competing interest

The authors (Anja Gosch, Florian J. Arbeiter, Silvia Agnelli, Michael Berer, Gerald Pinter, Francesco Baldi) declare that they have no known competing financial interests or personal relationships that could have appeared to influence the work reported in this paper (*J-testing of polymers via the load separation criterion based ESIS TC4 procedure: Effect of the specimen size*).

CRediT authorship contribution statement

Anja Gosch: Conceptualization, Methodology, Validation, Formal

Appendix

Relationships between specimen position in the plate and mechanical behaviour

The choice of the scheme adopted for the manufacturing of the bars from the plate, for the obtainment of the fracture specimens (section 3), was supported by the results obtained in a preliminary activity. This activity aimed at outlining the possible effects of the specimen position in the plate cross-section (orthogonal to the extrusion direction that is the x_1 -axis in Fig. 3) on the mechanical response of the ABS. These effects, if any, have to be put in relation with the different thermomechanical histories experienced by the polymer during the extrusion process, in the different points of the plate cross-section. In consideration of the symmetry characteristics of the plate, not only geometrical but also related to the die forming process, the attention was focused on two zones, between which the largest difference was expected: (i) the centre of the plate (core, at $x_3 = W_p/2$); (ii) the region close to the external surfaces (at $x_3 \rightarrow 0, W_p$) [ref. to Fig. 3]. The extremities of the plate along the x_2 -axis were disregarded.

Differential scanning calorimetry, DSC, analyses carried out on samples taken from the two zones of interest did not show any relevant difference in the calorimetric response of the material (results not reported here).

The mechanical response of the material, both at small strains and at yielding, was investigated by means of tensile and compression tests. The material was loaded along the direction of x_2 -axis, which is the loading direction for crack opening in the fracture tests. The specimens were milled from the plate. Dumbbells having a central narrow section with nominal length of 12 mm and cross-section of 10×4 mm², and cubes with 8 mm side length were used for tensile and compression tests, respectively. A Universal Testing System by Instron (model 3366), equipped with a 10 kN load cell, was employed. The experiments were carried out at room temperature, with a crosshead speed set in such a way to generate a nominal strain rate of 0.0625 min^{-1} in both tensile and compression tests. From each test, the material nominal stress-strain curve was constructed and the yield stress was determined. From additional tensile tests, carried out with an extensometer (with a gauge length of 10 mm), the Young's modulus was measured. The experiment was repeated three times for each combination of specimen position and test type.

The results are reported in Table A.1. At small strains, practically no difference is observed between the responses of the material in the two different zones examined (data of E in Table A.1). By contrast, a different response is noticed at yielding: the ABS close to the external surface of the plate shows a yield stress that is 5.6 and 8.6% higher than that of the material in the core, in tension and compression, respectively. Further analyses are necessary to explain these results. In spite of this, and on the basis of the results obtained here, it was decided to avoid mixing fracture data obtained from specimens, whose fracture process zones were at different x_3 -levels. Hence, the core of the plate was taken as the reference zone.

Table A1

Mean values (\pm standard deviation) of Young's modulus (E) and yield stress ($\sigma_{y,t}$ and $\sigma_{y,c}$, in tension and compression, respectively) from tests on specimens from core and external surface of the plate.

| Type of test | Mechanical property | Examined zone of the plate | |
|--------------|----------------------|----------------------------|------------------|
| | | Core | External surface |
| Tension | E ^a [MPa] | 2200 \pm 36 | 2170 \pm 28 |
| | $\sigma_{y,t}$ [MPa] | 28.5 \pm 0.10 | 30.1 \pm 0.64 |
| Compression | $\sigma_{y,c}$ [MPa] | 47.4 \pm 0.76 | 51.5 \pm 0.16 |

^afrom tests carried out with an extensometer.

Appendix A. Supplementary data

Supplementary data to this article can be found online at <https://doi.org/10.1016/j.polymertesting.2020.106637>.

References

- [1] G.E. Hale, F. Ramsteiner (Eds.), *J-fracture Toughness of Polymers at Slow Speed*, Elsevier, Oxford, UK, 2001.
- [2] ASTM D6068, Test Method for Determining J-R Curves of Plastic Materials, ASTM International, West Conshohocken, PA.
- [3] A. Gosch, F.J. Arbeiter, M. Berer, G. Pinter, Comparison of J-integral methods for the characterization of tough polypropylene grades close to the glass transition temperature, *Eng. Fract. Mech.* (2018), <https://doi.org/10.1016/j.engfracmech.2018.06.002>.
- [4] H. Ernst, P.C. Paris, J.D. Landes, Estimations on J-Integral and tearing modulus T from a single specimen test record, *American Society of Testing and Materials* (1981) 476–502.
- [5] C.R. Bernal, A.N. Cassanelli, P.M. Frontini, A simple method for J-R curve determination in ABS polymers, *Polym. Test.* 14 (1995) 85–96.
- [6] C. Bernal, A. Cassanelli, P. Frontini, On the applicability of the load separation criterion to acrylonitrile/butadiene/styrene terpolymer resins, *Polymer* 37 (1996) 4033–4039.
- [7] P.M. Frontini, L.A. Fasce, F. Rueda, Non linear fracture mechanics of polymers: load Separation and Normalization methods, *Eng. Fract. Mech.* 79 (2012) 389–414, <https://doi.org/10.1016/j.engfracmech.2011.11.020>.
- [8] F. Baldi, S. Agnelli, T. Rico, On the determination of the point of fracture initiation by the load separation criterion in J-testing of ductile polymers, *Polym. Test.* 32 (2013) 1326–1333, <https://doi.org/10.1016/j.polymertesting.2013.08.007>.
- [9] J. Wainstein, P.M. Frontini, A.N. Cassanelli, J-R curve determination using the load separation parameter Spb method for ductile polymers, *Polym. Test.* 23 (2004) 591–598, <https://doi.org/10.1016/j.polymertesting.2003.10.010>.
- [10] A. Salazar, J. Rodriguez, The use of the load separation parameter Spb method to determine the J–R curves of polypropylenes, *Polym. Test.* 27 (2008) 977–984, <https://doi.org/10.1016/j.polymertesting.2008.08.013>.
- [11] S. Agnelli, F. Baldi, B.R.K. Blackman, L. Castellani, P.M. Frontini, L. Laiarindrasana, A. pegoretti, M. Rink, A. Salazar, H.A. Visser, Application of the load separation criterion in J-testing of ductile polymers: a round-robin testing exercise, *Polym. Test.* 44 (2015) 72–81, <https://doi.org/10.1016/j.polymertesting.2015.03.019>.
- [12] T.L. Anderson, *Fracture Mechanics: Fundamentals and Application*, CRC Press - Taylor & Francis Group, 2005.
- [13] S. Agnelli, F. Baldi, A Testing Protocol for the Construction of the Load Separation Parameter Curve for Plastics, ESIS TC4 communication, 2015.
- [14] M.H. Sharobeam, J.D. Landes, The load separation and npl development in precracked specimen test records, *Int. J. Fract.* 59 (1993) 213–226.
- [15] M.H. Sharobeam, J.D. Landes, The load separation criterion and methodology in ductile fracture mechanics, *Int. J. Fract.* 47 (1991) 81–104.
- [16] C.R. Bernal, P.E. Montemartini, P.M. Frontini, The use of load separation criterion and normalization method in ductile fracture characterization of thermoplastic polymers, *J. Polym. Sci., Part B: Polym. Phys.* 34 (1996) 1869–1880.
- [17] F. Baldi, S. Agnelli, T. Ricco, On the applicability of the load separation criterion in determining the fracture resistance (JIC) of ductile polymers at low and high loading rates, *Int. J. Fract.* 165 (2010) 105–119, <https://doi.org/10.1007/s10704-010-9510-9>.
- [18] A. Salazar, J. Rodriguez, A.B. Martinez, The role of notch sharpening on the J-fracture toughness of thermoplastic polymers, *Eng. Fract. Mech.* 101 (2013) 10–22, <https://doi.org/10.1016/j.engfracmech.2012.07.006>.
- [19] A. Salazar, J. Rodriguez, A. Segovia, A.B. Martinez, Influence of the notch sharpening technique on the fracture toughness of bulk ethylene-propylene block copolymers, *Polym. Test.* 29 (2010) 49–59, <https://doi.org/10.1016/j.polymertesting.2009.09.004>.
- [20] A. Salazar, J. Rodriguez, F. Arbeiter, G. Pinter, A.B. Martinez, Fracture toughness of high density polyethylene: fatigue pre-cracking versus femtolaser, razor sharpening and broaching, *Eng. Fract. Mech.* 149 (2015) 199–213, <https://doi.org/10.1016/j.engfracmech.2015.07.016>.
- [21] C. Rodriguez, M.L. MasPOCH, F.J. Belzunce, Fracture characterization of ductile polymers through methods based on load separation, *Polym. Test.* 28 (2009) 204–208, <https://doi.org/10.1016/j.polymertesting.2008.12.004>.
- [22] S. Agnelli, F. Baldi, L. Castellani, K. Pisoni, M. Vighi, L. Laiarindrasana, Study of the plastic deformation behaviour of ductile polymers: use of the material key curves, *Mech. Mater.* 117 (2018) 105–115, <https://doi.org/10.1016/j.mechmat.2017.11.002>.
- [23] D.R. Moore (Ed.), *Application of Fracture Mechanics to Polymers, Adhesives and Composites*, Elsevier, 2003.
- [24] P. Frontini, E. Santarelli, The effects of specimen size and testing conditions on fracture toughness evaluation of polypropylene Homo polymer, *Polym. Eng. Sci.* 41 (2001) 1803–1814.

Publication 3

Bibliographic information

Title: Size induced constraint effects on crack initiation and propagation parameters in ductile polymers

Authors: Anja Gosch¹, Florian J. Arbeiter¹, Silvia Agnelli³, Michael Berer², Francesco Baldi³

Affiliation:

1. Materials Science and Testing of Polymers, Montanuniversitaet Leoben, Otto Glöckel-Strasse 2, 8700 Leoben, Austria
2. Polymer Competence Center Leoben GmbH, Roseggerstr. 12, 8700 Leoben, Austria
3. Dipartimento di Ingegneria Meccanica e Industriale, Università degli Studi di Brescia, Via Branze 38, Brescia 25123, Italy

Periodical: MDPI materials

Submitted

Relevant contributions to this publication

| | |
|-----------------------------|--|
| Conceptualization: | Anja Gosch, Florian Arbeiter, Silvia Agnelli, Francesco Baldi |
| Methodology: | Anja Gosch, Florian Arbeiter, Francesco Baldi |
| Validation: | Anja Gosch |
| Investigation: | Anja Gosch |
| Writing - Original Draft: | Anja Gosch |
| Writing - Review & Editing: | Florian Arbeiter, Silvia Agnelli, Michael Berer, Francesco Baldi |

Size induced constraint effects on crack initiation and propagation parameters in ductile polymers

Anja Gosch¹, Florian J. Arbeiter^{1,*}, Silvia Agnelli², Michael Berer³ and Francesco Baldi²

¹ Materials Science and Testing of Polymers, Montanuniversitaet Leoben, Otto-Gloeckel-Str. 2, 8700 Leoben, Austria;

² Università degli Studi di Brescia, Dipartimento di Ingegneria Meccanica e Industriale, Via Branze 38, Brescia 25123, Italy;

³ Polymer Competence Center Leoben GmbH, Roseggerstr. 12, 8700 Leoben, Austria;

* Correspondence: florian.arbeiter@unileoben.ac.at; phone: +43 3842 402 2122;

Abstract: Detailed knowledge about the influence of constraint and specimen size is gained for polymeric materials showing elastic plastic deformation behavior. Within this study, different sizes of single edge notched in bending SE(B) specimens, but constant geometrical ratios, were tested. The material key curve was used to investigate constraint issues, where changes for small and large specimen sizes were found. The found results were confirmed by testing of side-grooved specimens. Based on a size-independent crack resistance curve (J-R curve), two apparent initiation parameters were determined ($J_{0.2}$ and J_{bl}). Both initiation values display nearly a constant plateau for specimen sizes with a similar constraint state. The initiation parameter J_{ini} (based on the crack propagation kinetics curve) was determined and was found to be in the same range as the initiation parameter $J_{l,lim}$ (based on an ESIS TC 4 draft protocol). Both parameter (J_{ini} and $J_{l,lim}$) display a continuous increase with increasing specimen size, which is contrary to the found behavior of the initiation parameter based on the J-R curve ($J_{0.2}$ and J_{bl}). Based on the results, $J_{0.2}$ and J_{bl} can be used as crack initiation parameters, whereby J_{ini} and $J_{l,lim}$ as parameters indicative of the beginning of stable crack growth.

Keywords: material key curve; ABS; crack growth resistance; constraint; triaxiality; initiation parameter;

1. Introduction

Structural component design requires detailed information about the fracture behavior of a material in order to ensure the required safety. By the use of fracture mechanical approaches, it is possible to predict the toughness or even the service life of a component by considering the influence of load, toughness and inherent flaws in the material. In the case of linear elastic material behavior (linear elastic fracture mechanics LEFM), a single parameter is usually able to describe the fracture property (stress intensity factor, K , critical energy release rate G or crack tip opening displacement, CTOD) of a material. However, common applications of polymers often exceed the area of LEFM and show a material behavior, where elastic plastic fracture mechanics (EPFM) has to be considered. A typical result from EPFM is the so-called crack resistance curve (J-R curve, J-Integral depending on the crack advancement Δa), which can be used to describe the fracture behavior of a material based on crack initiation and crack growth parameters. When external loads exceed a certain level, a crack starts to grow, which is typically expressed by the crack growth initiation parameter. This parameter characterizes only the onset of crack growth, but provides no further information about the crack growth behavior of the material. The ability of the material to withstand crack growth is commonly known as crack growth resistance and is usually proportional to the shape and especially the slope of the J-R-curve [1].

In a fracture mechanical experiment on a plate with a defined crack, the stress state can vary along the crack front. A high constraint (triaxiality) is typically present in the middle of the plate (plane strain) and decreases close to the free surface (plane stress) [1]. Analogous, thickness variations within a component, which can lead to changing constraint levels, can influence the fracture behavior [1–3]. Therefore, it is important to assess the crack initiation and crack growth parameters for changing specimen sizes.

Citation: Lastname, F.; Lastname, F.; Lastname, F. Title. *Materials* **2021**, *14*, x. <https://doi.org/10.3390/xxxxx>

Academic Editor: Firstname Lastname

Received: date

Accepted: date

Published: date

Publisher's Note: MDPI stays neutral with regard to jurisdictional claims in published maps and institutional affiliations.



Copyright: © 2021 by the authors. Submitted for possible open access publication under the terms and conditions of the Creative Commons Attribution (CC BY) license (<http://creativecommons.org/licenses/by/4.0/>).

Generally, the initiation parameter was found to be not highly sensitive to geometry changes in literature for metals, whereas, the crack growth parameter usually displayed size dependent behavior and is influenced by the structural configurations [1,4]. However, previous research, dealing with the determination of the elastic plastic fracture behavior of up-scaled specimen sizes (increasing specimen size but identical geometrical ratios of width, thickness and initial crack lengths) of the well-known polymer, acrylonitrile-butadiene-styrene (ABS), showed a strong size dependency of the determined fracture parameters [5]. To assess this up-scaling behavior of ABS, a testing procedure [6] from the ESIS TC4 (European Structural Integrity Society, Technical Committee 4 on polymers and polymer composites) was used for the determination of a pseudo-crack initiation parameter, $J_{I,lim}$, and a parameter describing the crack growth process, m_s . The applied testing procedure [6], named TC4 LS-method hereafter, is based on the load separation theory [7] and requires only a few specimens for the evaluation of $J_{I,lim}$ and m_s . The TC4 LS-method was originally proposed to strengthen the results of the commonly used multispecimen method [8], and its applicability to various types of polymers was already investigated in a round robin test under the direction of the ESIS TC 4 [9,10].

Especially for the crack initiation phase, represented by $J_{I,lim}$, a clear trend with increasing specimen size was found. The observed size dependent behavior of $J_{I,lim}$ was not expected, since a crack initiation parameter should be independent of the specimen size when all preconditions regarding specimen size are fulfilled (exceed of minimum thickness for thickness independent fracture parameter) [1,4,11]. Interestingly, the presented J-R curve, determined via classical multispecimen approach [12], showed overlapping results and no indication of a size dependency. Subsequently, this raised the question, if the initiation values were depending on the size of the specimen, or if the applied procedure was inherently flawed. However, open questions about the level of constraint of the specimen size did not allow for a clear interpretation at that point.

Subsequently, the aim of the present study is to close this gap, by analyzing the effect of the constraint on the crack initiation and crack propagation phase for this material and specimen size in detail. As a starting point, the influence of specimen constraint is examined by resorting to the so-called calibration function. A common way to determine the calibration function is by the evaluation of the material key curve (normalized load, P_N , as a function of the normalized plastic displacement, u_{pl}/W) derived from the load separation principle (as shown in Ref. [2]). Further, to examine constraint effects in the crack growth phase, the stress state of specimens is deliberately changed by introducing side-grooves in specimens. Finally, the gained knowledge about the specimen constraint is used for a clearer interpretation of the fracture process (crack initiation and crack growth) with changing specimen size.

2. Theory/ calculation

The theoretical background for the used methods to evaluate constraint changes with increasing specimen size are described in detail in the next chapter. Furthermore, the applied procedure for the calculation of established crack initiation (J_{bl} , $J_{0.2}$ and J_{ini}) and crack growth parameters (crack resistance curve, J-R curve) are given. These values are also used to validate the results of $J_{I,lim}$, calculated via the TC4 LS-method from prior work [5].

2.1. Constraint effects in SE(B) specimens

In the present thesis two procedures were used to check the influence of constraint differences in the tested specimen sizes. In the first, the level of constraint is analyzed a posteriori via the material key curve construction for all the specimen sizes. This way, resulting crack growth initiation values can be compared to their corresponding stress states. Additionally, the local stress state in specimens was deliberately altered a priori by introducing side-grooves in selected specimens to examine differences in the crack growth phase.

2.1.1. Determination of constraint level in the crack initiation phase via the material key curve

The estimated material key curve is independent of the specimen geometry as long as the constraint is not modified. Therefore, the material key curve is a great tool to investigate changes in the constraint level during crack initiation. For a correct application of the material key curve, the load separation principle has to be verified beforehand as presented for several polymers in literature [9,13–21]. The material key curve is based on the load separation principle [7,22,23], in which the load, P , can be expressed as the product of two independent functions for a defined geometry, material and constraint (in the plastic region during a fracture test on a cracked specimen):

$$P = G \left(\frac{a}{W} \right) H \left(\frac{u_{pl}}{W} \right) \quad (1)$$

Here, G is the geometry function, H the material deformation function, a the notch length, W the specimen width, and u_{pl} the plastic displacement. The plastic displacement is given with:

$$u_{pl} = u - C\left(\frac{a}{W}\right) P \quad (2)$$

In which $C(a/W)$ is the elastic compliance of the tested specimens. The load separation principle (as proposed in equation 1) is only valid for fracture tests on a cracked specimen with a defined geometry, material and constraint as discussed in [7,23]. For SE(B) specimens, beam-shaped specimens with a single edge notch under three-point bending load, the geometry function, G , is defined by the following expression:

$$G = \left(1 - \frac{a}{W}\right)^{\eta_{pl}} \quad (3)$$

The geometry independent plastic calibration factor, η_{pl} , is given as 2 for SE(B) specimens in literature [23]. However, the parameter η_{pl} is only valid if the load can be expressed in its separable form like in equation 1 [7,13]. This precondition can be verified experimentally by the separability parameter, S_{ij} , as [7,23]:

$$S_{ij} = \frac{P(a_i)}{P(a_j)} \Bigg|_{u_{pl}} \quad (4)$$

where a is the remaining ligament length of the tested blunt notched specimens and $P(a_i)$ and $P(a_j)$ are the load values of blunt notched (bN) specimens with identical testing configuration and material but various crack length over width ratios, a_0/W (represented as a_i and a_j in equation 4). Based on these assumptions the presented separability parameter, S_{ij} , can be simplified as:

$$S_{ij} = \frac{G\left(\frac{a_i}{W}\right) H\left(\frac{u_{pl}}{W}\right)}{G\left(\frac{a_j}{W}\right) H\left(\frac{u_{pl}}{W}\right)} \Bigg|_{u_{pl}} = \frac{G\left(\frac{a_i}{W}\right)}{G\left(\frac{a_j}{W}\right)} \Bigg|_{u_{pl}} \quad (5)$$

where the material deformation function, H , is equal for same materials and the ratio of the geometry function, G , is representing S_{ij} . As mentioned above, equation 5 can be used to check the validity of the load separation parameter, which is expressed through the parameter η_{pl} . The theory assumes that the geometry function G is constant for stationary crack experiments. Therefore, the separability curve (S_{ij} - u_{pl} curve, S_{ij} depending on u_{pl}) of bN specimens with various a_0/W ratios has to be determined for verification. One bN specimen needs to be defined as reference specimen, for example the specimen with the highest a_0/W ratio (for our experiments the highest a_0/W was 0.8). Afterwards the parameter S_{ij} can be calculated with equation 4 and the S_{ij} - u_{pl} curve can be plotted (Figure 1a). The bN specimens display an almost constant value after the initial phase for all chosen a_0/W ratios. In this plateau area of the S_{ij} - u_{pl} curve, a fixed value for the evaluation of η_{pl} is defined (marked as " u_{pl}^* for the evaluation of η_{pl} " in Figure 1a). Subsequently, the values of the separability parameter S_{ij} at u_{pl}^* can be plotted over the used notch length (in Figure 1b the ligament length over the width $(W-a_0)/W$ of the tested bN specimens). For the used reference specimen (as aforementioned and in accordance with our experiments in this example a_0/W is 0.8), a theoretical point is added, where S_{ij} is equal to zero. The parameter η_{pl} is evaluated as the slope of the curve shown in Figure 1b. The slope displays a constant value when a separable form of the load exists for a set of material, geometry and constraint. Hence, the validity of the load separation principle can be assumed for the investigated specimens.

After the validation of the load separation principle, it is possible to determine the material key curve to examine constraint issues. The evaluation of the material key curve is based on the geometry function, H , evaluated from Eq. (1) and Eq. (3):

$$H\left(\frac{u_{pl}}{W}\right) = \frac{P}{G\left(\frac{a}{W}\right)} = \frac{P}{\left(1 - \frac{a}{W}\right)^2} \quad (6)$$

From equation 6 the normalized load, P_N , can be evaluated by normalizing the geometry function H , as follows:

$$P_N = \frac{P}{B W \left(1 - \frac{a}{W}\right)^2} \quad (7)$$

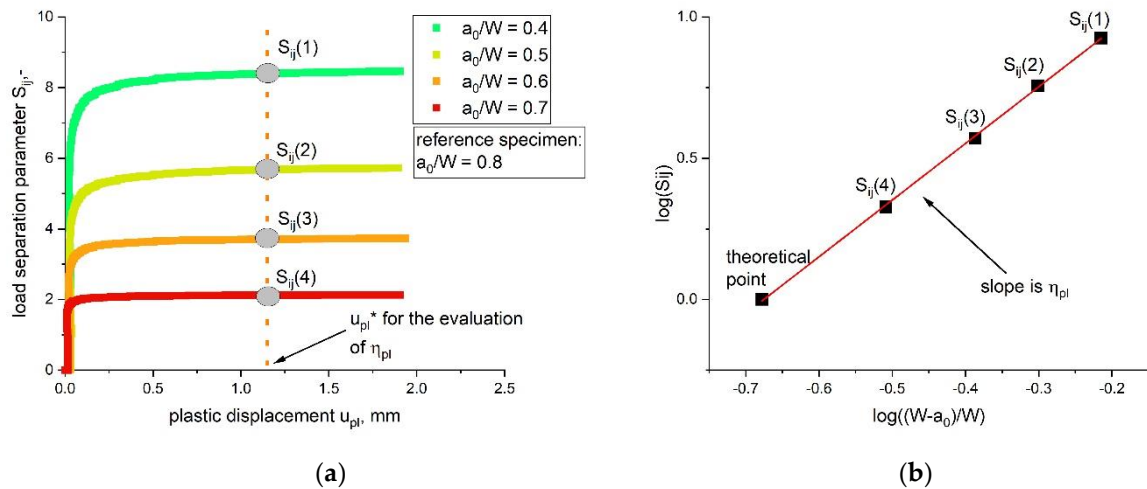


Figure 1. Determined load separation curves (S_{ij} as function of u_{pl}) of bN specimens with changing a_0/W ratio and the chosen limit value u_{pl}^* (a); evaluation of η_{pl} as the slope of the S_{ij} over $(W-a_0)/W$ plot (b).

The material key curve is defined as the normalized load P_N plotted against u_{pl}/W and it can provide information about changes in the constraint in front of the crack tip (see [19]). In this work, the material key curve is evaluated from stationary crack experiments on bN specimens, in which no crack growth is allowed. Previous studies showed a good agreement between sN and bN based material key curves [19,21]. Hence, a comparison of sN and bN specimens from the same material, tested with the same configurations and conditions can be used to determine differences in the specimen constraint.

Generally, the material key curve is depending on the material deformation behavior and the geometrical constraint [19,22,23]. Previous research [19], dealing with the application of the material key curves on polymers proposed a simplified relationship between P_N , the constraint, L , the span length over width ratio, S/W , and the yield stress, σ_y :

$$L = \frac{P_N}{\sigma_s} \frac{S}{W} \quad (8)$$

The application of equation 8 is limited to ideally elastic plastic materials and assumes a fully yielded net section. In spite of this, based also on the results presented in [19], the material key curves are used to gain information regarding the constraint degree in the ABS specimens examined in the present paper.

2.1.2. Changing the constraint level in the crack growth phase by testing of side-grooved specimens

To investigate constraint effects during actual crack growth, the testing of side-grooved specimens is a rather straight forward possibility. Side-grooves change the zone of low constraint near the outer surface of a specimen and reduce the possibility of shear lip formations, which leads to a higher constraint level. The testing of side-grooved specimens, with higher constraint and stress within the specimen, can provide information about the sensitivity of the fracture process to overall constraint changes during crack propagation.

2.2. Evaluation of crack initiation and crack growth parameter

After aforementioned detailed examination of the constraint in different specimen sizes it is possible to further investigate and especially validate determined fracture parameters. This knowledge will be used to interpret the results of the previous study [5], where the so-called pseudo initiation parameter $J_{I,lim}$, based on the TC4 LS-method [6], displayed a dependency with increasing specimen size. Furthermore, to not only validate these results with the examination of the level of constraint, but also to check for possible inherent flaws in the new testing procedure, established crack initiation and propagation values will also be included in the study.

2.2.1. Determination of the J-R curve

The most common method to determine fracture properties in an elastic plastic material is the so-called multi-specimen method. For this approach, several identical specimens are tested up to different amounts of crack advancement. Subsequently, the energy necessary for this amount of crack growth, usually expressed via the J-Integral, is plotted as a function of the produced crack advancement (Δa). In this work J-R curves were determined according to the

ESIS TC-4 method [8] for each examined specimen size. According to the ESIS TC-4 multispecimen method, valid data points are limited by two critical Δa values (Δa_{\min} and Δa_{\max}). The minimum Δa_{\min} is fixed at 0.05 mm crack advancement and the maximum Δa_{\max} is depending on the specimen size according to $0.1(W-a_0)$. In the case of cracks with a length higher than $0.1(W-a_0)$ the conducted measurements were corrected for high amounts of crack growth following the proposed formula in literature [7]:

$$J = J_0 \left[1 - \frac{0.75 \eta - 1}{W - a_0} \Delta a \right] \quad (9)$$

$$J_0 = \frac{\eta U_c}{B (W - a_0)} \quad (10)$$

where η is the geometry dependent calibration factor and is 2 for SE(B) specimens, U_c is the corrected area under the load displacement curve (corrected for the amount of indentation according to [12]), B is the specimen thickness, W is the specimen width and a_0 is the initial crack length. As a precondition for a successful application of the multispecimen procedure, the J-R curve data has to follow a simple power law routine [12]:

$$J = c \Delta a^b \quad (11)$$

where c and b are the fitting parameter (see **Figure 2**). It is possible to determine both initiation-, as well as propagation values of the examined material by using this fitting curve.

2.2.2. Determination of the crack initiation parameters

Based on the calculated J-R curve, several fracture initiation parameters can be determined for a quantitative description of the investigated material. However, one of the most important parameters evaluated from the J-R curve, is the technical crack initiation value $J_{0.2}$ at a crack advancement of 0.2 mm [12]. This amount of crack advancement was originally chosen, since it is large enough to experimentally characterize real crack growth and small enough to be close to the real initiation. The parameter $J_{0.2}$ is widely accepted and used for the characterization of crack initiation in polymers [5,9,13,24–26]. The second initiation parameter used in this study is J_{bl} , defined as the intersection of the blunting line with the J-R curve power law fit [12], where the blunting line is defined as:

$$J = 2 \sigma_y \Delta a \quad (12)$$

where σ_y is the yield stress of the investigated material. A schematic J-R curve with both initiation parameters ($J_{0.2}$ and J_{bl}) is shown in **Figure 2**.

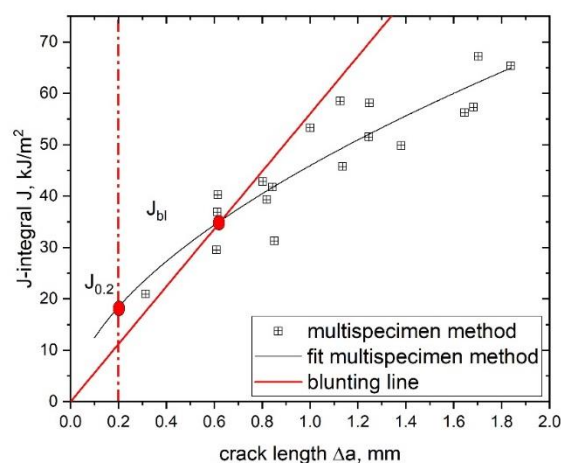


Figure 2. Evaluation of the initiation toughness parameters $J_{0.2}$ and J_{bl} from the J-R curve, according to [12].

A further crack initiation parameter used in this work is J_{ini} , which is based on the crack propagation kinetics where the produced crack length, Δa , is plotted against the testing time, t , of the experiment (**Figure 3**) [26–28]. Typical crack propagation kinetics curves exhibit three stages, where each stage is representing a characteristic process in the crack

growth mechanism during a fracture process. Stage I describes crack tip blunting and crack initiation, stage II non-stationary stable crack growth and stage III steady state stable crack growth. The transition from stage I to stage II is representing the physical crack initiation, which makes this method highly interesting for the present study [26–28].

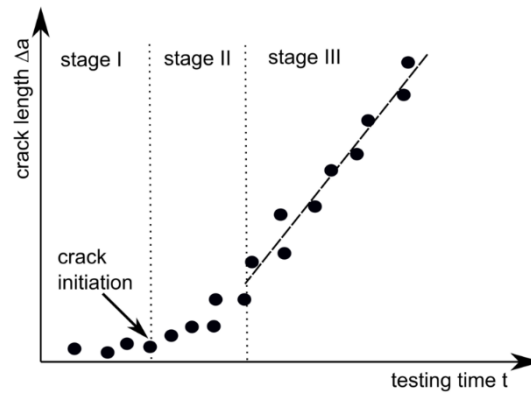


Figure 3. Crack propagation curve to evaluate the physical crack initiation, with three characteristic stages: stage I (crack tip blunting), stage II (non stationary stable crack growth) and stage III (stable crack growth).

For the measured specimens in this study no data points at very low testing time were available (stage I), hence, the initiation time had to be verified with a slightly modified procedure (Figure 4a). The Initiation time (t_{ini}) was determined as the intersection between the linear data fit of stage III and the x-axis. Afterwards the J-Integral was calculated using the area under the load displacement curve U up to the displacement at t_{ini} . The J-Integral was calculated according to the recommended formula from the ESIS TC-4 procedure [8]:

$$J_{ini} = \frac{\eta U_{ini}}{B(W - a_0)} \quad (13)$$

where η is the geometry dependent calibration factor and is 2 for SE(B) specimens, U_{ini} is area under the load displacement curve up to t_{ini} (see Figure 4b) and corrected for the amount of indentation according to [12], B is the specimen thickness, W is the specimen width and a_0 is the initial crack length.

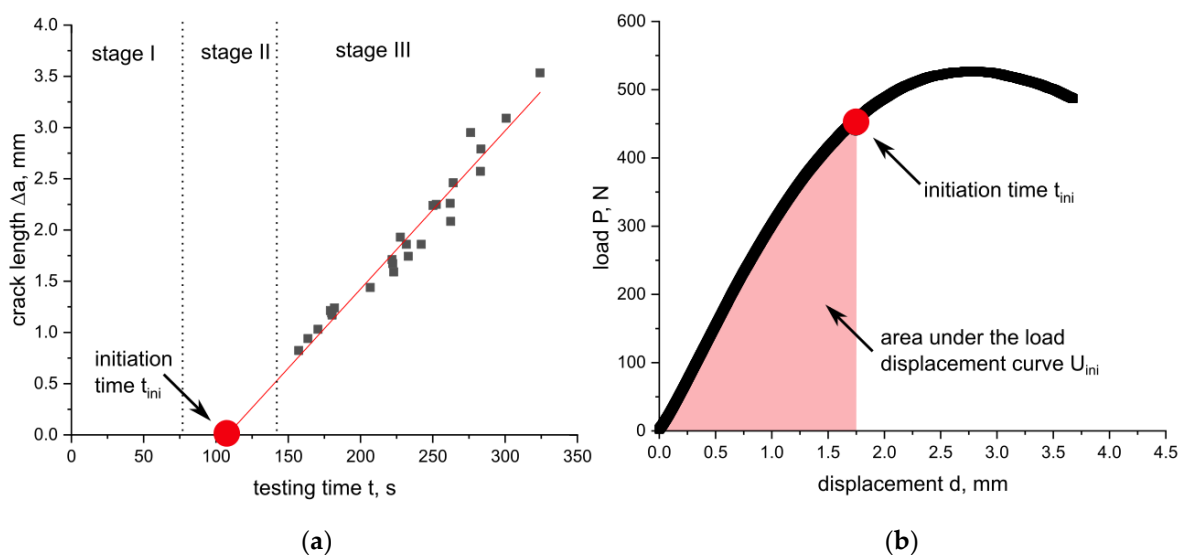


Figure 4. Crack propagation kinetics for the estimation of the initiation time t_{ini} (a) and the evaluation of U_{ini} (area under the load displacement curve up to t_{ini}) (b).

3. Materials and Methods

The material and specimen geometry used in this work was identical to the previous study on the influence of size effects on fracture mechanical parameters [5]. However, the experimental setup for the evaluation of constraint effects displays several differences, which are described in detail in the following section.

3.1. Specimen scale up

To analyse constraint effects during specimen-scale up, bN specimens of different sizes were manufactured. In addition to the bN specimens, sN specimens were made for the application of the multispecimen procedure in the same way as in the previous work [5]. The tested specimen geometry was single-edge notched in bending specimens (SE(B) as shown for a bN specimen in **Figure 5a**) with a specimen up-scaling ratio of 10 (specimen width, W , from 5 mm to 50 mm as shown in **Figure 5b**). The chosen width to thickness ratio, W/B , as well as the length to width ratio, L/W , were kept constant for all specimen sizes according to [12]. The used initial crack length over width ratio, a_0/W , was constant for the sN specimens (0.6). Side-grooves were added to three sN specimens of the size W is 10, 20, 30 and 40 mm, to evaluate constraint differences. The manufactured side-grooves had equal depth and showed a combined thickness reduction of 20 % of the thickness B . For the bN specimens, the a_0/W ratio varied from 0.3 to 0.8.

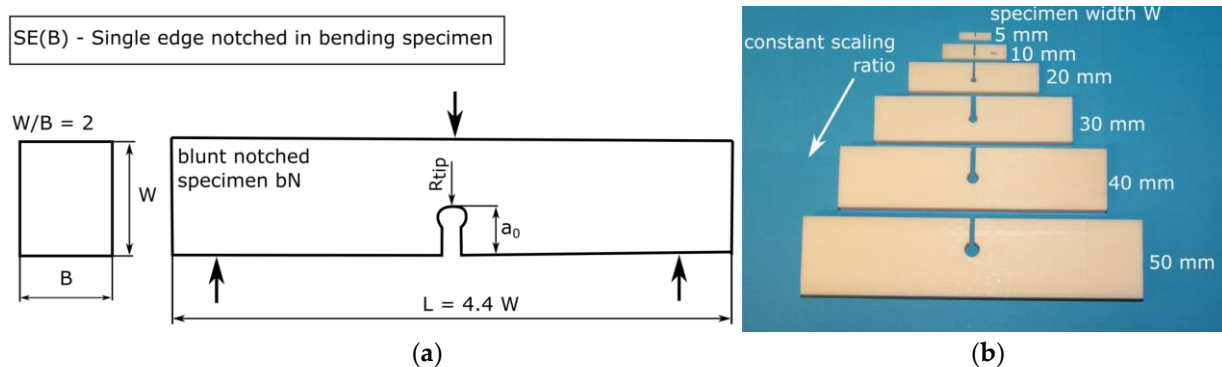


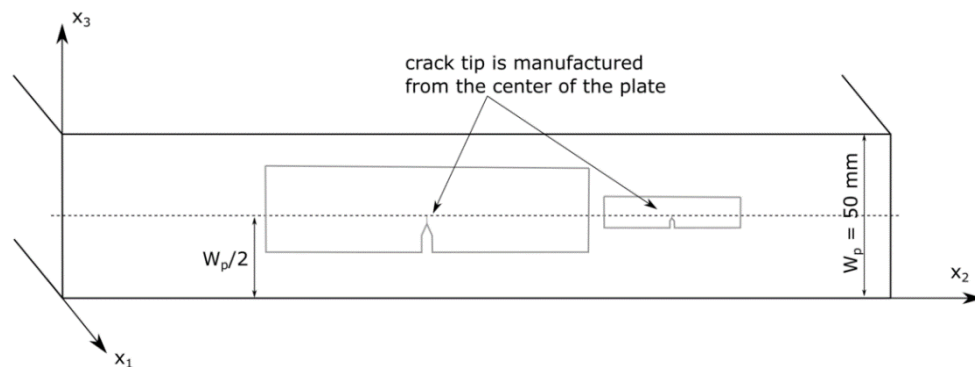
Figure 5. Blunt notched SE(B) specimen geometry and testing set-up (a); constant scale up ratio for specimen width W of manufactured blunt notched ABS-specimens (b) (adapted from [5]).

3.2. Material

The investigated material was ABS (acrylonitrile-butadiene-styrene), which was supplied as extruded plates with 1200 mm in length, 500 mm in width and 50 mm in thickness (identical to the previous study [5]). The high thickness of the plates was required to obtain a high up-scaling ratio (specimens with width values W from 5 to 50 mm) for the manufactured specimens. The extruded plate is commercially available at Faigle Kunststoffe GmbH (Austria).

3.3. Specimen preparation

The specimen preparation was made via cutting and milling. The blunt notch was introduced as a key hole notch with a size dependent notch tip radius R_{tip} , listed in **Table 1**. As discussed in the previous work, material property variations between the edge and the centre of the thick plates were detected, which were caused by variations in the manufacturing conditions. To guarantee similar testing material behavior close to the round tip of all bN specimen geometries, a fixed thickness position of the plate was chosen as reference. This reference position is defined as half of the thickness of the plate (" $W_p/2$ ") as shown in **Figure 6**.



232

Figure 6. Scheme of the specimen manufacturing from the centre of the ABS-plate to assure similar conditions near the crack tip (adapted from [5]).

233

234

3.4. Testing procedures

235

Three-point bending tests on bN and sN specimens were conducted to characterize constraint issues in the fracture mechanical behavior of ABS. All mechanical tests were performed on a Zwick Universal Testing System (Zwick GmbH & Co.KG, Germany), model Z010 or Z250, with different load cells listed in **Table 1**. The measurements were carried out at standardized conditions (23 °C air temperature, 50 % relative humidity) with a constant loading rate of 1 mm/min. The detailed parameters concerning the experimental setup for the tested geometries are listed in **Table 1**.

236

237

238

239

240

Table 1. Detailed information on the experimental setup and the crack tip radius of the bN specimen for all specimen sizes examined.

241

242

| Specimen width W | Span length S | Roller radius | Load cell capacity | Crack tip radius of bN specimen (R_{tip}) |
|-----------------------|--------------------|---------------|--------------------|--|
| [mm] | [mm] | [mm] | [kN] | [mm] |
| 5 | 20 | 1 | 1 | 0.5 |
| 10 | 40 | 3 | 10 | 1 |
| 20 | 80 | 3 | 10 | 2 |
| 30 | 120 | 5 | 10 | 3 |
| 40 | 160 | 5 | 10 | 4 |
| 50 | 200 | 10 | 10 | 5 |

All fracture mechanical results (J-Integral values) were corrected for the amount of indentation during the experiment. For this, the testing set-up was changed to an indentation configuration and unnotched specimens were used to evaluate the indentation curve. Afterwards this curve was subtracted from the measured load-displacement curves of the fracture mechanical specimens. Details concerning the indentation set-up and procedure are given in [12].

243

244

245

246

4. Results and Discussion

247

4.1. Evaluation of specimen constraint

248

The evaluation of the constraint is helpful to understand the influence of the specimen size and the up-scaling behavior of fracture mechanical parameters. In the present study, the material key curve is used to identify changes in the specimen constraint influencing the crack initiation process. Therefore, the applicability of the load separation principle is verified beforehand, since it is a precondition for the evaluation of the material key curve.

249

250

251

252

4.1.1. Applicability of load separation principle

Consequently, bN specimens with varying notch length (a_0/W) were tested to an amount of displacement, which did not lead to crack growth initiation. The load-displacement curves of tested bN specimens are presented in **Figure 7** for the smallest (W is 5 mm, **Figure 7a**) and the largest (W is 50 mm, **Figure 7b**) specimen sizes.

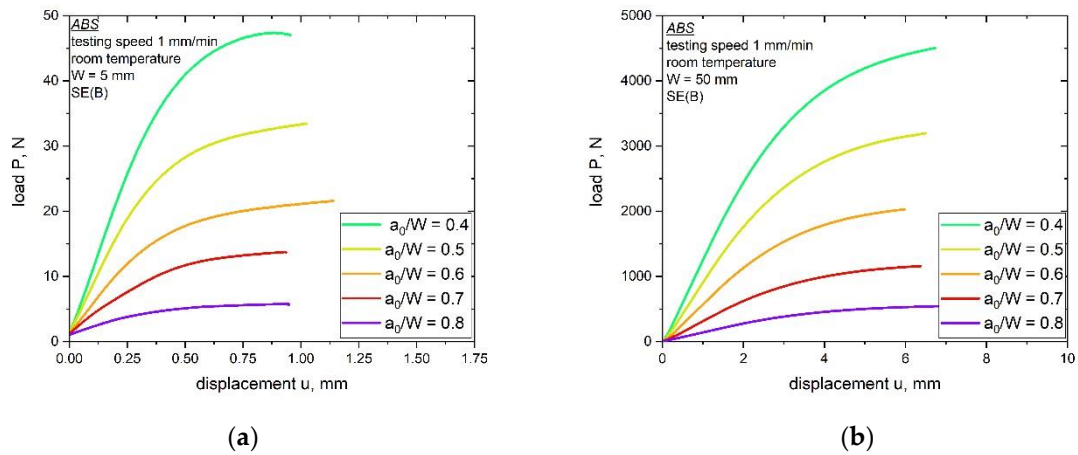


Figure 7. Decreasing load-displacement curves (P - u curves) with increasing ratios of notch length over width a_0/W for two tested bN ABS specimen sizes with W is 5 mm (a) and 50 mm (b).

For all geometries investigated, the measured force increases with lower a_0/W ratios. Furthermore, the measured load level is higher for a larger specimen size, as shown in **Figure 7** for the specimens with W is 5 mm (a) and W is 50 mm (b). There was no crack growth identified during testing of the bN specimens, which allows the assumption of stationary cracks. This precondition is especially important for a correct verification of the load separation property, which is done by the evaluation of the parameter η_{pl} as described in the theoretical part. The separability parameter, S_{ij} , calculated from bN specimens with varying notch length over width ratio, a_0/W , was calculated and plotted as a function of the plastic displacement, u_{pl} , in **Figure 8**. As discussed in the experimental part, for the used reference specimen (a_0/W is 0.8), a theoretical point is added, where S_{ij} is equal to zero.

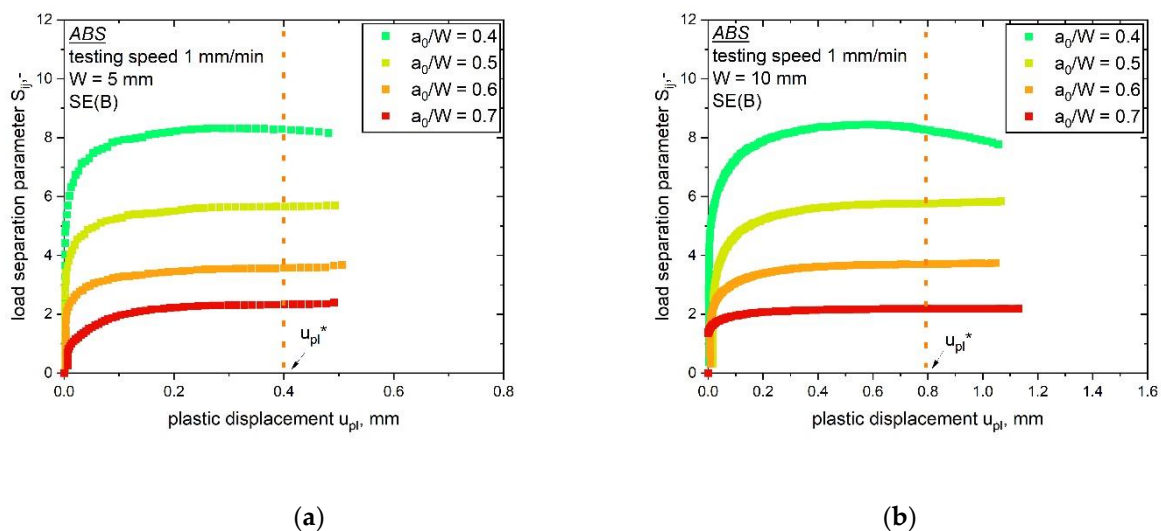
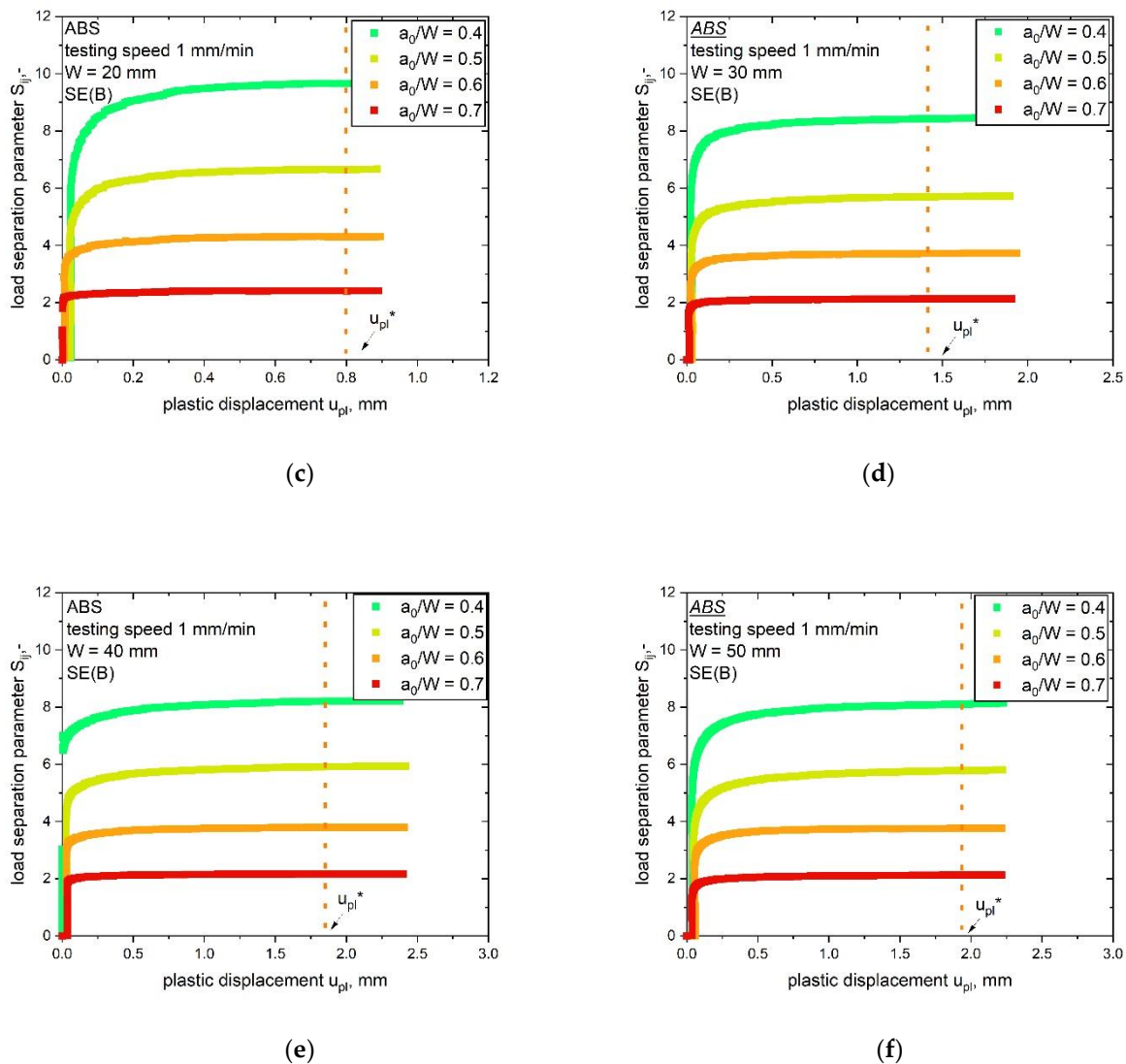


Figure 8. Load separation parameter S_{ij} vs plastic displacement u_{pl} for ABS specimens with varying notch length over width ratio, a_0/W .



270

271

Figure 8. Evaluation of the parameter η_{pl} from S_{ij} - u_{pl} curves determined from blunt notched specimens of ABS with various a_0/W ratios and up-scaling specimen sizes (W is 5 (a), 10 (b), 20 (c), 30 (d), 40 (e) and 50 mm (f)). The reference value of u_{pl} for the evaluation of η_{pl} (constant S_{ij} values) is marked as u_{pl}^* for every geometry.

272
273
274

The S_{ij} - u_{pl} curves were evaluated for all investigated specimen geometries (W is 5 to 50 mm). Nearly all curves meet the precondition of stationary cracks, as discussed in [13]. In stationary crack experiments, the curves display a constant S_{ij} -value (at high amounts of plastic displacement u_{pl}) after the initial phase. The first part of the S_{ij} - u_{pl} curves in **Figure 8**, at low amounts of u_{pl} , is representing the initial phase of the experiment, in which the parameter η_{pl} is not defined. Hence, this phase is not of importance for the validity check. However, not all tested specimens display a stationary crack behavior. Specimens with the smallest notch length of a_0/W is 0.4 show no clear plateau after the initial phase for the smallest two specimen sizes (W is 5 mm, **Figure 8a** and W is 10 mm, **Figure 8b**). This indicates that crack growth in these two bN specimens was not completely prevented. Consequently, optical analyses were conducted to examine possible signs of crack initiation or crack growth close to the round notch tip of the bN specimen. However, no signs of crack growth were found in these two specimens. Therefore, they were included in the determination of η_{pl} . The S_{ij} -values used for the evaluation of the parameter η_{pl} are indicated in every plot in **Figure 8** through the vertical line at u_{pl}^* . For all tested specimen geometries, the parameter η_{pl} , determined as the slope of the plot shown in **Figure 1b**, was evaluated with its statistical coefficient R^2 and is summarized in **Table 2**.

275
276
277
278
279
280
281
282
283
284
285
286
287
288

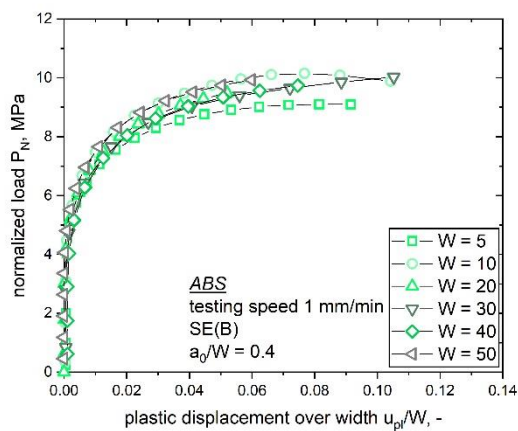
For all investigated specimen geometries, the value of the parameter η_{pl} was close to 2 with a good statistical correlation described via the parameter R^2 (Table 2). The estimated values are close to the theoretical value for this geometry (for SE(B) η_{pl} is 2). Hence, the load separation validity is given for all geometries examined in the present and in the previous work [5]. This first investigation of η_{pl} strengthens previously determined results from the TC4 LS-method dealing with the specimen size effect [5]. Subsequently, the constraint issues for the up-scaled ABS specimens are evaluated. This is done by applying the material key curve method to the results of this section.

Table 2. Values of η_{pl} with the corresponding statistical coefficient R^2 for all tested specimen geometries (W is 5, 10, 20, 30, 40 and 50 mm).

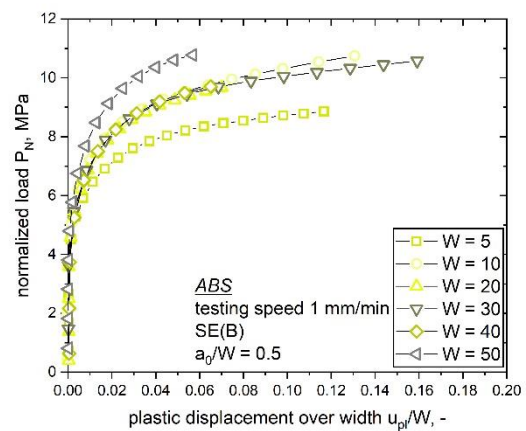
| Specimen width W [mm] | Parameter η_{pl} | R^2 |
|----------------------------|-----------------------|-------|
| 5 | 1.98 | 0.999 |
| 10 | 2.03 | 0.999 |
| 20 | 2.03 | 0.999 |
| 30 | 2.01 | 0.999 |
| 40 | 1.94 | 0.999 |
| 50 | 1.94 | 0.999 |

4.1.2. Determination of specimen constraint during crack initiation via material key curve

The material key curves with varying bN specimen size (W is 5 to 50 mm) but similar notch length (a_0/W ratio) were compared in Figure 9 (increasing a_0/W ratio from Figure 9a to Figure 9e). As discussed in the theory part of this publication, the normalized load P_N can be directly related to changes in the constraint, as long as the testing conditions are constant (yield stress of the material, σ_y , and span length over width ratio, S/W) [19]. Therefore, special attention was given to changes within the testing conditions. Small changes in σ_y related to the slightly different strain rates (see [5]) can be reasonably assumed to play a secondary role, and have been disregarded. Furthermore, the S/W ratio was kept constant. Hence, P_N can be used as an index for the constraint in front of the crack tip.



(a)

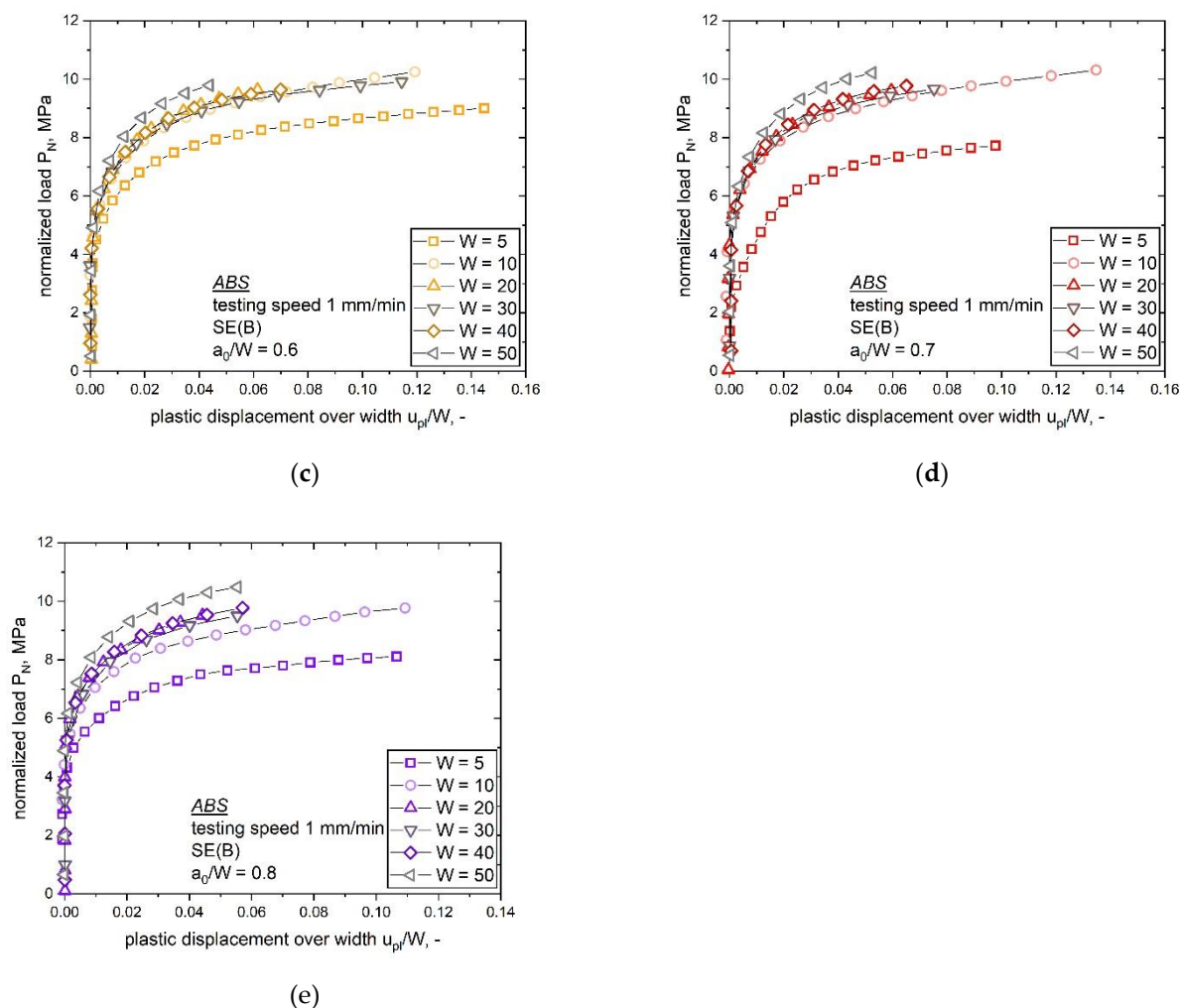


(b)

289
290
291
292
293
294
295
296

297
298
299
300
301
302
303
304
305

306
307



308

309

310

Figure 9. Material key curve of the investigated bN ABS specimens with different size (W is 5, 10, 20, 30, 40 and 50 mm) and varying a_0/W ratios 0.4 (a), 0.5 (b), 0.6 (c), 0.7 (d) and 0.8 (e).

311

312

The direct relationship between the material key curve and the level of constraint raised by the notch is demonstrated only for an ideally elastic plastic material, for which the material key curve is a horizontal line. In a real case, for a ductile polymer, the material key curve increases with increasing u_{pl}/W and if the displacement of the final point of the loading curve is sufficiently high, a plateau can be achieved. Even though it was not possible to determine a perfectly horizontal plateau region for specimens examined within this work, a clearly different trend is exhibited by the material key curves of the various sizes. In the present paper, the determined material key curves, at a given a_0/W , flatten after the initial phase toward a plateau level. Therefore, the presented curves in **Figure 9** can be seen as representative for the present constraint state.

313

314

315

316

317

318

319

320

The comparison of the different specimen sizes at a fixed a_0/W ratio displays some deviations in the observed P_N -values (**Figure 9**). Especially, with increasing a_0/W ratio the material key curves of the smallest (W is 5 mm) and the largest specimen size (W is 50 mm) differ significantly. For specimens with the lowest a_0/W ratio of 0.4 (**Figure 9a**), the observed material key curves show low deviation between the different specimen sizes. Hence, all ABS specimen sizes with an a_0/W ratio of 0.4 display a similar constraint situation in front of the notch tip. With increasing notch length (a_0/W ratio) the trend changes and differences in the constraint values with increasing specimen size are observed, as shown in **Figure 9b-d** (a_0/W ratio of 0.5, 0.6 and 0.7). However, for example, samples with W is 10 to 40 mm and an a_0/W ratio of 0.6 (**Figure 9c**), which is also the recommended a_0/W ratio for the multispecimen procedure, show similar material key curves, which indicates a similar crack tip constraint. The highest deviation in the values of P_N were observed for the largest specimen size (W is 50 mm). For the highest a_0/W ratio of 0.8 (**Figure 9e**), a higher deviation is observed,

321

322

323

324

325

326

327

328

329

330

but the trend is the same for the other configurations. These differences in the material key curves and subsequently stress states can be related to changes in the observed fracture initiation parameters. Hence, it is of high interest to evaluate these differences and consider geometry changes for accurate component design. To summarize this, P_N -values at a fixed ratio of u_{pl}/W were evaluated (shown in **Figure 10**). For this, an u_{pl}/W value of 0.04 was used since it is the highest level of u_{pl}/W for which P_N data are available for all the specimen sizes and a_0/W ratios explored.

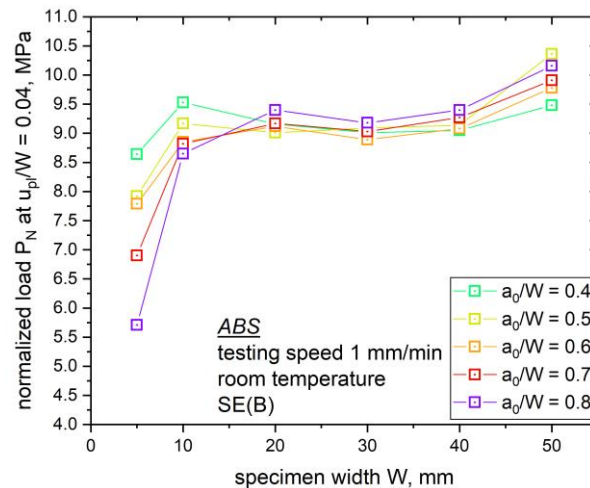


Figure 10. P_N at a fixed u_{pl}/W ratio of 0.04 for every bN specimen size examined (W is 5, 10, 20, 30, 40 and 50 mm) with varying a_0/W ratios (0.4 to 0.8).

Two trends can be noticed in the material key curve and the compared P_N -values in **Figure 10**:

- the influence of the a_0/W ratio for each investigated specimen size
- the influence of the specimen size on P_N -values at a fixed a_0/W ratio.

Starting with the influence of varying notch length (a_0/W ratio), the smallest specimen size (W is 5 mm) displays the highest deviations in the calculated P_N -values with increasing a_0/W ratio. As discussed in the previous section, also the largest specimen size shows high differences in the obtained P_N -values with changing a_0/W ratio. In contrast, the obtained P_N -values for specimen sizes from W is 10 mm to 40 mm display no significant influence of varying a_0/W ratio (P_N -values around 9 MPa were calculated for all notch lengths). By taking a closer look on the second influencing parameter shown in **Figure 10**, a constant a_0/W ratio and increasing specimen size, higher deviations in the obtained P_N -values for higher a_0/W ratios can be observed. For the lowest a_0/W ratio of 0.4 small differences in the obtained P_N -values (8.5 and 9.5 MPa) were observed. In comparison the highest a_0/W ratio of 0.8 resulted in P_N -values between 5.5 and 10.25 MPa. However, specimens with the highest a_0/W ratio can also be influenced by the small remaining ligament length, which can influence the full development of the plastic zone in front of the crack tip.

The discussed constraint information is of great interest, since size dependent fracture behavior was observed for up-scaled ABS specimens within a recently published work [5]. The previous study on sN ABS specimens was done at a fixed a_0/W ratio of 0.6. It is obvious from **Figure 9c** and **Figure 10** that for a fixed a_0/W ratio almost no differences in the material key curve can be observed for specimen sizes between W is 10 to 40 mm. However, material key curves from small (W is 5 mm) and large (W is 50 mm) specimen size show a significant difference. This supports the assumption of changing constraint close to the crack tip for different specimen sizes. Since all specimen sizes from W is 10 to 40 mm displayed similar constraint states, it is of high interest to examine if the crack growth phase of these specimen sizes exhibits also a similar constraint state.

4.2. Crack growth resistance curve

4.2.1. Crack growth resistance curve from the multispecimen procedure

In the previous study on size dependent fracture parameters [5], it was not possible to precisely discuss the shape of the combined J-R curve, due to a limited number of data points available at low values of Δa . This was due to the

experimental setup of the load separation method, where high Δa values are required. Subsequently, more data points at lower Δa values were generated for the combined crack growth resistance curve in this work. **Figure 11** shows the combined J-R curve of all specimen sizes (W is 5 to 50 mm) with these additional data points. The resulting crack growth resistance curve from **Figure 11**, including the additional test data, still displays one uniform curve.

366
367
368
369
370

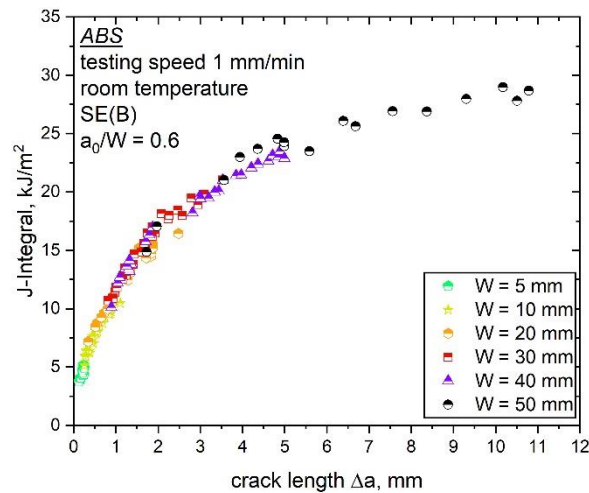


Figure 11. J-R curve for increasing specimen sizes (W is 5, 10, 20, 30, 40 and 50 mm) of ABS, determined following the ESIS TC 4 multispecimen procedure (adapted from [5]).

371
372

The J-R curve presented in **Figure 11** displays one overlapping curve for all investigated specimen sizes of ABS. However, by taking a closer look on the curve shape of each evaluated J-R curve it is no longer possible to describe the combined J-R curve (all data points of the investigated specimen sizes) via one power-law fit (according to equation 11). Especially, for the smallest and largest specimens examined a slightly deviating fracture behavior is observed, which is quantified via the application of a power law fit. The resulting fitting parameter c and b of each specimen size (listed in **Table 3**) show the expected deviations for the smallest (W is 5 mm) and the largest specimen size (W is 50 mm), particularly measurable in the variation of parameter c . All examined specimen sizes in between (W is 10 to 40 mm) showed similar fitting parameters. Hence, size independent crack growth behavior can be assumed, where all examined specimen sizes (from W is 10 to 40 mm) exhibit the same fracture resistance against crack growth.

373
374
375
376
377
378
379
380
381

The specimen up-scaling method used in the present and previous studies [5], where all geometry parameters (B , L , a_0) are dependent on the specimen width W , is rarely found in scientific work. This makes the comparison of the crack resistance curve determined here with results from literature challenging. However, evaluating plane stress and strain states with variations of the specimen thickness B at a constant specimen width W is portrayed in literature [11,29]. The variation of the specimen thickness is one of the most common procedures to investigate the influence of specimen size. With increasing B , thickness-independent material constants can be determined (transition from plane stress to plane strain state). In contrast to this, the specimen width W usually has almost no influence on the J-R curves, as long as boundary conditions are not modified [29]. The presented simultaneous up-scaling procedure in this study, where B increases with increasing W (fixed geometry ratio as in the present study) can also enable the calculation of size independent fracture parameters as shown in **Figure 11**.

382
383
384
385
386
387
388
389
390
391
392

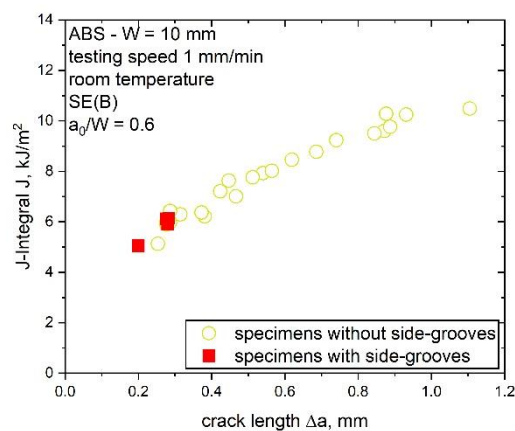
Table 3. Power law fitting parameter (c and b according to equation 11) of the J-R curve with the corresponding statistical coefficient R^2 and initiation toughness value $J_{0.2}$ for increasing specimen size (W is 5, 10, 20, 30, 40 and 50 mm) of ABS specimens, determined following the ESIS TC 4 multispecimen method.

| Specimen width W | Parameter c (power law fit) | Parameter b (power law fit) | R^2 | Crack initiation $J_{0.2}$ (apparent) | Crack initiation J_{b1} (apparent) |
|------------------|--|-----------------------------|-------|---------------------------------------|--------------------------------------|
| [mm] | [kJ/(m ² mm ^b)] | [-] | - | [kJ/m ²] | [kJ/m ²] |
| 5 | 8.7 | 0.41 | 0.718 | 4.5 | 2.4 |
| 10 | 10.4 | 0.45 | 0.972 | 5.0 | 2.7 |
| 20 | 11.3 | 0.45 | 0.978 | 5.5 | 3.0 |
| 30 | 11.9 | 0.47 | 0.969 | 5.6 | 3.0 |
| 40 | 12.3 | 0.41 | 0.984 | 6.3 | 4.2 |
| 50 | 14.6 | 0.29 | 0.936 | 9.1 | 8.4 |

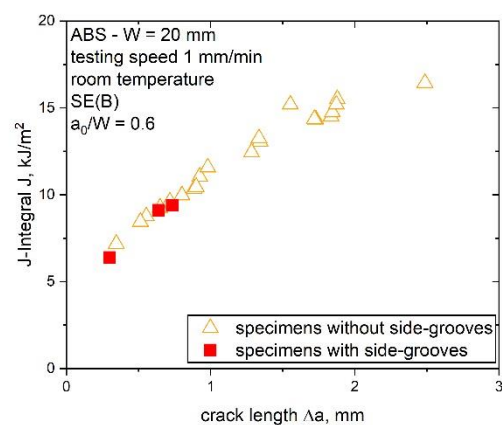
To increase the knowledge about the examined specimen sizes with similar fracture resistance curves (from W is 10 to 40 mm), the constraint situation was changed in the crack growth phase. Side-grooved specimens were tested for specimen sizes ranging from W is 10 to 40 mm and compared to the J-R curves presented in **Figure 11**. Side-grooves change the zone of low constraint near the outer surface of a specimen and reduce the possibility of shear lip formation, which leads to a higher constraint level. The testing of side-grooved specimens, with higher constraint and stress within the specimen, can provide information about the sensitivity of the fracture process to overall constraint changes during crack propagation.

4.2.2. Determination of specimen constraint during crack propagation via testing of side-grooved specimens

By the application of side-grooves, the constraint close to the edges is changed and the constraint is increased. Hence, it should be possible to confirm changes in the crack growth behavior by comparing the results of these specimens with the established J-R curves. Therefore, three side-grooved specimens of each specimen size (W is 10, 20, 30 and 40 mm) were tested according to the ESIS TC-4 multispecimen method [8]. The results from the side-grooved specimens were compared to the J-R curves of the previous study [5] and are shown in in **Figure 12**.



(a)



(b)

393
394
395396
397
398
399
400
401
402
403

404

405
406
407
408
409

410

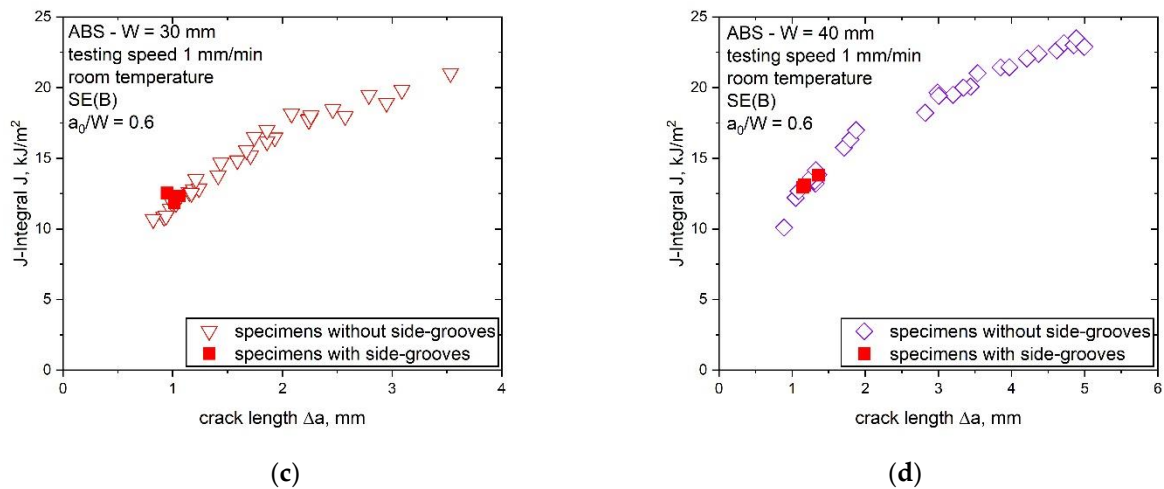


Figure 12. Resulting J-R curves of specimens tested with and without side-grooves for increasing specimen sizes (W is 10 mm (a), 20 mm (b), 30 mm (c) and 40 mm (d)) following the ESIS TC 4 multispecimen procedure (from [5]).

The determined J-R curves in **Figure 12** display no difference between specimens with and without side-grooves, in contrary to specimens with different sizes. The observed behavior denotes that the changing constraint in side-grooved specimens did not lead to a significant difference in the crack growth behavior. Similar behavior was also reported in a previous study on Polypropylene specimens [30], where several specimen sizes with and without side-grooves were compared. The results indicate that (for W is 10 to 40 mm), even if the constraint is artificially changed in the specimen, the crack growth behavior (at least as described by the J-R curve) does not change and a size-independent fracture behavior can be assumed.

4.3. Fracture initiation parameters

4.3.1. Initiation toughness parameter determined from the J-R curve

The initiation values $J_{0.2}$ for increasing specimen size, with the corresponding statistical coefficient R^2 of the fitted J-R curve, determined according to the ESIS TC 4 multispecimen method, are listed in **Table 3**. For the evaluation of $J_{0.2}$ values, the J-R curve of every specimen size examined is fitted (with the recommended power law according to equation 11 [12]) and afterwards the J-Integral is determined at 0.2 mm crack growth. Hence, the evaluated $J_{0.2}$ value is strongly dependent on the successful fitting of the J-R curve. Therefore, the statistical coefficient R^2 of every fitted J-R curve is also listed in **Table 3**. Based on the significant differences in the shape of the J-R curve from the largest specimen size (W is 50 mm), its initiation parameters are highly questionable. The observed $J_{0.2}$ values range from 4.5 kJ/m² (for the smallest specimen, W is 5 mm) to 9.1 kJ/m² (for the largest specimen, W is 50 mm). For the specimen sizes W is 10 to 40 mm, the observed initiation parameters display nearly constant values, only a slight increase from 5.0 kJ/m² to 6.3 kJ/m². However, the smallest and largest specimen size displayed a significant difference in the calculated initiation value. The resulting R^2 of the fitting procedure displays a low value for the smallest specimen size (W is 5 mm), due to the experimental difficulty of testing very small specimens (manufacturing accuracy, testing equipment, determination of the crack advancement using a light microscope). Hence, the determined crack initiation value, $J_{0.2}$, for the smallest specimen size is also questionable. All other specimen sizes displayed R^2 values from 0.936 to 0.984, which indicates that all data points can be fitted well with the applied power law.

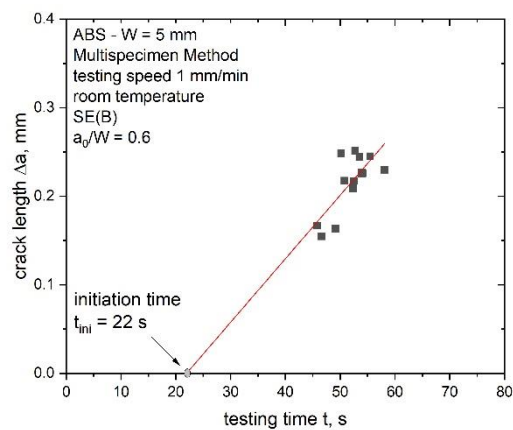
Furthermore, the initiation parameter J_{bl} was evaluated (listed in **Table 3**) as the intersection of the blunting line with the fit of each J-R curve. Therefore, the yield stress σ_y was used (28.5 MPa), which was investigated in the previous study [5]. J_{bl} displays fracture initiation values from 2.4 kJ/m² (W is 5 mm) to 4.2 kJ/m² (W is 40 mm), which are significantly lower than the evaluated values for $J_{0.2}$. However, both initiation values display a similar trend. Based on the multispecimen procedure [12], the lowest initiation value has to be taken as initiation toughness parameter, which in this case is the blunting value J_{bl} . However, also J_{bl} is depending on the successful fitting of the J-R curve, as discussed for $J_{0.2}$. Both initiation parameters ($J_{0.2}$ and J_{bl}) refer to a region of the J-R curve quite far from the experimental data points used for its construction, especially for larger specimen sizes. Hence, they have to be interpreted as apparent values. Furthermore, the fitting regions (Δa range) differ for the examined specimen sizes. In consideration of this, it

can be reasonably assumed that the values of the initiation parameter ($J_{0.2}$ and J_{bl}) can be influenced by computational effects, especially for the highest size examined (W is 50 mm). To improve the understanding of the present crack initiation behavior, further methods for the characterization of initiation parameters were conducted.

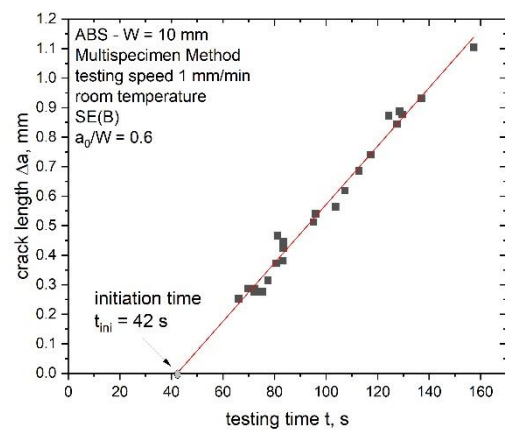
4.3.2. Initiation toughness parameter J_{ini}

The calculation of the crack propagation kinetics curve, where Δa is plotted against the testing time t , is an additional method for the investigation of entire fracture processes. Based on the crack propagation kinetics curve it is possible to evaluate the parameter J_{ini} , which is representing the crack initiation. Therefore, the crack initiation time, t_{ini} , is required beforehand. The determined crack propagation kinetics curve with its estimated initiation times, t_{ini} , are shown in **Figure 13** for the ABS specimens with different sizes.

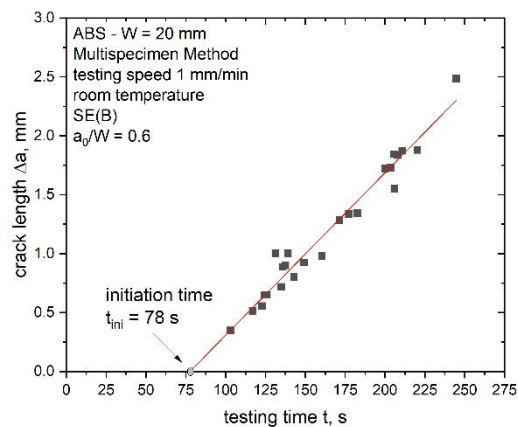
The limited data points at low testing times, representing the blunting process (stage I) and crack initiation (stage II), lead to a slightly modified experimental procedure for the determination of t_{ini} . The initiation time was estimated as the intersection of the linear fit of the available data points from stage III (representing crack growth) with the x-axis (details in the experimental section). The initiation time, t_{ini} , increases with increasing specimen size as shown in **Figure 13**. The linear fit was difficult to apply in the case of the smallest specimen size (W is 5 mm). For the other investigated geometries (W is 10 mm to 50 mm) a good application of a linear fit was possible. Additionally, the crack growth speed in stage III was determined and the increase was found to be small over the whole scaling range (increase from 0.4 to 1.5 mm/min from the smallest to the largest specimen size).



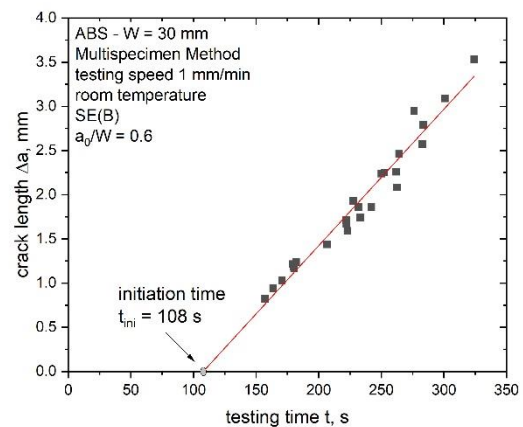
(a)



(b)



(c)



(d)

465

466

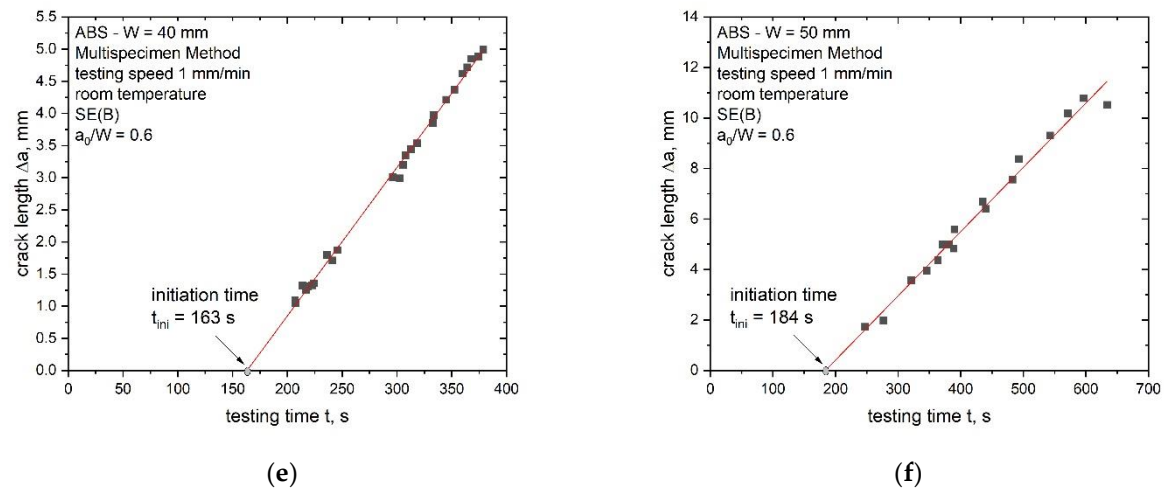


Figure 13. Determination of the crack initiation time, t_{ini} , via the crack propagation kinetics curve (produced crack length Δa depending on the testing time t) for all investigated specimen sizes of ABS (W is 5 (a), 10 (b), 20 (c), 30 (d), 40 (e) and 50 mm (f)).

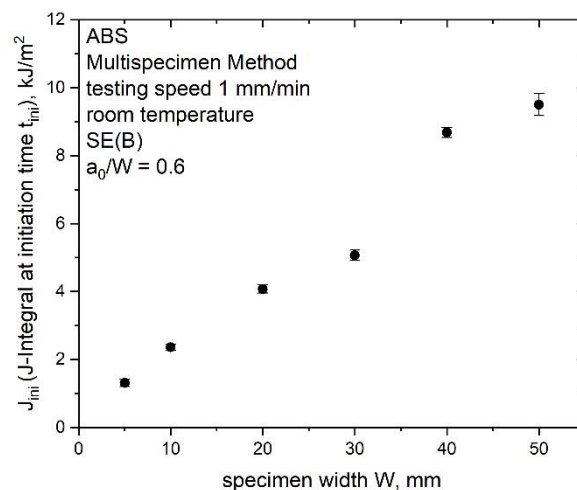


Figure 14. Growing initiation toughness value J_{ini} (J-Integral at the initiation time t_{ini}) for increasing specimen sizes (W is 5, 10, 20, 30, 40 and 50 mm) of ABS.

For a better comparison to the other crack initiation parameters, J_{ini} (J-Integral at the initiation time t_{ini}) was calculated and is presented in **Figure 14** for the up-scaled specimens of ABS. The physical crack initiation (J-Integral at initiation time t_{ini}) increases with increasing specimen size (from 0.8 kJ/m^2 for W is 5 mm to 9.5 kJ/m^2 for W is 50 mm). In comparison with the evaluated $J_{0.2}$ values (**Table 3**), the calculated J_{ini} is smaller and exhibits a strongly size-dependent behavior. Size dependent initiation toughness values were also found in literature [30], where methods from LEFM (stress intensity factor " K_Q ", " K_{max} ") were used to describe the elastic part of the J-R curve. Similar to results in this study, the linear elastic fracture parameters (" K_Q ", " K_{max} ") increased with increasing specimen size.

4.3.3. Comparison of crack initiation parameters

In the present study, additional tests on up-scaled sN ABS specimens were done to increase the completeness of the J-R curve data from the previous study [5]. In this previous work, the characterized J-R curve displayed size-independency, whereby, the initiation parameter ($J_{I,lim}$ from the ESIS TC 4 draft protocol [6]) exhibited strong size dependent behavior. A size independent crack resistance curve for specimen sizes from W is 10 to 40 mm was confirmed also by the additional data points measured following the ESIS TC 4 procedure. However, the calculated apparent initiation

toughness parameters $J_{0.2}$ and J_{bl} (based on the ESIS TC 4 multispecimen procedure) and J_{ini} (based on the crack propagation curve and t_{ini}) displayed different fracture initiation behavior for the examined specimen sizes (size dependent crack initiation parameter). For the sake of comparison, all calculated initiation toughness parameters ($J_{0.2}$, J_{bl} , J_{ini} and $J_{I,lim}$) are shown in **Figure 15**.

The initiation value $J_{0.2}$ displayed the highest values for small specimen sizes compared to the other assessed initiation parameters. For the specimen sizes W is 10 to 40 mm, $J_{0.2}$ displayed only a slight increase and indicating a plateau, whereby, the smallest (W is 5 mm) and the largest (W is 50 mm) specimen size display some differences. The observed fracture initiation behavior of $J_{0.2}$ is explained by the observed constraint differences for the smallest and largest specimen sizes and a simply computational effect arising with the chosen fitting range. J_{bl} showed a similar trend as $J_{0.2}$ (**Figure 15**). However, it showed the lowest fracture initiation values and is therefore the representative initiation toughness value according to the multispecimen procedure [12]. It has to be noted that J_{bl} is not only influenced by the computational effect of the fitting range. There is also the additional dependency on the evaluated σ_y . Since small changes in σ_y are assumed to play a secondary role [5], the influence on the initiation value can also be negligible. However, for a successful evaluation of an initiation value this aspect has to be kept in mind.

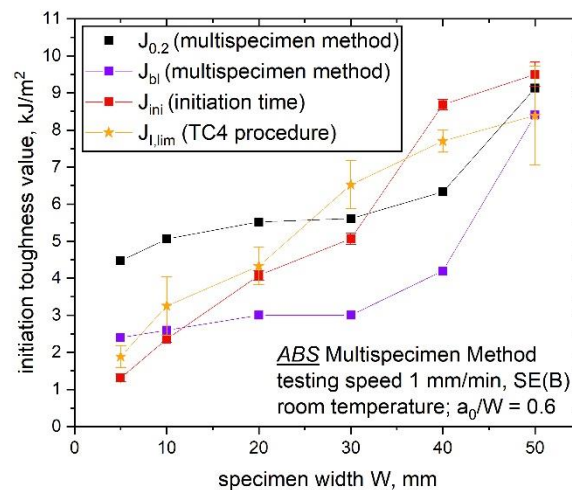


Figure 15. Comparison of initiation toughness parameters $J_{0.2}$ (multispecimen procedure), J_{bl} (multispecimen procedure) J_{ini} (based on the initiation time t_{ini}) and $J_{I,lim}$ (ESIS TC 4 draft protocol) for increasing specimen sizes W is 5, 10, 20, 30, 40 and 50 mm (adapted from [5]).

The calculated J_{ini} values (based on the initiation time t_{ini}) depicted a continuously increasing initiation value with increasing specimen size and the values are in the same range as the observed $J_{I,lim}$ data from the previous research [5]. These deviations between the initiation values based on the multispecimen method ($J_{0.2}$ and J_{bl}) and the other two initiation parameters (J_{ini} and $J_{I,lim}$) give rise to the assumption that these parameters mark two different stages during the fracture process. The estimated apparent values from the J-R curve ($J_{0.2}$ and J_{bl}) are representing crack initiation, whereby J_{ini} and $J_{I,lim}$ mark the beginning of stable crack growth. It is difficult to define crack initiation for ductile polymers, since it is a continuous process from blunting to crack advancement [18]. However, in this work, crack initiation is defined as the early starting of a progressive process of crack propagation. Typically, the crack starts to grow at the notch tip from the inner region of the specimen. Furthermore, the stable crack growth phase is related to a fully developed crack front along the whole thickness and a constant crack propagation rate. This was not experimentally checked within this work and is the topic of future work. The assumption that $J_{0.2}$ and J_{bl} represent crack initiation and J_{ini} and $J_{I,lim}$ mark the beginning of stable crack growth is based on the differences in the used experimental approach of the presented parameters. As discussed in the previous section, J_{ini} is calculated as the intersection between the linear data fit of stage III (area of stable crack growth) and the x-axis. Hence, the influence of the blunting phase is not represented in the estimation of J_{ini} , which strengthens the hypothesis that J_{ini} marks the point of stable crack growth instead of crack initiation. Also the parameter $J_{I,lim}$ is suggested as parameter for indicating stable crack growth, since a fixed value in the normalized load separation curve is defined as $J_{I,lim}$ in the ESIS TC 4 procedure [6]. This fixed value is defined after the blunting phase and at the beginning of stable crack growth. A slight overestimation of the crack initiation by the parameter $J_{I,lim}$ and the optical analysis of the fracture initiation was already discussed in literature [18].

Generally, fracture initiation and the point of stable crack growth must not be at the same level during a fracture experiment, which is also shown in **Figure 15**. For small specimen sizes crack initiation (marked by J_{bl}) and the point of stable crack growth (marked by J_{ini} or $J_{l,lim}$) are nearly at the same J-value. However, for increasing specimen sizes the crack initiation value is significantly lower compared to the point of stable crack growth. This can be explained by the increasing specimen thickness and the particular nature of crack initiation, which is typically a progressive process characterized by a slow development over the whole crack front [18]. Based on these new findings, the parameter $J_{0.2}$ is above the limit value of stable crack growth for small specimen sizes and below for large specimen sizes. Therefore, it is suggested to adapt the fixed initiation value $J_{0.2}$ to a more geometry dependent value to take changing specimen sizes into account.

4. Conclusion

It is necessary to acquire detailed knowledge of the up-scaling relationships of fracture parameters (crack initiation and crack growth parameter) and the constraint (crack tip triaxiality) to design complex components. The present work shows insights into the dependency of constraint and fracture behavior on the specimen size (SE(B) specimens with maximum up-scaling ratio of 10) of the investigated polymer ABS.

Changing constraint levels in the crack initiation and crack growth phase were evaluated by the application of the material key curve method for the smallest (W is 5 mm) and the largest (W is 50 mm) specimen size. However, all investigated specimen sizes in between (W from 10 to 40 mm) displayed a similar constraint for the crack initiation and crack propagation. With regard to crack propagation behavior it was found that the introduction of side-grooves, and a subsequent change in the overall stress state showed no influence on the results when compared to the J-R curve of non-grooved specimens.

The resulting J-R curve showed one overlapping curve for all tested specimen sizes of ABS. However, for the smallest and the largest specimen sizes some changes in the fitting parameters were detected, which support the results of changing constraint levels for these two specimen sizes. The changing constraint state for small and large specimens is also represented in the apparent initiation parameters based on the J-R curve ($J_{0.2}$ and J_{bl}).

Furthermore, the influence of the specimen size on the fracture initiation was investigated. Therefore, four parameters were analysed and compared in detail:

- $J_{0.2}$ (apparent), which is based on the technological evaluation of the J-R curve [12], displayed slowly increasing initiation values for specimens with W is 10 to 40 mm.
- J_{bl} (apparent), which is also based on the technological evaluation of the J-R curve [12], displayed the lowest initiation values and a similar behavior as $J_{0.2}$
- J_{ini} , which is based on the initiation time t_{ini} , displayed increasing crack initiation values with increasing specimen size, where small deviations were detected for changing constraint states
- $J_{l,lim}$, which is based on the ESIS TC4 LS method, displayed similar results as J_{ini} and supports the size-dependent fracture initiation behavior (initiation parameters increase with increasing specimen size)

The contrary behavior of the four initiation parameters is explained by a closer look on the evaluation and the experimental approach, where $J_{0.2}$ and J_{bl} are more technological parameters describing the crack initiation. J_{ini} and $J_{l,lim}$ are based on the physical crack initiation and mark the point of stable crack growth. In spite of the apparent character attributed to $J_{0.2}$ and J_{bl} , the results of the investigations suggest the use of the initiation parameters $J_{0.2}$ and J_{bl} for material ranking and comparison, due to the low differences in the resulting values of different geometries. Contrary, the parameters J_{ini} and $J_{l,lim}$ are of high interest to evaluate the point of stable crack growth.

In the future further investigations of the changing constraint state for small and large specimens are planned. Furthermore, the found experimental results will be compared with numerical simulations to gain more information about stress state and constraint close to the crack tip. In addition, the crack growth process has to be examined in detail and compared with the two types of initiation parameters found in this study.

Author Contributions: Conceptualization, A.G., F.J.A. and F.B.; methodology, A.G., F.J.A. and F.B.; validation, A.G.; formal analysis, A.G.; investigation, A.G.; data curation, A.G.; writing—original draft preparation, A.G.; writing—review and editing, F.J.A., M.B., S.A., G.P, F.B.; visualization, A.G.; supervision, F.J.A. and F.B.; project administration, F.J.A. and M.B.; All authors have read and agreed to the published version of the manuscript

Acknowledgments: The research work of this paper was performed at the Materials Science and Testing of Polymers/ Montanuniversitaet Leoben within the framework of the COMET-program of the Federal Ministry for Climate Action, Environment, Energy, Mobility, Innovation and Technology and the Federal Ministry for Digital and Economic Affairs with contributions by the

Polymer Competence Center Leoben GmbH and the Università degli Studi di Brescia (Dipartimento di Ingegneria Meccanica e Industriale).

Conflicts of Interest: The authors declare no conflict of interest

5. References

- [1] T.L. Anderson, *Fracture Mechanics: Fundamentals and Application*, CRC Press - Taylor & Francis Group, 2005.
- [2] J.R. Donoso, J.D. Landes, The role of constraint on the calibration functions for the prediction of ductile fracture behavior in structural components, *Int. J. Fracture* 63 (1993) 275–285.
- [3] J.R. Donoso, Common format for developing calibration curves in elastic plastic fracture mechanics, *Eng. Fract. Mech.* 47 (1994) 619–628.
- [4] X.-K. Zhu, J.A. Joyce, Review of fracture toughness (G, K, J, CTOD, CTOA) testing and standardization, *Eng. Fract. Mech.* 85 (2012) 1–46. <https://doi.org/10.1016/j.engfracmech.2012.02.001>.
- [5] A. Gosch, F.J. Arbeiter, S. Agnelli, M. Berer, G. Pinter, F. Baldi, J-testing of polymers via the load separation criterion based ESIS TC4 procedure: Effect of the specimen size, *Polym. Test.* 89 (2020) 106637. <https://doi.org/10.1016/j.polymertesting.2020.106637>.
- [6] S. Agnelli, F. Baldi, A testing protocol for the construction of the load separation parameter curve for plastics, ESIS TC4 communication (2015).
- [7] H. Ernst, P.C. Paris, J.D. Landes, Estimations on J-Integral and tearing modulus T from a single specimen test record, *American Society of Testing and Materials* (1981) 476–502.
- [8] G.E. Hale (Ed.), *An evaluation of the ESIS protocol for measurement of the J-fracture toughness of thermoplastics*, 1995.
- [9] S. Agnelli, F. Baldi, B.R.K. Blackman, L. Castellani, P.M. Frontini, L. Laiariandrasana, A. pegoretti, M. Rink, A. Salazar, H.A. Visser, Application of the load separation criterion in J-testing of ductile polymers: A round-robin testing exercise, *Polym. Test.* 44 (2015) 72–81. <https://doi.org/10.1016/j.polymertesting.2015.03.019>.
- [10] F. Baldi, S. Agnelli, L. Andena, B.R.K. Blackman, L. Castellani, P.M. Frontini, J. Kučera, L. Laiarinandrasana, A. Pegoretti, A. Salazar, L. Warnet, Determination of the Fracture Resistance of Ductile Polymers: The ESIS TC4 Recent Experience, *Matls. Perf. Charact.* 9 (2020) 20190175. <https://doi.org/10.1520/MPC20190175>.
- [11] M. Che, W. Grellmann, S. Seidler, Crack resistance behavior of polyvinylchloride, *J. Appl. Polym. Sci.* 64 (1997) 1079–1090. [https://doi.org/10.1002/\(SICI\)1097-4628\(19970509\)64:6<1079:AID-APP7>3.0.CO;2-I](https://doi.org/10.1002/(SICI)1097-4628(19970509)64:6<1079:AID-APP7>3.0.CO;2-I).
- [12] G.E. Hale, F. Ramsteiner (Eds.), *J-Fracture toughness of polymers at slow speed*, Elsevier, Oxford, UK, 2001.
- [13] P.M. Frontini, L.A. Fasce, F. Rueda, Non linear fracture mechanics of polymers: Load Separation and Normalization methods, *Eng. Fract. Mech.* 79 (2012) 389–414. <https://doi.org/10.1016/j.engfracmech.2011.11.020>.
- [14] C.R. Bernal, A.N. Cassanelli, P.M. Frontini, A Simple Method for J-R Curve Determination in ABS Polymers, *Polym. Test.* 14 (1995) 85–96.
- [15] C.R. Bernal, P.E. Montemartini, P.M. Frontini, The Use of Load Separation Criterion and Normalization Method in Ductile Fracture Characterization of Thermoplastic Polymers, *J. Polym. Sci., Part B: Polym. Phys.* 34 (1996) 1869–1880.
- [16] A. Salazar, J. Rodriguez, The use of the load separation parameter Spb method to determine the J–R curves of polypropylenes, *Polym. Test.* 27 (2008) 977–984. <https://doi.org/10.1016/j.polymertesting.2008.08.013>.
- [17] F. Baldi, T. Ricco, High-rate J-testing of toughened polyamide 6/6: Applicability of the load separation criterion and the normalization method, *Eng. Fract. Mech.* 72 (2005) 2218–2231. <https://doi.org/10.1016/j.engfracmech.2005.02.002>.
- [18] F. Baldi, S. Agnelli, T. Rico, On the determination of the point of fracture initiation by the load separation criterion in J-testing of ductile polymers, *Polym. Test.* 32 (2013) 1326–1333. <https://doi.org/10.1016/j.polymertesting.2013.08.007>.

- [19] S. Agnelli, F. Baldi, L. Castellani, K. Pisoni, M. Vighi, L. Laiarinandrasana, Study of the plastic deformation behaviour of ductile polymers: Use of the material key curves, *Mechanics of Materials* 117 (2018) 105–115. <https://doi.org/10.1016/j.mechmat.2017.11.002>.
- [20] S. Agnelli, F. Baldi, T. Riccò, The load separation criterion in elastic-plastic fracture mechanics: Rate and temperature dependence of the material plastic deformation function in an ABS resin, Ischia, Italy, AIP, 2012, pp. 114–116.
- [21] F. Baldi, S. Agnelli, T. Riccò, On the applicability of the load separation criterion in determining the fracture resistance (JIC) of ductile polymers at low and high loading rates, *Int. J. Fracture* 165 (2010) 105–119. <https://doi.org/10.1007/s10704-010-9510-9>.
- [22] M.H. Sharobeam, J.D. Landes, The load separation criterion and methodology in ductile fracture mechanics, *Int. J. Fracture* 47 (1991) 81–104.
- [23] M.H. Sharobeam, J.D. Landes, The load separation and npl development in precracked specimen test records, *Int. J. Fracture* 59 (1993) 213–226.
- [24] A. Gosch, F.J. Arbeiter, M. Berer, G. Pinter, Comparison of J-integral methods for the characterization of tough polypropylene grades close to the glass transition temperature, *Eng. Fract. Mech.* (2018). <https://doi.org/10.1016/j.engfracmech.2018.06.002>.
- [25] A. Salazar, J. Rodriguez, A.B. Martinez, The role of notch sharpening on the J-fracture toughness of thermoplastic polymers, *Eng. Fract. Mech.* 101 (2013) 10–22. <https://doi.org/10.1016/j.engfracmech.2012.07.006>.
- [26] R. Lach, T. Krolopp, P. Hutar, W. Grellmann, Influence of the interface and the additional layer on the stable crack propagation through polyolefin bilayered structures, *Procedia Mater. Sci.* 3 (2014) 867–872. <https://doi.org/10.1016/j.mspro.2014.06.141>.
- [27] R. Lach, S. Seidler, W. Grellmann, Resistance Against the Intrinsic Rate of Fracture Mechanics Parameters for Polymeric Materials Under Moderate Impact Loading, *Mech. Time-Depend. Mater.* 9 (2005) 103–119.
- [28] R. Lach, W. Grellmann, Time- and Temperature-Dependent Fracture Mechanics of Polymers: General Aspects at Monotonic Quasi-Static and Impact Loading Conditions, *Macromol. Mater. Eng.* 293 (2008) 555–567. <https://doi.org/10.1002/mame.200700417>.
- [29] O. Kolednik, A simple model to explain the geometry dependence of J-Da curves, *Int. J. Fracture* 63 (1993) 263–274.
- [30] P. Frontini, E. Santarelli, The Effects of Specimen Size and Testing Conditions on Fracture Toughness Evaluation of Polypropylene Homo polymer, *Polym. Eng. Sci.* 41 (2001) 1803–1814.

Publication 4

Bibliographic information

Title: Mixed Mode I/III fatigue fracture characterization of Polyoxymethylene

Authors: Anja Gosch¹, Michael Berer², Pavel Hutař³, Ondrej Slávik³, Tomáš Vojtek^{3,4}, Florian J. Arbeiter¹, Gerald Pinter²

Affiliation:

1. Materials Science and Testing of Polymers, Montanuniversitaet Leoben, Otto-Gloeckel-Str. 2, 8700 Leoben, Austria
2. Polymer Competence Center Leoben GmbH, Roseggerstr. 12, 8700 Leoben, Austria
3. Institute of Physics of Materials, Academy of Sciences of the Czech Republic, Žižkova 22, 616 62 Brno, Czech Republic
4. Central European Institute of Technology (CEITEC), Brno University of Technology, Purkyňova 123, 612 00 Brno, Czech Republic

Periodical: International Journal of Fatigue

doi.org/10.1016/j.ijfatigue.2019.105269

Relevant contributions to this publication

| | |
|-----------------------------|--|
| Conceptualization: | Anja Gosch, Michael Berer |
| Methodology: | Anja Gosch, Michael Berer, Pavel Hutař, Ondrej Slávik, Tomáš Vojtek |
| Validation: | Anja Gosch, Ondrej Slávik |
| Investigation: | Anja Gosch |
| Writing - Original Draft: | Anja Gosch |
| Writing - Review & Editing: | Michael Berer, Pavel Hutař, Ondrej Slávik, Tomáš Vojtek, Florian Arbeiter, Gerald Pinter |



ELSEVIER

Contents lists available at ScienceDirect

International Journal of Fatigue

journal homepage: www.elsevier.com/locate/ijfatigue

Mixed Mode I/III fatigue fracture characterization of Polyoxymethylene

Anja Gosch^a, Michael Berer^{b,*}, Pavel Hutař^c, Ondrej Slávik^c, Tomáš Vojtek^{c,d}, Florian J. Arbeiter^a, Gerald Pinter^{a,b}^a Materials Science and Testing of Polymers, Montanuniversitaet Leoben, Otto-Gloeckel-Str. 2, 8700 Leoben, Austria^b Polymer Competence Center Leoben GmbH, Roseggerstr. 12, 8700 Leoben, Austria^c Institute of Physics of Materials, Academy of Sciences of the Czech Republic, Žitkova 22, 616 62 Brno, Czech Republic^d Central European Institute of Technology (CEITEC), Brno University of Technology, Purkyňova 123, 612 00 Brno, Czech Republic

ARTICLE INFO

Keywords:

Mixed Mode loading
Polymers
Fatigue crack growth
Fracture mechanics
Equivalent stress intensity factor

ABSTRACT

The crack growth behaviour of thermoplastic polymers is a relevant topic in current research. While a dominant portion of studies in fracture mechanics investigates Mode I loading situations, very little is done to better understand Mixed Mode crack growth, which can be equally important to accurate live time predictions of polymer parts. In this research, fatigue tests on cylindrically notched specimens were performed in Mixed Mode I/III loading and compared via the so called equivalent stress intensity factor. Under these loading conditions, a significant reduction of the cycles to fracture occurred compared to pure Mode I.

1. Introduction

Bearing elements made of various materials are common in daily applications such as roller bearings, carrier rollers, deflector rolls, etc. Advantages of polymer bearing elements are for example the suitability for mass production of small-sized parts and a higher damping ability (noise reduction). However, the applicability of bearing elements made of polymers is limited by comparatively low load levels and the number of load cycles in service, which was also discussed in a previous research [1]. Especially wear and surface fatigue as well as global fatigue of the bearing element are limiting factors [2]. Furthermore, global [3] and local [4] creep deformations in static loading phases as a result of the viscoelastic material behaviour of polymers limit the lifetime.

Polymeric bearing elements are often made of semi-crystalline thermoplastics, which exhibit significant amounts of shrinkage during the cooling down from the melt due to crystallization processes. This shrinkage is compensated during the manufacturing process (injection moulding) by the so called holding pressure. However, the holding pressure is often not able to compensate for the total amount of shrinkage. Thus voids and also internal stresses remain in the core of the polymeric bearing element. These holes can act as initial defects for crack growth, or depending on the loading type, even lead to failure of the component. Due to the type of loading during the application of bearing elements, these holes are exposed to Mixed Mode crack opening conditions. To analyse the corresponding stress state of bearing elements during operation, numerical analyses were conducted previously

[1,5]. Similar failure modes are also discussed in literature for rolling bearing elements made of metals [6]. To gain more insight in shear load failure mechanisms in polymers, the investigation of Mixed Mode loading cases is of high interest.

In general, the propagation of Mixed Mode loaded cracks is described as non-self-similar. This expresses that the crack is changing its growth direction under Mixed Mode conditions [7]. Hence, not only the crack growth rate is an important parameter for Mixed Mode loaded components, but also the crack growth direction. For metals, several types of Mixed Mode test specimen geometries are discussed in literature [7–12]. Also for laminates, Mixed Mode loading analyses are documented in literature [13–16]. In this field, the in-plane shear situation, which ends up in Mode II loading of the crack tip is of high interest. Concerning bulk polymer materials, only little research data is available, which is dealing with Mixed Mode fracture behaviour. One recent example is a study by Lach et al. [17], in which the quasi-static fracture behaviour of brittle, amorphous poly-methyl-methacrylate (PMMA) under combined Mode I/II loading was examined. In the limited number of publications available, different types of specimen geometries were used to characterize the Mixed Mode fracture behaviour of bulk polymers under monotonic loading mainly. The determination of Mixed Mode fatigue crack growth characteristics is even more complicated for bulk materials and hence, hardly investigated. Two reasons are mainly responsible for the high complexity in this field. The first reason is caused by the Mode II and Mode III loading itself, where the crack flanks are not opened during loading as this is

* Corresponding author.

E-mail addresses: michael.berer@pcccl.at, michael.berer@gmail.com (M. Berer).<https://doi.org/10.1016/j.ijfatigue.2019.105269>

Received 3 July 2019; Received in revised form 9 September 2019; Accepted 12 September 2019

Available online 13 September 2019

0142-1123/ © 2019 Elsevier Ltd. All rights reserved.

the case in Mode I. During fatigue loading in Mode II and Mode III, the crack flanks stay more or less closed, which allows their contact. This leads to wear and friction forces generated by the sliding crack flanks, which decrease the final lifetime of the component [18]. The second reason is called “Mode I branching” and describes the competition between shear and tensile crack opening loading Mode during the crack growth of shear loaded specimens. Mode I branching, where the crack changes the direction from Mode II or Mode III loading directly to Mode I loading, is often observed in metals and highly discussed in literature [6,18,19]. The described influences complicate the evaluation of Mixed Mode driven fatigue crack propagation in bulk polymeric materials. Hence, in previous studies dealing with the fatigue lifetime of bearing elements, almost exclusively Mode I fatigue crack opening was examined [20,21], even though a significant Mode II and Mode III loading level was shown in literature [5]. Since the influence of such high Mixed Mode levels on the lifetime of polymer parts was completely unclear at the beginning of this study, it was of high interest to characterize it on specimen level.

In detail, the aim of this study was to characterize the influence of Mixed Mode loading on the fatigue fracture behaviour of a Polyoxymethylene (POM) homopolymer resin in comparison to pure Mode I. To fully understand the failure of bearing elements, both Mode II and III will have to be examined. However, as a starting point, the results of Mode III are discussed in this work. Circumferentially notched round bars were tested under two different loading conditions: tension (Mode I) and combined tension and torsion (Mixed Mode I/III). Their fracture surfaces were studied to obtain detailed information on the crack growth processes during the fatigue experiments.

2. Materials and methods

2.1. Materials and specimens

The material examined in this study was a Polyoxymethylen homopolymer (POM-H), which was supplied as extruded bars with a diameter of 20 mm (Faigle, Hard, Austria). The chosen polymer displays good mechanical properties, high abrasion resistance, a low friction coefficient and a high ductility down to 0 °C. POM-H is an engineering polymer and is able to withstand high constant or fatigue loads without fracture.

The specimen geometry examined in this study was a cracked round

bar (CRB) as shown in Fig. 1. The specimens were cut from the extruded POM-H bars using a buzz saw. Afterwards, a sharp notch at the circumference of the specimens was produced with a razor blade (blade thickness 0.1 mm, tip-radius < 5 µm). The notching procedure was adapted from a recently published standard [22], which uses the same specimen geometry, but for the testing of Polyethylene pipe materials. The depth of this notch was approximately 1 mm. In this way, CRB specimens with an outer diameter of 20 mm and an inner diameter of 18 mm were obtained and used for all tests (Fig. 1).

2.2. Methods

2.2.1. Experimental

To investigate the Mixed Mode I/III behaviour of the POM homopolymer, the CRB specimens were loaded in two different ways. First, several tensile fatigue load levels were applied to determine the pure Mode I crack growth characteristics (Fig. 1a). Secondly, Mixed Mode I/III conditions were achieved by applying both, tensile fatigue load (Mode I) and torsional fatigue load (Mode III) as shown in Fig. 1b. CRB specimens have the advantage that uniform Mode III loading can be induced without the influence of Mode II, since it does not contain any corner singularities. Rectangular-shaped specimens always contain corners, which induce coupling of Mode II and Mode III [23]. Details concerning the experimental conditions and the applied load levels are presented in Table 1. The tests were carried out at room temperature and 50% relative humidity, in load controlled mode and with a sinusoidal signal shape. An important detail here is that the maximum and the minimum of the sinusoidal signal shapes of Mode I and Mode III were synchronised to be in phase. To measure the specimen surface temperature during testing, an IR Camera of the type ImageIR (InfraTec GmbH, Dresden, Germany) was used.

For a more detailed examination of the deformation mechanisms, the fracture surfaces were analysed using an optical microscope “SZX12” from Olympus (Olympus Life Science Europe GmbH, Hamburg, Germany) and a scanning electron microscope “Vega II” from TeScan (Tescan Orsay Holding, a.s., Brno, Czech Republic). For a better understanding of the fracture surface structure, optical 3D measurements with an “Infinite Focus System” from Alicona (Alicona Imaging GmbH, Graz, Austria) were made.

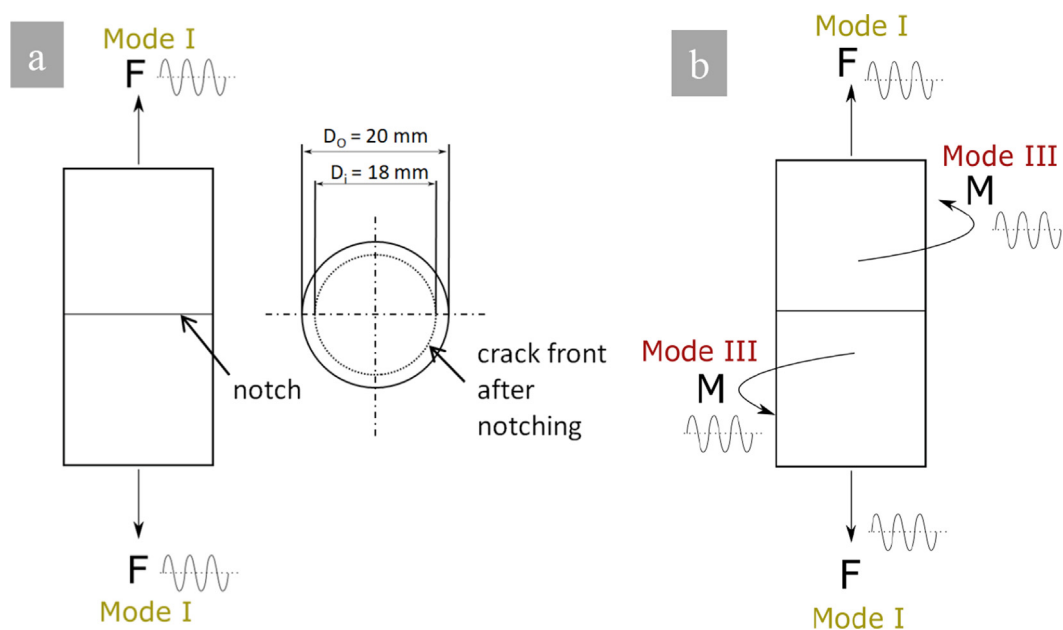


Fig. 1. Loading conditions used in this study – (a) Mode I loading of the CRB specimen and (b) Mixed Mode I/III loading of the CRB specimen.

Table 1

Details and parameters of the fatigue test series conducted in Mode I and Mixed Mode I/III (tensile load F, torsional moment M and stress intensity factor in Mode I K_I and Mode III K_{III}).

| | Mode I | Mixed Mode I/III (combined Mode I and Mode III loading) |
|--|--|--|
| Servo hydraulic testing machine | MTS 858 axial torsional (MTS systems GmbH, Minnesota, USA) | MTS 858 axial torsional (MTS systems GmbH, Minnesota, USA) |
| Frequency | 1 Hz, 5 Hz and 10 Hz | 5 Hz |
| R-ratio | 0.1 | 0.1 (for both loading cases) |
| Examined F regime (max. value) | 9000–13,500 N | 5000–12,000 N |
| Resulting K_I regime (max. K_I) | 1.3–2.5 MPa m ^{1/2} | 0.7–2.1 MPa m ^{1/2} |
| Examined M regime (max. value) | – | 25–50 Nm |
| Resulting K_{III} regime (max. K_{III}) | – | 0.9–1.8 MPa m ^{1/2} |
| Clamping distance | 35 mm | 35 mm |
| Data acquisition | Peak/valley data every 100 cycles Hysteretic data every 1000 cycles | Peak/valley data every 100 cycles Hysteretic data every 1000 cycles |

Table 2

Equations to calculate the initial stress intensity factor range in Mode I (ΔK_I).

$$\Delta K_I = \frac{\Delta F}{\pi b^2} \sqrt{\frac{\pi a_0 b}{1000r}} f_1 \left(\frac{b}{r} \right) \quad (1)$$

$$b = r - a_0 \quad (2)$$

$$f_1 \left(\frac{b}{r} \right) = \frac{1}{2} \left[1 + \frac{1}{2} \left(\frac{b}{r} \right) + \frac{3}{8} \left(\frac{b}{r} \right)^2 - 0.363 \left(\frac{b}{r} \right)^3 + 0.731 \left(\frac{b}{r} \right)^4 \right] \quad (3)$$

2.2.2. Analysis

In order to compare the different loading cases in the Mode I and Mixed Mode I/III conditions, the initial stress intensity factor range ΔK was calculated for each fatigue test. The corresponding equations are given in Tables 2 and 3. The stress intensity factor range in Mode I (ΔK_I) was determined according to [22,24] and the stress intensity factor range in Mode III (ΔK_{III}) was evaluated according to [25].

For the calculation of ΔK_I , ΔF is the difference between the minimum and maximum load, r the outer radius of the specimen, a_0 the initial crack length, b the ligament radius (which is the inner radius of the specimen) and $f_1(b/r)$ a geometry dependent factor typical for the CRB specimen in Mode I.

For the calculation of ΔK_{III} , τ is the shear stress and T is the torsional moment, $\Delta\tau$ and ΔT are the differences between the minimum and maximum values of shear stress and torsional moment, respectively, b is again the radius of the remaining ligament after notching, $f_3(b/r)$ is the geometry dependent factor for the CRB specimen in Mode III and r the outer radius of the bar.

In order to quantify the influence of the Mode III loading on the fatigue lifetime, K_I and K_{III} were combined to a so-called “equivalent stress intensity factor” (K_{eq}). Single-mode stress intensity factor values (K_I , K_{II} and K_{III}) cannot be simply added for different reasons. However, there are several approaches to determine K_{eq} from the single-mode K values. One possibility is to use the basic relationship between the energy release rate (G) and the K value obtained from brittle fracture Eq. (7). Since G is an energy value, the values for the three different modes can directly be combined to the total value:

$$G = \frac{K^2}{E} \quad (7)$$

$$G = G_I + G_{II} + G_{III} \quad (8)$$

where G_I , G_{II} and G_{III} are the values in Mode I, II and III and G is the total value. Using Eq. (7), this leads to the equation for the Mixed Mode

Table 3

Equations to calculate the initial stress intensity factor range in Mode III (ΔK_{III}).

$$\Delta K_{III} = \Delta\tau \sqrt{\pi b} f_3 \left(\frac{b}{r} \right) \quad (4)$$

$$\tau = \frac{2T}{\pi b^3} \quad (5)$$

$$f_3 \left(\frac{b}{r} \right) = \frac{3\sqrt{1-b/r}}{8} \left\{ 1 + \frac{1}{2} \frac{b}{r} + \frac{3}{8} \left(\frac{b}{r} \right)^2 + \frac{5}{16} \left(\frac{b}{r} \right)^3 + \frac{35}{128} \left(\frac{b}{r} \right)^4 + 0.208 \left(\frac{b}{r} \right)^5 \right\} \quad (6)$$

crack driving force under plane strain conditions, expressed in terms of K_{eq} [26]:

$$K_{eq} = \sqrt{K_I^2 + K_{II}^2 + \frac{1}{1-\nu} K_{III}^2} \quad (9)$$

where ν is the Poisson's ratio. Other equations for Mixed Mode are also available in literature, e.g., in [10,27]. It was found for fatigue cracks in metallic materials that under Mode III loading, the crack propagation is less pronounced than under Mode II [28]. Therefore, the coefficient $1/(1-\nu)$ in Eq. (9), which is theoretically 1.72 for POM-H, is expected to be somewhat smaller (according to our experience ν of POM-H is around 0.42). When this coefficient is denoted as λ and Eq. (9) is adapted for Mixed Mode I/III, the expression for K_{eq} changes to:

$$K_{eq} = \sqrt{K_I^2 + \lambda K_{III}^2} \quad (10)$$

According to [29,30], values for λ are between 0.9 and 1.2 for metallic materials. Since λ was unknown for POM-H at the beginning of this study, a value of 1 was used as a first step. This further simplified Eq. (10) to:

$$K_{eq} = \sqrt{K_I^2 + K_{III}^2} \quad (11)$$

3. Results and discussion

3.1. Evaluation of the equivalent stress intensity factor concept for POM-H

As mentioned in the experimental section, two types of tests were conducted in this study: pure Mode I fatigue tests and Mixed Mode I/III fatigue tests. The Mode I tests were intended as benchmark to determine the influence of the additional Mode III loading on the fatigue performance. In Fig. 2, the Mode I fatigue fracture curve (cycles to fracture in dependence on the load level, expressed as stress intensity factor range ΔK_I) is illustrated in combination with the results of the Mixed Mode I/III tests. For the latter, the ratio of the stress intensity factors in Mode III and Mode I ($\Delta K_{III}/\Delta K_I$) is given as captions in Fig. 2. A clear tendency towards fewer cycles to fracture with increasing Mode III level was observed for the Mixed Mode I/III loaded specimens. To quantify this influence, the equivalent stress intensity factor range ΔK_{eq} was evaluated.

As discussed in the experimental part, the equivalent stress intensity factor K_{eq} (Eq. (9)) takes both loading types into account. Hence, this parameter allows the comparison of pure Mode I and Mixed Mode I/III fatigue loading in one plot. For pure Mode I loading the equivalent stress intensity factor range ΔK_{eq} is the same as the stress intensity factor range ΔK_I . Hence, the pure Mode I fatigue fracture curves in Figs. 2 and 3 are identical. In the case of Mixed Mode loading several equations to evaluate ΔK_{eq} were presented in Section 2. As a starting point, the corresponding fatigue fracture curves based on the theoretical value ΔK_{eq} (Eq. (9)) are shown in Fig. 3(a). This first plot displays a longer lifetime of Mixed Mode I/III loaded specimens compared to pure

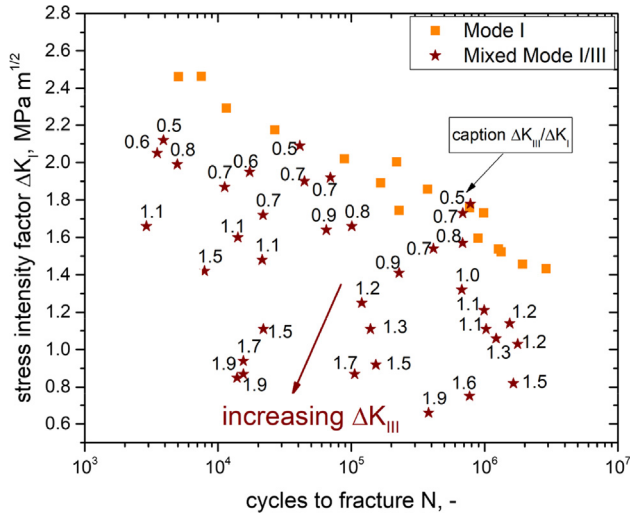


Fig. 2. Fatigue fracture behaviour of POM-H tested under Mode I and Mixed Mode I/III loading conditions (increasing Mode III loading leads to a lifetime reduction).

Mode I loading of POM-H. Hence, as it is usually assumed Mode I fatigue is more critical for the lifetime estimation of components in comparison to Mixed Mode I/III loading.

To quantify the influence of the additional Mixed Mode loading on the crack tip an adaption of the ΔK_{eq} equation and the evaluation of the

coefficient λ in Eq. (10) is recommended. As discussed in the experimental part, for polymeric materials λ is unknown. Hence, in a first step the simplified Eq. (11), where λ is 1 (ΔK_I and ΔK_{III} are simply combined), was used to determine ΔK_{eq} (shown in Fig. 3(b)). With the ΔK_{eq} values from Eq. (11), the fatigue fracture data of Mixed Mode I/III and pure Mode I loading overlap quite well but there is still some scattering in the data noticeable.

It is obvious from Fig. 2 that also the ratio of Mode III/Mode I influences the lifetime of the tested polymer. Small ratios of $\Delta K_{III}/\Delta K_I$, have little effect on fatigue lifetime under Mixed Mode I/III in comparison to pure Mode I. This behaviour is similar to metals, where Mode III is known to have relatively low efficiency [28–30]. For higher ratios of $\Delta K_{III}/\Delta K_I$, it is shown in Fig. 2 that the contribution of Mode III decreases the fatigue lifetime significantly. Such behaviour is opposite to that observed for metals. Higher ratios of $\Delta K_{III}/\Delta K_I$ result in a high level of friction between the fracture surfaces. In metallic materials, this always leads to a pronounced retardation of cracks and consequently in an increase of the fatigue lifetime. In polymers, the effect of friction is different due to the increase of temperature, which can reach levels, where the mechanical properties are influenced. On the other hand, the effect of friction can change during the test, since the fracture surface roughness is reduced due to abrasion.

As a consequence of the abrasion, the coefficient λ has to be adapted and furthermore the ratio of Mode III to Mode I loading should be represented in the evaluation of ΔK_{eq} . Therefore, the ratio $\Delta K_{III}/\Delta K_I$ is taken into account to reflect these effects and a new formula is proposed (Fig. 3(c)):

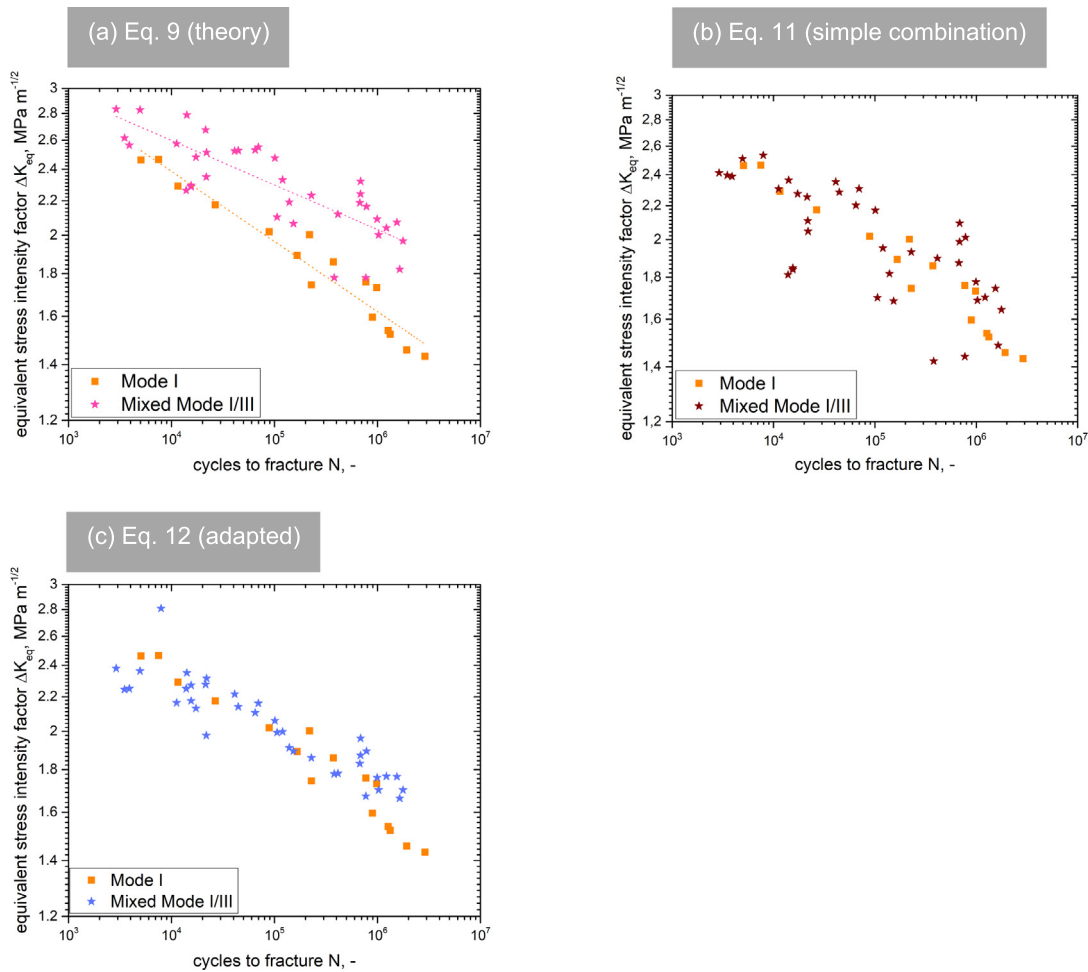


Fig. 3. Fatigue fracture test results of POM-H with the equivalent stress intensity factor range ΔK_{eq} as loading parameter to quantify combined loading in Mode I and Mode III – ΔK_{eq} was calculated with three alternative equations.

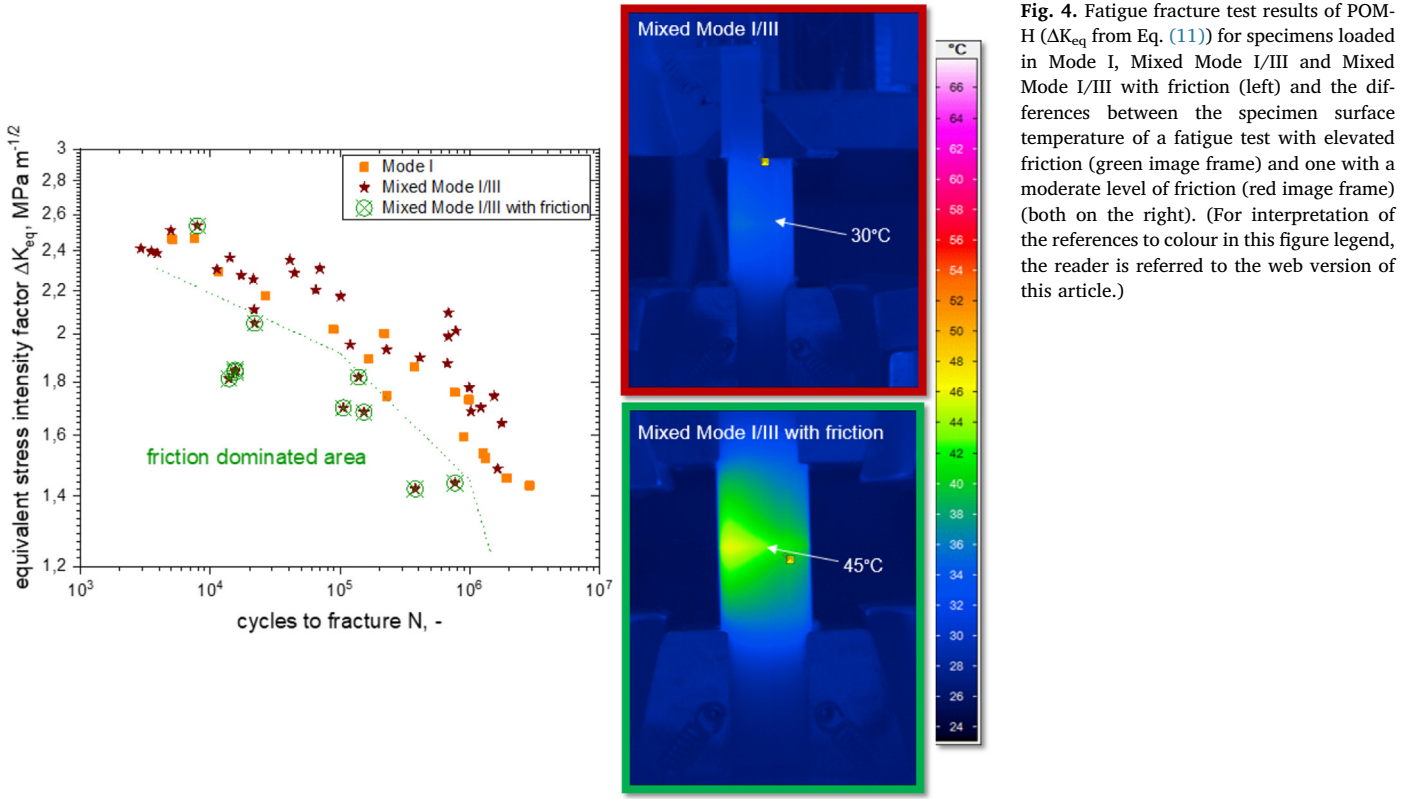


Fig. 4. Fatigue fracture test results of POM-H (ΔK_{eq} from Eq. (11)) for specimens loaded in Mode I, Mixed Mode I/III and Mixed Mode I/III with friction (left) and the differences between the specimen surface temperature of a fatigue test with elevated friction (green image frame) and one with a moderate level of friction (red image frame) (both on the right). (For interpretation of the references to colour in this figure legend, the reader is referred to the web version of this article.)

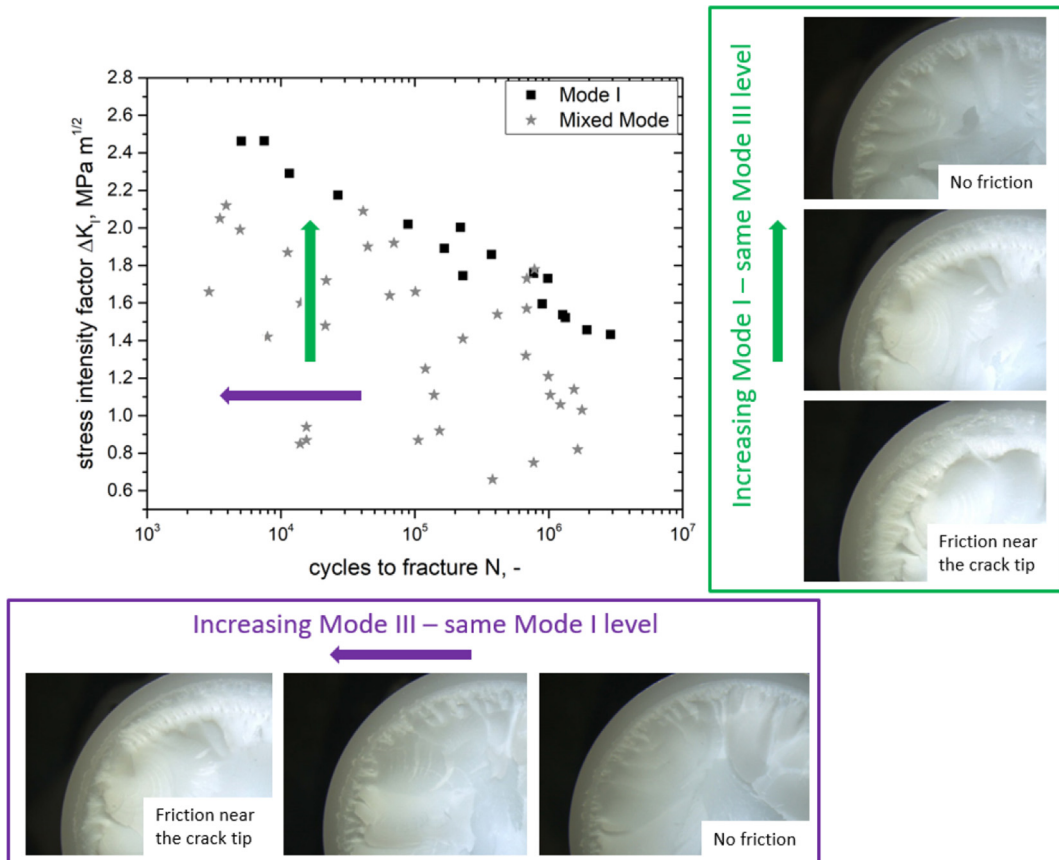


Fig. 5. Fracture surface appearance in Mixed Mode I/III fatigue loading in dependence on the different Mode I (ΔK_I) and Mode III (ΔK_{III}) contributions.

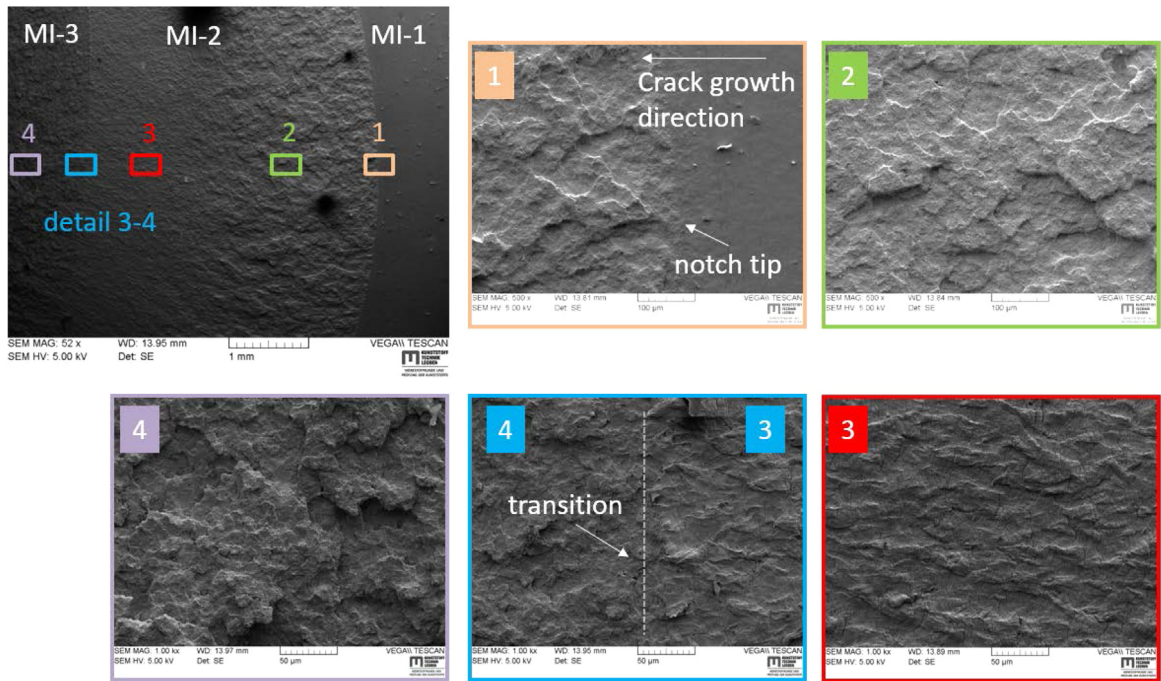
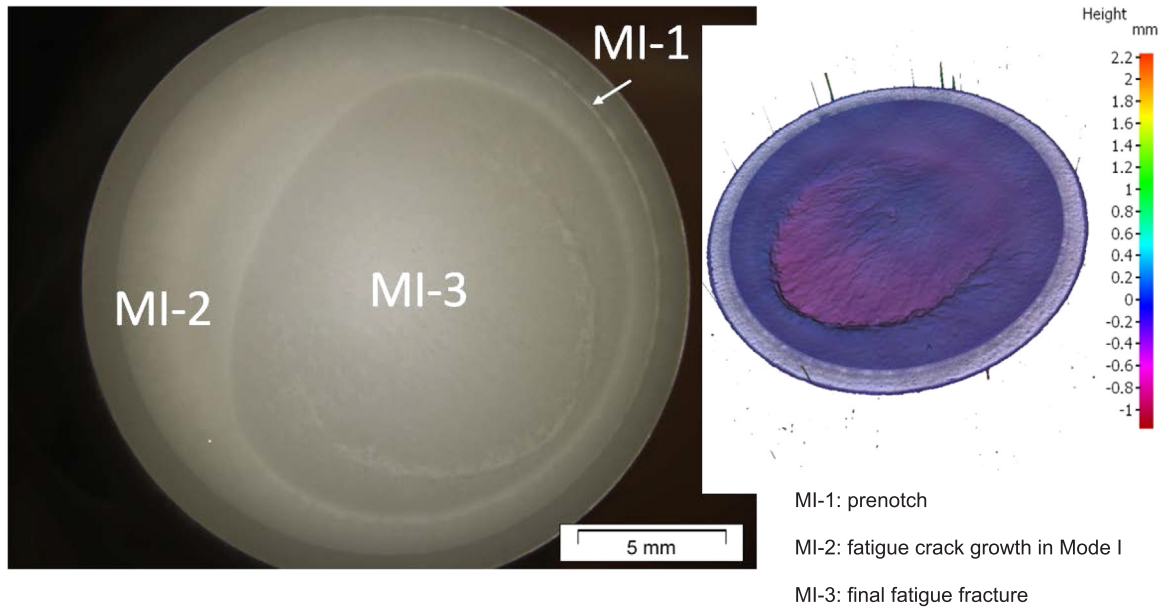


Fig. 6. Fracture surface images from a Mode I specimen (ΔK_I of $2.06 \text{ MPa m}^{1/2}$, frequency of 1 Hz) analysed using light microscopy, infinite focus 3D analysis and SEM – the areas with different crack growth mechanisms are: area close to the crack tip (1), fatigue crack growth region (2), transition region (3) and the final fracture region (4).

$$\Delta K_{eq} = \sqrt{\Delta K_I^2 + 0.9 \left(\frac{\Delta K_{III}}{\Delta K_I} \right) \Delta K_{III}^2} \quad (\text{valid for } \frac{\Delta K_{III}}{\Delta K_I} < 2.0) \quad (12)$$

It is obvious that the fatigue results of both, Mode I and Mixed Mode I/III loading follow very similar trend lines in Fig. 3(c) (with some experimental scatter, which is typical for fatigue tests). Generally, most of the Mixed Mode I/III data points evaluated with Eq. (12) overlap with the results from Mode I. This means that for Mixed Mode I/III loading, the fatigue performance of the specimens is indeed dependent on the Mixed Mode ratio. While for the higher $\Delta K_{III}/\Delta K_I$ ratios examined almost the theoretical values of λ in Eq. (9) (1.72 for POM-H) were reached, the lower ratios went down to λ values of around 0.45. In this case the Mode III loading had only half the effect of the Mode I loading. Eq. (12) describes the data sufficiently accurately and

therefore, it can be used for lifetime prediction. However, it should be considered that Eq. (12) was determined for a certain material (POM-H) and a certain loading frequency (5 Hz).

3.2. Influence of elevated friction on the Mixed Mode fatigue test results

The ΔK_{eq} values from the Mode I and the Mixed Mode I/III fatigue tests evaluated with Eq. (11) (λ value of 1) are shown again in Fig. 4. Some of the data points from the Mixed Mode I/III fatigue tests deviate strongly from the general tendency (marked green). These deviating Mixed Mode I/III data points display a significant temperature increase at the specimen surface, measured with an IR camera during fatigue testing. At the surface directly next to the crack tip, a temperature of around 45°C was measured during the fatigue test shown in Fig. 4

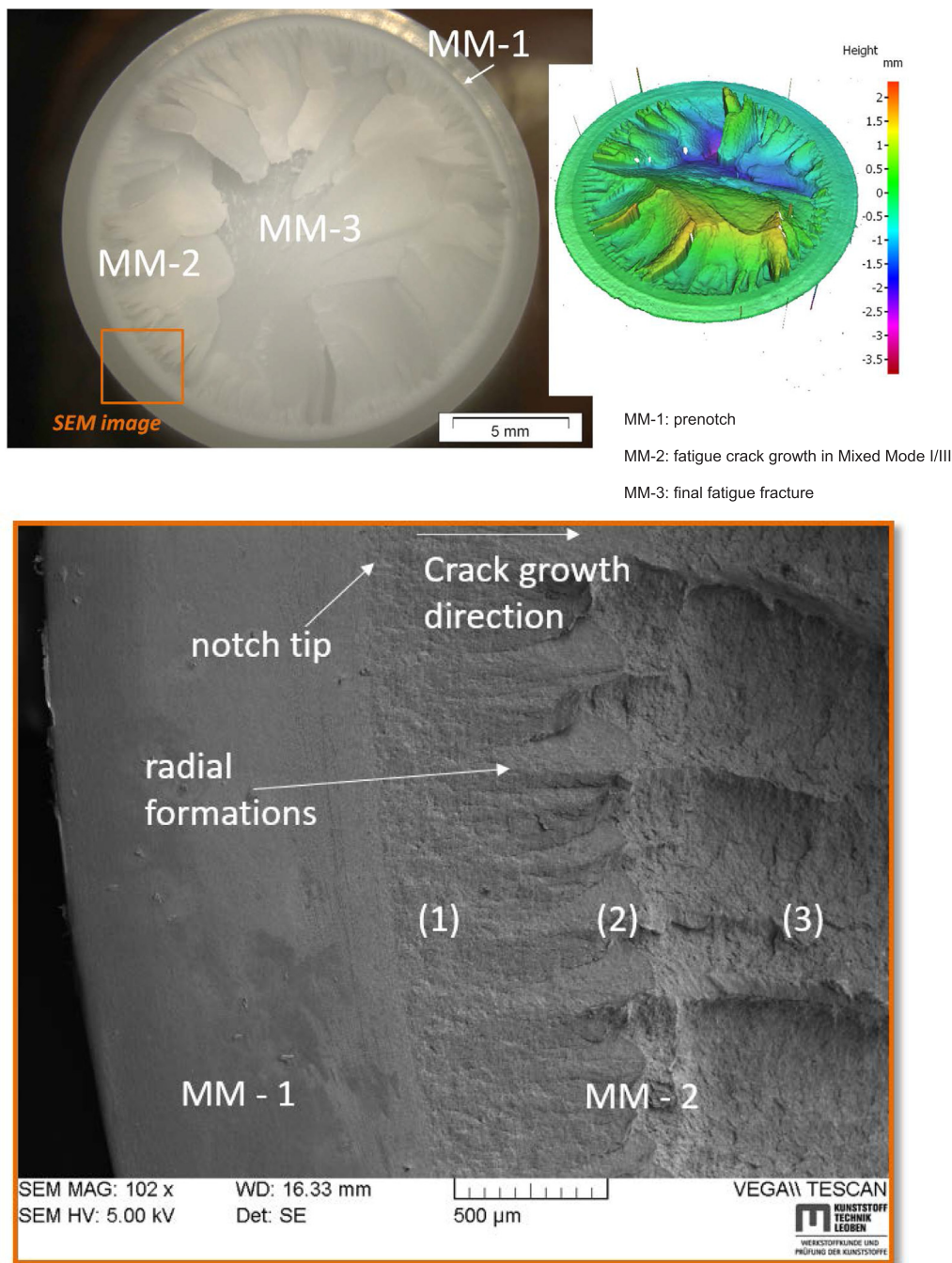


Fig. 7. Fracture surface images from a Mixed Mode I/III specimen (ΔK_{III} of $1.2 \text{ MPa m}^{1/2}$, ΔK_I of $2.0 \text{ MPa m}^{1/2}$, frequency of 5 Hz) analysed using light microscopy, infinity focus 3D analysis and SEM – the areas with different crack growth mechanisms are: start of crack growth (1), transition region with typical “factory roof”-formations which indicate the local change in crack growth direction to Mode I (2) and final fracture region (3).

(green image frame). As mentioned before, Mixed Mode I/III fatigue tests are influenced by friction and wear abrasion between the closed crack flanks during testing [18]. Especially polymers are highly sensitive to friction, because with this phenomenon a temperature increase is always present in the fatigue test. If the frictional forces reach very high levels, the resulting high temperature can significantly reduce the lifetime of the specimens [31]. Such tests cannot be considered as valid high cycle fatigue tests, since the lifetime reduction is an effect of the test set-up and the testing conditions, but not of the material itself.

For comparison, the surface temperature of a non-deviating Mixed Mode I/III specimen is also presented in Fig. 4 (red image frame). During the fatigue test, a specimen surface temperature of around $30 \text{ }^\circ\text{C}$

was measured near the crack tip. Thus it is possible to separate the friction dominated area, where the fatigue data points cannot be considered as valid, from valid Mixed Mode fatigue tests (marked red in Fig. 4). At least for the examined material and testing conditions, Eq. (11) with its simple character, was observed to be very useful to identify invalid data points within the Mixed Mode loading regime.

3.3. Detailed fracture surface analysis

An additional way to prove the appearance of friction between the crack flanks is with a detailed fracture surface analysis using light microscopy and SEM. With such a detailed analysis of the fracture

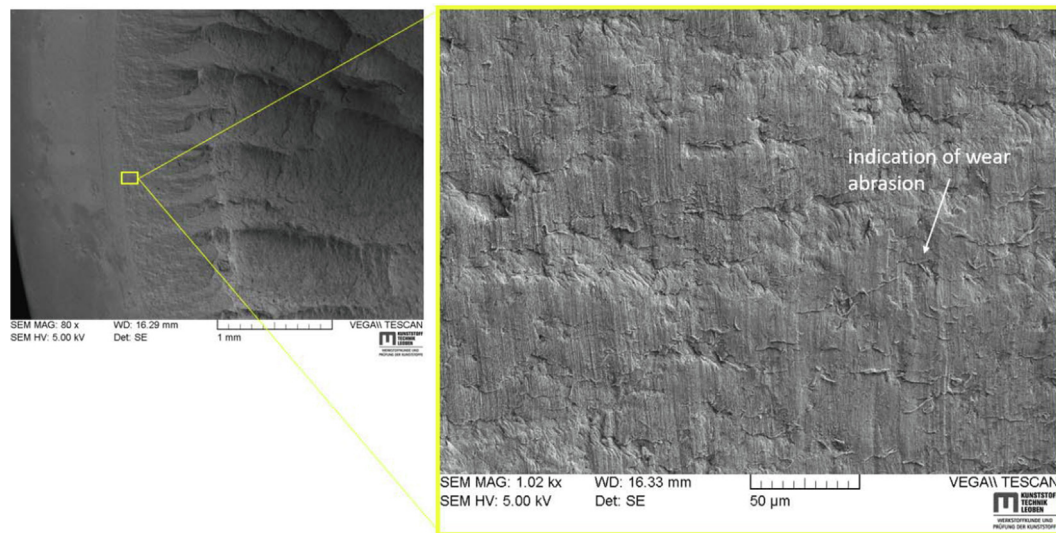


Fig. 8. Detailed fracture surface images from the area close to the crack tip of a Mixed Mode I/III specimen (ΔK_{III} of $1.2 \text{ MPa m}^{1/2}$, ΔK_I of $2.0 \text{ MPa m}^{1/2}$, frequency of 5 Hz) with wear abrasion indications.

surfaces, it was possible to examine the two main factors influencing the occurrence of wear abrasion, which is an indication of friction during Mixed Mode I/III fatigue tests (Fig. 5). Firstly, with higher torsional moment (higher stress intensity factor in Mode III) more effects of friction are observed on the fracture surfaces. Secondly, a higher tensile load (higher stress intensity factor in Mode I) ends up in less friction directly in front of the crack tip. The same interactions of loading and friction effects were reported for Mixed Mode I/III loaded specimens made of metals [32].

Generally, a detailed investigation of the fracture surface is a common method to gain more insight in the fracture process itself. This allows the identification of differences in the tested specimens caused by different fracture mechanism. Therefore, microscope images of fracture surfaces from Mode I, “valid Mixed Mode I/III” (marked red in Fig. 4) and “friction dominated Mixed Mode I/III” tests (marked green in Fig. 4) were made. The light microscope and detailed SEM images of the fractured specimen surfaces are shown in Figs. 6, 7 and 9. For the subsequent discussion the Mixed Mode I/III data points will be divided in two groups: “Mixed Mode I/III” and “Mixed Mode I/III with friction”. For all testing modes examined in Figs. 6, 7 and 9, different crack growth mechanisms were found on the corresponding fracture surfaces. The areas with different mechanisms are marked with numbers directly on the images. The areas 1 (prenotch) and 3 (final fatigue fracture) were similar for all test conditions (Mode I, Mixed Mode I/III and Mixed Mode I/III with friction). Contrary, the crack growth mechanism in between (area 2) changed depending on the type of test. To identify the different regions on the microscope images, the following abbreviations will be used together with the area number: “MI” for Mode I, “MM” for Mixed Mode and “MF” for Mixed Mode with friction.

The images in Fig. 6 show the fracture surface of a specimen loaded with pure Mode I conditions. Macroscopically, the pure Mode I fracture surface is flat (also represented in the 3D image in Fig. 6) and three characteristic crack growth mechanisms can be detected. The first area on the fracture surface (MI-1) is completely smooth and flat and represents the initial pre-notch. This pre-notch was made with a sliding razor blade and acts as starting point for fatigue crack growth. The second area (MI-2) shows the fatigue crack growth during the experiment. The area of fatigue crack growth is also rather smooth and plane with small patterns, which are shown in detail in the bottom SEM images in Fig. 6. The area marked with MI-3 represents the end of the fatigue test, where the critical K value was reached and the specimen ultimately failed during the loading of a single cycle. A similar fracture

behaviour in Mode I was previously mentioned for POM and other polymers [20,21,33].

The SEM images of the Mode I fracture surface, which are shown at the bottom of Fig. 6, are in accordance with the light microscope image. With their help, the fracture surface was investigated in detail concerning the different crack growth mechanisms present. Area “1” in Fig. 6 represents the initial notch and the starting region of fatigue crack growth in Mode I. Close to the notch tip small patterns were observed on the fracture surface. Similar appearance for this region was found previously [20,33]. Area “2” shows the region of fatigue crack growth. Here, the surface looks similar to the area near the crack tip with patterns and no indication of plastic flow. The next area is the transition region marked as “3” in Fig. 6, where the surface is covered with small ductile formations in crack growth direction. These formations are interpreted as fibrils formed before the final failure of the specimen [33]. Finally, there is the area of spontaneous crack growth (marked as “4” in Fig. 6), which represents the final fracture in the fatigue experiment. This area of spontaneous crack growth presents a craggy, texture like landscape. This also agrees with observations made for CT and CRB specimens [20,33]. Additionally, a detailed illustration of the transition region between area “3” and area “4” is presented in Fig. 6 (“detail 3–4”). This SEM image shows the change in the crack growth mechanism from the more ductile region (“3”) to the final fracture area (“4”).

Common to all presented specimens, Mode I (Fig. 6) and Mixed Mode I/III (Figs. 7 and 9), is the macroscopically flat fracture surface, where crack growth happens within the plane of the initial notch. This is especially visible in the 3D images obtained with the infinite focus analysis technique, which are included in Figs. 6, 7 and 9. For polymers only little literature is available dealing with Mixed Mode I/III fatigue loading. However, for other materials, similar macroscopically flat fracture surfaces were mentioned in literature [34].

As discussed for the Mode I loaded specimens, similar areas MM-1 (prenotch) and MM-3 (final fracture in fatigue loading) are present on the fracture surfaces of the Mixed Mode I/III specimens (Fig. 7). The differences are in the area of fatigue crack growth, which is marked with MM-2 on the fracture surface of the Mixed Mode I/III specimen in the corresponding Fig. 7. Formations in radial direction were detected on the whole fracture surface and they are especially distinct in area MM-2. These formations are also present in the infinity focus 3D image and the more detailed SEM image. A detailed SEM-image close to the crack tip of the same specimen (shown in Fig. 8) displays the presence

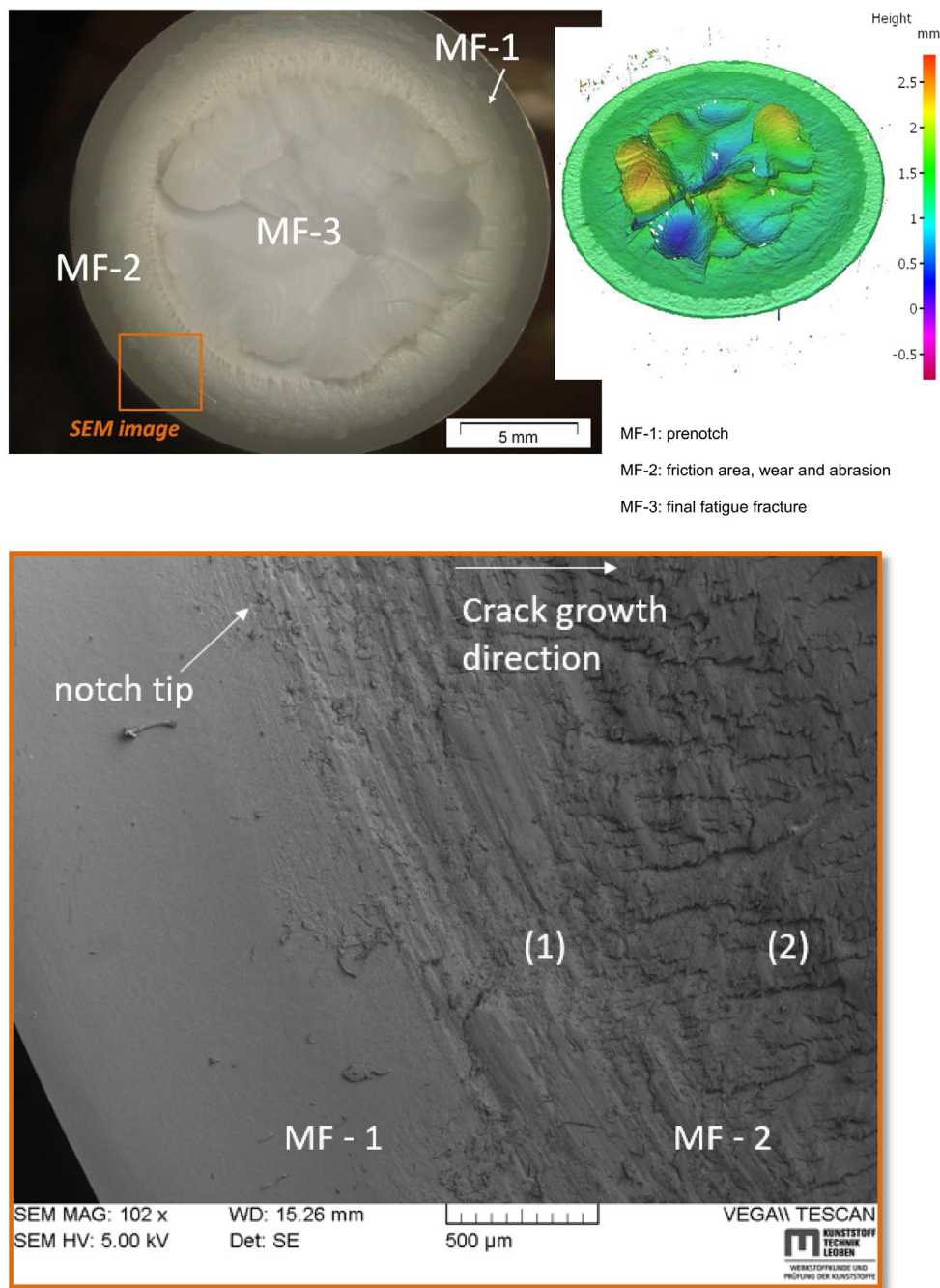


Fig. 9. Fracture surface images from a Mixed Mode I/III specimen (ΔK_{III} of $1.6 \text{ MPa m}^{1/2}$, ΔK_I of $0.9 \text{ MPa m}^{1/2}$, frequency of 5 Hz) analysed using light microscopy, infinity focus 3D analysis and SEM – the areas with different crack growth mechanisms: region with circumferential lines representing wear and abrasion between the crack flanks (1) and a follow-up region with radial surface cracks, which indicate Mixed Mode I/III crack formations (2).

of friction during testing represented as wear abrasion. It is the results of contact and relative movement between the crack flanks during testing and will be discussed in detail for the “Mixed Mode I/III with friction” specimens. Nevertheless, there was no significant surface temperature increase measured during fatigue testing for the specimen. The applied torque level on the tested specimen shown in Figs. 7 and 8 is too low to influence the surface temperature and finally the lifetime. This is also supported via the SEM-images in Fig. 7, where macroscopically no indications of wear abrasion on the fracture surface was detected. Therefore this specimen belongs to the group of “Mixed Mode I/III” specimens. This interaction of Mode I and Mode III is represented in Eq. (12) (Fig. 3(c)), which takes the ratio of $\Delta K_{III}/\Delta K_I$ into account.

After around $200 \mu\text{m}$ of crack propagation the mentioned radial

formations start (area “2” on the SEM image in Fig. 7). In literature, these radial formations are called “factory roof” formations and they indicate the local crack growth fracture in Mode I direction [35]. The initiation of these “factory roof” formations is started in Mixed Mode I/III. After a few μm crack growth the mechanism changes from Mixed Mode I/III into Mode I. In this research, especially for specimens with low cyclic torque amplitudes (Fig. 7) the cracks are commonly oriented in 45° , whereas for high cyclic torque amplitudes a more flat fracture surface was found. Finally, the area marked with “3” on the SEM image in Fig. 7, which represents the final fracture within the fatigue test, displays the same appearance as former area MI-3 from the Mode I specimen.

Specimens tested under the condition “Mixed Mode I/III with

friction" (Fig. 9) show a characteristic area (marked with MF-2), where wear abrasion dominates the fracture surface. The same appearance was also reported in literature for other materials examined under Mixed Mode I/III loading conditions [7,9,32,34]. This region is present directly after the initial notch (refer to Fig. 9).

Unlike in Mode I, friction can occur in Mode III, because the crack flanks are not torn apart during the loading and hence, they can rub during the fatigue loading in every cycle. With additional loading in Mode I, this friction can be reduced, especially at high Mode I levels. At the lower Mode I levels, the crack opening through the applied forces is not sufficient to totally separate the crack flanks during the cycle and this ends up in friction between them. In this case, Mixed Mode I/III loading (Mode I and Mode III) leads to wear abrasion on the fracture surface, to a reduction of the effectively acting torque (counterforce through friction) [35] and in case of polymers to a increase in the specimen temperature. These data points are marked as "Mixed Mode I/III with friction" data points in Fig. 4, because they are not only influenced by the applied load and torque level. It is obvious from Fig. 4 that the highly discussed influence of friction effects under shear mode crack opening (Mode II and Mode III) has to be identified separately in fatigue fracture curves. The friction effects are especially critical for the lifetime of polymers, because as shown before they cause elevated temperatures near the crack tip during testing. This temperature increase ends up in a cycle to fracture reduction and thus influences the resulting fatigue fracture behaviour.

The SEM image of the Mixed Mode I/III loaded specimen with friction on the fracture surface, which is part of Fig. 9, clearly shows the characteristics discussed above. An area with a smeared appearance (marked with (1) in Fig. 9) is present close to the crack tip. This smeared area is structured with lines parallel to the initial circumferential notch. Similar structures were also found in literature [8,9,32]. This effect is typical for wear abrasion between the crack flanks at the beginning of the crack growth process. This first area is followed by a region, where the abrasion lines disappear. Instead radial surface cracks become visible around 500 μm away from the notch tip. The level of friction present in the Mode I/III fatigue tests is dependent on the Mode I and Mode III loading: higher tension forces (Mode I loading) reduce the presence of friction, higher torsional moments (Mode III loading) support the presence of friction. This indicates that the applied load in Mode I becomes more effective with increasing crack length and the friction between the crack flanks becomes weaker (marked with (2) in Fig. 9). The area of final fatigue fracture "MF-3" is not shown in the SEM image, but is present on the light microscope picture in Fig. 9.

4. Conclusion

Efficient component design requires detailed information about the material behaviour during the application. The latter is also important to ensure the predicted lifetimes from the simulations. The simulation of crack growth starting from little defects, which can occur during the manufacturing, is one important task of component design. For this a lot of information about Mode I fatigue crack growth in polymers is available in literature. However, concerning Mixed Mode I/III fatigue loading of polymers only little information can be found. Hence, within this work the fatigue fracture behaviour of a selected polymer (POM-H) was studied in Mode I and Mixed Mode I/III loading to gain more information about component failure during the application. The determined results are summarized as followed:

- The conducted Mixed Mode I/III loading (represented as ratio of $\Delta K_{III}/\Delta K_I$) ends up in a clearly visible lifetime reduction of the specimens tested compared to pure Mode I loading.
- To take this Mixed Mode I/III loading into account for component design and simulation of components, the use of the equivalent stress intensity factor concept K_{eq} , where both loading types are represented, is suggested. Different equations were presented to

evaluate K_{eq} .

- The increasing specimen temperature during Mixed Mode I/III fatigue testing, caused by friction between the crack flanks, ends up in a lifetime reduction of the examined polymer.
- The level of friction present in the Mode I/III fatigue tests is dependent on the Mode I and Mode III loading: higher tension forces (Mode I loading) reduce the presence of friction, higher torsional moments (Mode III loading) support the presence of friction.
- Finally, a detailed fracture surface analysis of a specimen loaded in Mode I, Mixed Mode I/III and Mixed Mode I/III with friction was conducted. For the Mode I loaded specimen the fracture surface structures were in accordance with the literature. For the Mode I/III loaded specimen so called "factory roof formations" were found on the fracture surface. It was possible to observe the proposed wear abrasion area on the fracture surface of the Mixed Mode I/III loaded specimens with friction. No "factory roof formations" were found for the latter, but radial surface cracks instead.

For future research, it is of high interest to gain more insight in the still missing loading case of Mode II crack growth of polymers. Moreover, it is important to expand the application of the testing concept presented in this publication to various other polymers to develop a more generalized idea concerning the Mixed Mode crack growth behaviour of unreinforced polymeric materials.

Acknowledgement

The research work of this paper was performed at the Materials Science and Testing of Polymers/Montanuniversitaet Leoben within the framework of the COMET-program of the Federal Ministry for Transport, Innovation and Technology and the Federal Ministry of Science, Research and Economy with contributions by the Polymer Competence Center Leoben GmbH and the Institute of Physics of Materials "IPM" in Brno/Czech Republic.

References

- [1] Berer M, Mitev I, Pinter G. Finite element study of mode I crack opening effects in compression-loaded cracked cylinders. *Eng Fract Mech* 2017;175:1–14.
- [2] Berer M, Major Z, Pinter G. Elevated pitting wear of injection molded poly-etheretherketone (PEEK) rolls. *Wear* 2013;297(1–2):1052–63.
- [3] Berer M, Major Z. Characterization of the global deformation behaviour of engineering plastics rolls. *Int J Mech Mater Des* 2010;6(1):1–9.
- [4] Berer M, Major Z. Characterisation of the local deformation behaviour of engineering plastics rolls. *Strain* 2012;48(3):225–34.
- [5] Dlhý P, Poduska J, Nahlik L, Berer M, Gosch A, Pinter G, et al. Compression-loaded cracked cylinder – stress intensity factor evaluation. *Key Eng Mater* 2018;774:331–6.
- [6] Beretta S, Foletti S, Valiullin K. Fatigue crack propagation and threshold for shallow micro-cracks under out-of-phase multiaxial loading in a gear steel. *Eng Fract Mech* 2010;77(11):1835–48.
- [7] Qian J, Fatemi A. Mixed mode fatigue crack growth: A literature survey. *Eng Fract Mech* 1996;55:969–90.
- [8] Nayeb-Hashemi H, McClintock FA, Ritchie RO. Micro-mechanical modelling of mode III fatigue crack growth in rotor steels. *Int J Fract* 1983;23:163–85.
- [9] Nayeb-Hashemi H, McClintock FA, Ritchie RO. Effects of friction and high torque on fatigue crack propagation in mode III. *MTA* 1982;13(12):2197–204.
- [10] Richard HA, Schramm B, Schirmeisen N-H. Cracks on mixed mode loading – theories, experiments, simulations. *Int J Fatigue* 2014;62:93–103.
- [11] Pokluda J, Pippan R, Vojtek T, Hohenwarter A. Near-threshold behaviour of shear-mode fatigue cracks in metallic materials. *Fatigue Fract Eng Mater Struct* 2013;37:232–54.
- [12] Richard HA, Eberlein A. Material characteristics at 3D-mixed-mode-loadings. *Procedia Struct Int* 2016;2:1821–8.
- [13] Jones R, Stelzer S, Brunner AJ. Mode I, II and mixed mode I/II delamination growth in composites. *Compos Struct* 2014;110:317–24.
- [14] Stelzer S, Pinter G. Fatigue delamination growth in CFRP composites: from pure mode I and mode II to mixed mode I/II. *MSF* 2015;825–826:914–21.
- [15] Brunner AJ, Stelzer S, Pinter G, Terrasi GP. Mode II fatigue delamination resistance of advanced fiber-reinforced polymer-matrix laminates: towards the development of a standardized test procedure. *Int J Fatigue* 2013;50:57–62.
- [16] Brunner AJ, Stelzer S, Pinter G. Development of a test procedure for mode II fatigue delamination resistance of advanced fibre-reinforced polymer-matrix laminates.
- [17] Lach R. Mixed mode fracture mechanics behaviour of PMMA. *Weinheim*. 1–6; 2017.

- [18] Vojtek T, Pokluda J, Hohenwarter A, Pippan R. Three-dimensional morphology of fracture surfaces generated by modes II and III fatigue loading in ferrite and austenite. *Eng Fract Mech* 2013;108:285–93.
- [19] Doquet V, Pommier S. Fatigue crack growth under non-proportional mixed mode loading in ferritic pearlitic steel. *Fatigue Fract Eng Mater Struct* 2004;27:1051–60.
- [20] Berer M, Pinter G, Feuchter M. Fracture mechanical analysis of two commercial polyoxymethylene homopolymer resins. *J Appl Polym Sci* 2014:131.
- [21] Berer M, Pinter G. Determination of crack growth kinetics in non-reinforced semi-crystalline thermoplastics using the linear elastic fracture mechanics (LEFM) approach. *Polym Test* 2013;32:870–9.
- [22] ISO international organization for standardization. Polyethylene (PE) materials for piping systems – determination of resistance to slow crack growth under cyclic loading – cracked Round Bar test method (ISO 18489). Switzerland; 2015.
- [23] Pook LP. Crack profiles and corner point singularities. *Fatigue Fract Engng Mater Struct* 2000;23:141–50.
- [24] Scibetta M, Chaouadi R, Van Walle E. Fracture toughness analysis of circumferentially-cracked round bars. *Int J Fract* 2000;104:145–68.
- [25] Tada H, Paris P, Irwin GR. The stress analysis of cracks. Del Research Corporation; 2003.
- [26] Anderson TL. Fracture mechanics: fundamentals and applications. Taylor & Francis Group, LLC; 2005.
- [27] Tanaka K. Fatigue crack propagation from a crack inclined to the cyclic tensile axis. *Eng Fract Mech* 1974;6:493–507.
- [28] Pokluda J, Pippan R. Can pure mode III fatigue loading contribute to crack propagation in metallic materials? *Fatigue Fract Eng Mater Struct* 2005;28(1–2):179–85.
- [29] Doquet V, Bui QH, Bertolino G, Merhy E, Alves L. 3D shear-mode fatigue crack growth in maraging steel and Ti-6Al-4V. *Int J Fract* 2010;165(1):61–76.
- [30] Vojtek T, Pokluda J, Šandera P, Horníková J, Hohenwarter A, Pippan R. Analysis of fatigue crack propagation under mixed mode II + III in ARMCO iron. *Int J Fati* 2015;76:47–52.
- [31] Berer M, Major Z, Pinter G, Constantinescu DM, Marsavina L. Investigation of the dynamic mechanical behavior of polyetheretherketone (PEEK) in the high stress tensile regime. *Mech Time-Depend Mater* 2014;18:663–84.
- [32] Tschegg FK. Sliding mode crack closure and mode III fatigue crack growth in mild steel. *Acta Metall* 1983;9:1323–30.
- [33] Arbeiter F, Schrittmesser B, Frank A, Berer M, Pinter G. Cyclic tests on cracked round bars as a quick tool to assess the long term behaviour of thermoplastics and elastomers. *Polym Test* 2015;45:83–92.
- [34] Tschegg EK, Ritchie RO, McClintock FA. On the influence of rubbing fracture surfaces on fatigue crack propagation in mode III. *Int J Fati* 1983:29–35.
- [35] Tschegg EK. Mode III and Mode I fatigue crack propagation behaviour under torsional loading. *J Mater Sci* 1983;18:1604–14.

Publication 5

Bibliographic information

Title: Fatigue characterization of polyethylene under mixed mode I/III conditions

Authors: Anja Gosch¹, Florian J. Arbeiter¹, Michael Berer², Tomáš Vojtek^{3,4}, Pavel Hutař³, Gerald Pinter²

Affiliation:

1. Materials Science and Testing of Polymers, Montanuniversitaet Leoben, Otto-Gloeckel-Str. 2, 8700 Leoben, Austria
2. Polymer Competence Center Leoben GmbH, Roseggerstr. 12, 8700 Leoben, Austria
3. Institute of Physics of Materials, Academy of Sciences of the Czech Republic, Žižkova 22, 616 62 Brno, Czech Republic
4. Central European Institute of Technology (CEITEC), Brno University of Technology, Purkyňova 123, 612 00 Brno, Czech Republic

Periodical: International Journal of Fatigue

DOI: doi.org/10.1016/j.ijfatigue.2020.106084

Relevant contributions to this publication

| | |
|-----------------------------|---|
| Conceptualization: | Anja Gosch, Florian Arbeiter |
| Methodology: | Anja Gosch, Michael Berer, Pavel Hutař, Tomáš Vojtek |
| Validation: | Anja Gosch, Florian Arbeiter |
| Investigation: | Anja Gosch |
| Writing - Original Draft: | Anja Gosch |
| Writing - Review & Editing: | Florian Arbeiter, Michael Berer, Pavel Hutař, Tomáš Vojtek, Gerald Pinter |



Contents lists available at ScienceDirect

International Journal of Fatigue

journal homepage: www.elsevier.com/locate/ijfatigue

Fatigue characterization of polyethylene under mixed mode I/III conditions

Anja Gosch^a, Florian J. Arbeiter^{a,*}, Michael Berer^b, Tomáš Vojtek^{c,d}, Pavel Hutař^c, Gerald Pinter^{a,b}^a Materials Science and Testing of Polymers, Montanuniversität Leoben, Otto-Gloeckel-Str. 2, 8700 Leoben, Austria^b Polymer Competence Center Leoben GmbH, Roseggerstr. 12, 8700 Leoben, Austria^c Institute of Physics of Materials, Academy of Sciences of the Czech Republic, Žitkova 22, 616 62 Brno, Czech Republic^d Central European Institute of Technology (CEITEC), Brno University of Technology, Purkyňova 123, 612 00 Brno, Czech Republic

ARTICLE INFO

Keywords:

Mixed Mode I/III fatigue loading
Polyethylene
Fracture surface analysis
Equivalent stress intensity factor
Polymer

ABSTRACT

Mixed mode I/III fatigue fracture behaviour of bulk polymers is scarcely investigated. Thus, the aim of this work is to focus on the comparison of pure mode I and mixed mode I/III fatigue loading of polyethylene. During mixed mode I/III testing, both increases and decreases of lifetime were observed, depending on the levels of applied mode I and mode III loading. Additionally, the critical influence of friction and the accompanying increase of local temperature between the shear loaded crack flanks in mode III, as well as the dominant fracture mechanisms were discussed based on the fracture surface morphology.

1. Introduction

Mixed mode loading mechanisms in bulk polymers are rarely investigated, even though a significant amount of mixed mode loading close to the crack tip is likely to occur in several applications, such as randomly orientated cracks in a component which is used in rolling contact [1–5], twisting of a pipe during installation, etc. Therefore, it can be beneficial to possess detailed knowledge about mixed mode crack growth behaviour of polymers as shown in previous investigations [6]. For component design, the long-time performance of a polymer part can be evaluated via fatigue testing, which is usually performed only in mode I (tensile loading). However, mixed mode crack growth (in plane shear loading defined as mode II and out of plane shear loading as mode III) can display completely different crack growth behaviour and mechanisms. This is due to the complex nature of mixed mode crack growth, in which the crack flanks are closed during testing, which in turn can cause friction and wear abrasion and the effect of so called “mode I branching”. The latter mechanism is responsible for a change in the crack growth direction, where the local loading situation changes from mode II or mode III into mode I. This is commonly found in mixed mode loading tests on metals [7–9]. Furthermore, mixed mode crack propagation is known as non-self-similar, which means cracks change their direction during mixed mode loading [10].

As stated above, understanding mixed mode fatigue crack growth can provide additional information with regard to component design, as

shown in previous research [2,11]. This makes the topic highly interesting to gain more information about the behaviour of components in complex loading situations. In a recent study [12], mixed mode I/III fatigue loading was applied to cracked round bar specimens (CRB) of a polyoxymethylene homopolymer (POM-H) and the resulting fatigue fracture curve was compared to pure mode I fatigue tests. The work also presented an equivalent stress intensity factor (K_{eq}) concept, which can take both loading cases of mode I and mode III into account. Nevertheless, some open questions concerning the crack growth mechanisms during mixed mode loading remain due to the rather difficult fracture behaviour of POM-H. To better understand the complex mixed mode loading situation and the subsequent fracture behaviour of polymers, a study on a well-known reference material seems indispensable. Therefore, the mixed mode I/III fatigue fracture behaviour of high-density polyethylene (PE), which is well investigated for mode I, was characterized in the present study. PE is a commercially available polymer, which is used in daily applications (packaging, bottles, etc.) and technical components (gas or water pipes, tanks, etc.). Due to the increasing requirements in engineering applications, such as pressure piping, its fatigue behaviour in mode I is well characterized for the estimation of the life-time performance [13–19]. Furthermore, the occurring fracture mechanisms are well documented via optical methods (light-microscope and SEM analysis of the fracture surface) and are available as reference for the mixed mode testing.

* Corresponding author.

E-mail address: florian.arbeiter@unileoben.ac.at (F.J. Arbeiter).<https://doi.org/10.1016/j.ijfatigue.2020.106084>

Received 18 August 2020; Received in revised form 1 December 2020; Accepted 2 December 2020

Available online 15 December 2020

0142-1123/© 2020 The Author(s). Published by Elsevier Ltd. This is an open access article under the CC BY license (<http://creativecommons.org/licenses/by/4.0/>).

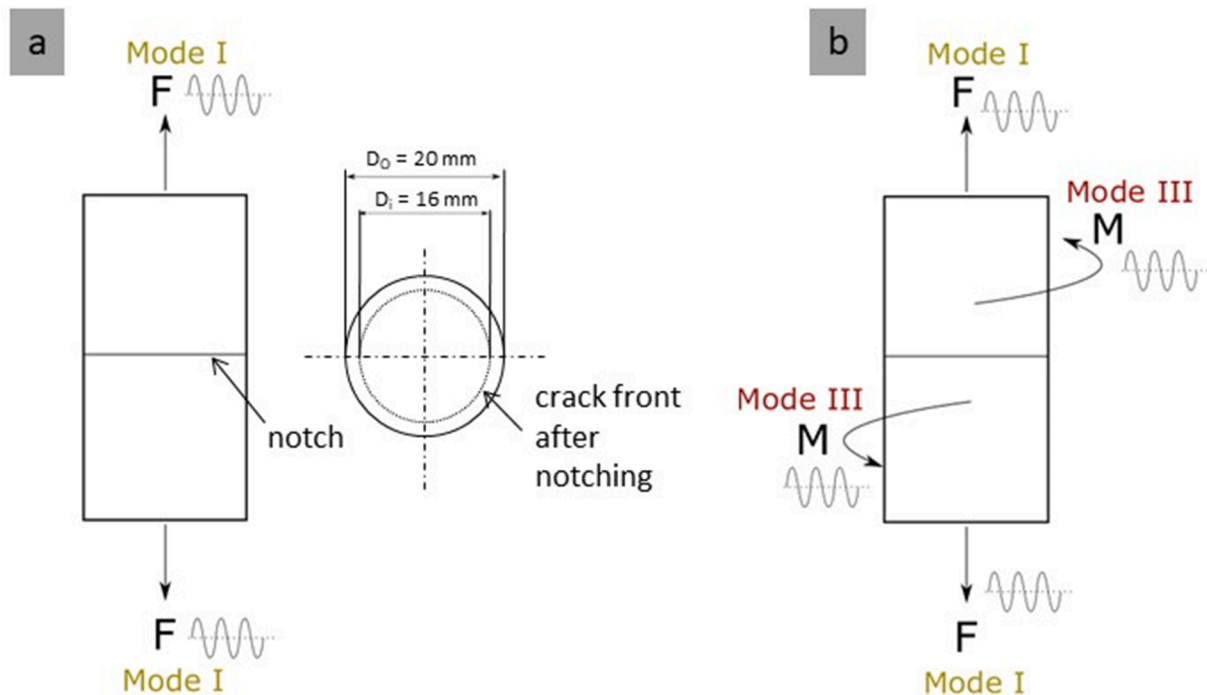


Fig. 1. Loading conditions of the PE - CRB specimens used in this work – (a) Mode I crack opening conditions realized as tensile fatigue load (b) Mixed mode I/III crack opening conditions realized as combined tensile and torsional fatigue load (adapted from [12]).

Table 1

Details and parameters of the fatigue test series conducted on PE specimens in mode I and mixed mode I/III (tensile load F , torsional moment M and stress intensity factor in mode I K_I and mode III K_{III}).

| | Mode I | Mixed Mode I/III (combined Mode I and Mode III loading) |
|--|--|--|
| Servo hydraulic testing machine | MTS 858 Axial Torsional (MTS Systems GmbH, Minnesota, USA) | MTS 858 Axial Torsional (MTS Systems GmbH, Minnesota, USA) |
| Frequency | 10 Hz | 5 Hz |
| R-ratio | 0.1 | 0.1 (for both loading cases) |
| Examined F regime (max. value) | 2200–3100 N | 2300–2600 N |
| Resulting K_I regime (max. K_I) | 0.6–0.9 MPa $m^{1/2}$ | 0.6–0.8 MPa $m^{1/2}$ |
| Examined M regime (max. value) | – | 5–10 Nm |
| Resulting K_{III} regime (max. K_{III}) | – | 0.3–0.6 MPa $m^{1/2}$ |
| Clamping distance | 35 mm | 35 mm |
| Data acquisition | Peak/valley data every 100 cycles Hysteretic data every 1000 cycles | Peak/valley data every 100 cycles Hysteretic data every 1000 cycles |

2. Materials and methods

2.1. Material

The used material in this work was a high-density polyethylene pipe grade material with high resistance against crack growth and a density of 0.95 kg/dm^3 (supplied as PE100-RC, extruded rods with a diameter of 20 mm, AGRU Bad Hall, Austria). To characterize the melting temperature and degree of crystallinity of the material, differential scanning calorimetry (DSC) measurements were performed according to ISO

11357-1:2016 (heating rate $\Delta T/\Delta t = 10 \text{ K min}^{-1}$, testing atmosphere N_2 50 mL min^{-1} , temperature range $0\text{--}160 \text{ }^\circ\text{C}$, 2 tested samples) on a DSC 1 (Mettler Toledo Schwarzenbach, CH). The investigated PE type has a melting temperature of $130 \pm 1 \text{ }^\circ\text{C}$ and a degree of crystallinity of $64 \pm 1.4\%$. Both values were determined at the first heating run. For the calculation of the degree of crystallinity the specific heat of fusion of a 100% crystalline PE, which is 290.0 J/g according to [20], was used.

2.2. Experimental

The experimental procedure used in this work was similar to a recently published paper dealing with the mixed mode I/III fatigue behaviour of POM-H [12]. However, to improve the readability, this section repeats the crucial details and parameters concerning the conducted experiments and data analysis.

The specimen type used for fatigue testing was the CRB specimen, for which the exact dimensions are shown in Fig. 1. A sharp circumferential notch was introduced with a razor blade (blade thickness 0.1 mm , tip radius $<5 \text{ }\mu\text{m}$) by mounting the specimens on a lathe. The notching depth was approximately 2 mm (10% of the initial diameter) for all specimens examined (following a recently published standard for PE [21]).

The CRB specimens were loaded in two different ways: (1) pure mode I tensile fatigue loading according to Fig. 1a and (2) mixed mode I/III through a combined tensile and torsional fatigue load as shown in Fig. 1b. All experimental details and testing conditions are summarized in Table 1., one can recognize a difference in frequency for the pure mode I and the mixed-mode I/III fatigue tests. This change for mixed-mode tests was due to technical limitations arising from the testing machine. However, published work shows, that this should have no influence on the results within the applied frequency range [22].

An optical microscope “SZX12” from Olympus (Olympus Life Science Europe GmbH, Hamburg, Germany), as well as a scanning electron microscope “Vega II” from TeScan (Tescan Orsay Holding, a. s., Brno, Czech Republic) were used for the detailed fracture surface analysis.

To investigate the formation and the path of growing cracks in mixed mode loading, so called “crack freezing” experiments were conducted

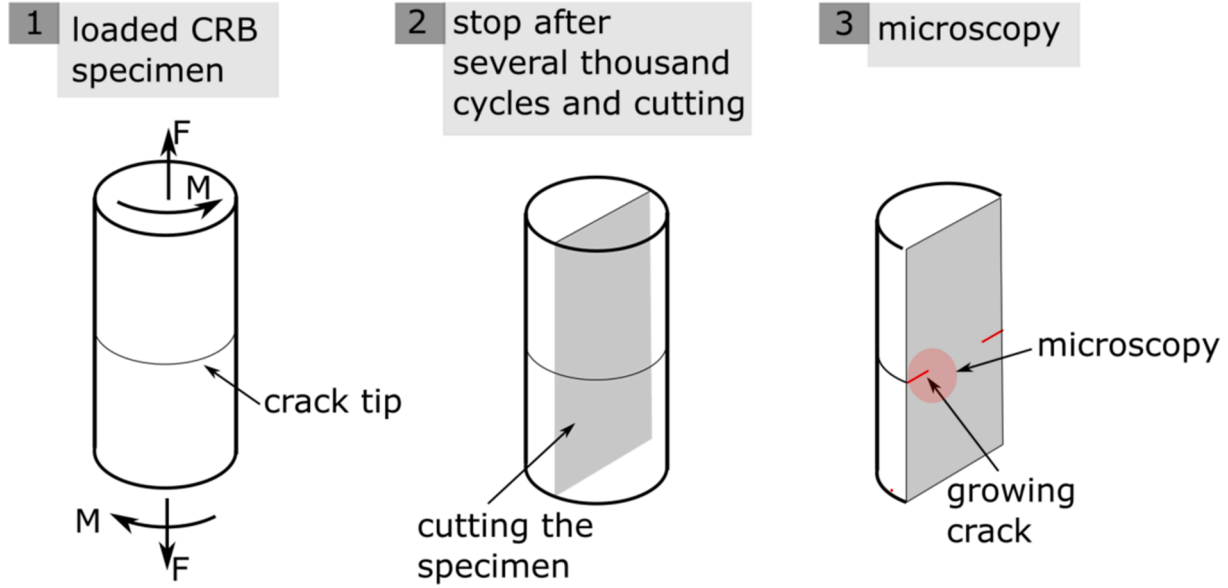


Fig. 2. Procedure for the “crack freezing” experiments: (1) Mixed mode loaded specimen with sharp notch; (2) test stopped after several thousand cycles before the complete fracture occurred and cut of the specimen; (3) Light-microscopy and SEM analysis of the crack extension (marked red). (For interpretation of the references to colour in this figure legend, the reader is referred to the web version of this article.)

Table 2

Equations to calculate the initial stress intensity factor range in mode I (ΔK_I) according to [21,23].

$$\Delta K_I = \frac{\Delta F}{\pi b^2} \sqrt{\frac{\pi a_0 b}{1000r}} f_1 \left(\frac{b}{r} \right) \quad (1)$$

$$b = r - a_0 \quad (2)$$

$$f_1 \left(\frac{b}{r} \right) = \frac{1}{2} \left[1 + \frac{1}{2} \left(\frac{b}{r} \right) + \frac{3}{8} \left(\frac{b}{r} \right)^2 - 0.363 \left(\frac{b}{r} \right)^3 + 0.731 \left(\frac{b}{r} \right)^4 \right] \quad (3)$$

Table 3

Equations to calculate the initial stress intensity factor range in mode III (ΔK_{III}) according to [24].

$$\Delta K_{III} = \Delta \tau \sqrt{\pi b} f_3 \left(\frac{b}{r} \right) \quad (4)$$

$$\tau = \frac{2T}{\pi b^3} \quad (5)$$

$$f_3 \left(\frac{b}{r} \right) = \frac{3\sqrt{1-b/r}}{8} \left\{ 1 + \frac{1}{2} \frac{b}{r} + \frac{3}{8} \left(\frac{b}{r} \right)^2 + \frac{5}{16} \left(\frac{b}{r} \right)^3 + \frac{35}{128} \left(\frac{b}{r} \right)^4 + 0.208 \left(\frac{b}{r} \right)^5 \right\} \quad (6)$$

(schematically shown in Fig. 2), before the complete fracture of the tested specimens. Experiments were stopped after several thousand cycles (close to the final failure), the specimens were cut along their longitudinal axis and the crack tip was investigated via microtome slices (light microscopy) and SEM images.

2.3. Expression of the mixed mode crack driving force using the equivalent stress intensity factor

The initial stress intensity factor range ΔK in mode I and mixed mode I/III was determined according to the corresponding equations given in Table 2 and Table 3.

In this equations ΔF is the difference between the minimum and maximum load, r the outer radius of the specimen, a_0 the initial crack length, b the ligament radius and $f_1(b/r)$ a geometry dependent factor for the CRB specimen in mode I [21,23].

In these equations τ is the shear stress, T is the torsional moment, $\Delta \tau$ and ΔT are the differences between the minimum and maximum values of shear stress and torsional moment, respectively; b is again the ligament radius after notching, $f_3(b/r)$ is the geometry dependent factor for

the CRB specimen in mode III and r the outer radius of the bar [24].

Furthermore, a so called “equivalent stress intensity factor” (K_{eq}) was calculated similar to our previous publication [12]. The parameter K_{eq} is able to combine stress intensity factors in different loading modes into a single value. The easiest expression for K_{eq} is based on the energy release rate (G) for brittle fracture. It is given by Eq. (7) for plane strain conditions [25]:

$$K_{eq} = \sqrt{K_I^2 + K_{II}^2 + \frac{1}{1-\nu} K_{III}^2} \quad (7)$$

where ν is the Poisson’s ratio. It should be mentioned at this point, that there are several equations for mixed mode loading and K_{eq} available in literature, e.g. in [7,26–28], based on different assumptions and/or boundary conditions. Under cyclic loading, the equivalent stress intensity factor range ΔK_{eq} is used instead of K_{eq} . The influence of mode II (K_{II}) is completely eliminated for the CRB specimen geometry used in the present study. This was verified via numerical simulations. Furthermore, the coefficient $1/(1-\nu)$ in Eq. (7) is expected to be smaller in reality, since mode III crack propagation is less efficient compared to the other loading modes. This aspect was also found in previous research for fatigue cracks in metallic materials [29] and for polymers [12]. Hence, a representative parameter λ was defined and ΔK_{eq} can be simplified for mixed mode I and mode III as shown in Eq. (10):

$$\Delta K_{eq} = \sqrt{\Delta K_I^2 + \lambda \Delta K_{III}^2} \quad (8)$$

According to [28,30], the values used for λ are typically between 0.9 and 1.2 for metallic materials. For POM-H, a value of 1 was used as a first step in [12] for the stress ratio of $R = 0.1$. For PE, the parameter λ is initially unknown. Therefore, the value of 1 was also used in a first step:

$$\Delta K_{eq} = \sqrt{\Delta K_I^2 + \Delta K_{III}^2} \quad (9)$$

Additionally, it is stated in literature that also the ratio of the applied mode I and mode III levels ($\Delta K_{III}/\Delta K_I$) influence the fatigue behaviour. Therefore, the parameter ΔK_{eq} can provide a much better fit of the experimental data, when this ratio is also included in the calculation. In [12] a new equation for ΔK_{eq} was proposed and successfully implemented for POM-H:

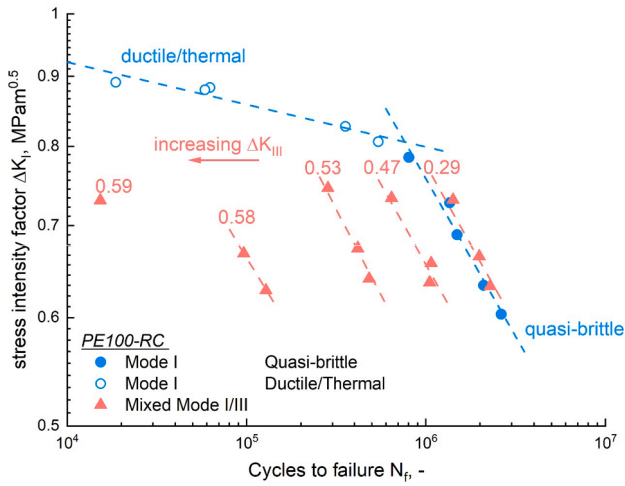


Fig. 3. Fatigue fracture behaviour of PE evaluated in pure mode I and mixed mode I/III fatigue testing: an increasing mode III amount (caption of mixed mode I/III data points is the mean value of ΔK_{III}) leads to a decrease in the cycles to fracture.

$$\Delta K_{eq} = \sqrt{\Delta K_I^2 + 0.9 \left(\frac{\Delta K_{III}}{\Delta K_I} \right) \Delta K_{III}^2} \quad (\text{valid for } \frac{\Delta K_{III}}{\Delta K_I} < 1.0) \quad (10)$$

3. Results and discussion

3.1. Mode I and mixed mode I/III fatigue behaviour of PE

To determine the influence of mixed mode I/III loading conditions on fatigue testing of PE, pure mode I tests were conducted to establish a benchmark of the material. The resulting mode I fracture curve (stress intensity factor range ΔK_I versus the cycles to failure N_f) is shown in Fig. 3.

In the current study, N_f was used for all presented figures. Usually, N_f can be separated into a crack initiation part (cycles to crack initiation $N_{initiation}$) and a crack propagation part (cycles during crack propagation $N_{propagation}$). The characterization of $N_{initiation}$ is often done by evaluation of the cyclic compliance of the specimen. For this, it is necessary to apply local strain sensors (e.g. clip on extensometers, placed in a circle around the specimen). In the case of mode I in PE-HD this has been done

many times before as shown in literature [31,32]. However, in the present work it was not possible to calculate $N_{initiation}$, since the mixed mode I/III loading situation requires a very complex biaxial measuring equipment. Subsequently, the compliance value documented by the testing machine itself (without the use of local extensometers) is too coarse for any detailed analysis of the mixed mode I/III crack growth behaviour (an example of this is shown in the Appendix A). Therefore, it is not reliably possible to determine the initiation point, or subsequently the evaluation of the crack growth kinetics curve based on the compliance data, which would be very desirable for further analysis and transferability to other components.

Looking at the results of the fracture curve, as expected from results in literature [14–19,33–35], two regions can be detected in the mode I fatigue curve:

- (1) the ductile/thermally controlled region, in which high ΔK_I values lead to a significant decrease in N_f , which is often accompanied by a significant amount of hysteretic heating and large-scale ductile deformation of the material. This behaviour was also observed for the investigated material in the present study.
- (2) the quasi-brittle region, at rather low values of ΔK_I and high corresponding values of N_f , in which the fracture surface appears rather brittle on a macroscopic scale, but shows signs of fibrillation on a microscopic level. This type of failure in PE is a rather complex process, consisting of void initiation at the crack tip, void growth and coalescence, craze formation and finally crack growth [32,36]. Contrary to (1) the deformation process is very localized in a very small area in front of the crack tip, allowing also for the application of linear elastic fracture mechanics [37–42]. For PE it was found, that the process is subsequently mostly governed by molecular disentanglement in the stretched craze fibrils [32,43–45].

Subsequently, mixed mode I/III tests were performed and the results added to Fig. 3 (caption is ΔK_{III}). Generally, when an additional loading mode is applied to pure mode I, a decrease in the measured life-time is expected, which was confirmed by most data shown in Fig. 3. It is worth noting that for low amounts of ΔK_{III} (around 0.3 $\text{MPam}^{1/2}$) no decrease in N_f was found, whereas, for higher amounts ($\Delta K_{III} \geq 0.5 \text{ MPam}^{1/2}$) a significant decrease in N_f occurred. Interestingly, a similar slope of the mixed-mode I/III failure curves and the mode I quasi-brittle curve can be observed. This indicates, that additional loading in mode III, produces a

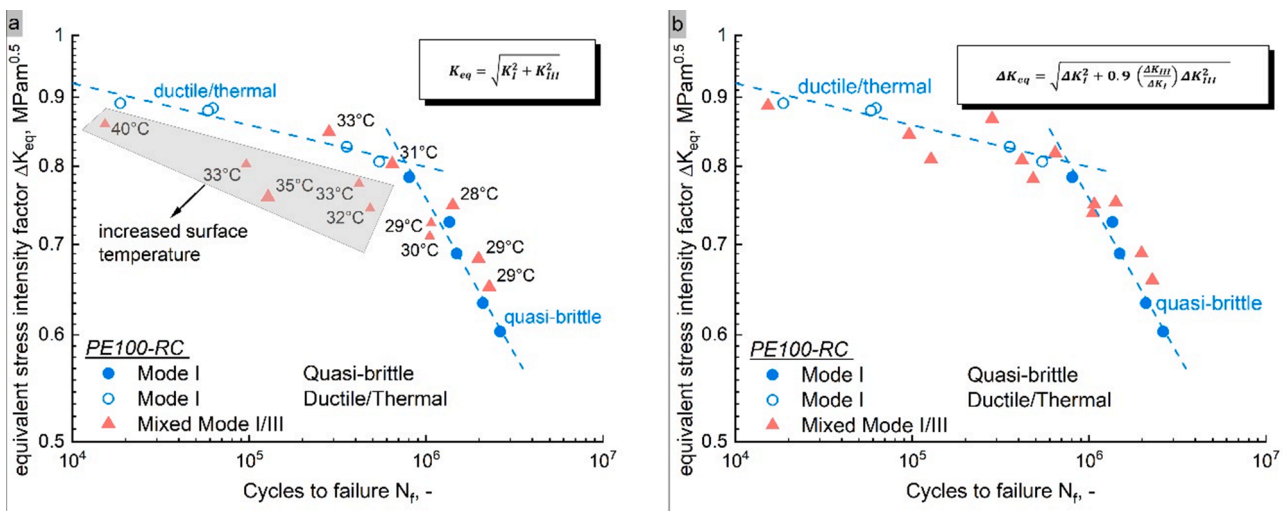


Fig. 4. Fatigue behaviour of pure mode I and mixed mode I/III loaded PE represented via the equivalent stress intensity factor ΔK_{eq} : (a) ΔK_{eq} calculated via Eq. (9), where the caption of mixed mode data points is the measured surface temperature during testing and (b) ΔK_{eq} calculated via Eq. (10), where the mode III/mode I ratio is taken into account.

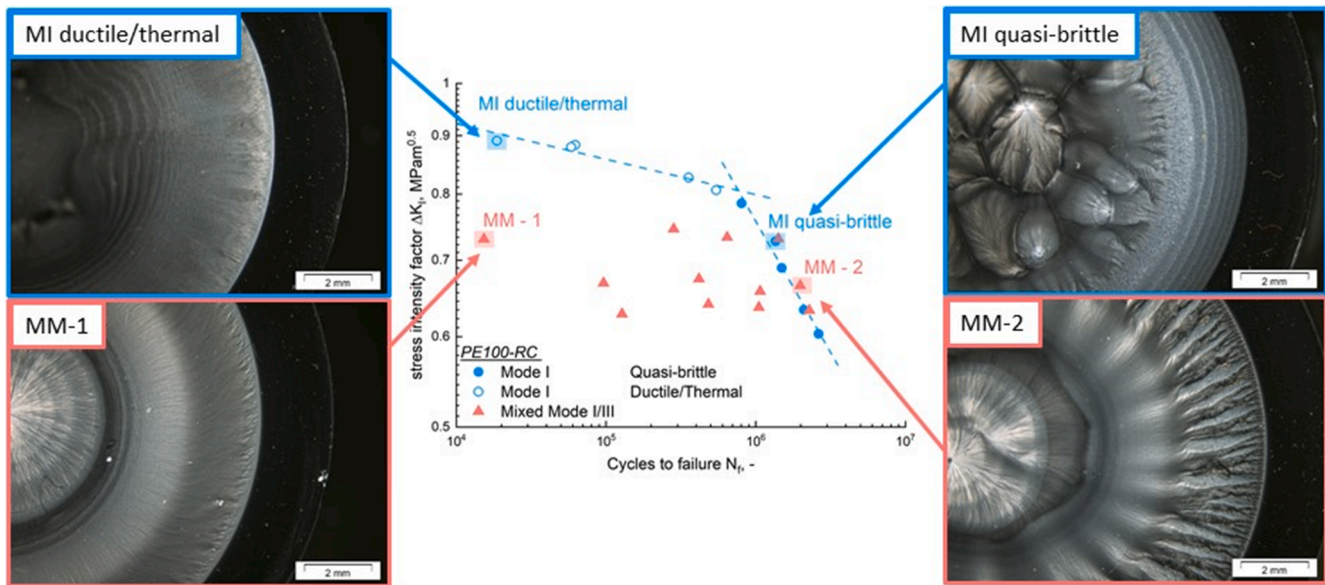


Fig. 5. Light microscope pictures of fracture surfaces in different parts of the fatigue fracture curve of PE: mode I loading (“MI ductile/thermal” and “MI quasi-brittle”) and mixed mode I/III loading (“MM-1” with high ΔK_{III} loading and “MM-2” with low ΔK_{III} loading).

similar trend between the applied loading and resulting cycles to failure, only shifted to lower values of N_f .

For a better comparison, it is of high interest to compare both loading cases via a representative parameter, which simultaneously takes mode I and mode III loading into account. This concept is based on the assumption that an absolute value, which is the sum of two loading cases, is able to fully characterize the fatigue crack growth of mixed mode I/III loading [10]. Previous investigations on POM-H showed promising results by using the equivalent stress intensity factor ΔK_{eq} , as defined in Eqs. (8) to (10) [12].

3.2. Equivalent stress intensity factor ΔK_{eq}

The use of ΔK_{eq} allows the combination of both loading cases and provides information about the partial contribution of pure mode I and mixed mode I/III loading. In the case of pure mode I, ΔK_{eq} is identical to ΔK_I . For mixed mode I/III specimens, the amount of ΔK_{eq} can be calculated using various equations proposed in literature [10]. As a starting point in this study, the interactions of mode I and mode III were neglected and it was assumed that both loading cases are affecting the results equally (Eq. (9)). Fig. 4-a displays the resulting fatigue fracture curve based on ΔK_{eq} calculated from Eq. (9) in addition with the maximum specimen surface temperature measured during the testing of the mixed mode I/III data points.

The evaluated data points from pure mode I and mixed mode I/III loading almost coincided with the application of ΔK_{eq} (calculated via Eq. (9)) in the area of low to moderate levels of ΔK_{III} . This indicates, that both loading cases contribute with a similar efficiency regarding the fatigue resistance of the material in the region of quasi-brittle fatigue crack growth. Interestingly, the specimens tested with the lowest amount of ΔK_{III} appear to be even slightly shifted towards higher lifetimes. At higher applied levels of pure mode I and mixed mode I/III, in the region of “hysteretic heating-induced thermal failure” [38], samples showed an increased surface temperature (up to 40 °C for the highest amount of ΔK_{III}). This is especially critical, since mechanical properties of polymers are highly sensitive to temperature and an increase in temperature can significantly change the life-time of the tests [12,46–48]. However, hysteretic heating should not significantly affect the region of quasi-brittle failure, since it was found that in this regime, the temperature increase in PE-HD is usually rather low (~2 to 4 K) and stabilizes after a few thousand cycles. This was also measured in prior

work via temperature sensors inside of the specimen, close to the crack tip itself [22].

Contrary to the results in the quasi-brittle region, tests at high levels of additional ΔK_{III} did not collapse onto the pure mode I results of the ductile/thermally controlled region by using Eq. (9). This indicates, that another contributing factor, besides mode I and mode III loading, as well as classical hysteretic heating, appears to be present. Based on the boundary conditions of the test setup and knowledge from previous research, this additional factor is most likely friction and wear abrasion [12]. Hence, the use of Eq. (9) appears to be a useful tool to identify loading conditions, which are significantly influenced by friction and wear abrasion of the crack flanks.

As shown in our previous research [12], it is possible to also consider friction and abrasion in ΔK_{eq} by including a ratio of $\Delta K_{III}/\Delta K_I$, as shown in Eq. (10). The results of using this equation are presented in Fig. 4-b. The data points of both loading cases coincide well, which means that the mode III/mode I ratio, which is also responsible for the amount of friction and abrasion during the test, influences the mixed mode I/III fatigue behaviour of PE significantly. The application of the adapted ΔK_{eq} equation (Eq. (10)) enables the explicit description of the relationship between applied loading and subsequent cycles to failure over the whole testing range. Based on the good correlation of the two loading cases, the adapted version of ΔK_{eq} according to Eq. (10) is expected to be usable for life-time prediction of mixed mode I/III loaded PE components.

3.3. Detailed fracture surfaces analysis

To gain more information about the fracture process during fatigue testing, it is common to investigate the fracture surfaces in detail via light microscopy and SEM analysis. Generally, the crack growth mechanisms observed on the fracture surface of a mode I loaded PE specimen are a series of complex processes involving cavitation, voiding, coarse fibril formation and rupture [49], which is commonly termed “crazing”. Adding a further loading case (mode III) leads to even more complex shapes on the fracture surfaces, which can be difficult to interpret as shown in the next chapter.

3.3.1. Fracture surface - Macroscopic level

In this section, an optical analysis of PE fracture surfaces is presented. To provide a rough overview, fracture surfaces of both loading

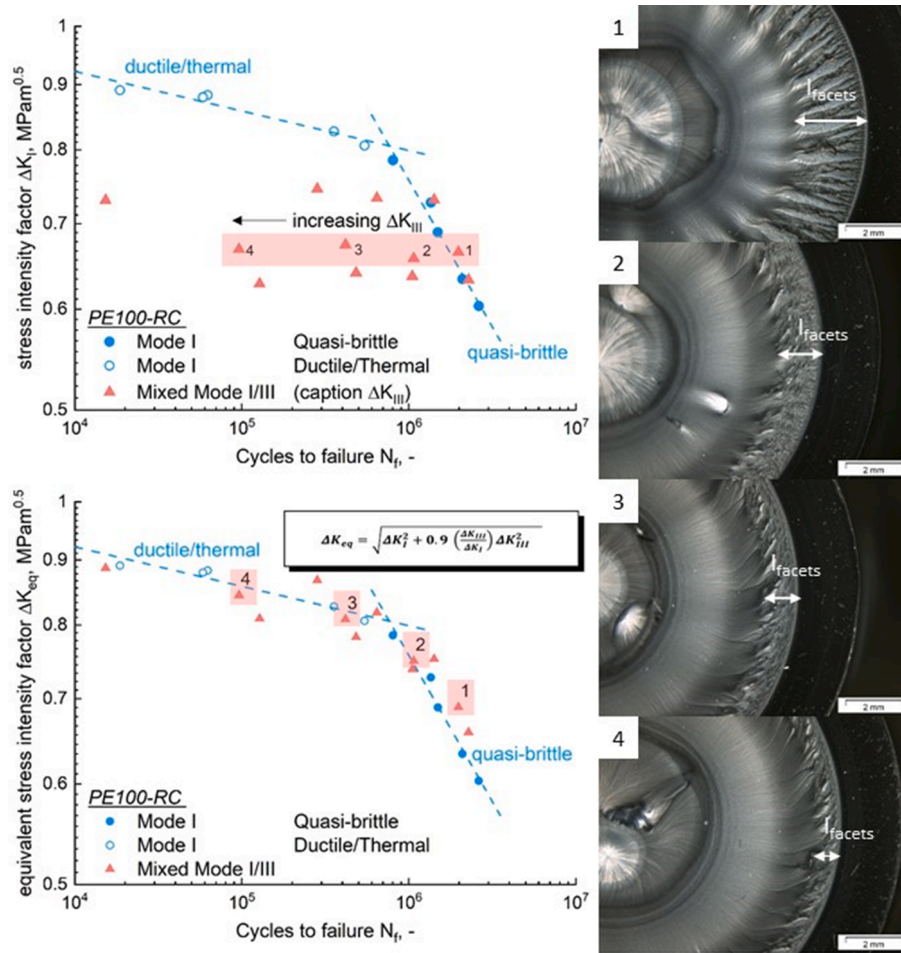


Fig. 6. Increasing mode III loading leads to a decrease in the facet length l_{facets} on the fracture surface of mixed mode I/III loaded PE specimens (for all investigated specimens, a similar mode I loading level was used during the tests).

cases in pure mode I and mixed mode I/III are compared in Fig. 5. Representative specimens from the ductile/thermal and quasi-brittle region of the mode I loaded specimens were chosen for a detailed optical analysis: “MI ductile/thermal” and “MI quasi brittle”. In the case of the mixed mode I/III loading two specimens with different amounts of mode III were chosen for the fracture surface investigations: “MM-1” was loaded with a very high amount of ΔK_{III} and “MM-2” was loaded with a low amount of ΔK_{III} .

The fracture surface of the ductile/thermal failure is shown in Fig. 5 (“MI ductile/thermal”), where high amounts of ΔK_I lead to relatively short cycles to failure. “MI ductile/thermal” specimens display large scale tearing on the fracture surface and the microscopic texture displays a rather smooth appearance, which was also found in literature for PE [33,50–52]. In the region of quasi-brittle failure, the fracture surfaces show a similar appearance as found in previous research [49–53]: Directly after the initial notch, the fracture surface displays indications of blunting and step wise discontinuous crack growth, detected as lines on the fracture surface. Discontinuous crack growth in polymers is caused by two mechanisms taking place at the same time: crazing and micro shear banding. The competition between these two crack growth mechanisms causes forward steps in the crack growth, which are known as discontinuous crack growth (DCG) bands [14,50,53]. The last state during a fatigue test of the “MI quasi-brittle” specimen displays indications of plastic flow towards the middle of the specimen and is the result of high loads and a ductile fracture of the remaining ligament.

The investigated material displays also a macroscopically flat fracture surface (crack growth in the initial crack plane) for all mixed mode

I/III loaded specimens, which is in agreement with literature for this type of specimen [10,54–57]. In the presence of mixed mode I/III loading, the area close to the initial crack tip is especially interesting. This area is highly influenced by mixed mode forces, which can lead to formations, significantly different from pure mode I loading, on the fracture surface. Macroscopically, these formations can be oriented in radial direction (compare “MM-2”) or have a smeared-out appearance (compare “MM-1”). The fracture surface of “MM-1” appears smooth and “smeared out” with signs of abrasion between the crack flanks. At low amounts of mode III loading, the “MM-2” displays large radial formations close to the initial crack tip, which are called “factory roof” formations [12,28,29,55,56]. Factory roof formations are mixed mode facet formations occurring directly after the crack initiation phase with a 45° sloping “roof”. This is the result of cracks, trying to propagate in local mode I by twisting the crack plane. Similar formations, although not as pronounced, were also found in previous research on polyoxymethylene [12]. The appearance of factory roof formations can lead to crack closure effects during testing, which is commonly known from metals [8,28,58–61]. This effect, which is also called “roughness induced” crack closure, is caused by the misfit of a microscopically rough fracture surface. During this state the crack is closed as a result of the contact between the fracture surfaces. Subsequently, the crack cannot propagate and the acting driving force is hindered, which can influence the measured cycles to failure. In this work, a slight increase in the measured life-time of mixed mode I/III specimens with low amounts of mode III loading compared to the pure mode I loaded specimens was detected (compare “MM-2” in Fig. 5). The measured cycles to failure

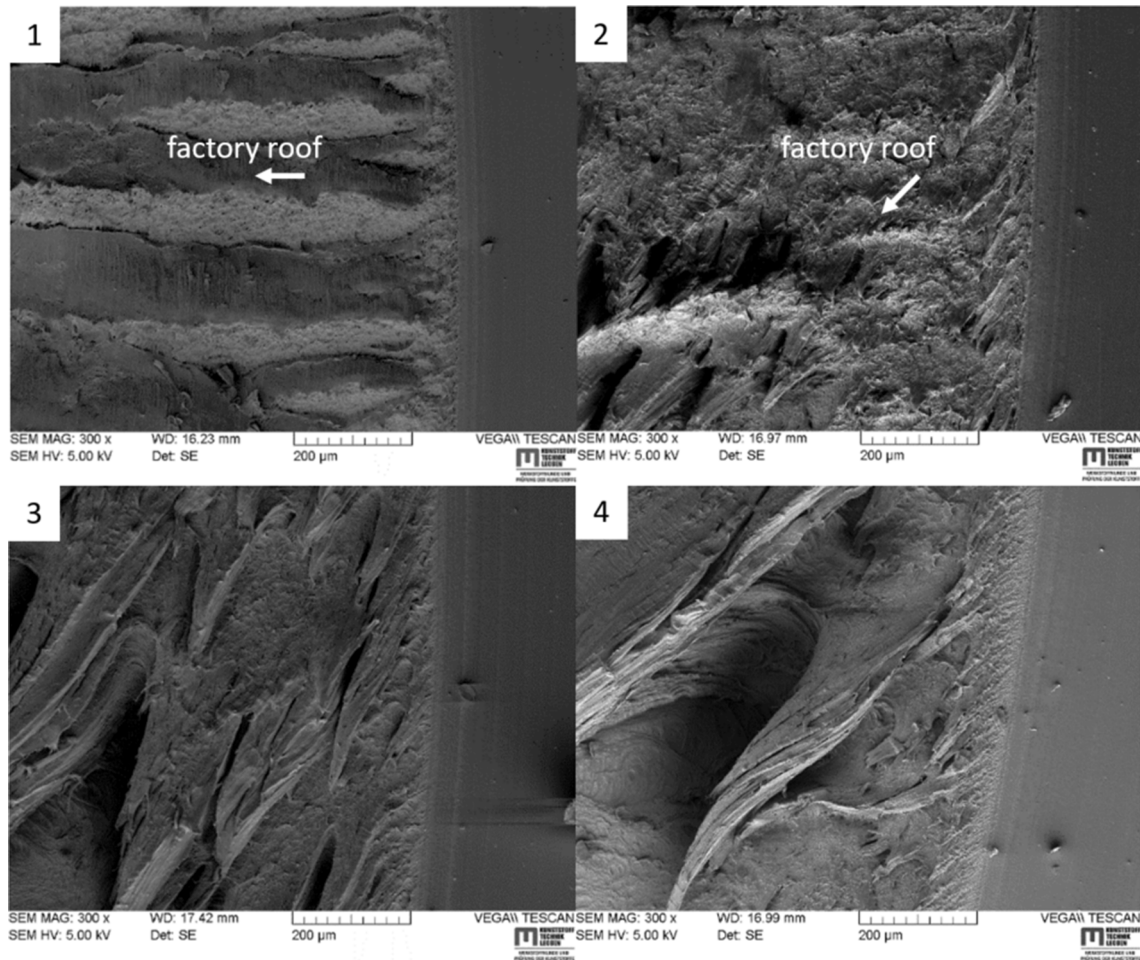


Fig. 7. SEM images from the fracture surfaces in Fig. 6 with a magnified view on the crack growth initiation area close to the notch tip show a change in the direction of the factory roof formations with increasing mode III loading.

slightly increase in comparison to the pure mode I loaded samples, even though an additional loading case (mode III) was applied. This could be an indication of a crack closure effect in the regime of low mode III loading amplitudes. The factory roof formations on the “MM-2” surface disappear after around 2 mm of crack growth, where the mechanism changes from mixed mode I/III loading to the final fracture (close to the specimen centre).

Based on the findings regarding the overall differences in fracture surface appearances, a more detailed analysis of the exact influence of the applied mixed mode I/III ratio is the logical next step. To discuss the influence of an increasing mode III amount on the appearance of the fracture surface, specimens at the same level of mode I but with increasing mode III loading were investigated and compared.

3.3.2. Influence of increasing mode III level on the fracture surface appearance

The influence of an increasing mode III amount on the fracture surface appearance of mixed mode I/III loaded PE specimens (nearly constant mode I loading) is presented in Fig. 6. Both variations of plotting the results with the applied ΔK_I value, as well as the ΔK_{eq} on the ordinate are presented.

The specimen with the lowest amounts of mode III displays the characteristic and aforementioned factory roof formations close to the notch tip, as shown in Fig. 6-(1). The factory roof formations display no indications of friction and wear abrasion on a macroscopical level. This argument is strengthened also by the fatigue fracture curve, where no decrease in life-time was measured compared to the pure mode I loaded

specimens. Contrary to expectations, the additional loading in mode III induces a slight increase of the life-time (as discussed in the previous section with the crack closure effect). With an increasing level of mode III (see specimen (2) and Fig. 6) the area on the fracture surface, where the typical factory roof formations are visible, decreases and the overall appearance of the area changes slightly. In the graph showing ΔK_{eq} , the specimens fall onto the line of the quasi-brittle failure in pure mode I. This might indicate, that no crack closure effect is present, but the applied amount of mode III also does not yet lead to significant abrasion and hysteretic heating, which would change the failure mode from quasi-brittle to thermally induced ductile failure. Further increases in mode III (specimens marked (3) and (4)) lead to an even smaller area of mixed mode indications, where in specimen (1) factory roof formations are visible. Furthermore, the structures in this area change the direction into a more tangential direction, which is in agreement with previous literature [54–56].

To get a better understanding of the exact formations in the first area close to the initial notch, a detailed investigation via SEM is shown for specimens (1) to (4) in Fig. 7. In the first picture (Fig. 7-(1)) the factory roof formations display no sign of deformation and the direction of the factory roof is pointed directly towards the specimen centre. For specimen (2), the area close to the crack growth initiation appears flatter and more smeared out with first signs of abrasion and deformation. Indications of factory roofs are still present, but change towards the direction of the mode III loading (tangentially). The examined area on the surfaces with higher amounts of mode III torsional loading (specimens (3) and (4), Fig. 7) do not show clear formations of factory roofs, but

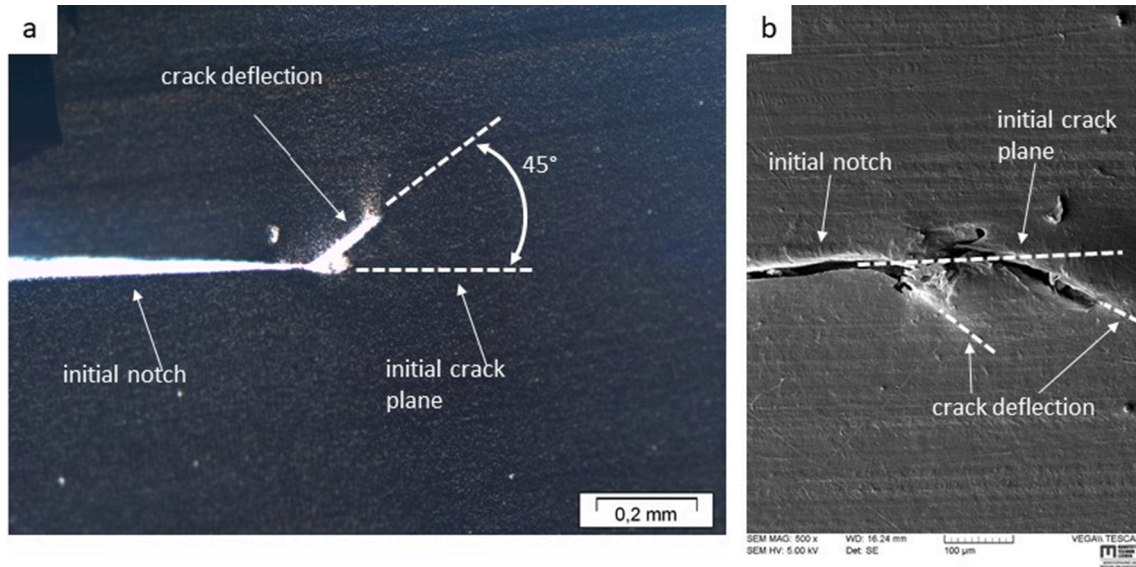


Fig. 8. Crack tip images of mixed mode I/III fatigue loaded PE specimens after the crack freezing experiments showing a branching from the initial crack plane directly after the initial crack tip (analysed using light microscopy (a) and SEM (b, c)).

rather a tangentially deformed texture, which is in agreement with fracture surfaces found on metals [55]. The visible indications of friction and wear abrasion in mode III testing are also supported by the increasing surface temperature measured during fatigue testing (33 °C for specimen 3 and 40 °C for specimen 4). This increase of temperature probably also further accelerates the plastic deformation of the formations on the fracture surface, since mechanical properties of polymers, e. g. the yield strength, are highly sensitive to temperature increases [22,38,39,62].

Interestingly, the governed area of factory roof morphology on the fracture surface seems to be dependent on the applied value of ΔK_{III} . The local stress intensity factor ΔK_{III} at the end of this area had similar values for all investigated specimens, which is shown as the length of the facet-zone l_{facets} in Fig. 6. The change is always accompanied by a local ΔK_{III} value of around 0.9 MPam^{1/2}. This indicates that the mode III amount during the experiment increases until a critical value is reached (in this case a ΔK_{III} value of around 0.9 MPam^{1/2}), at which point the fracture mechanism changes.

While the formations on the fracture surfaces of specimens with low

to moderate levels of ΔK_{III} allow for an interpretation of the fracture mechanism, it is not so clear on the specimens with high amounts of ΔK_{III} due to the smeared-out appearance after testing. To gain more information about the crack growth initiation process of highly deformed mixed mode specimens, like (3) and (4) in Fig. 6, so called crack freezing tests were conducted. Crack freezing experiments provide additional information about the developing crack path and subsequent formation of factory roofs at the beginning of the experiment before they are destroyed by friction and wear abrasion. Therefore, mixed mode I/III experiments were stopped after crack propagation had started but before the significant wear and abrasion, or even final failure occurred. Light-microscope and SEM images of different specimens with similar loading situations to specimen (4) in Fig. 6 (ΔK_I close to 0.7 MPa m^{1/2}, ΔK_{III} close to 0.6 MPa m^{1/2}) were performed and stopped after around 70 000 cycles. The results of the crack freezing experiments are shown in Fig. 8.

As discussed above, mode III can cause interactions during the tests, such as friction and wear abrasion due to the closed crack flanks, but also mode I branching. The latter phenomenon is a competition between

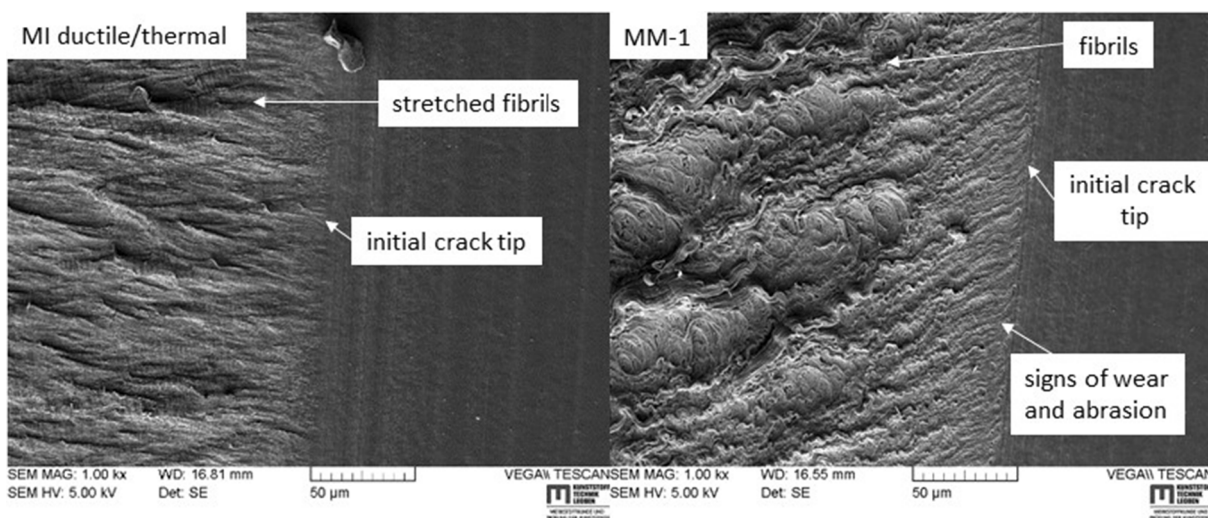


Fig. 9. SEM picture of the area close to the initial crack tip of fatigue loaded PE specimens: highly loaded mode I specimen (“MI ductile/thermal”) in comparison with a mixed mode I/III (“MM- 1”) specimen with a high level of mode III loading.

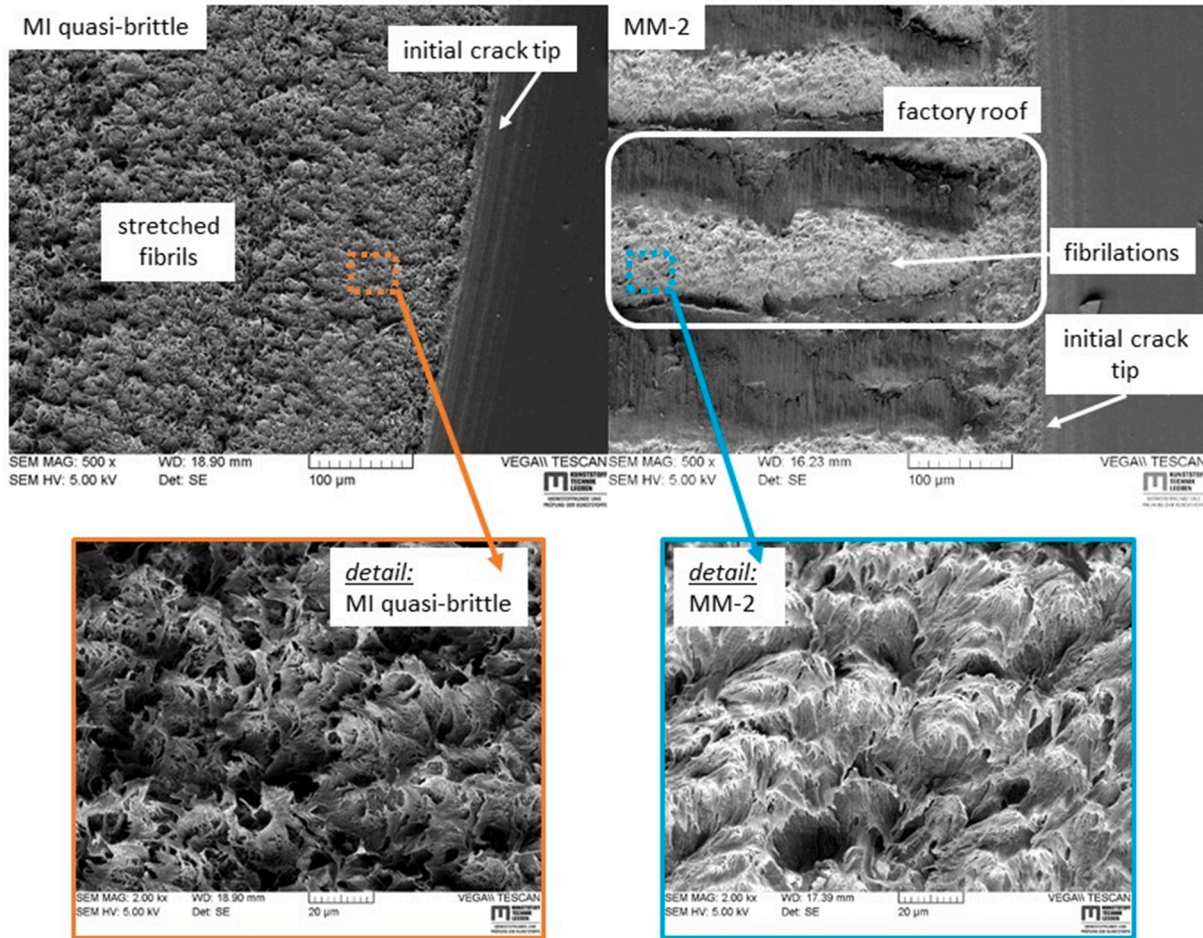


Fig. 10. SEM picture of the area close to the initial crack tip of fatigue loaded PE specimens: moderately loaded mode I specimen (“MI quasi-brittle”) in comparison with a mixed mode I/III specimen (“MM-2” with a low level of mode III loading) and a detailed comparison of the fibrillations.

the shear (mode II and mode III) and tensile (mode I) crack opening modes and leads to crack plane twisting (crack deflection) and subsequent factory roof formations on the fracture surface [8]. Although no clear factory roof formations are visible for specimens (3) and (4) on the fracture surfaces post mortem, the crack-freezing results in Fig. 8 show, that there are deflecting cracks with sloped crack fronts. This was also found for metals under mixed mode I/III loading [7,55,56,63]. The deflection of these cracks is marked in Fig. 8-a, where the light microscope image displays a nearly 45° kink of the crack front immediately after the initial crack tip. This is typically found during the formation of factory roofs. Also in the SEM images (Fig. 8-b), the crack plane rotation after the initial notch plane is clearly visible. In Fig. 8-b, the crack arrests in the first twisted crack before the crack growth continues to the next deflection. The growth happens close to the initial plane. This behaviour supports the appearance of factory roof formations as typical indications for mixed mode I/III crack growth also for highly loaded specimens, before these artefacts are destroyed by friction and wear abrasion.

Finally, after examination of the macro- and microscopic failure behaviour and appearance, it is also important to understand the underlying failure mechanism on a molecular level. As stated in the beginning, PE usually fails by the formation and breakdown of crazes in the quasi-brittle region. Since this area is especially interesting for lifetime estimations later on, it is necessary to investigate the influence of mode III loading with this regard as well.

3.3.3. Fracture surface - microscopic level

To examine the mechanisms occurring on the fracture surfaces, SEM

pictures were taken from the mode I and mixed mode I/III specimens presented in Fig. 5. Fig. 9 presents the mode I specimen in the region of “MI ductile/thermal” failure in comparison to the mixed mode I/III specimen with a high amount of mode III loading (“MM-1”).

The “MI ductile/thermal” fracture surface in Fig. 9 displayed indications of plastic deformation in the form of large stretched fibrils oriented in the direction of crack growth. These stretched fibrils are a sign of plastic surface flow [50,51,53]. The mixed mode I/III loaded specimen with high amounts of mode III presented in Fig. 9 (“MM-1”) displayed signs of wear and abrasion close to the initial crack tip, which, as previously stated, is also reflected by the comparatively high specimen surface temperatures measured for this specimen (around 40 °C).

In Fig. 10, SEM images of the area close to the initial crack tip are shown for a mode I quasi-brittle fracture surface (“MI quasi brittle”) and for a mixed mode I/III fracture surface with low amounts of mode III loading and suspected “crack closure” (“MM-2”).

The crack growth initiation area of the “MI quasi-brittle” specimen in Fig. 10 displays fine fibrillations on the fracture surface, which is an indication of creep and fatigue crack growth in combination with discontinuous crack, as previously discussed for PE [50,53]. The mixed mode I/III fracture surface in Fig. 10 with low amounts of mode III loading (“MM-2”) displays two clearly different mechanisms on the opposite side of the factory roofs. On one side of the factory roof also fibrillations, which show a similar appearance compared to pure mode I fibrillations (detail SEM pictures in Fig. 10), can be detected. On the other side of the factory roof the surface structure is more deformed and no fibrillation was observed. An explanation of the difference on the two

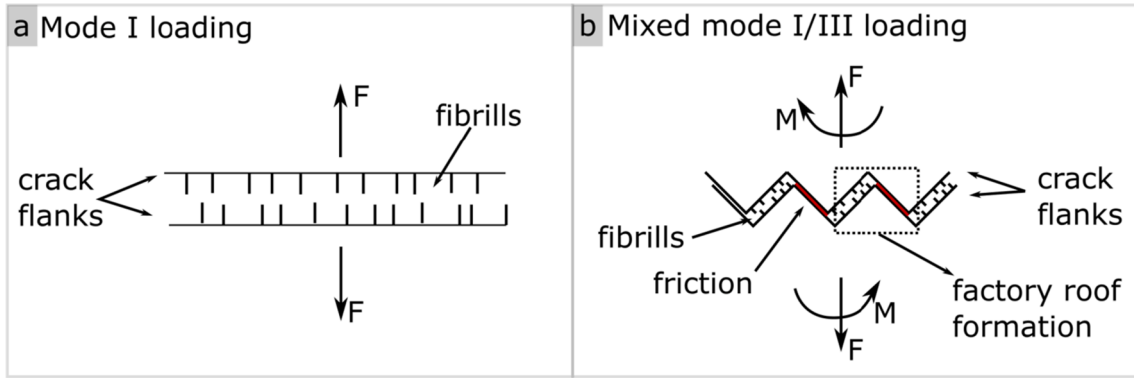


Fig. 11. Schematic illustration of the development of fibrills in pure mode I loading (a) and mixed mode I/III loading, where fibrills are present only on one side of the factory roof formation and friction and wear are supposed for the other side (b).

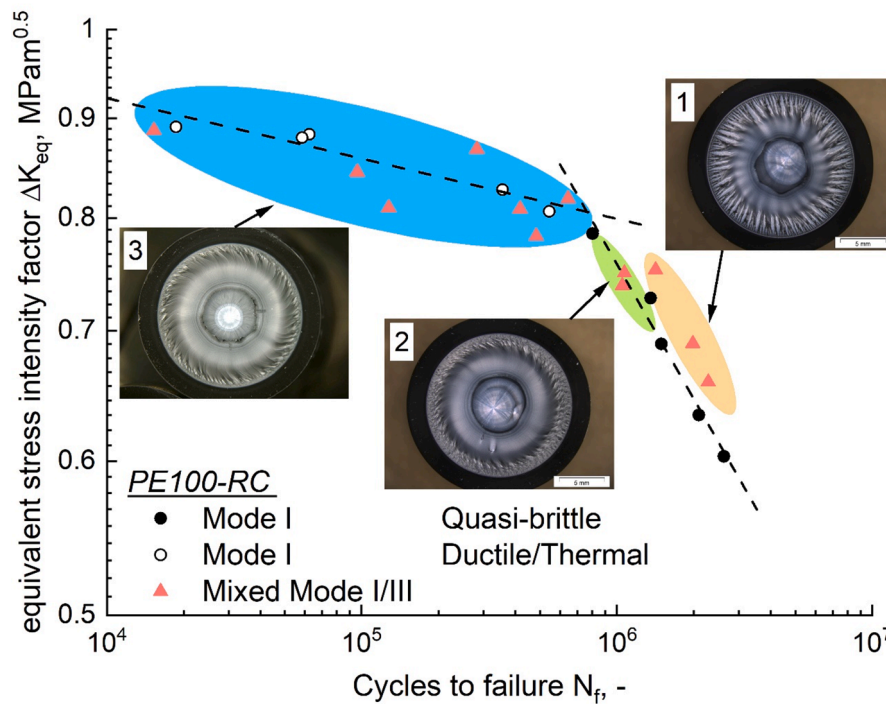


Fig. 12. The fatigue fracture behaviour of PE presented as the equivalent stress intensity factor ΔK_{eq} in pure mode I and mixed mode I/III fatigue testing is influenced by three effects marked as: (1) crack closure effect leads to increasing cycles to failure, (2) mixed mode fracture and (3) thermally induced failure.

sides of the factory roofs is schematically shown in Fig. 11, where pure mode I fibrills are compared to the factory roof formations in mixed mode I/III with fibrills on one side.

From the surface appearance in Fig. 10, it is supposed that the other side of the factory roof is exposed to friction and wear. The occurrence of fibrillation on only one side of the mixed mode facets is explained by the direction of the applied torque for the mode III loading. Since an R-ratio of 0.1 was applied, the specimen was deformed in mode III up to a certain value and afterwards unloaded to 10% of this value. Consequently, it was never completely unloaded or even loaded with a negative torque. Hence, only one side of the factory roof was loaded locally in positive mode I (through the crack plane rotation) and the fibrillations are only visible on this side. On the other side of these mixed-mode facets, wear and abrasion caused a smeared-out structure.

However, compared to specimens with high amounts of ΔK_{III} , the measured surface temperature increase was less pronounced. These results are a further indication, that the specimen is locally loaded in mode I due to a twisting of the crack plane. Therefore, the same underlying fracture mechanisms, which are often summarized as crazing, appear to be driving mechanisms of the failure of the PE material on one side of the factory roofs, while the other side shows clear indications of wear and abrasion.

4. Conclusions

The influence of mixed mode I/III fatigue loading on PE was characterized and compared to pure mode I fatigue results of this material. The aim was to continue the research on mixed mode fatigue loading of

polymers with a comparatively well analysed reference material (PE).

In a first comparison of applied ΔK_I and corresponding failure cycles N_f , the additional loading in mode III led to a significant decrease in the measured life-times compared to pure mode I fatigue experiments. For small amounts of mode III loading a similar slope as for the pure mode I quasi-brittle curve was observed only shifted to a lower life-time. For the comparison of both loading cases, the equivalent stress intensity factor ΔK_{eq} was evaluated, which led to a good correlation of pure mode I and mixed mode I/III experiments was observed. To provide an overview of the effects influencing mixed mode I/III fatigue crack growth in PE, the fatigue fracture curve based on the ΔK_{eq} was plotted again in Fig. 12, and the identified influences are marked as: (1) crack closure effect, (2) mixed mode I/III crack growth and (3) thermally induced failure.

For mixed mode I/III data points with low amounts of mode III (marked as (1) in Fig. 12) a slight increase in the measured cycles to failure was detected. This increasing life-time can be explained by the crack closure effect, where the driving force for crack growth is reduced due to a closed crack tip [8,28,58,59,61]. This is also visible on the investigated fracture surfaces, where characteristic factory roof formations, which are typical for mode III fracture, were observed. Mixed mode I/III specimens from the area (2) marked in Fig. 12, appear to be no longer influenced by crack closure effects and display a good correlation with the resulting ΔK_{eq} of pure mode I data points. Finally, the thermally induced failure (marked as (3) in Fig. 12), which is governed by abrasion between the crack flanks and hysteretic heating, is shown on the left side of the plot. The increasing temperature, friction and wear during testing also significantly alter the fracture surfaces, where a flat and smeared out appearance was detected. This aspect is especially critical for the measured life-time, since polymers are highly sensitive to temperature.

In future research, the results based on the equivalent stress intensity factor K_{eq} have to be compared with life-time simulations to further verify the results of this study. It is also important to expand this research by testing more materials to strengthen the knowledge of mixed mode I/III fatigue loading in plastics. Furthermore, mode II loading tests will be conducted to build a complete understanding for mixed mode crack growth effects in polymers.

Declaration of Competing Interest

The authors declare that they have no known competing financial

interests or personal relationships that could have appeared to influence the work reported in this paper.

Acknowledgement

The research work of this paper was performed at the Materials Science and Testing of Polymers/Montanuniversitaet Leoben within the framework of the COMET-program of the Federal Ministry for Transport, Innovation and Technology and the Federal Ministry of Science, Research and Economy with contributions by Polymer Competence Center Leoben GmbH and Institute of Physics of Materials AS CR/Czech Republic.

Appendix A

A.1. Specimen compliance and hysteretic loops

As mentioned in the manuscript, it was not possible to use the specimen compliance for a precise identification of the crack growth initiation or subsequent analysis of crack growth behavior via a compliance calibration. Due to the restrictions of the experimental setup, it is only possible to use the displacement data of the machine actuator. Therefore, the compliance data is too coarse for any detailed analysis of the mixed mode I/III crack growth behaviour. For illustration, the evaluated dynamic specimen compliance ($\Delta C = (\text{displacement}_{\max} - \text{displacement}_{\min}) / (\text{force}_{\max} - \text{force}_{\min})$) during a cycle from the machine data is shown in Fig. A1 for a mixed mode I/III specimen for both axial and torsional orientation.

Subsequent analysis of the whole load–displacement hysteresis, as shown in Fig. A2 for both regions in the failure curve and Fig. A3 for a mixed mode I/III specimen, did also not allow for further analysis of the crack growth kinetics, or point of crack growth initiation. All hysteresis loops shift towards higher displacements during testing due to creep of the whole specimen. However, a clear change of slope ($=1/\Delta C$) or shape of the hysteresis is only visible in the last few cycles before failure. Only the specimen failing in a ductile/thermal way (Fig. A3 on the right) shows a continuous change due to the steady increase in temperature.

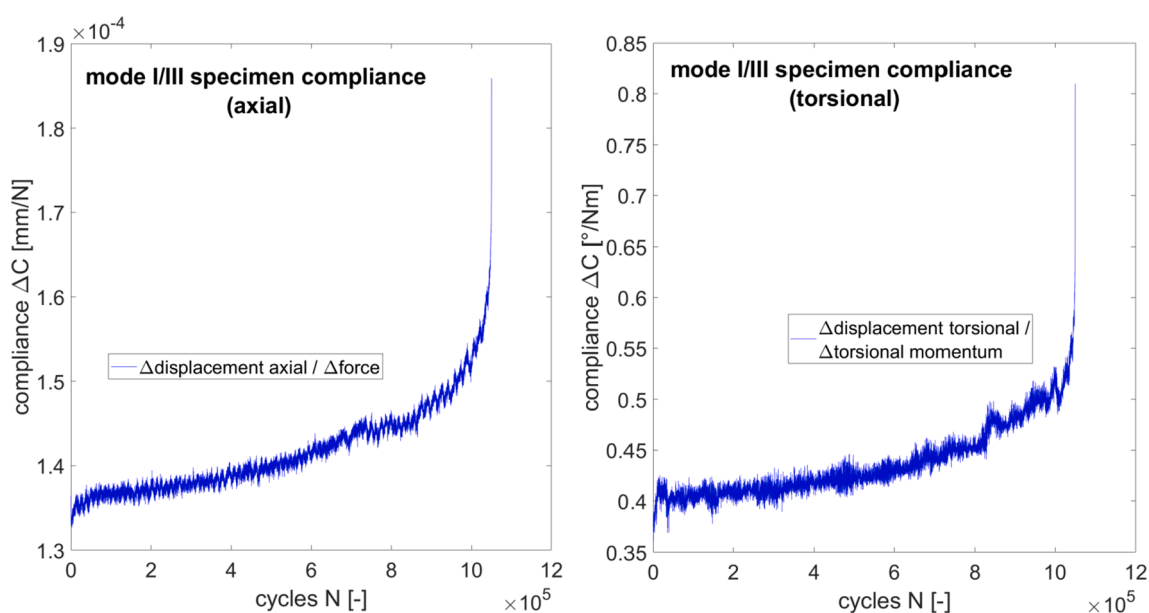


Fig. A1. Cyclic axial and torsional specimen compliance, recorded using the actuator of the testing machine during a mixed mode I/III test without clear indications of crack growth initiation.

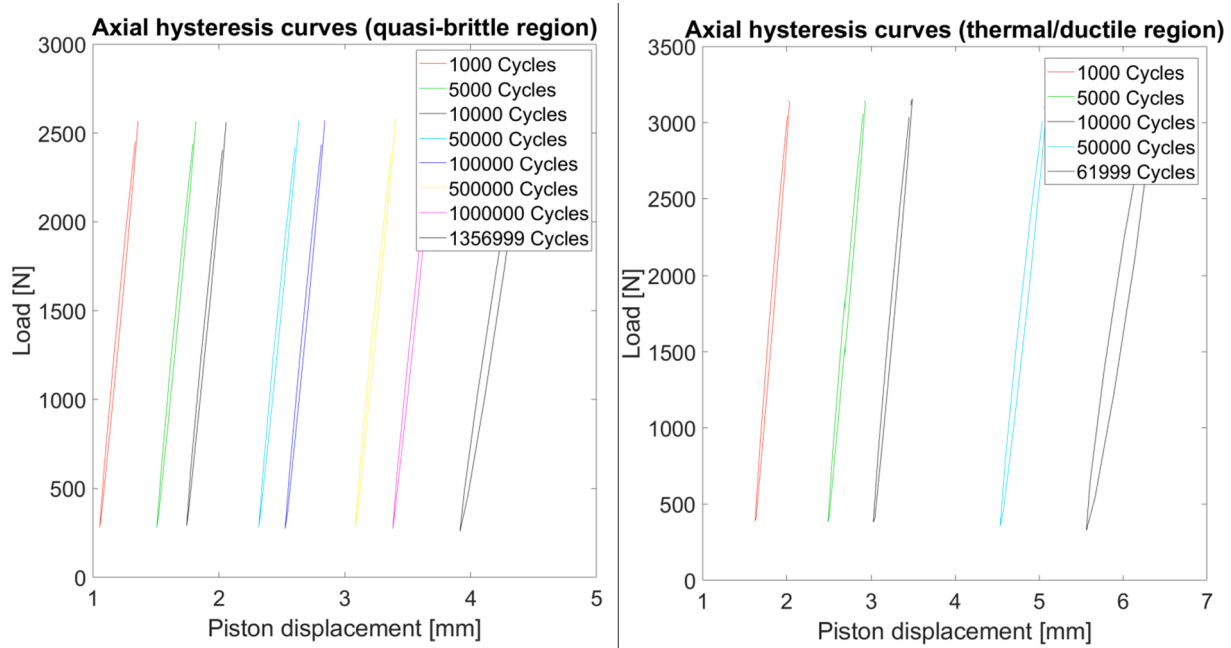


Fig. A2. Axial hysteresis curves in pure mode I loading tested samples in the quasi-brittle region and the thermal/ductile region.

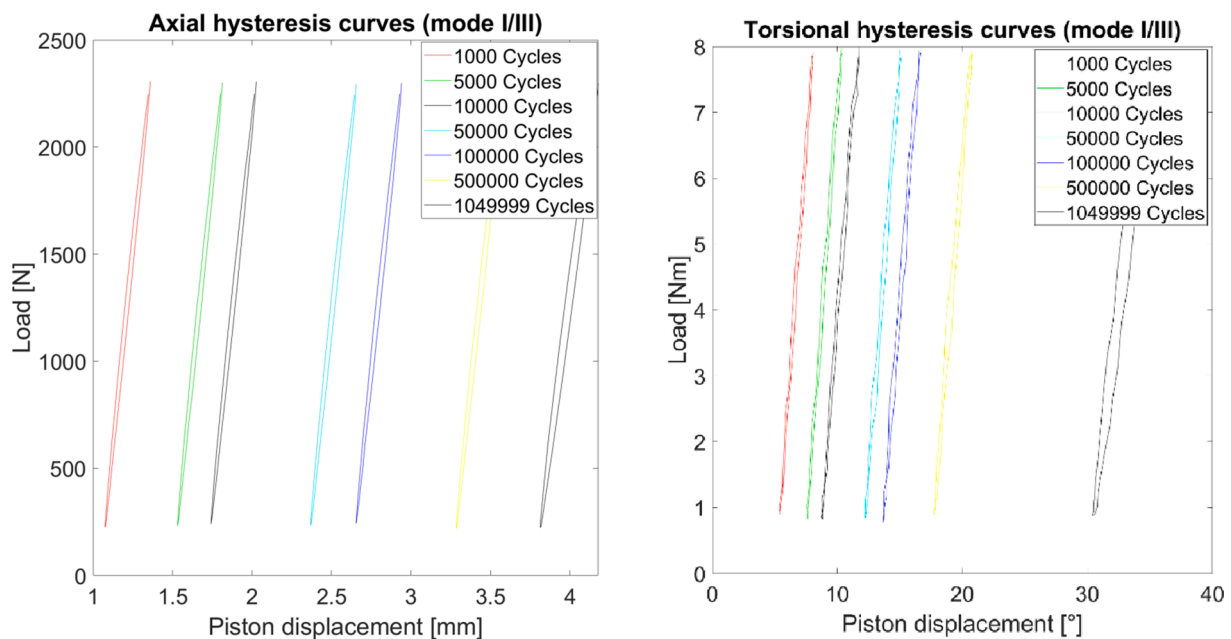


Fig. A3. Axial and torsional hysteresis curves in mixed mode I/III loading.

References

- [1] Rösler J. Zur Tragfähigkeitssteigerung thermoplastischer Zahnräder mit Füllstoffen [Dissertation]. Berlin: Technischen Universität Berlin; 2004.
- [2] Dlhý P, Poduska J, Nahlik L, Berer M, Gosch A, Pinter G, et al. Compression-loaded cracked cylinder - stress intensity factor evaluation. *Key Eng Mater* 2018;774: 331–6. <https://doi.org/10.4028/www.scientific.net/KEM.774.331>.
- [3] Berer M, Major Z. Characterization of the global deformation behaviour of engineering plastics rolls. *Int J Mech Mater Des* 2010;6(1):1–9. <https://doi.org/10.1007/s10999-010-9111-9>.
- [4] Berer M, Major Z. Characterisation of the local deformation behaviour of engineering plastics rolls. *Strain* 2012;48(3):225–34. <https://doi.org/10.1111/j.1475-1305.2011.00816.x>.
- [5] Berer M, Major Z, Pinter G. Elevated pitting wear of injection molded polyetheretherketone (PEEK) rolls. *Wear* 2013;297(1–2):1052–63. <https://doi.org/10.1016/j.wear.2012.11.062>.
- [6] Slávik O, Hutař P, Gosch A, Berer M, Vojtek T, Arbeiter F, et al. Fatigue crack propagation under mixed Mode I and III in polyoxymethylene homopolymer. *Key Eng Mater* 2019;827:404–9. <https://doi.org/10.4028/www.scientific.net/KEM.827.404>.
- [7] Beretta S, Foletti S, Valiullin K. Fatigue crack propagation and threshold for shallow micro-cracks under out-of-phase multiaxial loading in a gear steel. *Eng Fract Mech* 2010;77(11):1835–48. <https://doi.org/10.1016/j.engfracmech.2010.05.015>.
- [8] Vojtek T, Pokluda J, Hohenwarther A, Pippan R. Three-dimensional morphology of fracture surfaces generated by modes II and III fatigue loading in ferrite and austenite. *Eng Fract Mech* 2013;108:285–93. <https://doi.org/10.1016/j.engfracmech.2013.02.022>.
- [9] Doquet V, Pommier S. Fatigue crack growth under non-proportional mixed mode loading in ferritic pearlitic steel. *Fatigue Fract Eng Mater Struct* 2004;27:1051–60. <https://doi.org/10.1111/j.1460-2695.2004.00817.x>.
- [10] Qian J, Fatemi A. Mixed mode fatigue crack growth: A literature survey. *Eng Fract Mech* 1996;55:969–90.

- [11] Berer M, Mitev I, Pinter G. Finite element study of mode I crack opening effects in compression-loaded cracked cylinders. *Eng Fract Mech* 2017;175:1–14. <https://doi.org/10.1016/j.engfracmech.2017.03.008>.
- [12] Gosch A, Berer M, Hutař P, Slávik O, Vojtek T, Arbeiter FJ, et al. Mixed Mode I/III fatigue fracture characterization of Polyoxymethylene. *Int J Fatigue* 2020;130:105269. <https://doi.org/10.1016/j.ijfatigue.2019.105269>.
- [13] Arbeiter FJ, Frank A, Pinter G. Influence of molecular structure and reinforcement on fatigue behavior of tough polypropylene materials. *J Appl Polym Sci* 2016;133(38):1237. <https://doi.org/10.1002/app.43948>.
- [14] Pinter G, Haager M, Balika W, Lang RW. Cyclic crack growth tests with CRB specimens for the evaluation of the long-term performance of PE pipe grades. *Polym Test* 2007;26(2):180–8. <https://doi.org/10.1016/j.polymertesting.2006.09.010>.
- [15] Barker MB, Bowman J, Bevis M. The performance and causes of failure of polyethylene pipes subjected to constant and fluctuating internal pressure loadings. *J Mater Sci* 1983;18:1095–118.
- [16] Lang RW, Stern A, Doerner G. Applicability and limitations of current lifetime prediction models for thermoplastics pipes under internal pressure. *Angew Makromol Chem* 1997;247:131–45.
- [17] Sehanobish K, Moet A, Chudnovsky A, Petro PP. Fractographic analysis of field failure in polyethylene pipe. *J Mater Sci* 1985;4:890–4.
- [18] Lu X, Brown N. A test for slow crack growth failure in Polyethylene under a constant load. *Polym Test* 1992;11:309–19.
- [19] Haager M, Pinter G, Lang RW. Estimation of slow crack growth behavior in polyethylene after stepwise isothermal crystallization. *Macromol. Symp.* 2004;217(1):383–90. <https://doi.org/10.1002/masy.200451334>.
- [20] Abdel-Bary EM. *Handbook of plastic films*. UK: Shawbury; 2003.
- [21] ISO International Organization for Standardization. Polyethylene (PE) materials for piping systems — Determination of resistance to slow crack growth under cyclic loading — Cracked Round Bar test method (ISO 18489). Switzerland; 2015.
- [22] Frank A, Redhead A, Pinter G. The influence of test frequency and eccentric crack growth on cyclic CRB tests. Unpublished; 2012.
- [23] Scibetta M, Chaouadi R, Van Walle E. Fracture toughness analysis of circumferentially-cracked round bars. *Int J Fract* 2000;104:145–68.
- [24] Tada H, Paris P, Irwin GR. *The stress analysis of cracks*. Del Research Corporation; 2003.
- [25] Anderson TL. *Fracture mechanics: Fundamentals and applications*. Taylor & Francis Group, LLC; 2005.
- [26] Richard HA, Schramm B, Schirmeisen N-H. Cracks on Mixed Mode loading – Theories, experiments, simulations. *Int J Fatigue* 2014;62:93–103. <https://doi.org/10.1016/j.ijfatigue.2013.06.019>.
- [27] Tanaka K. Fatigue crack propagation from a crack inclined to the cyclic tensile axis. *Eng Fract Mech* 1974;6:493–507.
- [28] Vojtek T, Pokluda J, Sandera P, Horníková J, Hohenwarter A, Pippan R. Analysis of fatigue crack propagation under mixed mode II+III in ARMOCO iron. *Int J Fatigue* 2015;76:47–52. <https://doi.org/10.1016/j.ijfatigue.2014.09.018>.
- [29] Pokluda J, Pippan R. Can pure mode III fatigue loading contribute to crack propagation in metallic materials? *Fatigue Fract Eng Mater Struct* 2005;28(1–2):179–85. <https://doi.org/10.1111/j.1460-2695.2004.00843.x>.
- [30] Doquet V, Bui QH, Bertolino G, Merhy E, Alves L. 3D shear-mode fatigue crack growth in maraging steel and Ti-6Al-4V. *Int J Fract* 2010;165(1):61–76. <https://doi.org/10.1007/s10704-010-9504-7>.
- [31] Frank A, Freimann W, Pinter G, Lang RW. A fracture mechanics concept for the accelerated characterization of creep crack growth in PE-HD pipe grades. *Eng Fract Mech* 2009;76(18):2780–7. <https://doi.org/10.1016/j.engfracmech.2009.06.009>.
- [32] Frank A, Arbeiter FJ, Berger IJ, Hutař P, Nahlík L, Pinter G. Fracture mechanics lifetime prediction of polyethylene pipes. *J Pipeline Syst Eng Pract* 2019;10(1):4018030. [https://doi.org/10.1061/\(ASCE\)PS.1949-1204.0000356](https://doi.org/10.1061/(ASCE)PS.1949-1204.0000356).
- [33] Brown N, Donofrio J, Lu X. The transition between ductile and slowcrack- growth failure in polyethylene. *Polymer* 1987;28:1326–30.
- [34] Gedde UW, Ifwarson M. Molecular structure and morphology of crosslinked polyethylene in an aged hot-water pipe. *Polym Eng Sci* 1990;30(4):202–10. <https://doi.org/10.1002/pen.760300403>.
- [35] Krishnaswamy RK. Analysis of ductile and brittle failures from creep rupture testing of high-density polyethylene (HDPE) pipes. *Polymer* 2005;46(25):11664–72. <https://doi.org/10.1016/j.polymer.2005.09.084>.
- [36] Deblieck RAC, van Beek DJM, Remerie K, Ward IM. Failure mechanisms in polyolefines: The role of crazing, shear yielding and the entanglement network. *Polymer* 2011;52(14):2979–90. <https://doi.org/10.1016/j.polymer.2011.03.055>.
- [37] Lu X, Brown N. Unification of ductile failure and slow crack growth in an ethylene-octene copolymer. *J Mater Sci* 1991;26(3):612–20. <https://doi.org/10.1007/BF00588295>.
- [38] Lang RW. *Applicability of Linear Elastic Fracture Mechanics to Fracture in Polymers and Short-Fiber Composites [Dissertation]*: Leigh University; 1984.
- [39] Hertzberg RW, Manson JA. *Fatigue of engineering plastics*. New York, NY: Acad. Press; 1980.
- [40] Stern A, Novotny M, Lang RW. Creep crack growth testing of plastics—I. test configurations and test system design. *Polym Test* 1998;17(6):403–22. [https://doi.org/10.1016/S0142-9418\(97\)00067-6](https://doi.org/10.1016/S0142-9418(97)00067-6).
- [41] Stern A. *Fracture mechanical characterization of the long-term behavior of polymers under static loads [Ph.D. Dissertation]*. Leoben: Montanuniversitaet; 1995.
- [42] Lang RW, Balika W, Pinter G. Applicability of linear elastic fracture mechanics to fatigue in amorphous and semi-crystalline polymers. In: Moore DR, editor. *The application of fracture mechanics to polymers, adhesives and composites: European Structural Integrity Society ESIS Technical Comitee 4 (TC4)*. Elsevier; 2004. p. 83–92.
- [43] Barenblatt GI. *The mathematical theory of equilibrium cracks in brittle fracture*. In: Dryden HL, von Kármán T, Kuerti G, van den Dungen FH, Howarth L, editors. *Advances in applied mechanics*. Elsevier; 1962. p. 55–129.
- [44] Kausch-Blecken von Schmeling H-H. *Polymer fracture*. Berlin, Heidelberg: Springer; 1978.
- [45] Parsons M, Stepanov EV, Hiltner A, Baer E. The damage zone ahead of the arrested crack in polyethylene resins. *J Mater Sci* 2001;36(24):5747–55. <https://doi.org/10.1023/A:1012935517866>.
- [46] Berer M, Major Z, Pinter G, Constantinescu DM, Marsavina L. Investigation of the dynamic mechanical behavior of polyetheretherketone (PEEK) in the high stress tensile regime. *Mech Time-Depend Mater* 2014;18:663–84. <https://doi.org/10.1007/s11043-013-9211-7>.
- [47] Berer M, Tscharnuter D, Pinter G. Dynamic mechanical response of polyetheretherketone (PEEK) exposed to cyclic loads in the high stress tensile regime. *Int J Fatigue* 2015;80:397–405. <https://doi.org/10.1016/j.ijfatigue.2015.06.026>.
- [48] Arbeiter F, Pinter G, Frank A. Characterisation of quasi-brittle fatigue crack growth in pipe grade polypropylene block copolymer. *Polym Test* 2014;37:186–92. <https://doi.org/10.1016/j.polymertesting.2014.05.016>.
- [49] Favier V, Giroud T, Strijko E, Hiver JM, G'Sell C, Hellinckx S, et al. Slow crack propagation in polyethylene under fatigue at controlled stress intensity. *Polymer* 2002;43:1375–82.
- [50] Hamouda HBH, Simoes-betbeder M, Grillon F, Blouet P, Billon N, Piques R. Creep damage mechanisms in polyethylene gas pipes. *Polymer* 2001;42:5425–37.
- [51] Parsons M, Stepanov EV, Hiltner A, Baer E. Correlation of fatigue and creep slow crack growth in a medium density polyethylene pipe material. *J Mater Sci* 2000;35:2659–74.
- [52] Pinter G, Lang RW. Creep crack growth in high density polyethylene. In: Moore DR, editor. *The application of fracture mechanics to polymers, adhesives and composites: European Structural Integrity Society ESIS Technical Comitee 4 (TC4)*. Elsevier; 2004. p. 47–54.
- [53] Arbeiter F, Schrittester B, Frank A, Berer M, Pinter G. Cyclic tests on cracked round bars as a quick tool to assess the long term behaviour of thermoplastics and elastomers. *Polym Test* 2015;45:83–92. <https://doi.org/10.1016/j.polymertesting.2015.05.008>.
- [54] Nayeb-Hashemi H, McClintock FA, Ritchie RO. Effects of friction and high torque on fatigue crack propagation in Mode III. *MTA* 1982;13(12):2197–204. <https://doi.org/10.1007/BF02648390>.
- [55] Tschegg EK. Mode III and Mode I fatigue crack propagation behaviour under torsional loading. *J Mater Sci* 1983;18:1604–14.
- [56] Tschegg EK, Ritchie RO, McClintock FA. On the influence of rubbing fracture surfaces on fatigue crack propagation in Mode III. *Int J Fatigue* 1983;29–35.
- [57] Tschegg FK. Sliding mode crack closure and Mode III fatigue crack growth in mild Steel. *Acta Metall* 1983;9:1323–30.
- [58] Pippan R, Hohenwarter A. Fatigue crack closure: a review of the physical phenomena. *Fatigue Fract Eng Mater Struct* 2017;40(4):471–95. <https://doi.org/10.1111/ffe.12578>.
- [59] Suresh S, Ritchie RO. A geometric model for fatigue crack closure induced by fracture surface roughness. *MTA* 1982:13A.
- [60] Vojtek T, Pippan R, Hohenwarter A, Holan L, Pokluda J. Near-threshold propagation of mode II and mode III fatigue cracks in ferrite and austenite. *Acta Mater* 2013;61:4325–635. <https://doi.org/10.1016/j.actamat.2013.04.033>.
- [61] Pokluda J, Pippan R, Vojtek T, Hohenwarter A. Near-threshold behaviour of shear-mode fatigue cracks in metallic materials. *Fatigue Fract Eng Mater Struct* 2013;37:232–54. <https://doi.org/10.1111/ffe.12131>.
- [62] Hertzberg RW, Vinci RP, Hertzberg JL. *Deformation and fracture mechanics of engineering materials*. 5th ed. Hoboken, NJ: Wiley; 2013.
- [63] Zhizhong H, Lihua M, Shuzhen C. A study of shear fatigue crack mechanisms. *Fatigue Fract Eng Mater Struct* 1992;15(6):563–72.

Publication 6

Bibliographic information

Title: Fracture of Thin-Walled Polyoxymethylene Bulk Specimens in Modes I and III

Authors: Peer Schrader¹, Anja Gosch², Michael Berer³, Stephan Marzi¹

Affiliation:

1. Institute for Mechanics and Materials, Technische Hochschule Mittelhessen, 35390 Gießen, Germany;
2. Materials Science and Testing of Polymers, Montanuniversitaet Leoben, Otto-Gloeckel-Str. 2, 8700 Leoben, Austria
3. Polymer Competence Center Leoben GmbH, Roseggerstr. 12, 8700 Leoben, Austria

Periodical: MDPI materials

DOI: 10.3390/ma13225096

Relevant contributions to this publication

| | |
|-----------------------------|--|
| Conceptualization: | Peer Schrader, Anja Gosch, Stephan Marzi |
| Methodology: | Peer Schrader, Anja Gosch, Stephan Marzi |
| Validation: | Peer Schrader, Anja Gosch |
| Investigation: | Peer Schrader, Anja Gosch |
| Writing - Original Draft: | Peer Schrader |
| Writing - Review & Editing: | Anja Gosch, Michael Berer, Stephan Marzi |

Article

Fracture of Thin-Walled Polyoxymethylene Bulk Specimens in Modes I and III

Peer Schrader ^{1,*} , Anja Gosch ², Michael Berer ³  and Stephan Marzi ¹ 

¹ Institute for Mechanics and Materials, Technische Hochschule Mittelhessen, 35390 Gießen, Germany; stephan.marzi@me.thm.de

² Materials Science and Testing of Polymers, Montanuniversität Leoben, 8700 Leoben, Austria; anja.gosch@unileoben.ac.at

³ Polymer Competence Center Leoben GmbH, Roseggerstraße 12, 8700 Leoben, Austria; michael.berer@pccl.at

* Correspondence: peer.schrader@me.thm.de

Received: 16 October 2020; Accepted: 7 November 2020; Published: 12 November 2020



Abstract: Thin-walled polymeric components are used in many applications. Hence, knowledge about their fracture behavior in bulk is beneficial in practice. Within this study, the double cantilever beam (DCB) and out-of-plane double cantilever beam (ODCB) tests are enhanced to enable the testing of such bulk specimens in mode I and mode III on the basis of the *J*-integral. This paper then presents and discusses the experimental results following the investigation of a semicrystalline polymer (polyoxymethylen) under quasi-static load conditions. From the experiments, fracture energies of similar magnitude in both mode I and mode III were determined. In mode III, pop-in fracture was observed. Furthermore, the fracture surfaces were investigated regarding the mode I and mode III dominant crack growth mechanisms, based on the morphology of the tested material. For specimens tested in mode I, no signs of plastic deformation were observed, and the fracture surface appears flat. In mode III, some samples display a twisted fracture surface (twisting angle close to 45°), which indicates local mode I crack growth. A transfer of the presented methodology to other (more ductile) polymeric materials is deemed possible without further restrictions. In addition, the presented setup potentially enables an investigation of polymeric bulk specimens in mixed mode I+III.

Keywords: polyoxymethylene; fracture mechanical testing; polymers; quasi-static loads; experimental procedures; *J*-integral; tensile and shear dominated fracture

1. Introduction

Polymers are used in a wide range of applications, from daily use (packaging, bottles, etc.) to mechanical components (pipes, rollers, gearwheels, etc.). Unfortunately, compared to other materials such as metals or ceramics, there is still a large variety of open questions that remain to be addressed regarding the design of polymeric assemblies. To guarantee the safety of polymeric components, it is beneficial to possess good knowledge of their fracture mechanical properties. Especially when used as tube materials, information about their behavior as thin-walled components is also necessary, as fracture mechanical tests are generally conducted under plain strain conditions and, hence, greater specimen widths are tested.

Due to its material properties such as high stiffness, dimensional stability and fatigue resistance, polyoxymethylene (POM) is currently used in many technical applications [1–3]. While the fracture mechanical properties of POM are already available in mode I and mixed mode I+III under monotonic loading and cyclic fatigue tests [4–8], to the authors' knowledge, little is known about its fracture

mechanical properties in pure mode III. This paper addresses the need for the determination of fracture mechanical characteristics of POM for thin-walled components, so far lacking scientific literature.

Generally, only a few methods are available for determining the fracture energy of polymeric materials in pure mode III, of which many have drawbacks either in terms of experimental effort, costs or unwanted contributions in other modes that cannot be deemed negligible [9]. Furthermore, previous studies and therein proposed experimental setups have exclusively focused on linear elastic fracture mechanics, limiting their field of application to brittle and quasi-brittle materials. Hence, a number of questions regarding the mode III fracture of ductile polymers remain to be addressed.

To determine the fracture mechanical properties of POM and possibly other polymers in both pure modes I and III, we propose experimental setups based on the double cantilever beam (DCB) and out-of-plane double cantilever beam (ODCB) tests evaluated by using the J -integral. DCB tests with this method of data reduction have historically mostly been used for the experimental investigation of adhesives or composites, see [10–13] for example, whereas the ODCB test was exclusively used for the investigation of adhesives thus far [14]. The proposed modifications to the DCB and ODCB tests offer the possibility to determine the fracture energy in pure modes I and III on the basis of the J -integral. Hence, non-linear fracture behavior can also be characterized with the herein proposed setups, implying that the presented experiments are also used for materials that are not necessarily brittle or quasi-brittle. Conveniently, for the special case of linear elastic and brittle or quasi-brittle materials, the obtained J -integral measurements can be directly converted to approximate the fracture toughness values K_{Ic} and K_{IIIc} .

This paper begins by examining the theoretical background of the experimental determination of the J -integral in pure modes I and III. We will then describe the modifications made to the DCB and ODCB tests, which enabled the determination of the energy release rate (ERR) of a POM homopolymer (POM-H) in modes I and III. Then, after the determination of the ERR in modes I and III, a comparison with relevant literature is sought to classify the generated results in mode I and III. After an examination of the fracture surfaces and methodological critique, we will then present a summary of the most important results.

2. Theoretical Background

The ERR G is central to the field of fracture mechanics. It can generally be defined as the decrease in potential energy W per increase in fracture surface area, yielding

$$G = -\frac{\Delta W}{b\Delta a} \quad (1)$$

for plane problems. Here, a denotes the crack length, and b is the out-of-plane thickness of the body. For a crack to propagate, the ERR must equal the critical ERR $G = G_c$.

Next to the ERR, the J -integral according to Rice [15]

$$J = \int_S \left(W dy - t_i \frac{\partial \delta_i}{\partial x} dS \right) \quad (2)$$

represents an alternative approach to determine the release of energy during fracture. Here, t_i are the components of the traction vector, δ_i are the components of the displacement vector along an arbitrary path S containing the crack tip in counter-clockwise direction, and x is the direction of crack propagation (see Figure 1 for reference). This two-dimensional integral is path independent. It should be noted that the J -integral, according to its initial definition, strictly only applies to materials for which a strain energy density exists, implying that it may only be used for materials that behave in a hyperelastic manner. One should also note that the strain energy density must not explicitly depend on the x -coordinate for J to be path independent. However, the J -integral was also found to be path independent for small scale yielding and even during hardening at the crack tip under a monotonically increasing load [16,17]. An important key factor resulting from this path independence

is that contributions from external loads are in equilibrium with the value of J at the crack tip if the path is chosen around the outer bounds of the tested specimen, allowing the determination of J at the crack tip from the outer loading conditions. Furthermore, the J -integral and the ERR are equivalent if the crack grows straight ahead, the deformation at the crack tip is largely linear elastic, and only small-scale yielding is present [18].

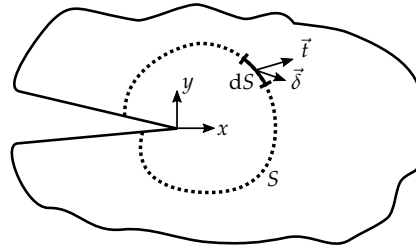


Figure 1. Schematic representation of the line J -integral around a notch for a plane problem.

In the following, we will briefly present the necessary equations for the evaluation of the conducted experiments in modes I and III and state the most important findings of prior studies. For more detailed derivations, we would like to refer to relevant literature, e.g., [10,11,14,19,20].

Consider a specimen with the corresponding external loads as displayed in Figure 2. Under these given forces F and moments M , the J -integral yields

$$J = \frac{F_y (\theta_1 + \theta_2)}{b} + \frac{M_y \kappa}{b} + \frac{M_{x,\text{up}}^2 + M_{x,\text{low}}^2}{2b} \frac{1}{\mu I_t} + \frac{M_z^2}{2b} \frac{1}{EI_z} \quad (3)$$

with the measured rotational angle at the points of load introduction θ_i and the curvature κ . E and μ denote the elastic Young's and shear modulus of the specimen. I_z and I_t are the second moment of area around the z -axis and the torsional second moment of area around the x -axis, respectively. By deconstructing the above equation, one obtains the contributions to J in the individual modes:

$$J_I = \frac{F_y (\theta_1 + \theta_2)}{b} \quad (4)$$

is the contribution in pure mode I,

$$J_{III} = \frac{M_y \kappa}{b} \quad (5)$$

is the pure mode III contribution,

$$J_{I^*} = \frac{M_{x,\text{up}}^2 + M_{x,\text{low}}^2}{2b} \frac{1}{\mu I_t} \quad (6)$$

is an unintended contribution to J by an “out-of-plane mode I”—loading due to the specimen twisting, and

$$J_{I+II} = \frac{M_z^2}{2b} \frac{1}{EI_z} \quad (7)$$

is an unintended contribution in modes I and II due to the finite width of the specimen.

The instantaneous experimental determination of the ERR based on the J -integral is relatively unsophisticated in mode I, as only force and rotational angle at the points of load introduction have to be measured [10]. To obtain the curvature κ in mode III, an increased experimental effort and the use of additional measuring equipment are required. Provided that the load is introduced to the crack tip by linear-elastically deforming beams, this experimental effort can be reduced by using the Irwin–Kies Equation

$$G_{III} = \frac{M_y^2}{2b} \frac{dC_{III}}{da} \quad (8)$$

with the change of compliance dC_{III} in shear direction, and the change of the lever arm da during crack propagation [14]. Loh and Marzi were able to establish a connection between the two evaluation methods from Equations (5) and (8) using Bernoulli beam theory, and determined that $J_{III} = G_{III}$ for this evaluation method [14]. Their beam theory approach yields

$$\kappa = \frac{M_y}{2} \frac{dC_{III}}{da}, \quad (9)$$

offering the possibility to significantly reduce the experimental effort, if dC_{III}/da is determined beforehand.

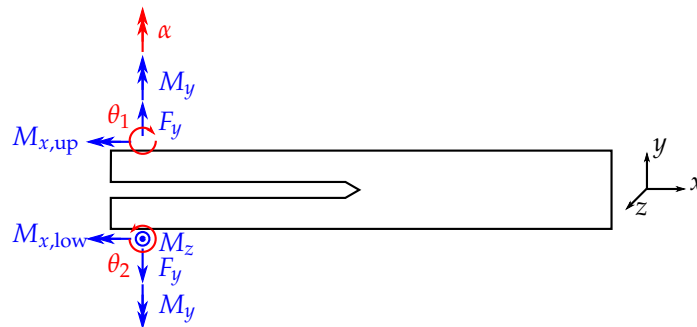


Figure 2. Schematic drawing of a loaded specimen. Measured forces and moments are displayed in blue color; measured or prescribed rotations are displayed in red.

Furthermore, it should be mentioned that the unintended contributions due to the mode III load were found to be negligible in the studies of Loh and Marzi [14,20,21], in which adhesives were investigated. Because of the changed specimen geometry we use within our study, it must be investigated to which extent these unintended contributions are present at the point of material failure with our proposed mode III setup to determine the “purity” of the mode III fracture.

3. Materials and Methods

3.1. Tested Material—Polyoxymethylene Homopolymer

The investigated material is a POM-H (Delrin 111PF) from DuPont (DuPont de Nemours, Wilmington, NC, USA) supplied as tubular granules, with a nominal diameter of 4 mm and a nominal height of 2 mm. POM-H shows good mechanical properties (Young’s Modulus E around 3500 MPa and Poisson’s ratio ν around 0.42) [1,22–24], high ductility down to 0 °C, high abrasion resistance and a low friction coefficient. Furthermore, the material is able to resist high amounts of constant loading or fatigue loading. Therefore, POM-H is used in more advanced applications with higher requirements concerning the material properties. POM-H is categorized as a technical thermoplastic material. In preliminary investigations, a glass transition temperature for the tested POM-H of -64 °C was obtained using dynamic mechanical thermal analysis.

3.2. Specimen Preparation

The geometry of the tested POM-H specimens is displayed in Figure 3. The specimens were milled and cut from plates (dimensions approx. $200 \times 200 \times 5.5$ mm), which were produced by compression molding (Hydrostat 300, Schwabenthan, Germany) with an immersion edge tool (TT-260, Tool-Temp). We want to note that extreme caution was taken during the milling and cutting processes, to ensure minimum temperature yield. For a better overview, the different stages of processing as well as the used tools and milling parameters are disclosed in Appendix A.

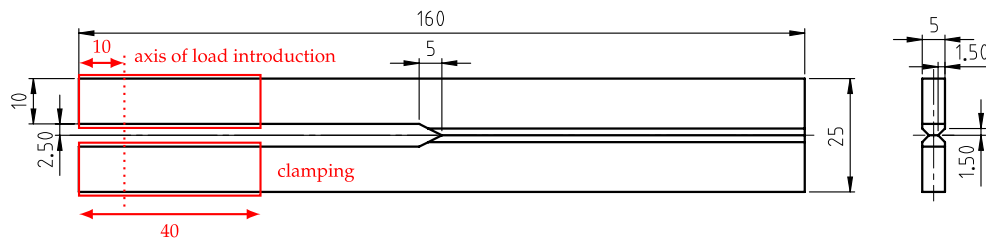


Figure 3. Geometry of the tested polyoxymethylene homopolymer (POM-H) specimens (in mm). The specimens were notched via pushing with a thin razor blade (notch depth ≈ 1 mm).

Prior to experimental investigation, the specimens were notched via pushing with a thin razor blade. The depth of the notches lay in the range between 1.0 ± 0.4 mm (mean and standard deviation). We want to mention that notching proved to be very difficult because of the brittle material behavior, leading to a larger standard deviation of the achieved notch length.

In the mode III investigation, aluminum reinforcements with a length of 160 mm and the cross-section area displayed in Figure 4 are connected to the POM-H specimens. The aluminum reinforcements were milled from an aluminum alloy (AlZn5.5MgCu, material grade number 3.4365) by a professional supplier (Feiler GmbH, Ehringshausen, Germany). The aluminum reinforcements were added to avoid energy dissipation outside of the crack tip due to plastic deformations in the lever arms caused by the introduction of an external moment. Furthermore, as the aluminum reinforcements are very much stiffer than the POM-H specimens and behave linear-elastically, it is ensured that possible influences of material nonlinearities are repressed so that the evaluation of the mode III ERR remains possible with Equation (8).

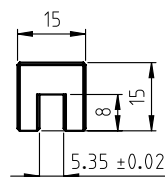


Figure 4. Geometry of the aluminum specimen holder (in mm). The nominal geometrical moments of inertia for the given geometry equate to $I_y = 4116.66 \text{ mm}^4$, $I_z = 3343.02 \text{ mm}^4$, and $I_t = 7459.68 \text{ mm}^4$ around the area's centroid.

The POM-H specimens and the reinforcements were joined using thermal clamping. For this purpose, the specimens were cooled to a temperature of -60 °C with an ultra-deep freezer Herafreeze Basic (Thermo Electron LED GmbH, Langenselbold, Germany) and, hence, subjected to thermal shrinkage. After two to three hours of cooling, the POM-H specimens were removed from the industrial freezer and inserted into the aluminum reinforcements. Then, steel gauge tape with a thickness of 0.20 mm is inserted into the small gaps between specimen and reinforcement on each side. Through thermal expansion of the POM-H specimens, the specimens and the aluminum reinforcements are, hence, uptight at room temperature. It should be noted that the glass transition temperature of POM-H is close to being reached during the cooling procedure, which could, although deemed very unlikely, influence the fracture behavior observed in the experiments. For reasons of space, the investigation of this influencing factor is postponed to possible future works. For a better overview, the specimens in the mode I and mode III investigation are shown in Figure 5.

Overall, 29 specimens were produced (eleven for the mode I investigation, 18 for the mode III investigation).

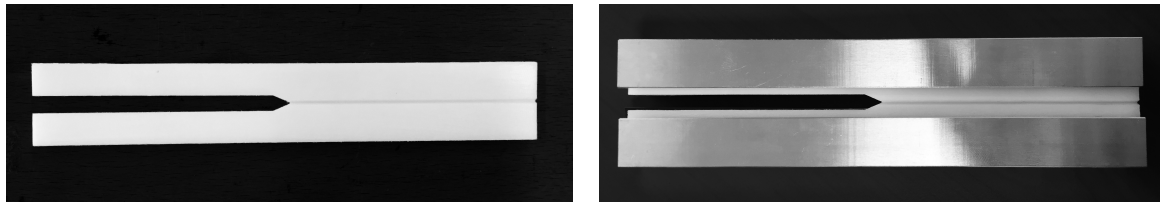


Figure 5. Specimen in mode I investigation (left) and mode III investigation (right). In mode I, the specimen is clamped directly into the test setup whereas in mode III, aluminum specimen holders are added.

3.3. Experimental Setups and Test Evaluation

In Figure 6, the test setup as realized in a biaxial tension-torsional servo-hydraulic test machine of type MTS Landmark Bionix (MTS Systems, Eden Prairie, MN, USA) is displayed. For both the mode I and the mode III setup, a distance between the point of load introduction and crack tip of 70 mm was maintained. It should be noted that for every tested specimen, the width of the specimen at the initial crack tip was measured with an optical microscope prior to evaluation. All tests were performed under laboratory conditions (20–23 °C, approx. 40% RH).

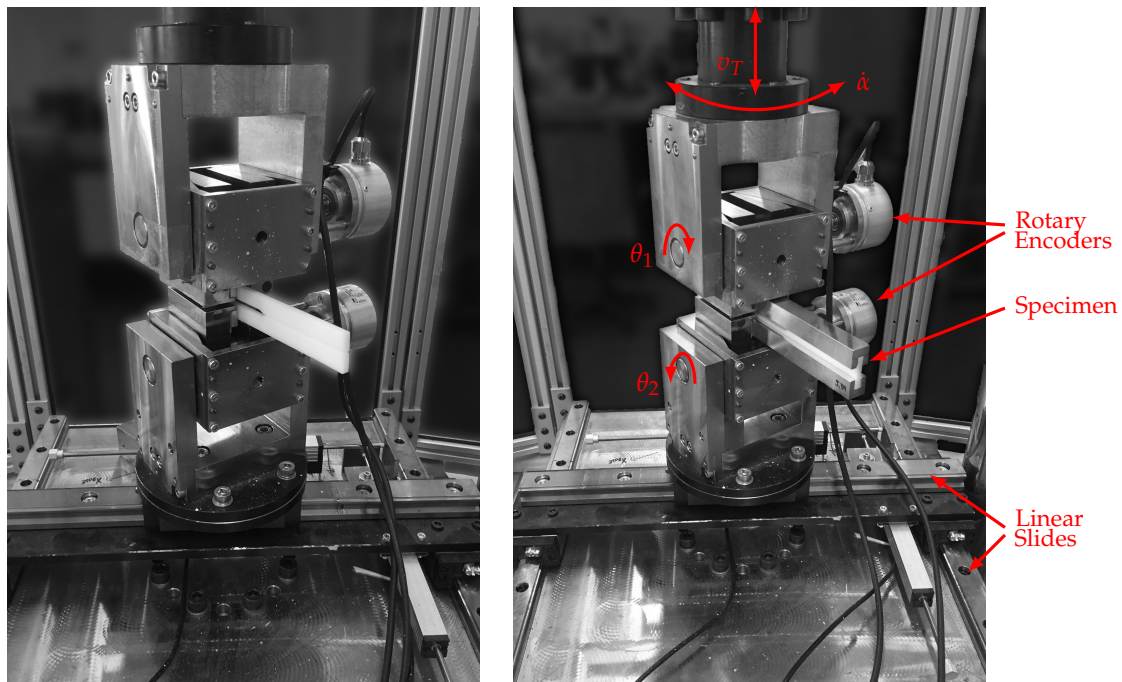


Figure 6. Experimental setup with POM-H specimens. Mode I setup (left) and mode III setup (right).

For the mode I tests, the specimen is clamped directly into the test machine without attaching reinforcements. The angles at the points of load introduction θ_1 and θ_2 are measured with two high resolution rotary incremental shaft encoders. A cross head velocity of $v_T = 0.05$ mm/s was selected during the mode I investigation. To determine the critical ERR in mode I, eleven specimens were tested. The tests were terminated after the first brittle crack extension for being able to measure the generated crack length after the experiment.

Next to the determination of the mode I ERR using the J -integral, the modified beam theory approach according to ASTM standard D5528 [25] is also used to determine the ERR. In this method of data reduction, the ERR is calculated from

$$G_I = \frac{3}{2} \frac{F\delta}{b(a + \Delta)} \quad (10)$$

with the correction term Δ , which is derived from a regression between the cube root of compliance and crack length. Prior to the analysis, the displacement measurement was corrected with the experimentally obtained compliance of the test setup (561.6 Nmm).

In mode III, the specimen is loaded with an angle-rate of $\dot{\alpha} = 0.05$ deg/s. To achieve pure mode III and avoid lateral forces, the setup contains two orthogonal linear slides below the bottom clamping device. Furthermore, axial forces are controlled to be naught by the control system of the test machine, leading to a vanishing mode-I-contribution. To directly obtain the mode III ERR from the J -integral, the curvature of three specimens is measured using two strain-gauges in half-bridge circuit at the external surface of the aluminum reinforcements. With the measured averaged strain ε and the width c of the aluminum parts, the curvature is computed with $\kappa = 2\varepsilon/c$. Thereupon, dC_{III}/da is determined from the given measured values in order to enable the calculation of the ERR via Equation (8), which leads to a reduction of experimental requirements, as the external moment is solely needed for evaluation. At last, using 15 more specimens, the critical mode III ERR of POM-H is determined.

3.4. Crack Length Determination and Fracture Surface Analysis

The produced crack length during the experiment in mode I was determined after testing. Therefore, the crack path of the mode I specimens, which were not fully fractured, were covered with a black ink to mark the crack advancement. Afterwards, the specimens were completely broken and the crack length was obtained as the length of the covered area via a digital calliper (Kellner & Kunz AG, Wels, Austria), with a measurement accuracy of 0.02 mm.

To obtain more information about the fracture process, a detailed analysis of the fracture surfaces was conducted. Therefore, an optical microscope SZX12 (Olympus Life Science Europe GmbH, Hamburg, Germany) was used. The investigation of the fracture surface provides valuable information about the fracture mechanisms and crack path formations in modes I and III.

4. Results and Discussion

4.1. Experimental Results in Mode I

In Figure 7, the measured force-displacement curves are displayed. As shown, the relationship between force and displacement is almost completely linear up until the point of a sudden, brittle fracture. Furthermore, the cube root of the specimen compliance is displayed over the crack length with the 5% confidence bands of the performed regression, from which a correction factor Δ of 37.66 mm can be derived. Using the modified beam theory approach according to Equation (10) yields a critical ERR of (6.58 ± 1.09) kJ/m².

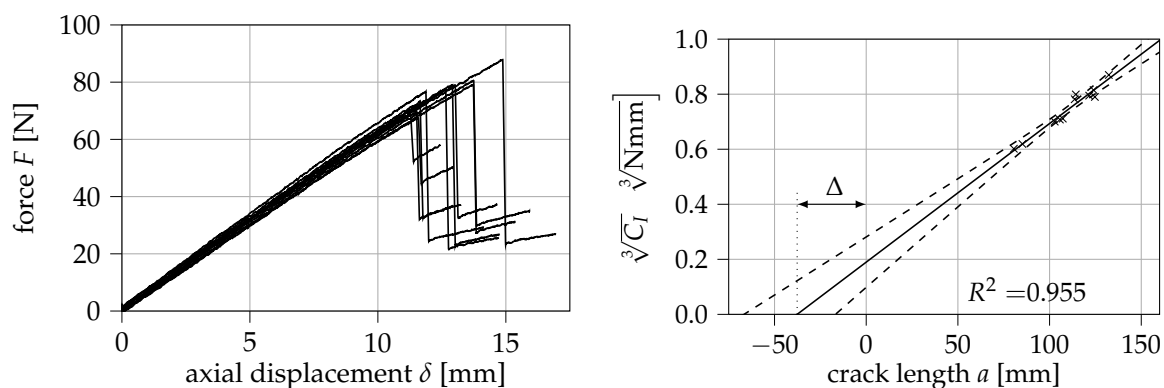


Figure 7. Measured force-displacement curves in mode I (left) and cube root of compliance over crack length with 5% confidence bands (right). Eleven specimens were tested.

However, the confidence bands suggest that the determination of Δ leads to a considerably large uncertainty in the calculation of G_{Ic} in this case. To roughly quantify this uncertainty, the critical ERR and its standard deviation depending on the obtained correction factor Δ is displayed in Figure 8. At the 5% confidence bands of Δ , ERRs between $(5.18 \pm 0.85) \text{ kJ/m}^2$ and $(8.13 \pm 1.34) \text{ kJ/m}^2$ are obtained. It is therefore argued that the calibration of the corrected crack length in this method of data reduction may be a strong source of error, which would be eliminated in the calculation of the J -integral via Equation (4).

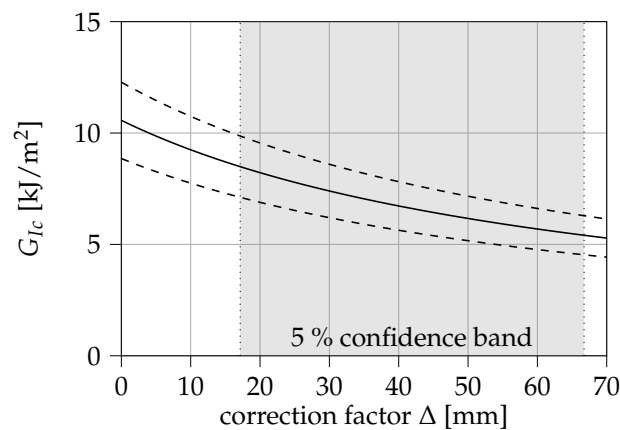


Figure 8. Influence of the correction factor Δ on the energy release rate (ERR) obtained from modified beam theory.

The measured mode I J -integral is shown over the cross head displacement δ in Figure 9. From the conducted experiments, a value for J_{Ic} of $(8.84 \pm 1.39) \text{ kJ/m}^2$ can be obtained. On the right side of Figure 9, both the maximum values of J_I as well as the values at crack arrest $J_{I,rest}$ are displayed over the generated crack surface. Interestingly, these results imply that J_{Ic} increases linearly with the generated crack surface, whereas $J_{I,rest}$ linearly decreases. In Table 1, the parameters of both of these linear regressions are summarized. Both regression lines just narrowly fail to meet in the intersection with the ordinate axis. However, within the confidence bands of the regression analyses, it is possible that an intersection of both lines exists on the ordinate axis. One may hypothesize that this intersection is the minimum possible value of J able to cause crack propagation. Considering the overlaps between both confidence bands, the intersection is most likely located in the range between 4.56 and 6.19 kJ/m^2 .

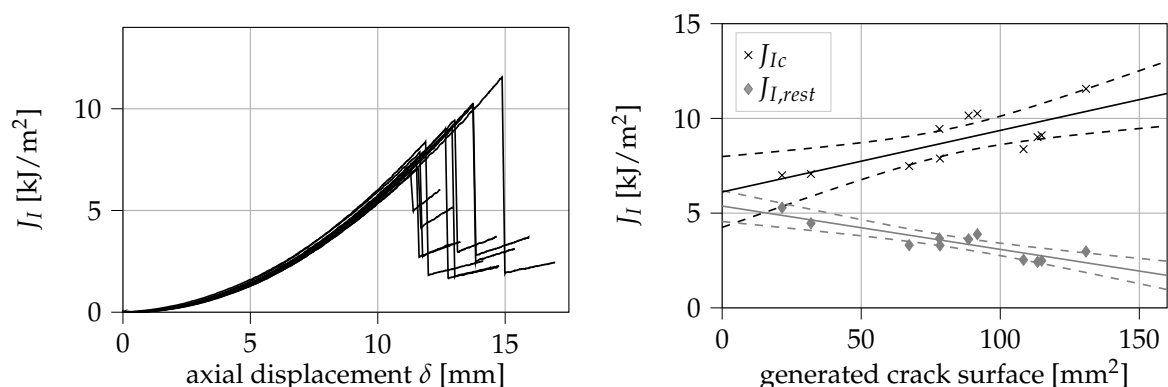


Figure 9. Measured values of the mode I J -integral (left) and obtained values for J_{Ic} and $J_{I,rest}$ over the generated crack surface (right).

Table 1. Function parameters and correlation coefficients of the linear regressions between J_{Ic} and $J_{I,rest}$ vs. crack length.

| | Slope [(kJ/m ²)/mm ²] | Intercept [kJ/m ²] | R ² [-] |
|--------------|--|-----------------------------------|-----------------------|
| J_{Ic} | 3.249×10^{-2} | 6.12 | 0.583 |
| $J_{I,rest}$ | -2.286×10^{-2} | 5.37 | 0.783 |

In practical application, these results can be advantageous: Firstly, knowing the relationships between J_{Ic} and $J_{I,rest}$ with the generated crack surface allows a rough determination of the fracture energy of a thin-walled component (with a similar geometry to the tested specimens) in hindsight, by simply measuring the area of the fracture surface. Secondly, the intersection between the regression lines is a useful parameter for the design of a thin-walled polymeric component, as it represents a lower limit to the crack driving force. We suggest that further research is performed in these areas to determine whether the obtained results also remain valid for larger sample sizes, other specimen geometries, and different polymeric materials.

4.2. Experimental Results in Mode III

4.2.1. Determination of dC_{III}/da

Within this study, three specimens are used to experimentally determine the constant dC_{III}/da . In Figure 10, the measured moment M is displayed over the rotational angle of the biaxial testing machine α .

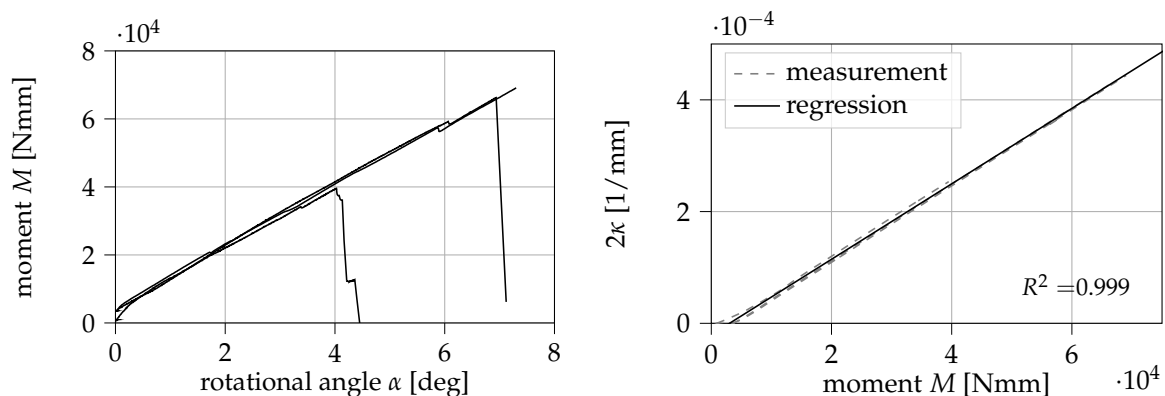


Figure 10. Measured moment M_y over the rotational angle α (left) and linear regression between the curvature 2κ and the measured moment M_y (right) obtained with three specimens.

As can be seen in Equation (9), dC_{III}/da can be obtained from the relationship $2\kappa/M_y$. Here, dC_{III}/da is determined from a linear regression between 2κ and M_y up until the measured maximum of J_{III} . The value for dC_{III}/da is then derived from the slope of the regression line. The measured values of curvature κ on the outside of the reinforcements and the bending moment M_y as well as the performed regression are also displayed in Figure 10. The slope of the regression line equates to $(6.75 \pm 0.01) \times 10^{-9} \text{ 1/Nmm}^2$ ($\pm 5\%$ confidence interval of regression slope). It can be observed that the measured values are captured by the regression line with great accuracy (correlation coefficient $R^2 = 0.999$).

For verification purposes, dC_{III}/da is also determined analytically with $dC_{III}/da = 2/(EI_y)$, the aluminum's elastic modulus of $E = (70 \pm 1) \text{ GPa}$ and the specimen holders area moment of inertia $I_y = 4116.66 \text{ mm}^4$. From this, a value of $(6.940 \pm 0.101) \times 10^{-9} \text{ 1/Nmm}^2$ can be derived, which fits with the experimentally obtained dC_{III}/da , given that the compliance of the aluminum reinforcements itself should be greater than the compliance of the holder with an inserted POM specimen. Because of the

relatively good agreement between experimentally measured and analytically determined dC_{III}/da , the evaluation of the unintended contributions according to Equations (6) and (7) is performed with the moments of inertia of the reinforcements.

4.2.2. Critical Mode III ERR

The experimental results with 15 additional specimens are displayed in Figure 11. From this, a critical mode III ERR of (7.59 ± 1.19) kJ/m² can be derived. We note from the diagram that prior to critical failure all samples show at least one significant, sudden drop in J_{III} . This so-called pop-in phenomenon has been mostly observed for steels or weldments in mode I testing. Studies found that pop-ins can both result from a local unstable crack growth that is then stabilized by the surrounding material [26] or by the formation of cracks perpendicular to the plane of the initial pre-crack [27]. To our knowledge, pop-in in pure mode III fracture of polymers is observed for the very first time within this study.

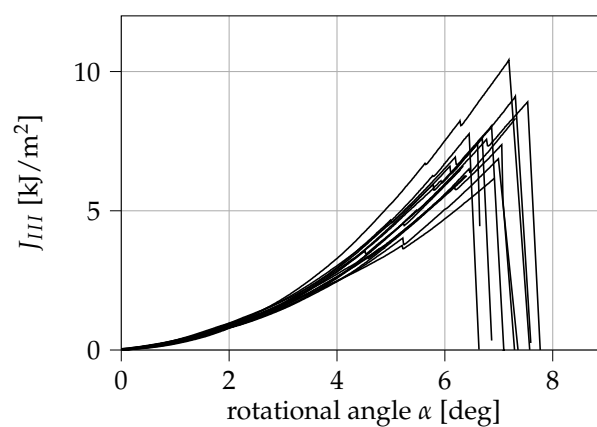


Figure 11. Experimental results of the mode III investigation. The shown mode III ERR of 15 specimens was determined from the Irwin-Kies Equation.

In Figure 12 the ratio between the values of J_{III} at which pop-ins occurred and J_{IIIc} is displayed. Here, pop-in ratios between 53% and 93% can be observed. For the given sample size, the results do not allow any statement as to whether the pop-in-ratio is dependent on the measured J_{IIIc} . The occurrence of pop-ins can be critical for the structural integrity of a thin-walled POM-H component loaded in shear as cracks could grow prior to critical failure, potentially weakening thin-walled components to a significant extent. Because pop-ins were already observed shortly above 50% of J_{IIIc} , it is indicated that shear loads could be very much critical for a thin-walled POM-H component.

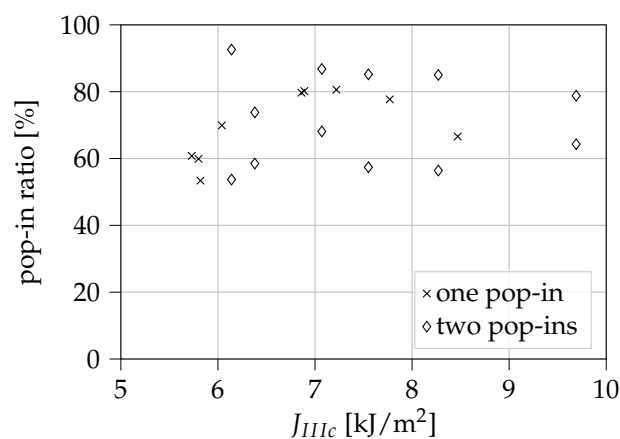


Figure 12. Ratio between the observed pop-in values of J_{III} and J_{IIIc} .

The measured unintended contributions normalized to the current measured mode III ERR are displayed over J_{III}/J_{IIIc} in Figure 13. One should note that the contribution of J_{I^*} is considerably larger than the measured mode III ERR at the start of the test. This may be partly attributed to the fact that the breakaway force of the linear slides must first be overcome at the beginning of the test. The load history is therefore not to be considered as a pure mode III loading process. However, it can also be observed that the unintended contributions are, in fact, negligible at the points of fracture. At fracture, J_{I^*} takes up $(3.02 \pm 1.01) \%$ of J_{III} and tends further towards naught, whereas J_{I+II} only takes up $(0.04 \pm 0.04) \%$. This means that, according to the measurements, the fracture process can be considered as a pure mode III fracture.

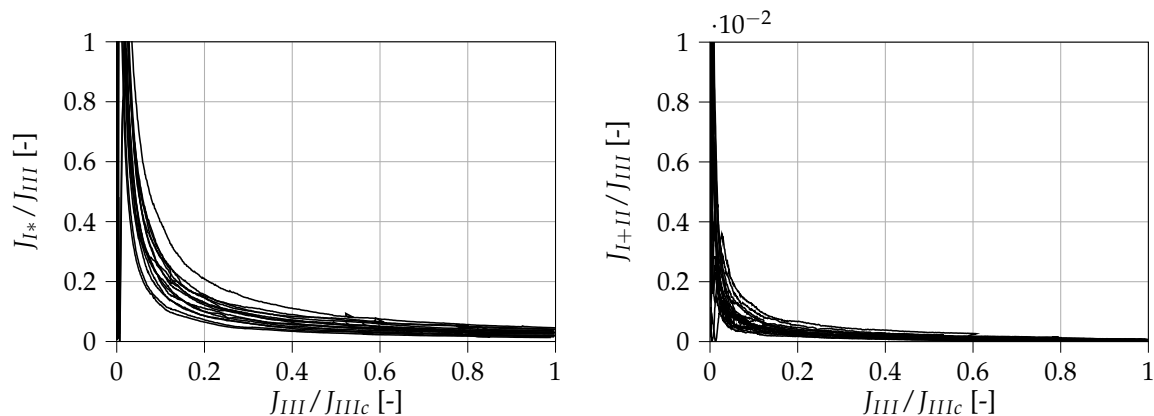


Figure 13. Artificial contributions determined within the mode III investigation. The unintended out-of-plane mode I load J_{I^*} (left) and the mode I/II contribution J_{I+II} (right) are displayed normalized on J_{IIIc} over J_{III}/J_{IIIc} .

4.3. Approximate Determination of the Stress Intensity Factors K_{Ic} and K_{IIIc}

As a side effect, for the special case of linear elastic, isotropic, and brittle or quasi-brittle materials, the stress intensity factors in mode I and mode III can directly be related to the critical values of G (and J) in a given loading mode. In mode I, the stress intensity factor K_{Ic} is calculated with

$$K_{Ic} = \sqrt{E'J_{Ic}} = \sqrt{E'G_{Ic}} \quad (11)$$

with $E' = E$ in plane stress and $E' = E/(1 - \nu^2)$ in plane strain. Unfortunately, it is unclear at this point, whether the crack tip was loaded in plane stress or plane strain due to the necessary addition of the side-grooves to the specimen. Although the thin geometry of the specimens should induce a plane stress state, the addition of side-grooves is known to induce stress triaxialities that could lead to a state of plain strain [28].

In mode III, i.e., for antiplane shear, the stress intensity factor K_{IIIc} can be derived with

$$K_{IIIc} = \sqrt{2\mu J_{IIIc}} = \sqrt{2\mu G_{IIIc}}. \quad (12)$$

As shown in Section 4.1, a critical ERR J_{Ic} of $(8.84 \pm 1.39) \text{ kJ/m}^2$ was determined from the experiments performed in this study, which roughly equates to a mode I stress intensity factor K_{Ic} of $5.6 \text{ MPa m}^{1/2}$ (plane stress) or K_{Ic} of $6.1 \text{ MPa m}^{1/2}$ (plane strain), respectively. In mode III, a fracture energy of $(7.59 \pm 1.19) \text{ kJ/m}^2$ was obtained, which equates to a K_{IIIc} of about $4.3 \text{ MPa m}^{1/2}$.

4.4. Summary and Discussion of the Obtained Fracture Mechanical Properties

In this section, we want to shortly summarize and discuss the obtained fracture mechanical properties displayed in Table 2.

Table 2. Summary of the most important experimentally obtained parameters.

| | Mode I | Mode III |
|--|--|----------------------------------|
| G_c from modified beam theory | $(6.58 \pm 1.09) \text{ kJ/m}^2$ | n.a. |
| critical value of J | $(8.84 \pm 1.39) \text{ kJ/m}^2$ | $(7.59 \pm 1.19) \text{ kJ/m}^2$ |
| approx. fracture toughness K | 5.6 MPa $\text{m}^{1/2}$ (plane stress) 6.1 MPa $\text{m}^{1/2}$ (plane strain) | 4.3 MPa $\text{m}^{1/2}$ |
| min. of J to cause crack propagation | 4.56–6.19 kJ/m^2 | n.a. |
| pop-in ratio | not observed | 53–93% |

In the mode I investigation, a relatively large discrepancy between the experimentally obtained mode I G_{Ic} and J_{Ic} was found. The authors believe that this discrepancy is due to a large uncertainty in the determination of the corrected crack length Δ from the crack length measurement and specimen compliance. We want to point out that using the J -integral method of evaluation offers the possibility to determine the fracture energy of a polymeric bulk specimen without measuring crack length or the elastic properties of the material. As only force and rotational angle have to be measured for the determination of the mode I J -integral, a simultaneous determination of the fracture energy during the experiment is possible. This allows controlling the experiments on specific values of J , which poses an interesting topic for future research.

Regarding the obtained mode III J -integral, we want to point out two important factors: Firstly, we want to emphasize that the evaluation of the J -integral with the measured curvature κ might be necessary in some cases. With the aluminum reinforcements, a constant dC_{III}/da could be ensured in this study, rendering J_{III} and G_{III} equivalent. However, this may change if the reinforcements are removed. Furthermore, if the material was more ductile, a determination of J_{III} with the curvature κ may prove to be more accurate. Secondly, it should also be mentioned that J_{III} can be determined with both evaluation methods (κ or dC_{III}/da) instantaneously during the experiment. This, as in mode I testing, allows controlling the experiments on specific values of J in future studies.

A review of literature provided mode I stress intensity factors K_{Ic} for POM-H between 2.5 and 6.9 MPa $\text{m}^{1/2}$ [4,6,7]. Thus, the obtained mode I stress intensity factor between 5.6 and 6.1 MPa $\text{m}^{1/2}$ lies within the range of reference measurements from literature. We want to emphasize that our results match with the plane strain fracture toughness of the same material determined with compact tension specimens [6,7]. Unfortunately, we were unable to better investigate the stress state at the crack tip within the scope of this work, and we cannot report the mode I stress intensity factor at a greater accuracy. To the authors' knowledge, no comparative values are available under pure mode III. Hence, one of the highlights of our study is that the determination of the pure mode III fracture toughness of POM was made possible with our setup for the first time. However, future studies on the topic are suggested in order to verify the determined mode III fracture energy and fracture toughness.

4.5. Investigation of the Fracture Surfaces

4.5.1. Mode I

An optical analysis of the fracture surface was conducted in this study to gain more information about ongoing crack growth mechanisms during testing. This is a common method to investigate the crack growth process after testing and to identify changes in the latter with the surface structure. An overview picture of the fracture of a specimen tested in mode I and a light microscope image of the fracture surface close to the initial notch are shown in Figure 14.

The macroscopically observed fracture surface of monotonically loaded mode I specimens is flat (see overview picture in Figure 14), with three different areas on the fracture surface (marked with (1) to (3) on the images in Figure 14). The first area represents the pre-notch, which was generated via a razor blade before testing. Area (2) marks the produced crack growth during testing and area (3) was generated after testing to determine the ligament length.

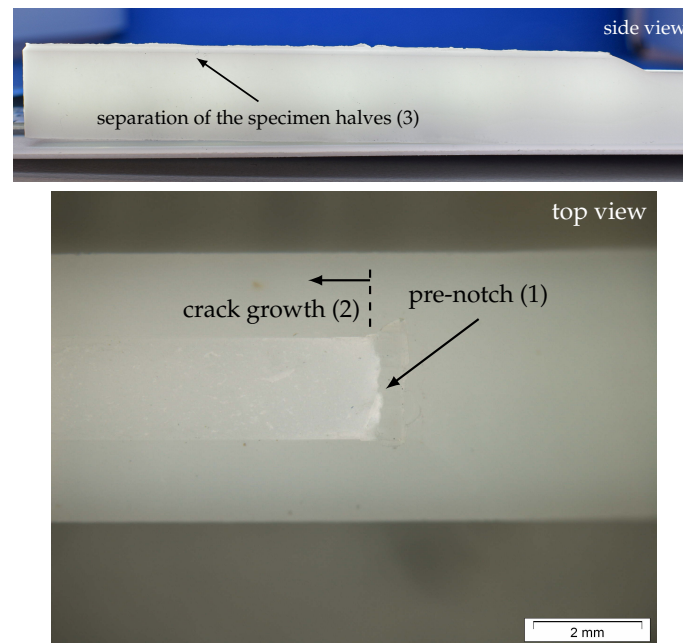


Figure 14. Fracture surface images from a monotonically loaded mode I specimen analyzed using a light microscope ($16\times$ magnification)—three areas of different crack areas were observed: pre-notch before testing (1), the crack growth area (2) and the area produced during the separation of the two specimen halves (3).

The quality of the pre-notch (sharp crack tip without any signs of deformation) has a major influence on the resulting fracture mechanical parameters. Therefore, it is of high interest to guarantee a similar notch quality for all investigated specimens. For the used POM-H specimens, the notching procedure was found to be challenging because of the rather brittle material behavior. This difficulty manifests itself as small imperfections at the crack tip, as shown in Figure 14. Hence, small variations of the produced pre-notch led to an increased standard deviation of the determined fracture mechanical parameters.

No indications of plastic deformation, which would have been visible as intensive white zones on the fracture surfaces, were found in the investigation. Furthermore, as already observed during the experimental investigation, the specimens fractured in a brittle manner. This observation is in contrast to previous monotonic mode I tests on the same material class [6], in which an intensive white zone was found whose formation is attributed to crazes and micro-voids within the material.

In general, deformation rate, specimen thickness, and the added side-grooves also have a large influence on the size of the plastic zone. Based on the fracture surface investigation and the brittle fracture without any indications of plastic deformations, it is suggested that the specimens fractured in a plane strain state. This is also supported by the addition of the side-grooves, which lead to an increased triaxiality along the crack front. However, this finding suggests that further investigations are required to gain a better understanding of the influence of specimen thickness and groove shape on the fracture behavior of POM-H.

4.5.2. Mode III

To examine the fracture process of the mode III samples, a fracture surface analysis via an optical microscope was conducted similar to the mode I procedure. An overview of two representative fracture surfaces loaded in mode III is shown in Figure 15. Interestingly, two different types of mode III fracture surfaces were observed. A larger group of the mode III specimens displayed extensive twisting and crack plane deflection (Figure 15a), whereas in some cases, a less deflected crack flank was observed (Figure 15b).

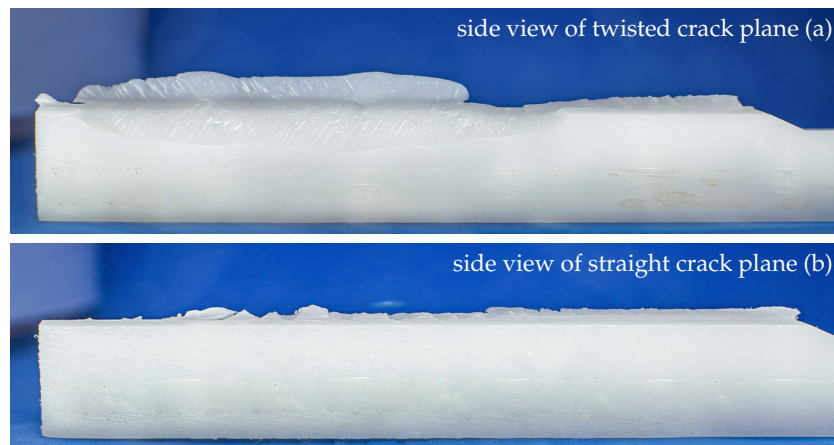


Figure 15. Fracture surface images from monotonically loaded mode III specimens (side view)—two different types of surface structure were observed: twisted crack planes along the fracture surface (a) and a nearly straight crack plane with little deflections (b).

The twisting of the crack during propagation is known as mode I branching. Here, the crack deflects under mixed-mode conditions to a local mode I loading [29,30]. Such mode I branches were also observed in a previous study on the same material in mode I/III fatigue tests [8]. Furthermore, the occurrence of shear lips and slant crack growth is quite common for thin specimens subjected to mode III [31–33]. As the measurements obtained in Section 4.2.2 demonstrated that the fracture was initiated in pure mode III and the fracture surfaces show typical signs of mode III fracture and the subsequent mixed-mode crack propagation, we can conclude that our adaption to the ODCB test allows the determination of the mode III fracture energy without further restrictions.

After a comparison with the results shown in Figure 12, a dependency of the macroscopically observed angle of the fracture surface and the pop-in ratio is suggested. A small ratio of $J_{III, \text{pop-in}} / J_{IIIc}$ seems to lead to a more flat and straight fracture, as shown in Figure 15b. This means that the macroscopically twisted and deflected fracture surfaces may be related to a higher pop-in ratio. However, to prove this assumption, further investigations are necessary. Especially a determination of the twisting angle at the crack tip using optical methods could be of huge benefit. Apart from the implied change in pop-in ratio, no connection between other experimental results and the twisting angle of the fracture surfaces could be found within the framework of this study.

Akin to the mode I fracture, no indications of plastic deformation were observed on the mode III fracture surfaces. Figure 16 presents a detailed picture of the fracture surfaces of a macroscopically twisted specimen (Figure 16a) and a specimen with a less deflected fracture surface (Figure 16b). The pre-notch is marked as area (1) and the mode III crack growth is marked as area (2).

4.6. Advantages, Limitations and Research Proposals

Before summarizing the most important results obtained within our paper, we would like to discuss the advantages and limitations of our work and propose topics for future studies.

We are aware that our research may have limitations: As we mainly tried to enable the testing of thin-walled polymeric components, we were unable to examine some possible influencing factors in more detail, unfortunately. It is generally well known that both the thickness of the specimen as well as the position of the initial crack tip may have a large influence on the fracture behavior. Furthermore, the stress state at the crack tip is likely influenced by the geometry of the grooves on the side of the specimen. As previously mentioned, the absence of signs of plastic deformation at the crack tip suggests a fracture in plane strain, although the slender specimen geometry should lead to a plane stress state. Hence, the impact of the grooves' geometry is unclear at this point. In this case, a simulative study using finite element analysis should provide important insights, but as we primarily focused on the experimental setup and the methods of evaluation, we have refrained from

performing simulations at this point in time. Such detailed analyses would not have been possible within the framework of this study without neglecting other important areas of our investigations. We propose that further research be undertaken in these areas.

In our investigation, we had to rely on thermal clamping of the specimens. Currently, we also cannot certainly rule out that the cooling procedure has influenced the overall fracture behavior of the specimen in mode III. Furthermore, one could argue that the addition of the aluminum reinforcements influences the load introduction to the crack tip, possibly impacting the measured results. We are aware of this limitation and, hence, propose that further research is undertaken to improve the specimen geometry. An alternative can be a change of specimen thickness at the lever arms, which may allow omitting the aluminum reinforcements in the first place.

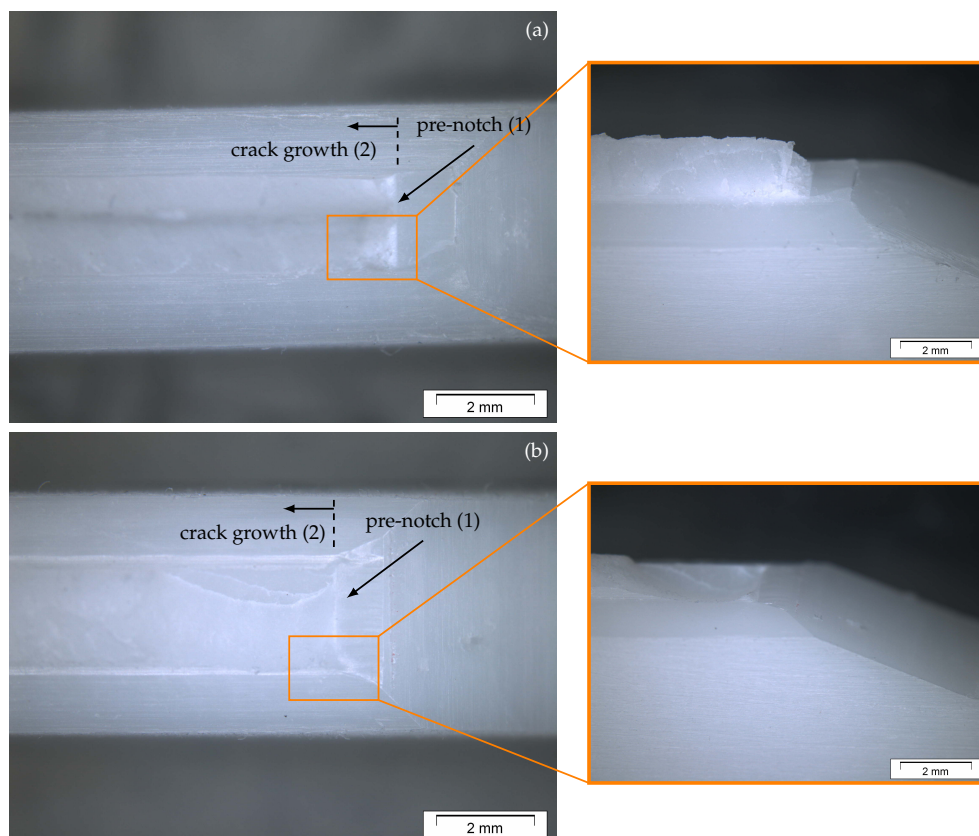


Figure 16. Fracture surface images from two mode III specimens analyzed using a light microscope ($16\times$ magnification). Image of a deflected fracture surface (a) and a flat fracture surface (b)—two different crack areas were observed on the fractured specimen half: pre-notch before testing (1) and area of crack growth during testing (2).

As discussed above, the instantaneous determination of J during the experiment in both modes I and III can be used to control the experiments on J . This enables testing in mixed-mode I+III under constant mixed-mode ratios, which can help to better understand the fracture behavior of polymeric bulk specimens. A revision of the sample geometry will therefore be required so that the aluminum holders become obsolete. In future studies, this should be investigated in more detail.

We also want to emphasize that the proposed setups should also be tested with other polymeric materials, as we exclusively focused on POM-H in our research. The selection of POM for this study was mainly due to its high relevance among engineering plastics and our prior knowledge of the material. Another advantage of POM is its limited dependency on strain rate in the elastic range [34], which allows the strain energy density to be considered as rate-independent in good approximation.

One of the obvious advantages of our methodology is that using the J -integral allows for the investigation of ductile materials. As a nice side effect, in case of a brittle or quasi-brittle failure,

the stress intensity factors in modes I and III can be determined. Furthermore, we found evidence to suggest that our mode III setup enables pure mode III testing of various kinds of polymers, as our setup allows for a precise experimental determination of the contributions to the fracture process in other fracture modes.

5. Conclusions

Within the limitations of our study, the following conclusions can be drawn:

- Our proposed methodology provides the possibility to determine the energy release rate of a polymeric material in pure mode I on the basis of the J -integral. It also allows us to measure the energy release rate in pure mode III, which is not yet possible with setups found within literature. For isotropic, brittle or quasi-brittle materials, the results can approximately be converted into the stress intensity factors in mode I and mode III.
- The observed pop-in fracture in mode III could be crucial for the structural integrity of thin-walled POM-H components. Crack growth prior to reaching the critical energy release rate can significantly weaken a structure when loaded in shear.
- The analysis of the fracture surfaces showed no signs of plastic deformation close to the initial notch in both modes I and III. The mode I specimens displayed a macroscopically flat fracture surface, whereas the mode III samples showed a deflection of the crack plane. The twisting of the crack path was attributed to a mixed-mode crack propagation and requires further investigation.

Additionally, we suggest that further research should be undertaken in the following areas:

- Future studies should address the applicability of the presented test setups to other materials, especially more ductile polymers.
- A simulative study of the experimental design could provide information on the validity of the test setups proposed in this study. Furthermore, an investigation of the influence of thermal clamping and the stress state at the crack tip using finite element analysis is suggested.
- The influences of specimen thickness, initial crack position, groove geometry, and influences due to notching have not been investigated within this study. We suggest that further studies focus on this, as their influence on the fracture behavior determined from the given test setup is not yet foreseeable.
- The test setups can be modified and "superimposed" to achieve a mixed mode I/III load. For this, it may be necessary to revise the clamping procedure.
- The fracture surface investigation should be expanded to obtain more information about the influence of pop-ins and the deflection of the crack-plane in the mode III tests.

Author Contributions: Conceptualization, P.S., A.G. and S.M.; methodology, P.S.; investigation, P.S. and A.G.; formal analysis, P.S.; data curation, P.S.; writing—original draft preparation, P.S. and A.G.; writing—review and editing, P.S.; visualization, P.S.; supervision, M.B. and S.M. All authors have read and agreed to the published version of the manuscript.

Funding: This research received no external funding.

Acknowledgments: This article is part of P. Schrader's doctoral thesis at the Doctoral Center for Engineering Sciences of the Research Campus of Central Hessen under the supervision of the Justus-Liebig-University Gießen in cooperation with the University of Applied Sciences of Central Hessen (Technische Hochschule Mittelhessen). The authors want to thank Bernd Haar for the production of the POM plates.

Conflicts of Interest: The authors declare no conflict of interest.

Abbreviations

The following abbreviations are used in this manuscript:

| | |
|------|--|
| POM | Polyoxymethylene |
| DCB | Double cantilever beam |
| ODCB | Out-of-plane-loaded double cantilever beam |
| ERR | Energy release rate |

Appendix A. Production of the POM-H Specimens

For a better overview, we want to disclose the manufacturing steps and parameters for the production of the POM-H specimens in greater detail:

- Step 1: Compression molding tubular granules into plates of approx. 200 × 200 × 5.5 mm; Hydrostat 300 (Schwabenthan, Germany) with an immersion edge tool (TT-260, Tool-Temp)
- Step 2: Cutting the pressed plates into a rectangular shape of size 160 × 25 mm; Bäuerle tablesaw KSW-7 (Riston Werkzeug GmbH, Fellbach, Germany)
- Step 3: Milling the rectangles to correct thickness; universal milling machine Deckel FFP3 (Friedrich Deckel AG, München, Germany) with HSS face-milling cutter ø60 mm at 500 rpm
- Step 4: Milling the slit between the lever arms; universal milling machine Deckel FFP3 (Friedrich Deckel AG, München, Germany) with HSS prismatic disk cutter ø250 mm at 80 rpm
- Step 5: Cutting the sidegrooves; Bäuerle tablesaw KSW-7 (Riston Werkzeug GmbH, Fellbach, Germany) with prismatic sawblade

References

1. Berer, M.; Major, Z. Characterization of the global deformation behaviour of engineering plastics rolls. *Int. J. Mech. Mater. Des.* **2010**, *6*, 1–9. [[CrossRef](#)]
2. Berer, M.; Major, Z. Characterisation of the Local Deformation Behaviour of Engineering Plastics Rolls. *Strain* **2012**, *48*, 225–234. [[CrossRef](#)]
3. Berer, M.; Mitev, I.; Pinter, G. Finite element study of mode I crack opening effects in compression-loaded cracked cylinders. *Eng. Fract. Mech.* **2017**, *175*, 1–14. [[CrossRef](#)]
4. Hashemi, S.; Elmes, P.; Sandford, S. Hybrid effects on mechanical properties of polyoxymethylene. *Polym. Eng. Sci.* **1997**, *37*, 45–58. [[CrossRef](#)]
5. Berer, M.; Pinter, G. Determination of crack growth kinetics in non-reinforced semi-crystalline thermoplastics using the linear elastic fracture mechanics (LEFM) approach. *Polym. Test.* **2013**, *32*, 870–879. [[CrossRef](#)]
6. Berer, M.; Pinter, G.; Feuchter, M. Fracture mechanical analysis of two commercial polyoxymethylene homopolymer resins. *J. Appl. Polym. Sci.* **2014**, *131*, n/a–n/a. [[CrossRef](#)]
7. Ramoa, B.; Berer, M.; Schwaiger, M.; Pinter, G. Effect of cyclic fatigue on the fracture toughness of Polyoxymethylene. *J. Physics Conf. Ser.* **2017**, *843*, 012052. [[CrossRef](#)]
8. Gosch, A.; Berer, M.; Hutař, P.; Slávik, O.; Vojtek, T.; Arbeiter, F.J.; Pinter, G. Mixed Mode I/III fatigue fracture characterization of Polyoxymethylene. *Int. J. Fatigue* **2020**, *130*, 105269. [[CrossRef](#)]
9. Aliha, M.; Bahmani, A.; Akhondi, S. Determination of mode III fracture toughness for different materials using a new designed test configuration. *Mater. Des.* **2015**, *86*, 863–871. [[CrossRef](#)]
10. Anthony, J.; Paris, P. Instantaneous evaluation of J and C. *Int. J. Fract.* **1988**, *38*, R19–R21. [[CrossRef](#)]
11. Olsson, P.; Stigh, U. On the determination of the constitutive properties of thin interphase layers—An exact inverse solution. *Int. J. Fract.* **1989**, *41*, R71–R76. [[CrossRef](#)]
12. Sørensen, B.F.; Jacobsen, T.K. Determination of cohesive laws by the J integral approach. *Eng. Fract. Mech.* **2003**, *70*, 1841–1858. [[CrossRef](#)]
13. Gunderson, J.D.; Brueck, J.F.; Paris, A.J. Alternative test method for interlaminar fracture toughness of composites. *Int. J. Fract.* **2007**, *143*, 273–276. [[CrossRef](#)]
14. Loh, L.; Marzi, S. An Out-of-plane Loaded Double Cantilever Beam (ODCB) test to measure the critical energy release rate in mode III of adhesive joints: Special issue on joint design. *Int. J. Adhes. Adhes.* **2018**, *83*, 24–30. [[CrossRef](#)]

15. Rice, J.R. A Path Independent Integral and the Approximate Analysis of Strain Concentration by Notches and Cracks. *J. Appl. Mech.* **1968**, *35*, 379–386. [[CrossRef](#)]
16. Hutchinson, J.W. Singular behaviour at the end of a tensile crack in a hardening material. *J. Mech. Phys. Solids* **1968**, *16*, 13–31. [[CrossRef](#)]
17. Rice, J.R.; Rosengren, G.F. Plane strain deformation near a crack tip in a power-law hardening material. *J. Mech. Phys. Solids* **1968**, *16*, 1–12. [[CrossRef](#)]
18. Zehnder, A.T. *Fracture Mechanics; Lecture Notes in Applied and Computational Mechanics*; Springer Science+Business Media: London, UK; New York, NY, USA, 2012; Volume 62.
19. Loh, L.; Marzi, S. Mixed-mode I+III tests on hyperelastic adhesive joints at prescribed mode-mixity. *Int. J. Adhes. Adhes.* **2018**, *85*, 113–122. [[CrossRef](#)]
20. Loh, L.; Marzi, S. A Mixed-Mode Controlled DCB test on adhesive joints loaded in a combination of modes I and III. *Procedia Struct. Integr.* **2018**, *13*, 1318–1323. [[CrossRef](#)]
21. Loh, L.; Marzi, S. A novel experimental methodology to identify fracture envelopes and cohesive laws in mixed-mode I + III. *Eng. Fract. Mech.* **2019**, *214*, 304–319. [[CrossRef](#)]
22. Tscharnuter, D.; Gastl, S.; Pinter, G. Modeling of the nonlinear viscoelasticity of polyoxymethylene in tension and compression. *Int. J. Eng. Sci.* **2012**, *60*, 37–52. [[CrossRef](#)]
23. Brandstetter, D. Überprüfung eines Zugkriechprüfstands auf Genauigkeit und Reproduzierbarkeit. Bachelor's Thesis, Montanuniversität Leoben, Leoben, Austria, 2014.
24. Usman, K. Mechanical Behaviour of POM in Dependence on Molar Mass, Temperature and Loading Regime. Master's Thesis, Technische Universität Chemnitz, Chemnitz, Germany, 2019.
25. D30 Committee. *ASTM D5528–13, Test Method for Mode I Interlaminar Fracture Toughness of Unidirectional Fiber-Reinforced Polymer Matrix Composites*; ASTM International: West Conshohocken, PA, USA, 2013; doi:10.1520/D5528-13. [[CrossRef](#)]
26. Berejnoi, C.; Perez Ipiña, J.E.; Llorente, C.L. Reproducibility of pop-ins in laboratory testing of welded joints. *Mater. Res.* **2000**, *3*, 139–146. [[CrossRef](#)]
27. Pisarski, H.G.; Hammond, R.; Watt, K. Significance of Splits and Pop-Ins Observed During Fracture Toughness Testing of Line Pipe Steel. In Proceedings of the 2008 7th International Pipeline Conference, Calgary, AB, Canada, 29 September–3 October 2008; Volume 3, pp. 473–482. [[CrossRef](#)]
28. Anderson, T.L. *Fracture Mechanics: Fundamentals and Applications*, 4th ed.; Chapman and Hall/CRC: Boca Raton, FL, USA, 2017.
29. Pokluda, J.; Pippan, R.; Vojtek, T.; Hohenwarter, A. Near-threshold behaviour of shear-mode fatigue cracks in metallic materials. *Fatigue Fract. Eng. Mater. Struct.* **2014**, *37*, 232–254. [[CrossRef](#)]
30. Vojtek, T.; Pokluda, J.; Šandera, P.; Horníková, J.; Hohenwarter, A.; Pippan, R. Analysis of fatigue crack propagation under mixed mode II+III in ARMCO iron. *Int. J. Fatigue* **2015**, *76*, 47–52. [[CrossRef](#)]
31. Pook, L.P. Crack profiles and corner point singularities. *Fatigue Fract. Eng. Mater. Struct.* **2000**, *23*, 141–150. [[CrossRef](#)]
32. Pook, L.P. Five decades of crack path research. *Eng. Fract. Mech.* **2010**, *77*, 1619–1630. [[CrossRef](#)]
33. Pook, L.P. The linear elastic analysis of cracked bodies and crack paths. *Theor. Appl. Fract. Mech.* **2015**, *79*, 34–50. [[CrossRef](#)]
34. Plummer, C.J.G.; Béguélin, P.; Kausch, H.H. The temperature and strain-rate dependence of mechanical properties in polyoxymethylene. *Polym. Eng. Sci.* **1995**, *35*, 1300–1312. [[CrossRef](#)]

Publisher's Note: MDPI stays neutral with regard to jurisdictional claims in published maps and institutional affiliations.



© 2020 by the authors. Licensee MDPI, Basel, Switzerland. This article is an open access article distributed under the terms and conditions of the Creative Commons Attribution (CC BY) license (<http://creativecommons.org/licenses/by/4.0/>).